DISSERTATION

FURTHERING THE DEVELOPMENT OF THE JAMAICAN FRUIT BAT AS AN ANIMAL MODEL FOR IMMUNOLOGY

Submitted by

Bradly E. Burke

Department of Microbiology, Immunology, and Pathology

In partial fulfillment of the requirements

For the Degree of Doctor of Philosophy

Colorado State University

Fort Collins, Colorado

Spring 2023

Doctoral Committee:

Advisor: Tony Schountz
Co-Advisor: Marcela Henao-Tamayo

Mark Zabel
Angela Bosco-Lauth
Tod Hansen

Copyright by Bradly E. Burke 2023

All Rights Reserved

ABSTRACT

FURTHERING THE DEVELOPMENT OF THE JAMAICAN FRUIT BAT AS AN ANIMAL MODEL FOR IMMUNOLOGY

Bats are the only flying mammals capable of powered sustained flight and encompass over 1,400 species. Bats interconnect important ecological services, agricultural crop services, agricultural husbandry health, and human health. The order of chiroptera is largely understudied for immunological research even though bats are reservoirs for viruses that are transmissible to livestock and humans including, henipaviruses, filoviruses, coronaviruses, and lyssaviruses. In 2006 Colorado State University established a breeding colony of Jamaican fruit bats (*Artibeus jamaicensis*) for use in the study of bat-borne viral infections.

Establishment of a bat colony is only the first step to the development of an animal model. The next step to develop an animal model is to elucidate the immunological systems and functionality of them. To elucidate the immunological systems, bat specific reagents are needed to characterize and perform hypothesis driven research. However, the paucity of bat specific reagents largely limits hypothesis driven research. Antibodies and cell lines are foundational reagents to immunology and virology. Antibodies are integral reagents used for many immunological and biochemical assays: ELISAs, ELISPOTs, western blots, cytometric bead assays, magnetic bead pull-down, surface plasmon resonance, microscopy, *in vivo* cellular depletion, and flow cytometry. Cell lines allow for *in vitro* assays and the propagation of viruses to be performed.

The production and validation of Jamaican fruit bat specific antibodies targeting CD3γ, CD4, and CD8α epitopes for the investigation of cytotoxic CD8 T cells, and CD4 T helper cells

are described in this study. Furthermore, the identification and validation of commercially available cross-reactive antibodies targeted to epitopes for various proteins and glycolipids: asialo GM1, CD3ε, CD8α, CD19, CD34, CD40, CD44, CD45, CD80, CD104, CD154, CD161, and MHC-II. This work has described their use in highly quantitative flow cytometric analysis, enrichment of cell populations by fluorescently activated cell sorting, and highly qualitative anatomical data by microscopy. This study has identified a novel $CD19^{+}CD3^{+}$ T cell population under homeostatic conditions of the Jamaican fruit bat immune system that has not been identified in humans, mice, or other bat species under a homeostatic state. The use of anti-asialo GM1 *in vivo* treatment of Jamaican fruit bats to target natural killer cells is also described in this work. Lastly the construction of plasmids for the production of Jamaican fruit bat growth factors: epidermal growth factor, wnt3a, R-Spondin-2, noggin, and gastrin are described for their use in culturing Jamaican fruit bat primary cells – especially gastrointestinal crypt stem cells.

Validation of cellular markers and reagents is a crucial first step in the investigative process that allows for the generation of informed conclusions – in any study. Furthermore, validation of cellular markers holds a higher level of imminent need and accuracy in underdeveloped animal models. This work provides a framework for other researchers in the advancement of underdeveloped animal models for immunology to more rigorously test antibody cross-reactivity. Furthermore, this work highlights the need to build a robust body of literature of cross-reactive antibodies for underdeveloped animal models.

ACKNOWLEDGEMENTS

I would like to first acknowledge my mentors Tony Schountz, and Marcela Henao-Tamayo. When I was rotating through laboratory groups, I had every intention to join a mycobacteria research lab – specifically Marcela's lab. I decided for my last rotation I should see a laboratory that was not doing mycobacteria research just to try something new. Mark Zabel pointed me to Tony's lab and told me Tony studies Jamaican fruit bats, and I thought that was cool. However, throughout my rotation I had no intention to join Tony's lab. Towards the end of my rotation, I began to love the work I was doing in his lab. As my last rotation came to an end, I had to decide. To my surprise and Tony's, I found myself in Tony's office and said "If I can do immunology and flow cytometry in your lab, and if you and Marcela will co-mentor me… I will join your lab". I would not have the knowledge I do about flow cytometry if Marcela had not given me the opportunity to work at the CSU flow cytometry core facility throughout my doctoral studies. Thank you, Tony and Marcela, for mentoring me. The work I have done would not have been possible without the guidance and support you both have given me.

I would like to thank my doctoral committee, Mark Zabel, Angela Bosco-Lauth, and Tod Hansen for your support and guidance throughout my doctoral studies

I would also like to thank my parents, husband, family, and friends who have supported me throughout my doctoral studies – I could not have done it without your support. Thank you all for putting up with my absences and cancelations because I was working late or needed to go home to get some sleep.

I would like to thank my best friend and collaborator Savannah Rocha; your friendship is more valuable than gold. I will always cherish the science we have done and the time we have spent in the lab together.

I would like to thank my friend Lizzy Creissen. You are the best coworker anyone could ask for. Thank you for helping every day I was working in the flow core and the days you set up the cytometer and cell sorter for them to be ready the moment I arrived with samples so I could hit the ground running.

DEDICATION

This work is dedicated to my parents Bryan and Tena Burke, to my husband Jacob Wilmoth, and to all first-generation students past, present, and future.

TABLE OF CONTENTS

LIST OF TABLES

LIST OF FIGURES

LIST OF KEYWORDS

AGM1
AGM1 antibody depletion
Antibody validation
Artibeus jamaicensis
Asialo GM1
Bats
CD104
CD154
CD161
CD19
CD19+ CD3+ double positive cells
CD28
CD34
CD3ε
CD40
CD44
CD45
CD80
CD8α
Cell sorting
Cellular immunity
Chiroptera
Cross-reactive antibodies
Crypt cells
Cytotoxic T lymphocytes
Desmodus rotundus
FACS
flow cytometry
Hybridoma production
Immune cell population enrichment
Immunology
Jamaican fruit bat and human homology
Jamaican fruit bat and mouse homology
Jamaican fruit bat and porcine homology
Jamaican fruit bat growth factors
Jamaican fruit bats
Keyhole limpet hemocyanin
KLRB1B
KLRB1C
KLRF1
MHC-II
Microscopy

Mucosal immunity
Natural killer cell depletion
PBMCs
Phylogeny of humans, bats, and mice
Protein homology
Pteropus alecto
Pteropus giganteus
Pteropus medius
Rhinolophus ferrumequinum
Rhinolophus sinicus
Rousettus aegyptiacus
Spectral Flow Cytometry
Splenocytes
Stem cells
T helper Lymphocytes

CHAPTER 1
A SHORT HISTORY OF FLOW CYTOMETRY IN RELATION TO THE ADVANCEMENT OF IMMUNOLOGY AND WHY FLOW CYTOMETRY IS NEEDED FOR BAT IMMUNOLOGY

Summary

The first flow cytometer was developed in 1968 by German scientist Wolfgang Göhde, and since then flow cytometry has become an indispensable tool for immunology. However, foundational milestones in multiple disciplines, including physics, chemistry, and immunology, needed to occur to develop flow cytometry as a powerful tool for cell biology and immunology. Florescence is critical component of quantum physics related to flow cytometry; Niels Bohr established in 1904 that photons can excite electrons and when the electrons return to their ground state they emit photons. Another milestone in quantum physics related to flow cytometry is the photoelectric effect. The construction of photomultiplier tubes and avalanche photodiodes, vital components of flow cytometers, are reliant on photoelectric effect which was observed by Heinrich Hertz in 1887. In 1950, the law of the photoelectric effect was established by Albert Einstein. Antibodies are a critical reagent for flow cytometry and were first described, though not fully as understood as they are today, by three individuals in the late 1800s and early 1900s Emil von Behring, Shibasaburo Kitasato, and Paul Ehrlich. The first published paper using fluorescently conjugated antibodies to visualize localization of antigen in tissues cells was in 1950 by Albert H. Coons and Melvin H. Kaplan using fluorescein isocyanate, also known as FITC, and is still used today to conjugate antibodies. In 1975 Georges J.F. Köler and César Milstein received a Nobel Prize for Medicine for describing the technique to produce monoclonal antibodies – the hybridoma technique.

These milestones were critical in the formation of the flow cytometry technique. Flow cytometry is used by scientists across the globe as a high-thruput multi-parametric

technique. It allows scientists to measure and monitor immune cell populations during infections, responses to vaccines and drug therapies, and to diagnose and monitor diseases in a variety of animal species. One group of mammals that has not been well-studied by flow cytometry are bats, which are major reservoir hosts for viruses that cause disease in humans and livestock including, henipaviruses, filoviruses, coronaviruses, and lyssaviruses. Few studies that have been performed on bats using flow cytometry to characterize their immune systems and responses. The primary limitation of using flow cytometry to characterize bat immune systems the paucity of bat specific reagents. As such this limitation is hindering the understanding of the selection pressures bat-borne viruses have undergone and continue to undergo. Studies characterizing bat immune systems and immune responses can give us insight as to how bat-borne viruses result in high morbidity and mortality when spilled-over into human and other mammal populations.

Flow Cytometry: The Fundamentals

Fluorescence and Photoelectric Effect

Before discussing the components of flow cytometry two areas of quantum mechanics need to be discussed: fluorescence and photoelectric effect. Fluorochromes, or fluorophores, are molecules that become excited by a specific wavelength of light (excitation wavelength) and the fluorochromes will emit light (emission wavelength) when they fall from their excited state back into their ground state. The classic Bohr's model demonstrates fluorescence in a simplified manner[3,4]. Absorption of light (violet) causes an atom's ground state electron to move to a higher energy state, when the electron returns to its ground state it releases photons (**Figure 1.1**)[4-7]. This excitation and emission are

depended upon the molecule. For example, fluorescein isothiocyanate (FITC) a common fluorophore in flow cytometry is predominantly excited by blue light – typically a 488nm laser– and emits green light with a peak emission wavelength of 525nm (**Figure 1.2**). In contrast allophycocyanin (APC) another common fluorophore in flow cytometry is predominantly excited by red light – typically 650nm laser – and emits red light with a peak emission wavelength of 660nm (**Figure 1.2**).

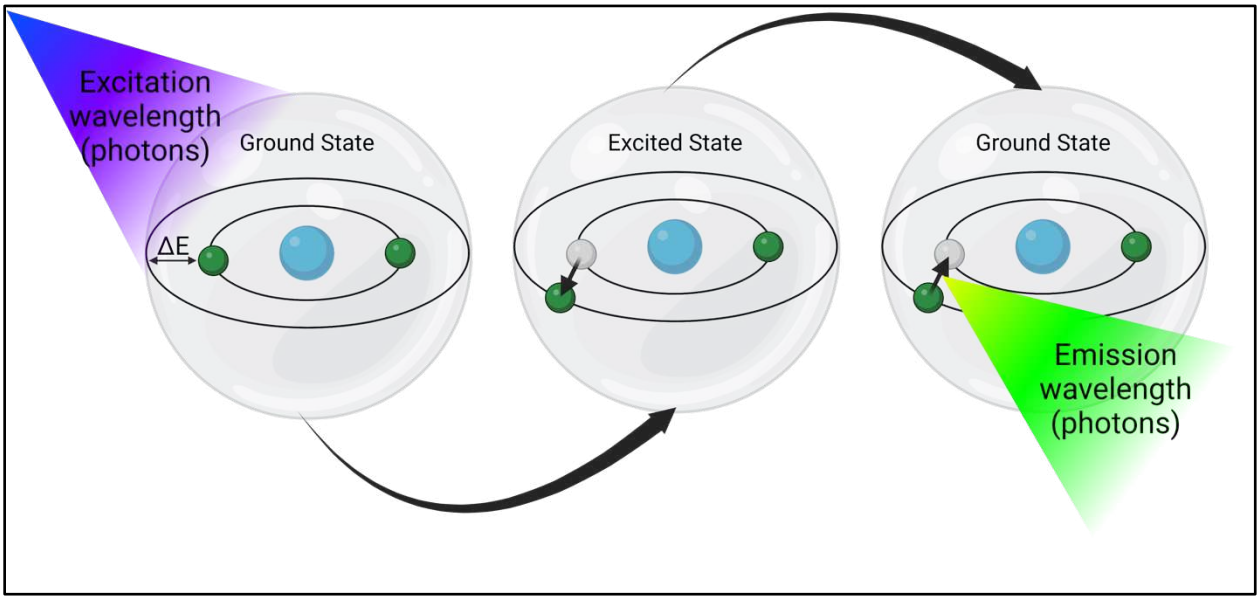

Figure 1.1) Bohr's model demonstrating excitation and emission. An atom's electrons absorbing violet light (left) causing it to move to a higher energy state (ΔE) (middle), and the excited electron falling back into ground state and emitting green light (right). Created with BioRender.com

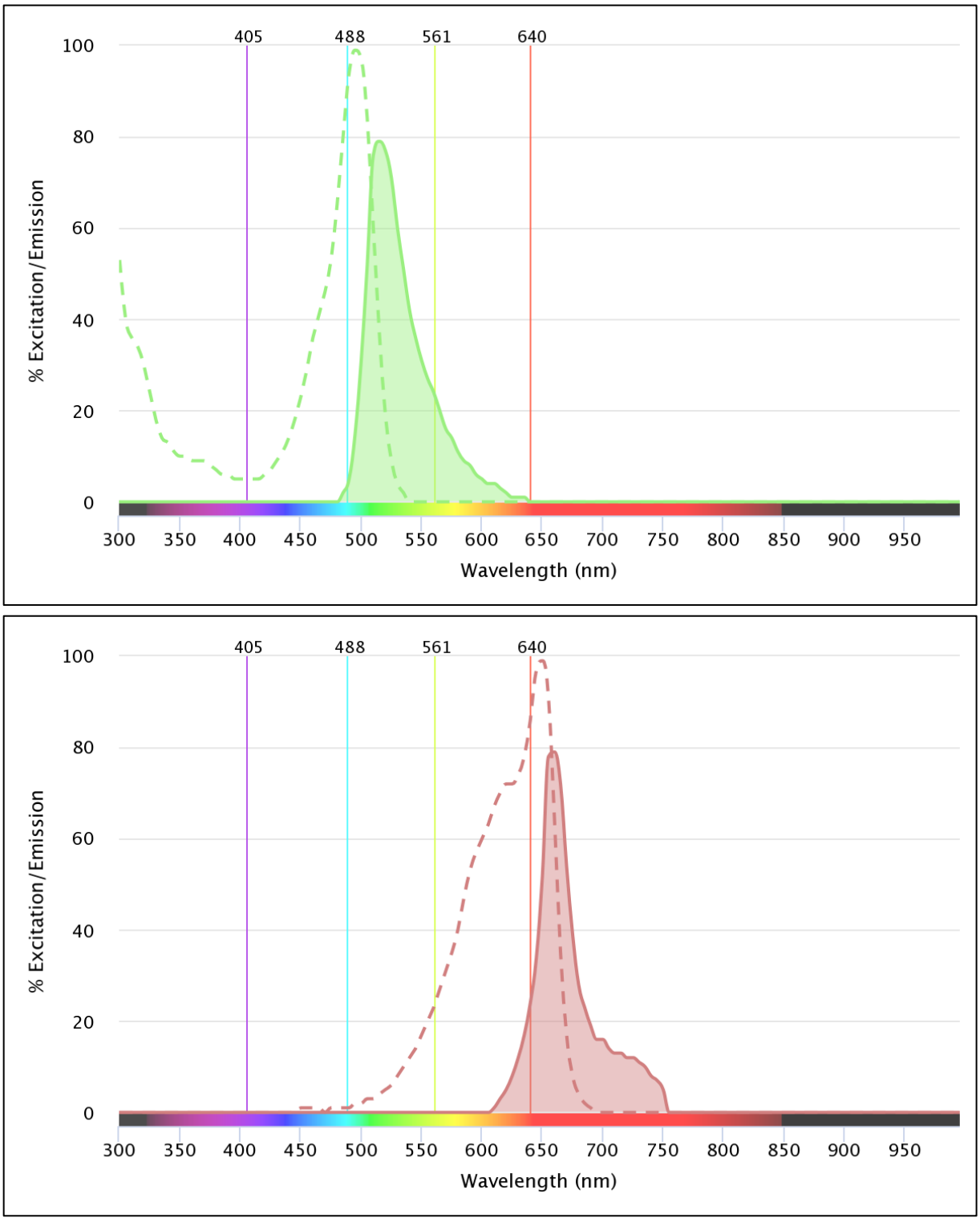

Figure 1.2) FITC (Fluorescein isothiocyanate) excitation (dashed line) and emission (solid line with filled area) spectra normalized to 488nm blue laser line (Top).
APC (Allophycocyanin) excitation (dashed line) and emission (solid line with filled area) spectra normalized to 640nm red laser line (Bottom). Generated by FluoroFinder.

The photoelectric effect is the process in which photons generate electrons and was first observed by Heinrich Hertz in 1887, but Albert Einstein established the law of the photoelectric effect in 1905 and received a Nobel Prize in Physics in 1921 “for his services to Theoretical Physics, and especially for his discovery of the law of the photoelectric effect"[8-10]. Traditionally photomultiplier tubes (PMT) have been used in flow cytometers. This process occurs by an incident photon hitting the photocathode producing the primary electron. The primary electron then collides with the first electrode (dynode) causing a secondary shower of electrons, this process is repeated multiple times until the electrons impact the anode which generates an electronic impulse that is recorded by a computer (**Figure 1.3**)[11].

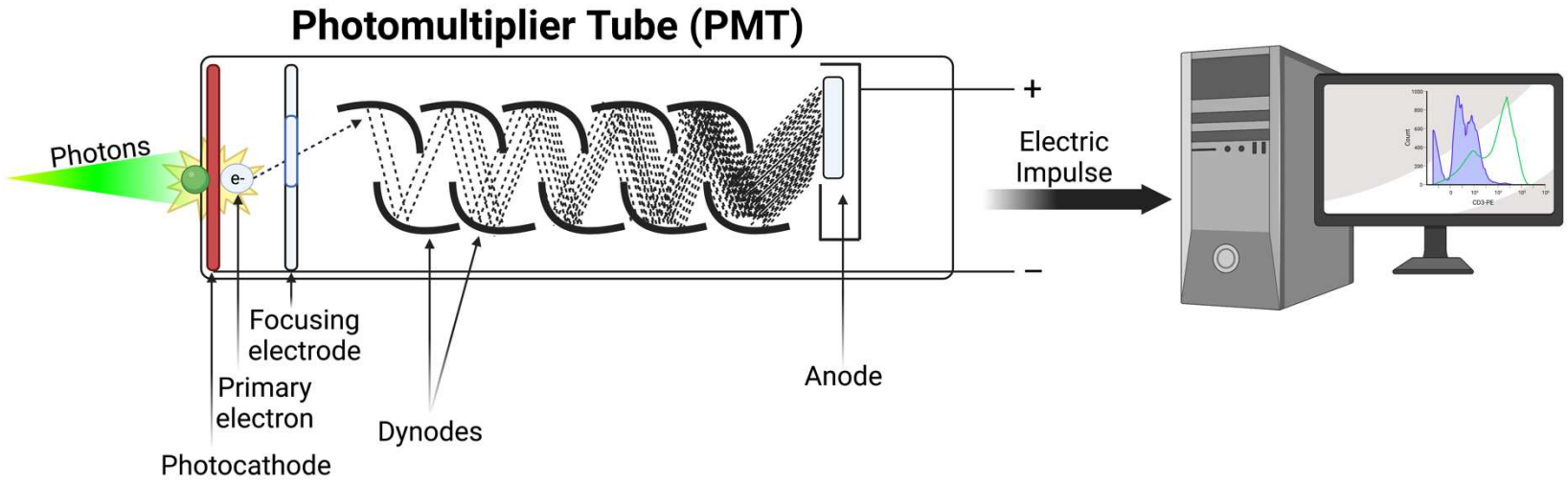

Figure 1.3) Photoelectric effect in a Photomultiplier tube. Incident photons bass through the photocathode, causing a primary electron to collide with the first electrode (dynode). Electrons that impact a dynode causes a secondary electron shower to occur. This process occurs in multiple stages thereby multiplying electrons many times over. These electrons hit the anode and produce an electrical impulse which can be recorded by a computer. Created with BioRender.com

With the advancement of technology, reach-through avalanche photodiodes (APD) are beginning to replace PMTs because they have a higher quantum efficiency, with an upper bound of 90%, whereas PMTs have no more than 40% quantum efficiency[12]. APDs are silicone-based semiconductors containing two pn junctions (the boundary between the P and N regions) created by positively doped P regions and a negatively doped N region surrounding the pn junctions are the depletion region and the avalanche multiplication region. Incident photons pass though the APD into the depletion region where the photon generates an electron-hole pair, the hole travels to the anode and the electron travels to the cathode. The electron while traveling to the cathode collides with other molecules in the silicon lattice in the avalanche multiplication region where it generates another electron-hole pair – this occurs multiple times[13-17]. The avalanche process generates an electronic impulse that is recorded by a computer (**Figure 1.4**). As such, this process is comparable to an electron shower observed in PMTs (**Figure 1.3**).

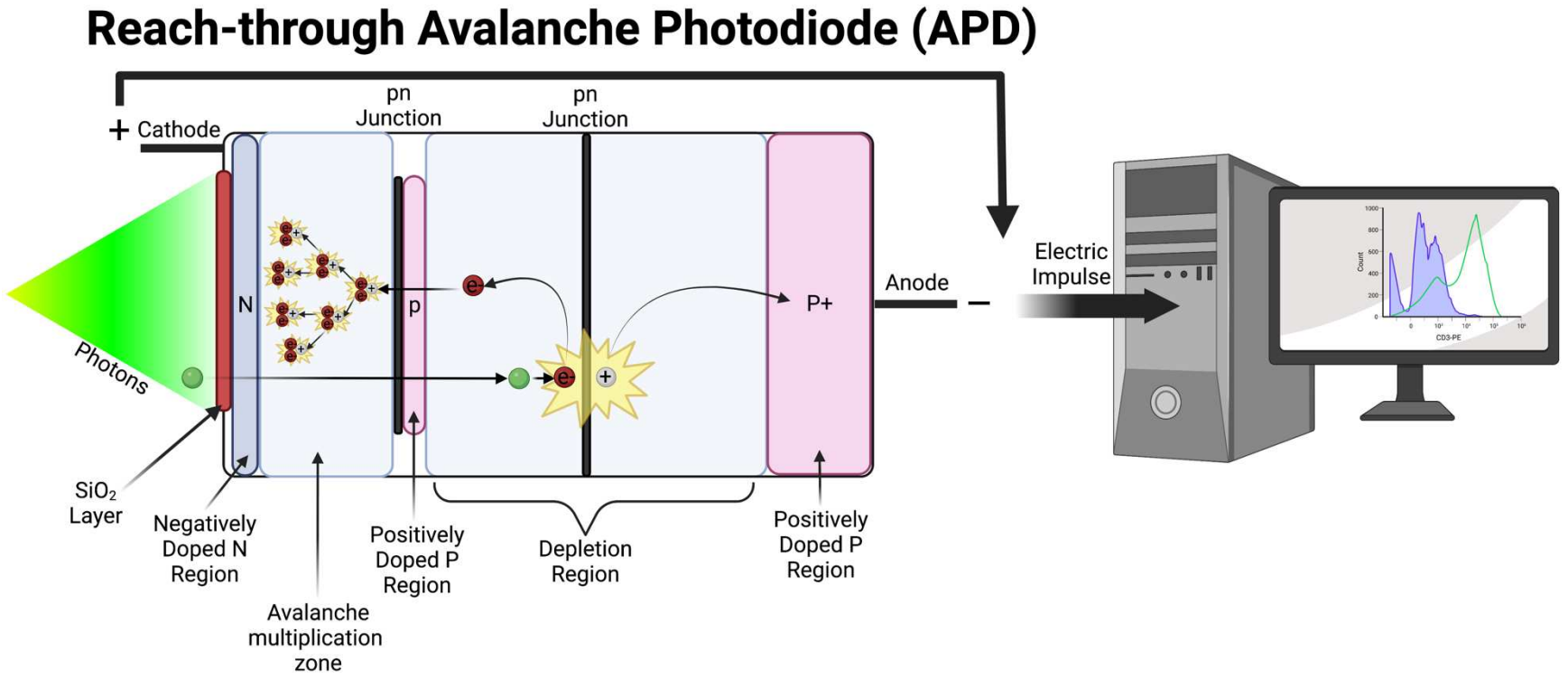

Figure 1.4) Photoelectric effect in a reach-through avalanche photodiode. Incident photons pass through the APD into the depletion region where photons generate electron-hole pairs. Energetic free electrons travel towards the cathode, and generated holes travel to the anode. As electrons travel to the cathode, they collide with the silicon lattice generating more electron-hole pairs – similar to the electron shower generated by dynodes in a PMT. Created with BioRender.com

Staining Cells

Labeling or staining cells with fluorochromes permit gathering of specific information about cells and there are multiple ways to label or stain cells. Cells can be manipulated to produce reporter fluorescent proteins, such as green fluorescent protein. Florescent molecules can be used to stain various components of cells directly, for example, nucleic acid dyes like DAPI, propidium iodide, and 7-AAD. Cells can be indirectly stained with fluorochrome labeled proteins – such as immunoglobulins or antibodies. Antibodies were first described, though not fully as understood as they are today, by three individuals in the late 1800s and early 1900s Emil von Behring, Shibasaburo Kitasato, and Paul Ehrlich[18-20]. Here, I will focus on fluorescently labeled immunoglobulins –specifically IgG. The structure of IgG is comprised of two heavy chains and two light chains held together by disulfide bonds [21]. The N terminus region of an IgG

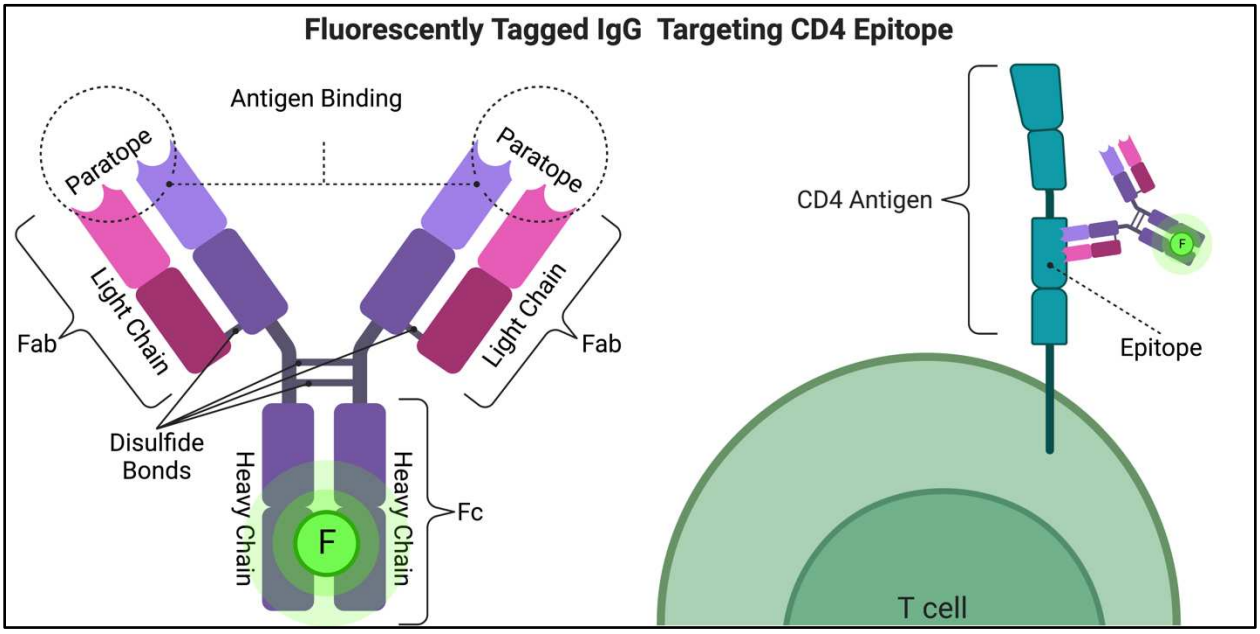

Figure 1.5) Structure (left) of an immunoglobulin (IgG) fluorescently tagged binding to the antigen's epitope (Right). IgG is comprised of two heavy chains and two light chains bound together by disulfide bonds. The tail of the immunoglobulin is called the Fc region. The two arms of the immunoglobulin are called the Fab regions. The antigen binning site is called the paratope. The paratope binds to the epitope of the antigen (in this example CD4). This antibody is conjugated to a green fluorochrome, therefore measured green fluorescence measures antibody bound to CD4. Created with BioRender.com

protein is the antigen binding domain, also known has the paratope [21,22]. The paratope binds to the epitope, or antigenic determinant, of the antigen (**Figure 1.5**). Antibodies are generated to target an antigen of interest by immunizing an animal, typically mice, rabbits, chickens, and goats, with the antigen of interest [23]. The immunized animal will generate an immune response which will produce antibodies from activated B cells[21,23,24]. Antibodies can then be purified from the serum known as polyclonal antibodies. Polyclonal antibodies are immunoglobulins that arise from many different B cells, as such, they can target many different epitopes on the same antigen[21,23]. Polyclonal antibodies are still used today for flow cytometry; however, monoclonal antibodies are preferred in many cases because they target a single epitope. In 1975 Georges J.F. Köler and César Milstein received a Nobel Prize in Medicine for describing the technique to produce monoclonal antibodies – the hybridoma technique (**Figure 1.6**) [21,25]. Splenocytes from hyperimmunized mice and immortal mouse myeloma cancer cells are fused using polyethylene glycol (PEG). After myeloma and splenocyte cells are fused, the cells are cultured in hypoxanthine-aminopterin-thymidine (HAT) medium. HAT medium selects for hybrid cells; unfused myeloma and splenoytes die. The unfused myeloma cells die because they lack hypoxanthine:guanine phosphoribosyl transferase (HGPRT) to detoxify HAT. The splenocytes have HGPRT, but they are not immortal and, therefore, also die. The fused cells have both the immortal characteristics of the myeloma cells and the HGPRT enzyme, as such they can grow in HAT medium. Once the hybridomas are selected, they are then cloned into 96 well. From here the hybridoma clones will replicate and secrete monoclonal antibodies that can then be screed for reactivity to the antigen of interest[21,25]. Reactive clones can then be cultured to collect secreted

antibody in the cell culture supernatant. Collected antibody monoclonal or polyclonal can then be labeled with a fluorochrome.

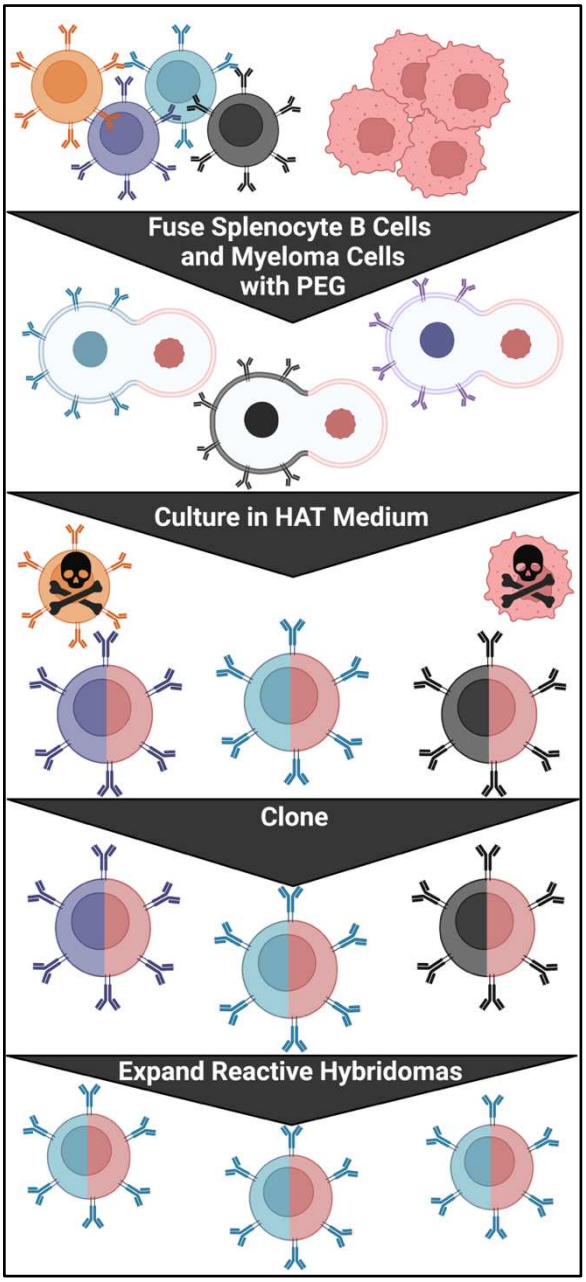

Figure 1.6) General overview of hybridoma generation to produce monoclonal antibodies. After immunizing a mouse with an antigen of interest, the spleens are harvested and processed into a single cell suspension. The splenocytes and myeloma cells are then fused with polyethylene glycol (PEG). Fused cells are then cultured in hypoxanthine-aminopterin-thymidine (HAT) medium which selects for hybridoma cells. Hybridoma cells are then cloned by seeding 96 well plates in a dilute manner such that one well is seeded with one hybridoma. Reactive clones to the antigen of interest are then expanded, and the cell culture supernatant is collected to isolate excreted monoclonal antibody. Created with BioRender.com

The process of labeling immunoglobulins with a fluorochrome is called conjugation. The first published paper using fluorescently labeled antibodies to visualize localization of antigen in tissues cells was in 1950 by Albert H. Coons and Melvin H. Kaplan[26]. Coons and Kaplan could not have done this without the previous work performed in 1933 by Sydney J. Hopkins and Arthur Wormall who described isocyanate conjugation to proteins, in which they deduced the reaction site was on lysine[27]. The work of Hugh J. Creech and R. Norman Jones performed in 1941 was also pivotal in Coons' and Kaplan's success in which they elucidated the conditions for antibodies to be conjugated to fluorescein isocyanate[28,29]. Fluorescein isocyanate (FITC) is still used today to conjugate antibodies. Currently antibodies are predominantly conjugated on three different types of sites, amine, thiol, and carbohydrates, because immunoglobulins are rich in lysine and cystine residues, and carbohydrate groups on glycans (**Figure 1.7**) [24,30-33]. As such, chemical reactions can be carried out on purified antibodies – monoclonal or polyclonal. The primary amines found predominantly on lysine residues form bonds with fluorochromes that have various functional groups: N-hydroxysuccinimidyl esters (NHS-ester), isocyanates, isothiocyanates, and benzoyl fluorides. The thiol groups found on cysteines form bonds with fluorochromes that have various functional groups: maleimides, iodoacetamides, 2-thiopyrdone, and 3-carboxy-4-nitrothiophenol. Carbohydrates found on glycans, such as galactose, can be oxidized with periodate ($NaIO_4$) to form aldehyde groups. The aldehyde groups can form stable bonds with fluorochrome hydrazides (**Figure 1.7**) [24,30-33].

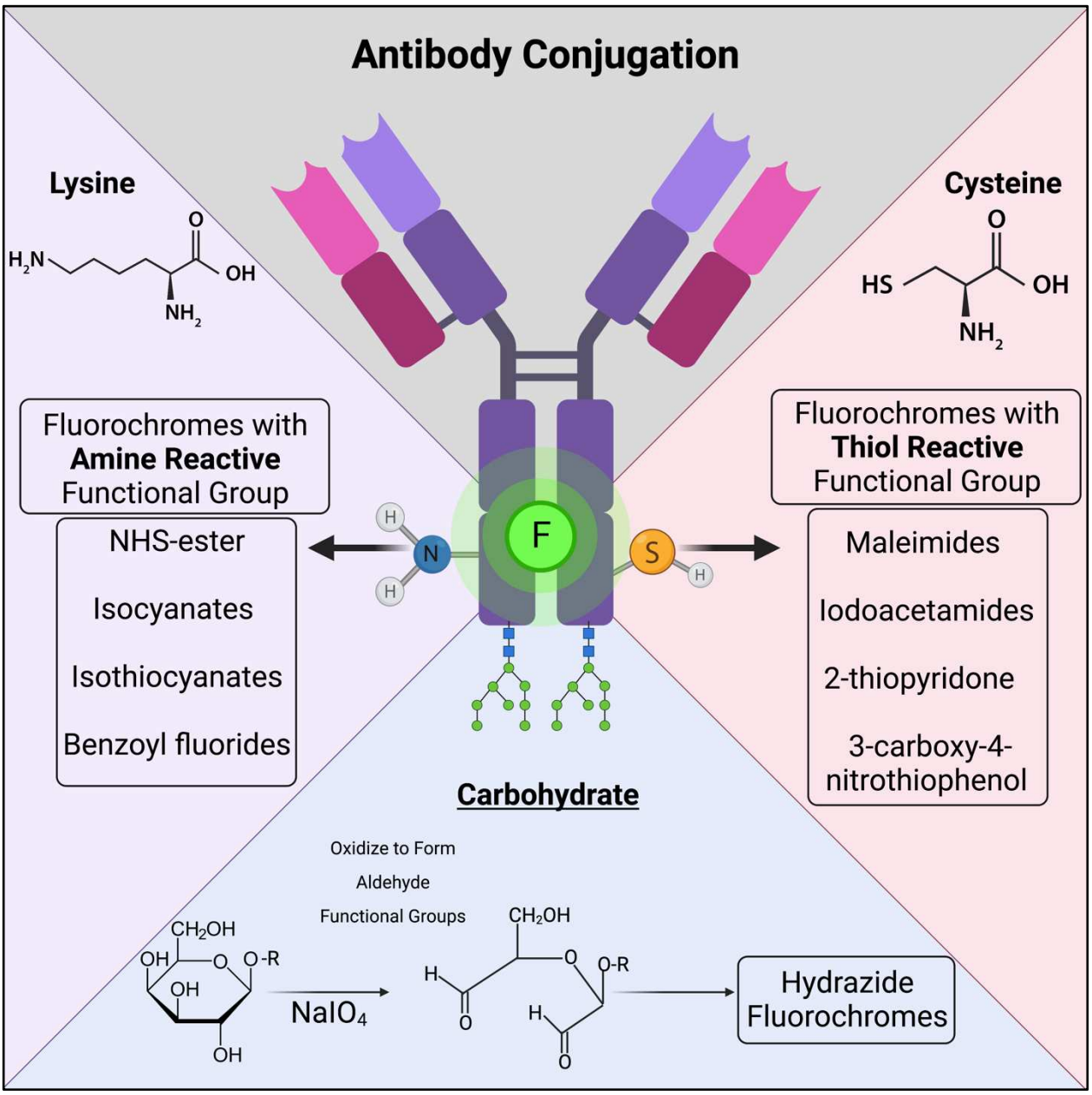

Figure 1.7) Antibody conjugation targeting three sites: amines (left), thiols (right), and carbohydrates (bottom). Amine conjugation largely targets lysine residues. Thiol conjugation largely targets cysteines. Carbohydrate conjugation targets glycosylation sites. Created with BioRender.com

Fluorescence, Photoelectric Effect, and Staining Put Together in a Flow Cytometer

All of the previous discussed topics – fluorescence, photoelectric effect, and cell staining span the disciplines of physics, immunology, and chemistry are foundational to flow cytometry and are vital to understand flow cytometry as a technique and technology. The first flow cytometer was developed in 1968 by German scientist Wolfgang Göhde (Patent DE1815352), since then flow cytometry has become an indispensable tool for immunology. Flow cytometry permits measurement and monitoring of immune cell populations during infections, responses to vaccines and drug therapies, and to diagnose and monitor diseases[34-37].

The basics of any flow cytometer can be divided into three components: fluidics, optics, and electronics (**Figure 1.8**). The sample of interest is disassociated into a single cell liquid suspension which allows the instrument to aspirate the sample into the instrument's fluidics system. The cells are then hydrodynamically focused into a single file stream. Once in a single file stream, the optics component comes into play. The cells then pass through the interrogation point – where the cells pass through the laser or lasers. As a cell passes through the laser, forward scatter (FSC) light and side scatter (SSC) light detectors (PMTs or APDs) measure cell size (FSC) and complexity (also known as granularity) (SSC) (**Figure 1.8**). Additionally, if fluorescent molecules are used to label the cell a specific nanometer wavelength laser excites (excitation wavelength) the fluorochromes and the fluorochromes will emit light into specific nanometer wavelengths (emission wavelength). The emitted light is split by being reflected or passing through dichroic mirrors into specific nanometer wavelengths, this can simply be thought of as colors (violet, blue, green, yellow, and red) – this is called optical configuration (**Figure 1.8**). This information is measured by additional detectors (PMTs or APDs) for each wavelength of light in the optical configuration.

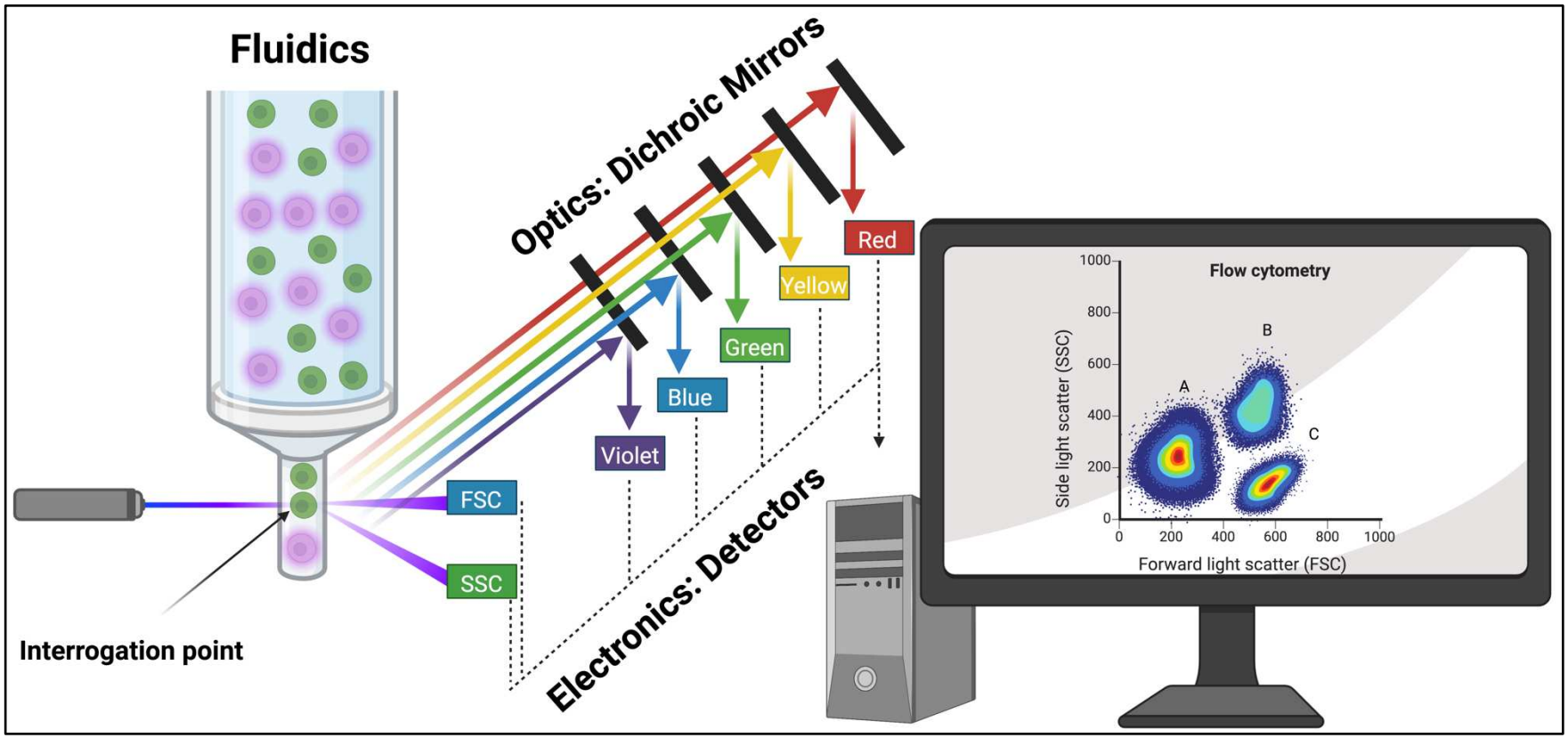

Figure 1.8) Flow cytometer systems: fluidics, optics, and electronics. The single cell suspension is being aspirated into the fluidics system where the cells are hydrodynamically focused and pass through the interrogation point. FSC and SSC light determines cell size and granularity, Light being emitted by the fluorochromes passes through or is reflected by dicrotic mirrors and band pass filters (optics) and directed to their intended detectors. The detectors then transmit electronic pulses to the computer to be recorded (electronics). Created with BioRender.com

The start of the electronics component are detectors that detect photons and convert the photons into electrons (**Figures 1.3 and 1.4**). These elections can then me measured and recorded as an electronic pulse by a computer.

In traditional cytometry one fluorochrome is assigned to one detector[38,39]. Spectral cytometry has an ADP array, meaning every fluorochrome is measured across all detectors[38,39]. As such a polychromatic panel in traditional cytometry and spectral cytometry use different methods to calculate the intensities of each fluorochrome present on each cell. Traditional flow cytometry uses compensation which calculates overlap of other fluorochromes that are not assigned to the detector[40]. After calculating spillover coefficients, which can be thought of as precents, is used to correct – compensate – the data[40]. Spectral cytometry uses unmixing to calculate vectors of each fluorochrome[39,41]. Vector regression is calculated using ordinary least squares which is in turn used to extract – unmix – the contribution of each fluorochrome from the total emission signal from a sample[39,41]. Single color controls of each fluorochrome to perform traditional compensation and spectral unmixing[39,40]. Using traditional cytometers a maximum amount of fluorochromes that can be used simultaneously in a panel is about 18[38]. Spectral cytometers currently can use 50 fluorochromes simultaneously[38,42].

Immune Cell Populations and Flow Cytometry Panels

The immune system can be defined by two facets – the innate and adaptive. Innate immunity can rapidly respond to pathogens but it lacks specificity (**Figure 1.9**). Adaptive is slower to respond to pathogens; however, it escalates rapidly and has high specificity. The innate immune system is comprised of various cells and proteins: neutrophils, eosinophils, basophils, macrophages, dendritic cells, mast cells, complement proteins, and pattern recognition receptors. The adaptive immune system is comprised of $CD4^+$ T helper cells, $CD8^+$ cytotoxic T cells, and B cells that secrete antibodies. There are also additional cells, such as γδ T cells, natural killer cells,

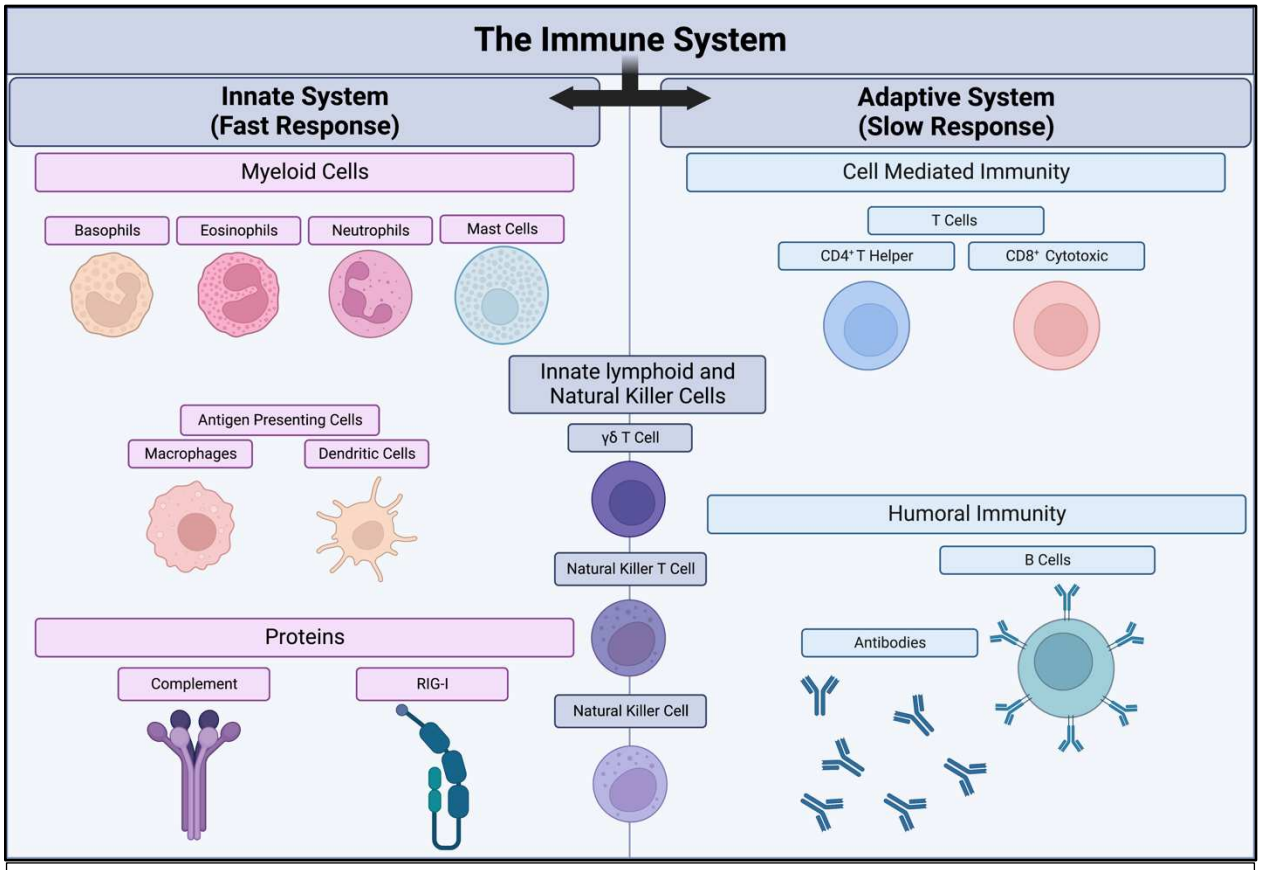

Figure 1.9) Overview of the mammalian immune system and it's cell types. The innate immune system is comprised of cells and proteins: neutrophils, eosinophils, basophils, macrophages, dendritic cells, mast cells, complement proteins, and RIG-I proteins. The adaptive immune system is comprised of $CD4^+$ T helper cells, $CD8^+$ Cytotoxic T cells, and B cells that secrete antibodies. There are also additional cells, such as γδ T cells, natural killer cells, and natural killer T cells that have characteristics of both innate and adaptive cells. Created with BioRender.com.

and natural killer T cells that have characteristics of both innate and adaptive cells. However, the generalized groups of cells can be further classified into different functionalities. These immune cells can be identified by flow cytometry, to determine their abundance, how they are responding and functioning to a pathogenic assault, vaccine, or drug[34-37]. Identifying immune cell types is termed *immunophenotyping* and is largely done by staining cells with fluorochrome conjugated antibodies that bind to various clusters of differentiation (CD) markers, other markers, and various cytokines to determine responses and functionality. The CD nomenclature was established and is maintained by the human leucocyte differentiation antigens (HLDA) workshop. The HLDA workshop and conference was first held in 1982 and has characterized CD1 to CD350 [43]. A well-designed flow cytometry panel that combines markers and cytokines is critical to identify and characterize immune cell populations of interest. Designing a flow cytometry panel is a tedious process that requires the optical configuration of the flow cytometer that will be used to determine the fluorochromes that can be used and knowing each fluorochromes' brightness and antigen density of each target. For example, one cannot use a fluorochrome that is excited by a laser that the flow cytometer does not have, nor can one use a fluorochrome that emits into a wavelength that the flow cytometer does not have a filter and detector set for. Additionally, multiple fluorochromes that have highly similar excitations and emissions should not be used in the same panel. Antigen density and fluorochrome brightness are critical in polychromatic flow cytometry. A bright fluorochrome to an antigen that is expressed at low levels or is only found on a rare cell population (**Figure 1.10**). Dim fluorochromes should be assigned to an antigen that is expressed at high levels or is found on an abundance of cells.

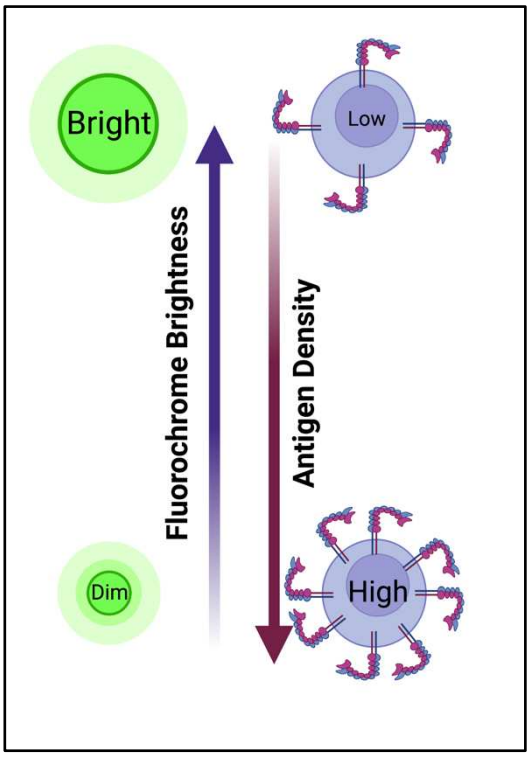

Figure 1.10) Panel design considering antigen density and fluorochrome brightness. Assign bright fluorochrome to antigens that are expressed at low levels, or found on rare cell populations. Assign dim fluorochrome to antigens that are highly expressed or is found on an abundance of cells. Created with BioRender.com

(**Figure 1.10**). Conjugated antibodies must be titrated to calculate staining indexes to determine the optimal concentrations to use of a particular antibody to stain a sample. A standard method is to do an 8-point titration, then gating on positive and negative cells, then the median fluorescent intensities are used from the negative and positive populations, and the negative population robust standard deviation to calculate staining indexes[44,45]. Staining index calculations are a signal-to-noise ratio calculation – the higher the staining index the better[44,45]. Too much antibody increases background negative noise, and too little antibody decreases positive signal –both of which lower the staining index[44,45]. Each component previously discusses is critical to producing and optimized flow cytometry panel.

Currently there are 85 *Optimized Multicolor Immunofluorescence Panels* (OMIPs), which are peer reviewed publications that meet the International Society for Advancement of

Cytometry and are excellent resources to find optimized panels to use as is or build on to [46]. For example, *OMIP-038: Innate Immune Assessment with a14 Color Flow Cytometry Panel* is an optimized flow cytometry panel that utilizes a variety of CD markers and cytokines to identify innate immune cells and their function (**Table 1.1**). The OMIP-038 panel identifies multiple subsets of monocytes, dendritic cells, T cells, natural killer cells, B cells, and neutrophils (**Table 1.2**). TNF, IL-6, and IL-12 are proinflammatory cytokines that determine functionality of the antigen presenting cells. The two other inflammatory cytokines in OMIP38 TNFα and IFNγ determine the functionality of pDCs (TNF) and T cells (IFNγ).

Table 1.1) OMPI-038 Panel

OMPI-038 Panel

Specificity	Clone	Fluorochrome	Purpose
Viability Dye	N/A	eFluor780	Live/Dead
TNF	MAb11	Alexa 700	Function
CD11c	S-HCL-3	APC	cDC
CD123	6H6	PE-Cy7	pDC
CD3	UCHTI	PE-CF594	T Cell Lineages
IFNα	7N4-1	PE	Function
IL-6	MQZ13A5	PerCP-eFLuor 710	Function
γδTCR	B1.1	FITC	γδ T cell
CD66	ASL-32	Biotin	Neutrophils
Streptavidin	N/A	BV786	N/A
IFNγ	4S.B3	BV711	Function
CD16	3G8	BV650	NK, NK T cells, and Mocytes
HLA-DR	LN3	eFluor 605	B cells, Monocytes
CD14	M5E2	V500	Monocytes
IL-12	C8.6	eFluor 450	Function

Table 1.2) OMIP-038 Immunophenotypes

OMIP-038 Immunophenotypes

Immunophenotype	Markers
Neutrophils	CD66+
Plasmocytoid Dendritic Cells (pDC)	CD66- HLA-DR+ CD11c- CD123+
Conventional Dendritic Cells (cDC)	CD66- HLA-DR+ CD11c+ CD123-
B Cells	CD66- HLA-DR+ CD11c- CD123-
Classical Monocytes	CD66- CD14+ CD16-
Inflammatory Monocytes	CD66- CD14+ CD16+
Patroling Monocytes	CD66- CD14dim CD16+
T cells	CD66- CD3+ γδ-
γδ T Cells	CD66- CD3+ γδ+
Natural Killer Cells	CD66- CD3- γδ- CD16+ CD56+

Bat Immunology

The Interconnection of Bats, Ecology, Agriculture, and Human Health

Bats encompass over 1,400 species which interconnect important ecological services, agricultural crop services, agricultural husbandry health, and human health. Agricultural crop services include pollination and seed dispersal, and consumption of insects such as crop and forest pests [47]. Additionally, some of the pests that bats consume are also vectors of pathogenic viruses and bacteria to plants [47,48]. Bats also consume mosquitos and midges that spread arthropod-borne diseases to livestock and humans such as West Nile virus, Japanese encephalitis virus, dengue, chikungunya, Zika, bluetongue viruses, and malaria parasites [47,49-52]. Bats are major reservoir hosts for viruses that are transmissible to humans and livestock including, henipaviruses, filoviruses, coronaviruses, and lyssaviruses [53]. For example, Nipah virus has caused outbreaks in pig farming, but also directly from bats to humans though consumption of date palm sap [54-56]. Additionally, SARS-CoV2 and the global pandemic of COVID-19 likely originated from a spillover event from horseshoe bats [57]. Interestingly, bats usually do not show signs of disease from these viruses, in contrast to the high morbidity and mortality caused by these viruses in humans and other mamals[53]. However, bats are susceptible to other pathogens such as rabies virus and *Pseudogymnoascus destructans*, the causative agent of white nose syndrome (WNS) that has killed millions of North American bats. A recent study has reported that three species of North American bats (*Myotis septentrionalis*, *Myotis lucifugus*, and *Perimyotis subflavus*) have been reduced by more than 90% by WNS [58]. As such, these interconnections of ecological services, agricultural crop services, agricultural husbandry health, and human health demonstrate – in part – the significance of bats.

Bats Have Unique Immunological Attributes

Notwithstanding the significance of bats interconnecting ecological, agricultural, and human health, bats are largely underdeveloped animal models. Despite this fact, some unique immunological attributes have been demonstrated in bats that warrant further study. Bats have unusual aspects of their immune systems and responses compared to humans. Some bat species have a constitutively expressed innate type I interferon (IFN) system with higher basal expression of the *Ifna* genes compared to humans and other mammals [59]. This constitutive expression of *Ifna* induces the expression of IFN-stimulated genes without inducing chronic inflammatory pathology [60]. Some species of bats differ in their VDJ recombination for immunoglobulins in B cells. Humans have 40 functional V segments, 24 D segments, and 6 J segments in the heavy-chain locus giving rise to the potential 5,760 heavy chain combinations [61]. Some bats have a higher diversity in their immunoglobulin heavy chain repertoire. For example, the little brown bat (*Myotis lucifugus*) has at least 236 V segments, 24 D segments, and 13 J segments giving rise to a potential 73,632 heavy chain combinations from VDJ recombination alone [62]. Furthermore, little brown bats may use affinity maturation of antibodies to a lesser degree than humans [62]. Interestingly, Jamaican fruit bats produce low antibody titers with poor neutralizing capabilities in responses to H18N11 influenza A virus, Tacaribe virus, Zika virus, and Middle East respiratory syndrome coronavirus [63-66]. However, when Jamaican fruit bats are vaccinated with rabies virus nucleocapsid protein emulsified in complete Freund's adjuvant they make high antibody titers (T. Schountz, pers. comm). Jamaican fruit bats seroconvert 17 days post inoculation with H18N11, and ferrets seroconvert 7 days post inoculation [66]. Similar to ferrets, waterfowl, swine, and mice all seroconvert about 7 days post inoculation with other avian influenza A viruses [67-69]. As such, it

does not appear that Jamaican fruit bats are inherently deficient in their ability to produce antibodies, but the innate immune response is highly efficient, and the adaptive immune response is needed to a lesser extent.

Bat Cellular Immune Systems and Immune Responses are Largely Uncharacterized.

The attributes of bat immune systems discussed above bring about questions of how the bat cellular immune system responds to viral infections. The primary limitation of developing an animal model such as a bat animal model is the paucity of bat specific reagents. Antibodies are foundational reagents to immunology. As mentioned before, antibodies are integral reagents used for many immunological and biochemical assays: ELISAs, ELISPOTs, western blots, cytometric bead assays, magnetic bead pull-down, surface plasmon resonance, microscopy, *in vivo* cellular depletion, and flow cytometry. Without bat-specific reagents, specifically antibodies for immunophenotyping, characterizing bat immune systems and immune responses is limited.

There are some studies that have been performed on bats using flow cytometry to characters bat immune systems. There have been some reported cross-reactive antibodies: CD3, CD4, CD8, CD14, CD44, CD11b, Ig, CD21, CD27, CD206, NK1.1 and MHC-II for surface markers and Tbet. Gata3, Eomes, TNF, IL-10 for intracellular markers that react with black flying fox (*Pteropus Alecto*), and/or cave nectar bat *(Eonycteris spelaea*) antigens [70-72]. These studies permitted limited characterization of B, T, and NK cell populations and functionality in old world these species. In human ACE2 transduced Jamaican fruit bats (*Artibeus jamaicensis*) SARS-CoV-2, antigen-specific T helper cells have been shown to respond to SARS-CoV-2 nucleocapsid peptide antigens. This study used flow cytometry in conjunction with a Jamaican fruit bat specific anti-CD4 antibody and cross-reactive CD40 and CD154 antibodies[73].

Understanding bat immune systems and responses are vital to understanding the selection pressures bat-borne viruses have undergone and continue to undergo; this can provide insight as to how bat-borne viruses result in high morbidity and mortality when spilled-over into human and other mammal populations. Studies investigating bat-borne viruses to develop immunomodulatory treatments that mimic bat immune responses in other animal models, thereby leading to immunomodulatory treatments for humans infected with bat-borne viruses for improved patient outcome. Furthermore, understanding bat immune systems and immune responses can bolster conservation efforts. However, bat-specific reagents will be required to generate good hypotheses to perform these types of investigations.

CHAPTER 2
REGULATORY T CELL-LIKE RESPONSE TO SARS-COV-2 IN JAMAICAN FRUIT BATS TRANSDUCED WITH HUMAN ACE2

Summary

Insectivorous Old World horseshoe bats (*Rhinolophus* spp.) are the likely source of the ancestral SARS-CoV-2 prior to its eventual spillover into humans and causing the COVID-19 pandemic. Natural coronavirus infections of bats appear to be principally confined to the intestines, suggesting fecal-oral transmission; however, little is known about the biology of SARS-related coronaviruses in bats. Previous experimental challenges of Egyptian fruit bats (*Rousettus aegyptiacus*) resulted in limited infection restricted to the respiratory tract, whereas insectivorous North American big brown bats (*Eptesicus fuscus*) showed no evidence of infection. In the present study, we challenged Jamaican fruit bats (*Artibeus jamaicensis*) with SARS-CoV-2 to determine their susceptibility. Infection was confined to the intestine for only a few days with prominent viral nucleocapsid antigen in epithelial cells, and mononuclear cells of the lamina propria and Peyer's patches, but with no evidence of infection of other tissues; none of the bats showed visible signs of disease or seroconverted. Expression levels of ACE2 were low in the lungs, which may account for the lack of pulmonary infection. An additional group of bats was intranasally inoculated with a replication-defective adenovirus encoding human ACE2 and 5 days later challenged with SARS-CoV-2. Viral antigen was prominent in lungs for up to 14 days, with loss of pulmonary cellularity during this time; however, the bats did not exhibit weight loss or visible signs of disease. From day 7, bats had low to moderate IgG antibody titers to spike protein by ELISA, and one bat on day 10 had low-titer neutralizing antibodies by a VSV pseudotyped virus assay. $CD4^+$ helper T cells became activated upon ex vivo recall stimulation with SARS-CoV-2 nucleocapsid peptides and exhibited elevated mRNA expression of the regulatory T cell cytokines interleukin-10 and transforming growth factor-β, which may have limited inflammatory pathology. Collectively,

these data show that Jamaican fruit bats are of low susceptibility to SARS-CoV-2, but that expression of human ACE2 in their lungs leads to robust infection and an adaptive immune response with low-titer antibodies and a regulatory T cell-like response that may explain the lack of prominent inflammation in the lungs. This model will allow for insight into how SARS-CoV-2 infects bats and how bat innate and adaptive immune responses engage the virus without overt clinical disease.

Introduction

The ancestral severe acute respiratory syndrome coronavirus 2 (SARS-CoV-2), in all likelihood, originated in insectivorous bats prior to spillover to humans through two or more intermediate bridge hosts in live animal markets in Wuhan, China [74-77]. SARS-CoV-2 is a sarbecovirus (genus *Betacoronavirus*, subgenus *Sarbecovirus*) that uses angiotensin converting enzyme 2 (ACE2) as a cellular entry receptor in humans. Although hundreds of distinct sarbecovirus sequences have been detected in bats in Asia and Europe, principally in horseshoe bats (*Rhinolophus* spp.) [76,78-84], not all can use human ACE2 as an entry receptor [85].

Field studies of natural coronavirus infections of bats show that infections are localized to the gastrointestinal tract with likely shedding through feces, suggesting maintenance of virus in natural bat populations is via fecal-oral transmission [74,78-80]. However, few studies have experimentally examined coronavirus infections in bats, and those have relied exclusively on surrogate models. Experimental challenge determined that Jamaican fruit bats (*Artibeus jamaicensis*), one of the most abundant and largest bats in the Americas, are susceptible to the merbecovirus, Middle East respiratory syndrome coronavirus (MERS-CoV) [86]. In this study, viral antigen and RNA were detected in several organs up to 14 days post challenge, and viral RNA was

detected in oral and rectal swabs up to 9 days post challenge. Inoculation of Jamaican fruit bat primary kidney cells (Ajk cells) led to robust virus replication and cytopathic effect, with destruction of the Ajk cell monolayer. Despite clear evidence of infection, no conspicuous disease occurred, only one bat seroconverted, and they remained healthy. MERS-CoV likely emerged from insectivorous bats in Africa [87-89] that used dromedary camels (*Camelus dromedarius*), which then became a secondary reservoir host species [90], as a bridge to humans.

Considering the wide species tropism of SARS-CoV-2, which includes mustelids, cervids, felines, canines and cricetid rodents, including Syrian hamsters and North American deer mice [91-97], it might be expected that SARS-CoV-2 can readily infect a variety of bat species. A significant limitation for conducting meaningful studies on the biology of bat-borne viruses is the lack of relevant captive breeding colonies of specific pathogen-free (SPF) bats. A few established colonies of SPF fruit bats and nectarivorous bats are available for infectious disease studies [98-100]; however, insectivorous bats are substantially more difficult to colonize because of the need for live insect species that are often not natural food sources of the bats. Thus, insectivorous bats are typically captured and used for one-off experimental infection studies. Despite these limitations, previous work using Egyptian fruit bats (*Rousettus aegyptiacus*) and insectivorous big brown (*Eptesicus fuscus*) and Brazilian/Mexican free-tailed (*Tadarida brasiliensis*) bats have examined susceptibility to SARS-CoV-2 infections [101-104]. Although Egyptian fruit bats were moderately susceptible without disease, with detection of virus in the respiratory tract for several days and transmission to other Egyptian fruit bats, big brown bats were not susceptible. Two studies demonstrated low susceptibility in Brazilian free-tailed bats [103 104]. Thus, it is clear host specificity of SARS-CoV-2 infection cannot be determined simply by taxonomic assignment of a given

mammalian species. In this study, we sought to expand the knowledge surrounding bat susceptibility to SARS2 by performing experimental infections in Jamaican fruit bats.

Results

We sought to determine the susceptibility of Jamaican fruit bats to SARS-CoV-2. Initial challenge of bats with SARS-CoV-2 WA1 isolate was confined to the small intestine for only 2 days before antigen could no longer be detected, bats held 21 days failed to seroconvert, and contact transmission did not occur. Viral antigen or RNA was not detected in other tissues, suggesting an abortive infection that is poorly adapted to Jamaican fruit bats, that infection was controlled by the innate immune response, or both. We were interested in determining whether ACE2 was a restriction factor for SARS-CoV-2 infection of Jamaican fruit bats; therefore, we intranasally inoculated bats with an adenovirus that expresses human ACE2 [105-107] and subsequent challenge of the bats with SARS-CoV-2 led to robust infection in the lungs for up to 14 days and low-titer seroconversion. Histopathology revealed moderate inflammation in the lungs, including neutrophil infiltration, lymphoblasts and macrophage syncytia, and loss of pulmonary cellularity. Bats appeared healthy and experienced no weight loss, suggesting only mild disease. Splenic $CD4^+$ helper T cells were activated upon ex vivo stimulation with nucleocapsid peptide library and three of four bats expressed the regulatory T cell cytokines IL-10 and TGFβ but not inflammatory cytokines. Collectively, this study shows that Jamaican fruit bats are poorly susceptible to SARS-CoV-2; however, they are permissive when a suitable ACE2 receptor is provided but which only leads to minimal pathology, and that a virus-specific adaptive immune response occurs that may be mediated by regulatory T cells. Importantly, this study provides the first example of a robust

infection of bats with SARS-CoV-2, virus-specific bat T cell responses, and demonstrates the use of adenovirus vectors for *in vivo* expression of genes of interest in Jamaican fruit bat lungs.

SARS-CoV-2 Causes Restricted Infection of Jamaican Fruit Bats That is Confined to the Small Intestine.

Intranasal inoculation of Jamaican fruit bats with SARS-CoV-2 WA1 did not result in visible signs of disease, nor did they lose weight. However, viral antigen was readily detected in intestinal sections on day 2 (**Figure 2.1A**) but not on day 4 or thereafter. Antigen was particularly prominent in the periphery of Peyer's patches that are typically populated with macrophages, mononuclear cells of the lamina propria, and intestinal crypts. No antigen was detected in intestinal sections of unchallenged bats (**Figure 2.1B**). Oral swabs, but not rectal swabs, from bats were positive for viral RNA (vRNA) on days 2 and 4 post challenge (**Figure 2.1C**), but negative thereafter. Despite clear evidence of antigen staining, both ELISA to recombinant nucleocapsid antigen and virus neutralization assay were negative for antibodies. To determine why virus was not detected in the lungs, we examined ACE2 gene expression levels and found that it was very low (**Figure 2.1D**), suggesting this may be a restriction factor for infection in the lungs.

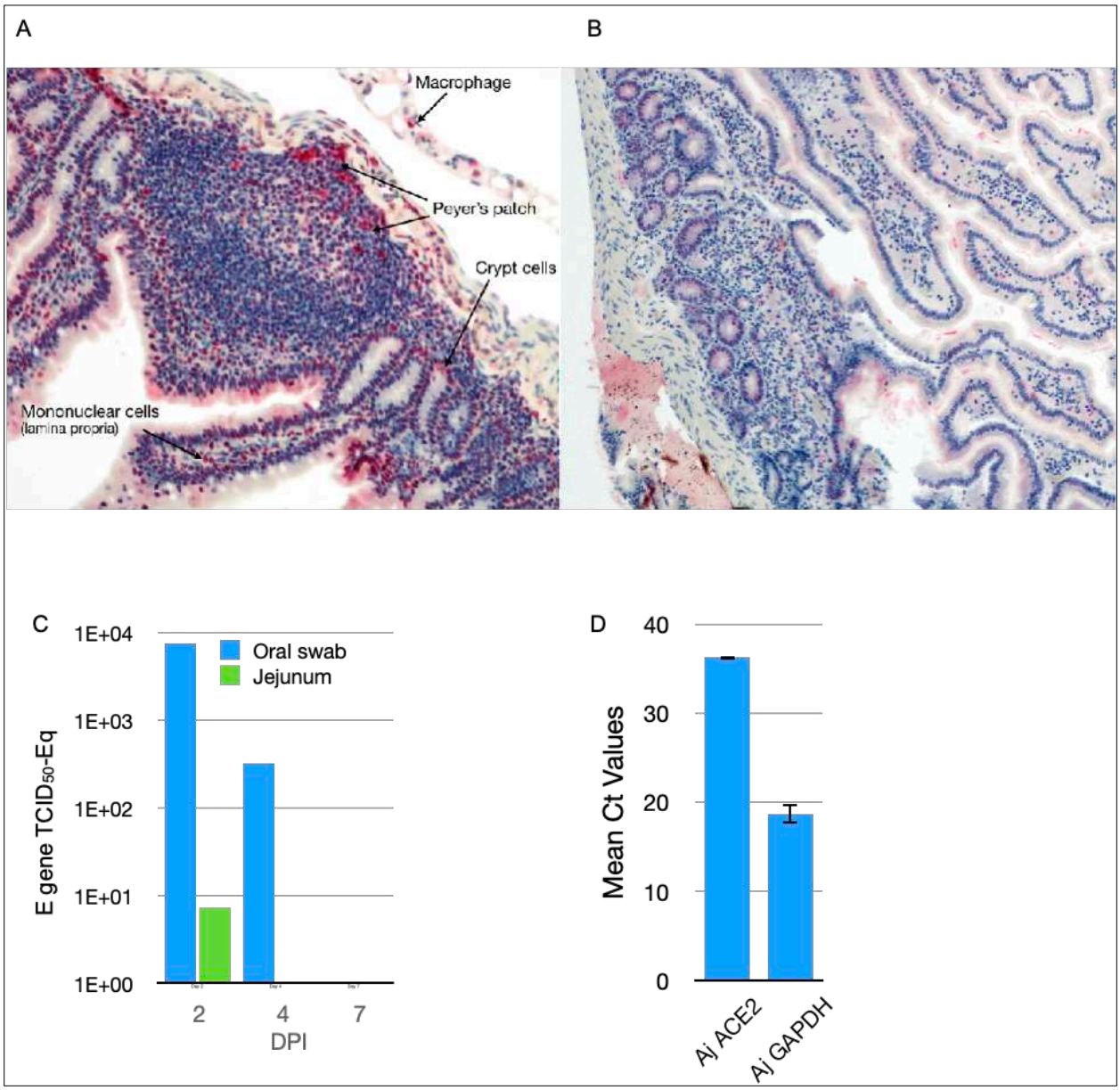

Figure 2.1) Immunohistochemistry of intestines of Jamaican fruit bats challenged with SARS-CoV-2. **A**. Two days after challenge, but not thereafter, antigen was detected in mononuclear cells of the lamina propria and periphery of Peyer's patches where macrophages are typically found. Crypt cells also were infected. **B**. Unchallenged control bat intestine showed no antigen staining. **C**. SARS-CoV-2 E gene vRNA was detected only on days 2 and 4 in oral swabs, and only on day 1 in jejunum. **D**. Endogenous ACE2 expression measured by RT-qPCR in lungs of Jamaican fruit bat appears to be low and may account for the lack of detectable virus in lungs.

Defective Adenovirus Encoding Human ACE2 Transduces Jamaican Fruit Bat Cells.

A replication-defective adenovirus serotype 5 that encodes human ACE2 (Ad5/hACE2) has been used to study SARS-CoV-1 and SARS-CoV-2 infections of nonsusceptible laboratory mice [105,106]. Examination of the mouse receptor for Ad5, the coxsackievirus and adenovirus receptor (CAR), revealed that it has 85% identity and 92% similarity to Jamaican fruit bat CAR, suggesting that Jamaican fruit bats may be susceptible to Ad5. To test this hypothesis, we inoculated primary Jamaican fruit bat kidney (Ajk) cells with Ad5/hACE that also encodes eGFP and examined the cells daily. By 24 hours, fluorescence was observed, and it was maximal on days 2 through 6 when the study was terminated (**Figure 2.2A**). Ajk cells, transduced for 48 hours, and Vero E6 cells (positive control) were inoculated with 0.1 MOI of SARS-CoV-2 and supernatants were collected at 1 hour and daily for 4 days, followed by titration on Vero E6 cells. No increase in SARS-CoV-2 was detected from hACE2-transduced Ajk cells (**Figure 2.2B**), suggesting the cells were not permissive for SARS-CoV-2 replication.

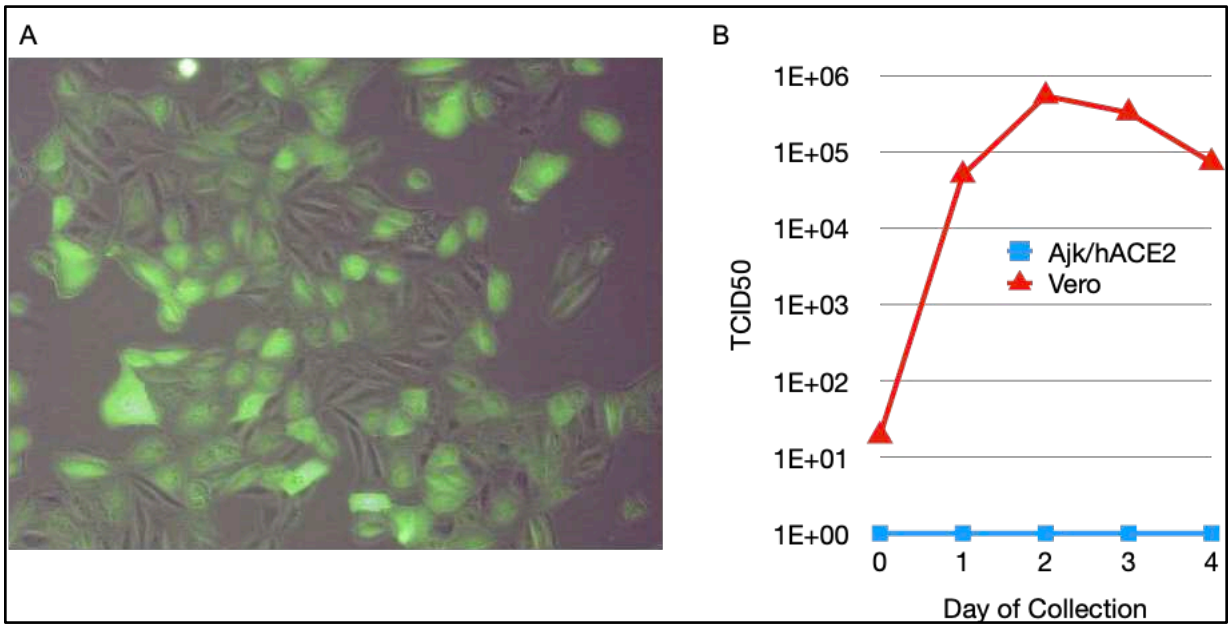

Figure 2.2) Adenovirus serotype 5 encoding human ACE2 (Ad5/hACE2) transduces Jamaican fruit bat cells in vitro. **A.** Transduction of Jamaican fruit bat primary kidney epithelial (Ajk) cells with Ad5/hACE2/eGFP. Jamaican fruit bat primary kidney cells were inoculated with 10 MOI of Ad5/hACE2/eGFP for 1 hour, washed and incubated in fresh medium for 4 days. Most, but not all, cells exhibited fluorescence, suggesting a heterogeneous population with some susceptible and some nonsusceptible cells. **B**. Ad5/hACE2 transduced Jamaican fruit bat kidney cells are not productively infected with SARS-CoV-2. Ajk/hACE2 cells (blue) and Vero cells (red) were inoculated with 0.1 MOI of SARS-CoV-2 WA1 for 1 hour, washed and cultured for 4 days. Supernatants were collected each day and titrated on Vero E6 cells to determine virus titers. Despite evidence of human ACE2 expression on Ajk cells, inoculation failed to produce infectious virus, suggesting the cells were not permissive.

Bat Lung Cells Transduced with Human ACE2 are Susceptible and Permissive to SARS-CoV-2 Infection.

To determine if lung cells of Jamaican fruit bats transduced with human ACE2 become susceptible and permissive to SARS-CoV-2, 21 bats were intranasally inoculated with $2.5x10^8$ pfu of Ad5/hACE2 and 5 days later they were challenged with SARS-CoV-2 (**Figure 2.3A**). Groups of bats (four on days 2, 4, 7; two on days 10, 14, 21) were serially euthanized. On day 2, lungs of all four euthanized bats had detectable viral RNA (vRNA); however, on days 4 and 7 only one bat from each group had vRNA, and none of the lungs from bats thereafter had vRNA (**Figure 2.3B**). Serum antibody to recombinant spike was detected by ELISA in one bat on day 4, and all bats euthanized thereafter, with peak response on day 10. Only one bat, euthanized on day 10, had weak, but detectable, neutralizing antibody using a D614G VSV pseudotype assay (**Figure 2.4**); this bat also had the highest O.D. value on the ELISA (2.957).

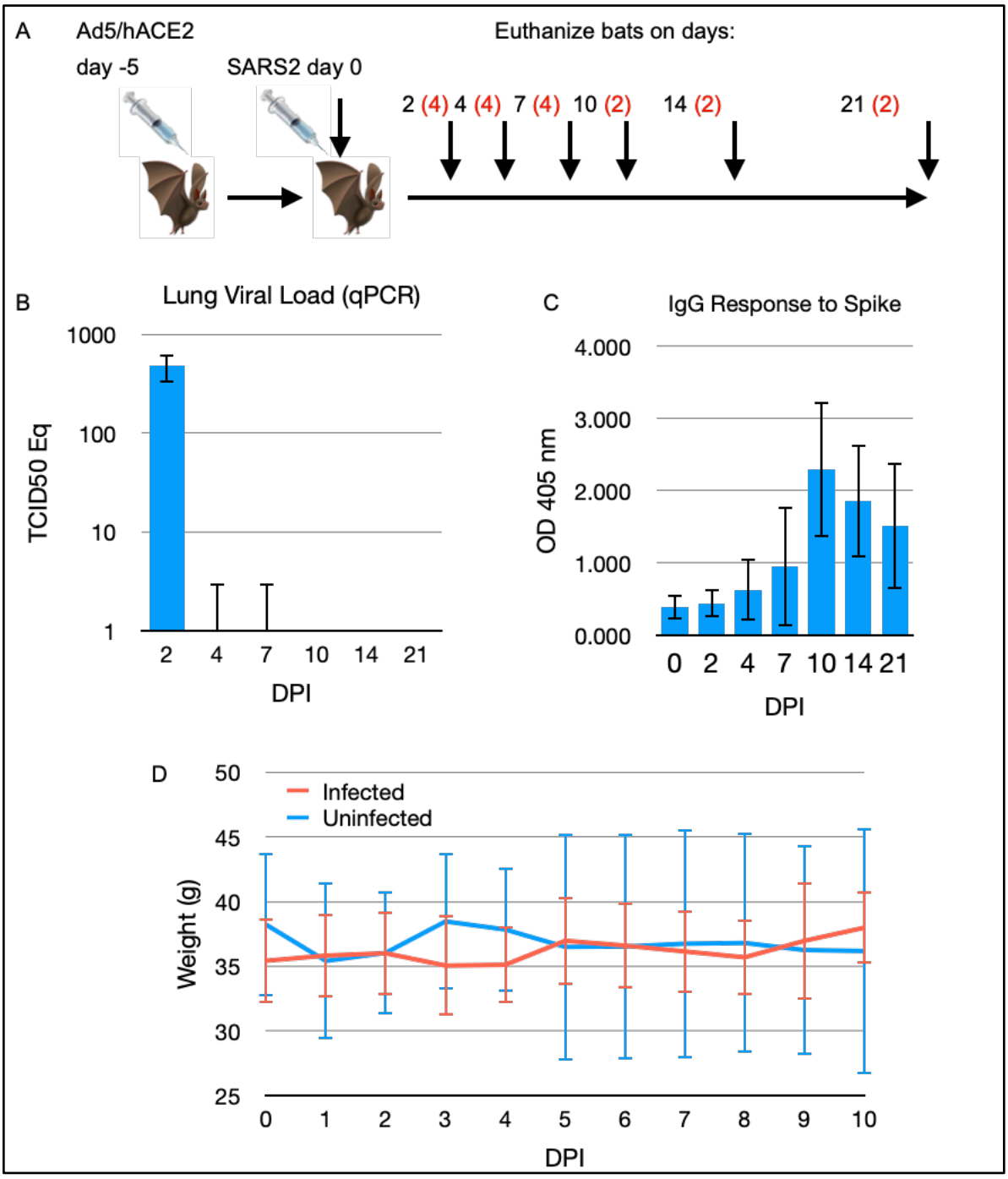

Figure 2.3) SARS-CoV-2 infection of Jamaican fruit bat lungs transduced with hACE2. **A.** Experimental design. Jamaican fruit bats were intranasally inoculated with Ad5/hACE2, then challenged with SARS-CoV-2 WA1. Groups of bats (n=red numerals) were euthanized at intervals and evaluated for infection. **B**. Viral RNA was detected in all bats on day 2 but only one bat on each of days 4 and 7. **C**. Serum antibody titers to recombinant spike antigen became elevated by day 4 in one bat, and all bats thereafter. **D**. Bats did not lose weight during the first ten days of the study, nor did they show other signs of disease.

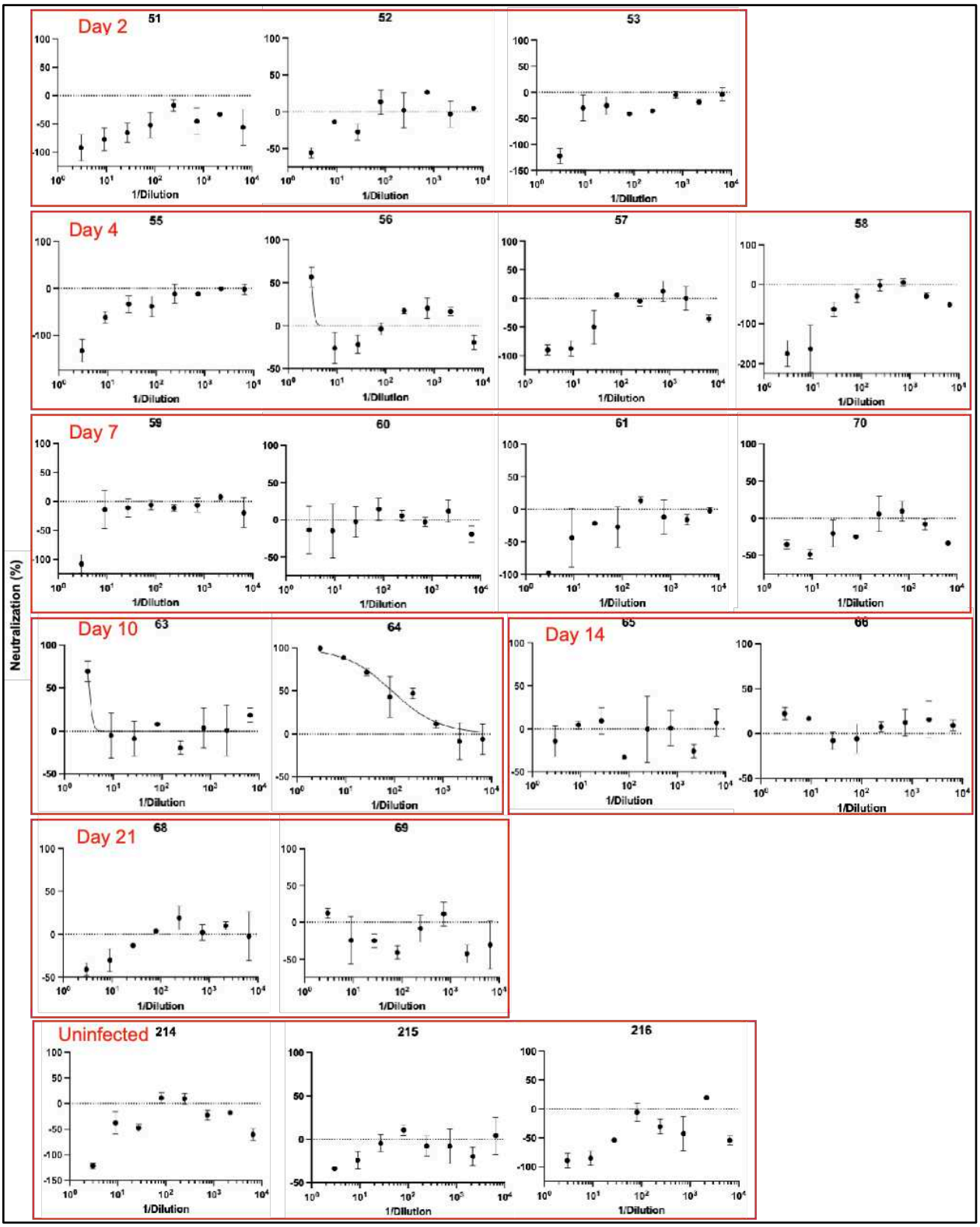

Figure 2.4) Neutralizing antibody titers from hACE-tranduced Jamaican fruit bats. Only bat, # 64, produced antibodies that neutralized VSV pseudotype virus expressing SARS-CoV-2 spike.

SARS-CoV-2 Lung Pathology and Localization in hACE2-Transduced Bats.

Infection of the lungs was principally localized around the main stem bronchi, with destruction of cilia corresponding with neutrophil infiltration, and lymphoid follicle formation (**Figure 2.5A**). Perinuclear SARS-CoV-2 nucleocapsid antigen was readily detected in the lungs of challenged bats for up to 14 days, whereas in unchallenged bats no antigen was detected (**Figure 3C**). On day 21, all bats were negative for nucleocapsid antigen, suggesting viral clearance. Epithelial, goblet and parenchymal cells had perinuclear staining for nucleocapsid antigen, suggesting these cells were susceptible to the adenovirus delivery of human ACE2 (**Figure 2.5C**). Analysis of pulmonary cellularity found slight reduction at 2 DPI that became maximal at 4 DPI, followed by gradual recovery (**Figure 2.5D**). Despite the clear evidence of infection, none of the bats exhibited conspicuous disease.

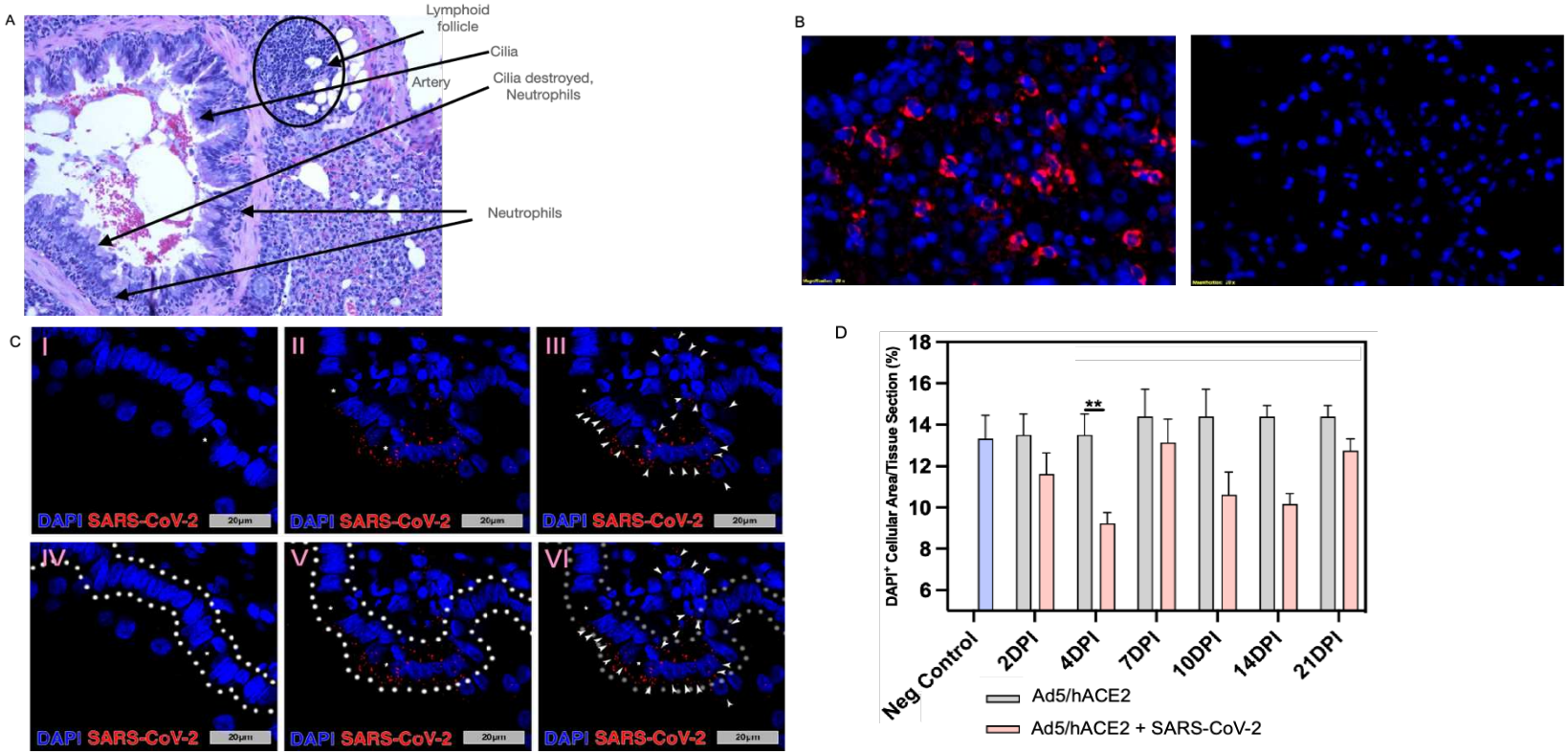

Figure 2.5) SARS-CoV-2 infection of Jamaican fruit bat lungs transduced with hACE2. **A.** Histopathology of Jamaican fruit bat lungs transduced with Ad5/hACE2 and infected with SARS-CoV-2, 4 DPI. Cilia destruction, neutrophil infiltration, and lymphoid expansion occurred. **B**. Fluorescent imaging of Ad5/hACE2 bat lung sections on day 7 infected with SARS-CoV-2 (left) or uninfected (right) showed perinuclear nucleocapsid antigen staining (red) (200x). **C.** Main stem bronchi (100x) in bats that received Ad5/hACE2 but no SARS-CoV-2 (I, IV) and bats that received Ad5/hACE2 followed by viral infection with SARS-CoV-2 at post-infection day 14 (14 DPI; II, III, V, VI). Asterisks identify goblet cells within the respiratory epithelium. Arrowheads identify cells that contain positive perinuclear SARS-CoV-2 nucleocapsid staining, that are composed of epithelium, goblet cells and cells of the lung parenchyma. White outlines highlight the respiratory epithelial layer (including goblet cells) of the bronchi for reference (IV, V, VI). **D**. SARS-CoV-2 causes loss of cellularity in hACE2-transduced bat lungs. A trend downward was observed on day 2 and was maximal on day 4, with reduced cellularity thereafter that was not significantly different.

$CD4^+$ T Cells Responded to SARS-CoV-2 in Infected Bats.

To determine if helper T cells may play a role in bat immune responses during infection, we adopted an activation-induced marker (AIM) test to identify $CD4^+$ T cell responses (32-34). This assay relies on increased expression of CD154 on helper T cells that occurs within hours of TCR engagement of MHC-II/peptide and its signal-to-noise ratio is augmented by blocking CD40 on the antigen presenting cells.

We also screened several anti-CD4 antibodies for cross reactivity; however, none were useful. Therefore, we generated a monoclonal antibody (designated 1-D5) using a Jamaican fruit bat CD4 peptide (ENRKVSVVKTRQDRR) predicted to be extracellular and solvent-accessible and conjugated to KLH for mouse immunizations (**Figure 2.6**). Based upon structural homology (**Figure 2.7**), we determined that commercially available anti-mouse CD40 (Tonbo, clone FGK45) and anti-human CD154 (Tonbo, clone 5C8) monoclonal antibodies were cross reactive with Jamaican fruit bat orthologs (**Figure 2.8**).

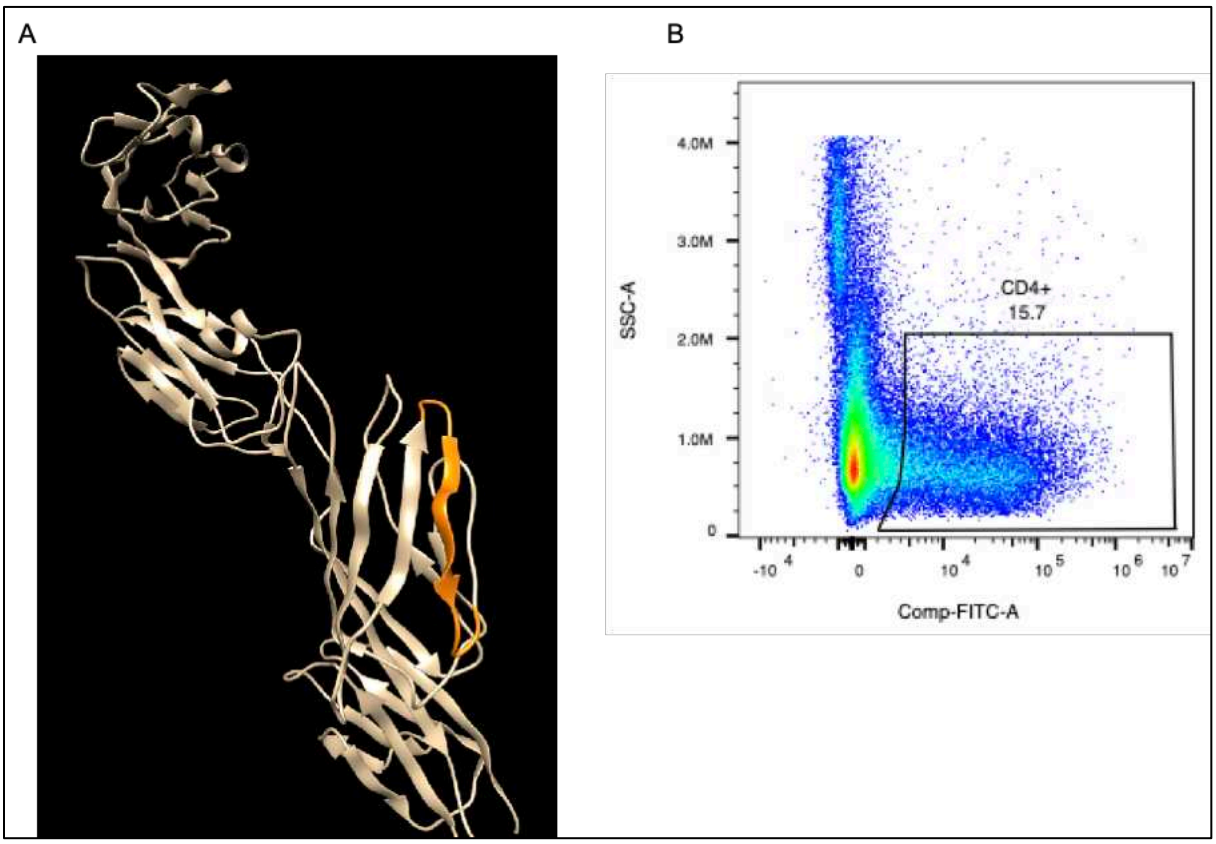

Figure 2.6) (A) Predicted extracellular structure of Jamaican fruit bat CD4 with immunizing peptide in orange, and (B) flow cytometric staining of naive bat splenocytes with monoclonal antibody 1-D5.

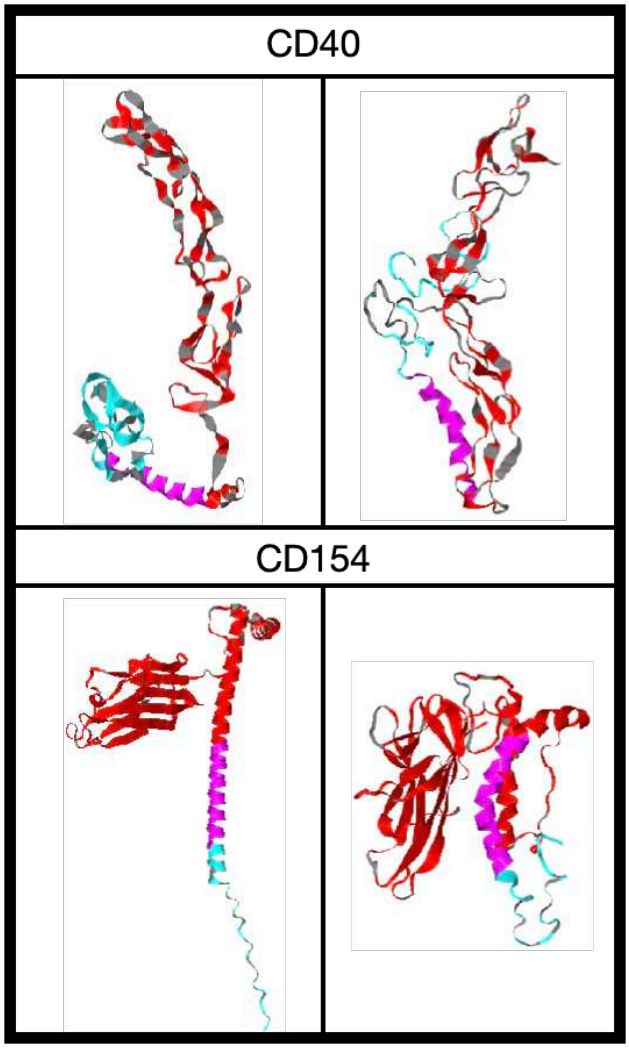

Figure 2.7) Protein homology of Jamaican fruit bat, mouse, and human CD40 and CD154. CD40 protein structures mouse (top left) and Jamaican fruit bat (top right). CD154 protein structures human (bottom left) and Jamaican fruit bat (bottom right). Protein structures are represented with signal peptides removed and transmembrane domains (magenta) highlighted for orientation. Jamaican fruit bat CD40 and mouse CD40 protein alignment identified 90 identical extracellular sites (red) or 53.39% identical extracellular domains with a BLOSUM62 value of 71.3%. Jamaican fruit bat CD40 and mouse CD40 protein alignment identified 39 identical cytoplasmic sites (cyan) or 72% identical cytoplasmic domains with a BLOSUM62 value of 84%. Jamaican fruit bat CD154 and human CD154 protein alignment identified 190 identical extracellular sites (red) or 88.4% identical extracellular domains with a BLOSUM62 value of 92.1%. Jamaican fruit bat CD154 and mouse CD154 protein alignment identified 18 identical cytoplasmic sites (cyan) or 61.9% identical cytoplasmic domains with a BLOSUM62 value of 73%.

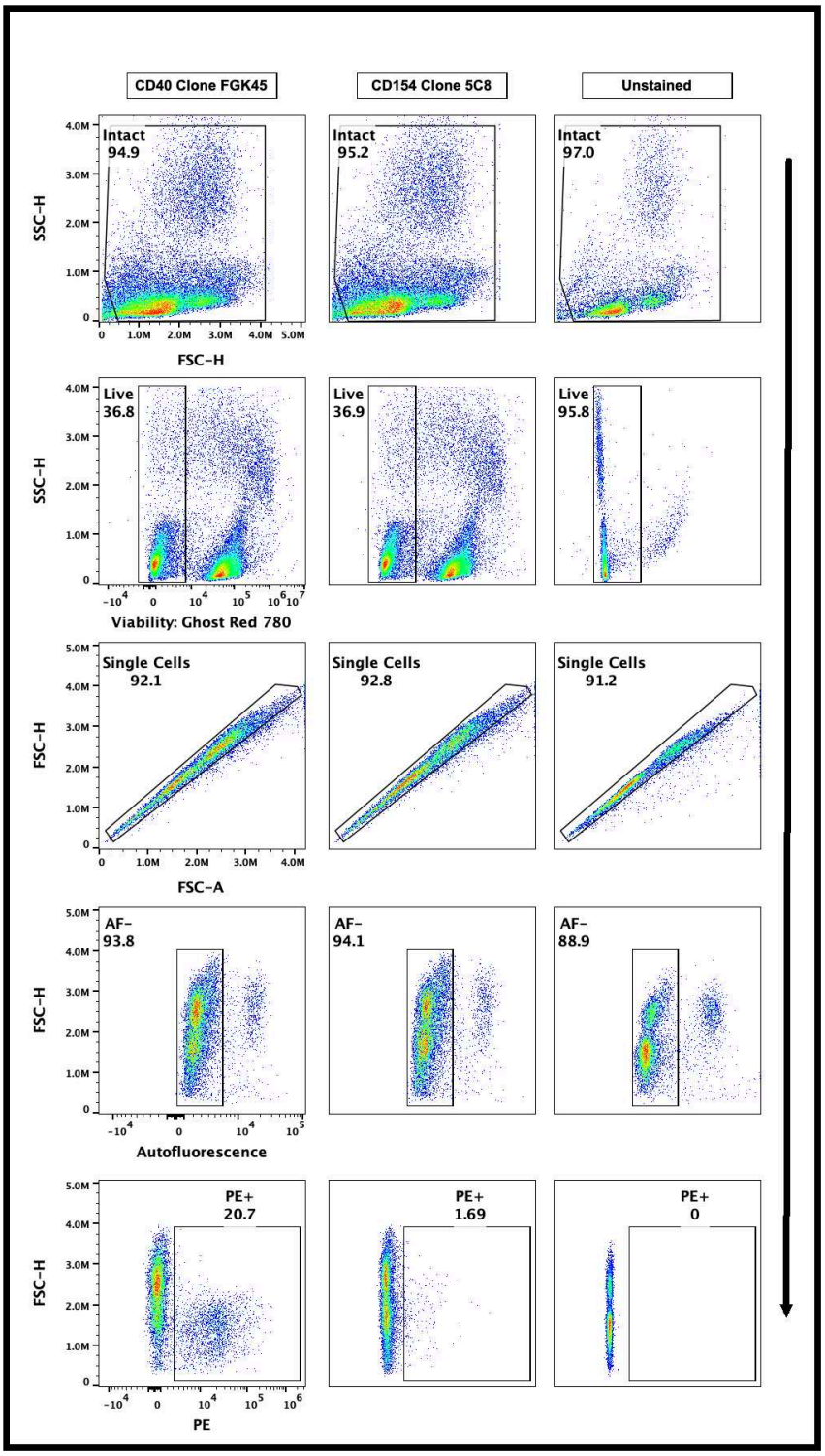

Figure 2.8) Anti-mouse CD40 (FGK45) and anti-human CD154 (5C8) PE conjugated antibody staining of Jamaican fruit bat splenocytes. Gating strategy: Intact > Live > Single Cells > AF- > PE^{+}. Anti-mouse CD40 cross reactive antibody demonstrated 20.7% positive splenocytes. Anti-human CD154 cross reactive antibody demonstrated 1.69% positive splenocytes.

Four bats transduced with Ad5/hACE2 and challenged with SARS-CoV-2 were euthanized 12 days later (**Figure 2.9A**). Splenocytes were cultured with or without SARS-CoV-2 nucleocapsid peptide library and anti-CD40 blocking antibody in duplicate for 6 hours. The cells were then co-stained for CD4 and CD154, markers of activated helper T cells. $CD4^+CD154^+$ cells were gated on (**Figure 2.10**), and evaluated for CD154 expression by flow cytometry. Less than 2% of the $CD4^+$ cells also expressed CD154, which was significantly elevated on these cells that were stimulated by peptide ($p<0.0001$) compared to paired samples without peptide stimulation (**Figure 2.9B**). Replicate cells from the bats were cultured 24 hours with or without peptide library and RNA extracted for RT-qPCR for T cell gene expression profiling. Three of the four bats had increased expression of several genes; however, one bat did not exhibit changes in gene expression (**Figure 2.C**), suggesting it was not responsive to antigen. Excluding this bat, IL-10, TGFβ, Cxcr4 and CD4 were elevated >2 fold, whereas IL-2, IL-4 and IL-21 expression were substantially downregulated (**Figure 2.9D**).

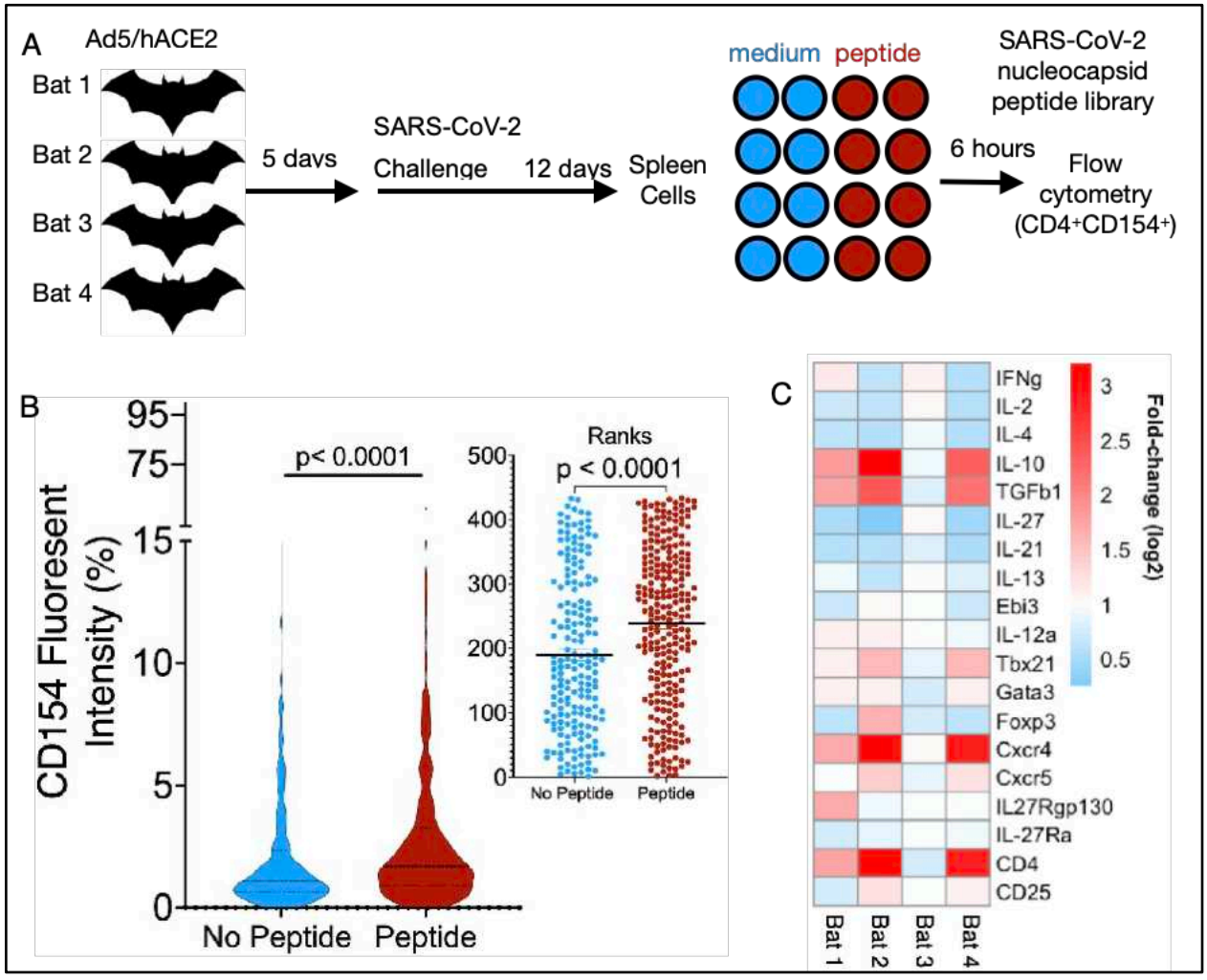

Figure 2.9) Activation of CD4+ Helper T cells in SARS-CoV-2-infected Jamaican fruit bats. (A) Splenocytes from four Ad5/hACE2-transduced bats 12 days post infection with SARS-CoV were cultured with or without SARS-CoV-2 nucleocapsid peptide library for 6 hours in the presence of anti-CD40 blocking antibody. Cells were stained with anti-CD154 and anti-CD4 and analyzed by flow cytometry. (B) In the presence of peptide, CD154 expression was significantly increased on splenocytes (red) compared to no peptide controls (blue) (Wilcoxon rank sum test). (C) Heat map of splenocyte gene expression in response to peptide stimulation determined 3 of the 4 bats expressed a profile consistent with a regulatory T cell response. (D) Gene expression changes in bats 1, 2 and 4.

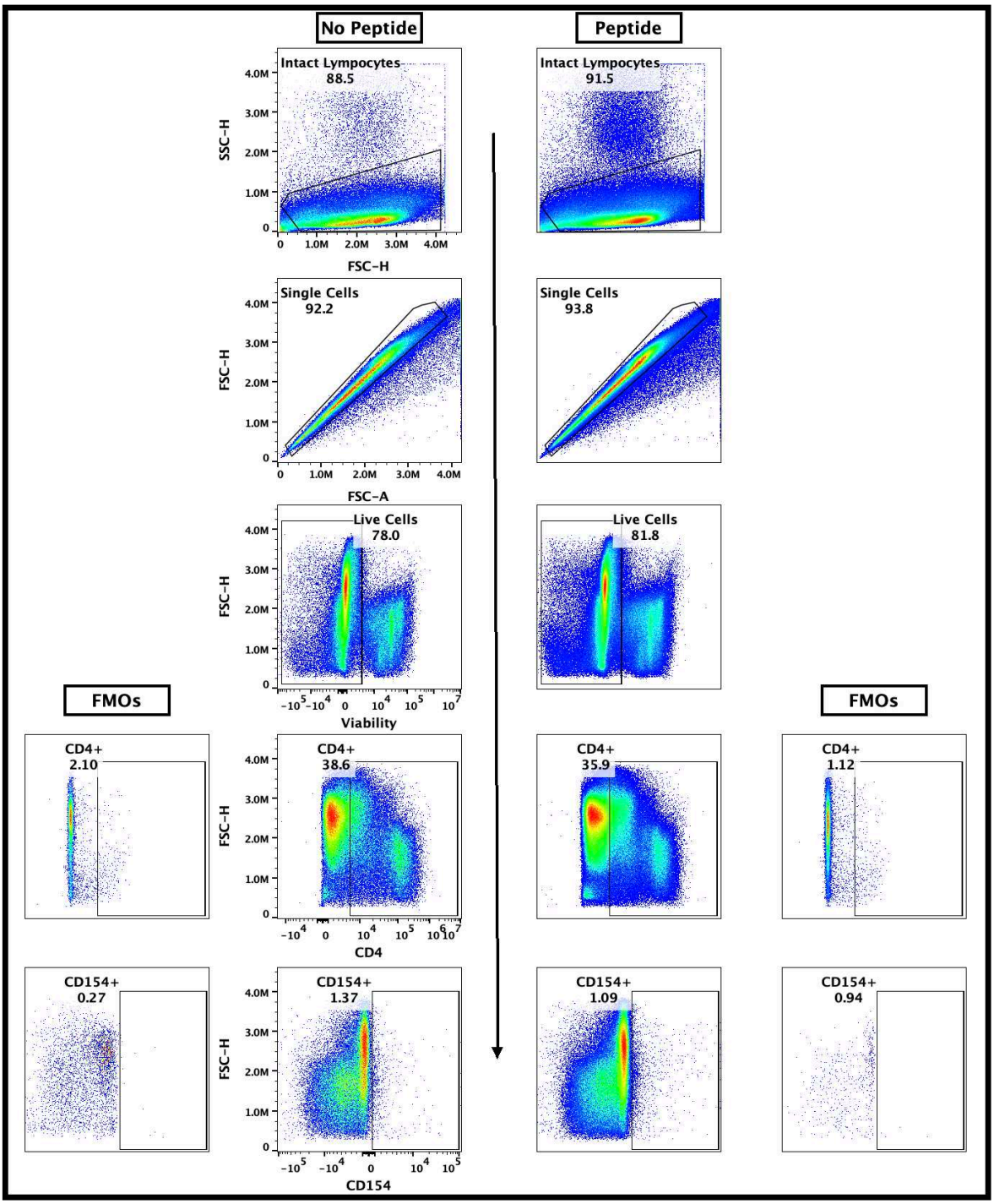

Figure 2.10) Gating strategy to obtain $CD4^+$ $CD154^+$ splenocytes. Concatenated no peptide samples and FMOs (left) and concatenated peptide samples (right) were gated as follows: Intact Lymphocytes > Single Cells > Live Cells > $CD4^+$ > $CD154^+$. CVS files of $CD4^+CD154^+$ cells were then exported from FlowJo to obtain fluorescent intensities of CD154 on each cell for statistical analysis in Graph Pad Prism 9.

Discussion

A significant limitation for studying how coronaviruses infect bats is the lack of relevant colonized bat species and the availability of coronaviruses that are naturally hosted by those species. Sarbecoviruses are naturally hosted by insectivorous horseshoe bats (*Rhinolophus* spp.) and there are more than 80 species in the genus. Until such colonies are established, research on bats and coronaviruses will require surrogate bat models, similar to how the laboratory mouse is routinely used as a surrogate model. We established a breeding colony of Jamaican fruit bats in 2006 and have used bats from this colony for a number of infection studies with several viruses, including MERS-CoV [86,108-110].

The initial challenge study determined that SARS-CoV-2 replicates poorly in Jamaican fruit bats for only a few days without visible signs of disease, is confined to the intestine with detection of virus in the Peyer's patches and mononuclear cells of the intestinal lamina propria, no apparent shedding in feces, and without a detectable antibody response, even by highly sensitive ELISA to nucleocapsid antigen. The lack of detectable virus in the lungs is consistent with what is known about coronavirus circulation in wild bat populations, where virus is typically found in the intestines and shed through feces. One possible explanation for this is that very low levels of endogenous ACE2 mRNA was detected in Jamaican fruit bat lungs. The only other experimental SARS-CoV-2 challenges of bats have yielded varying results. An experimental challenge of Egyptian fruit bats (*Rousettus aegyptiacus*) led to a limited infection without visible signs of disease, but with detectable virus in several tissues, including lungs and lymph nodes, and transmission to one contact bat [101]. Challenge of big brown bats (*Eptesicus fuscus*) did not lead to infection [102]. Two studies of Mexican/Brazilian free-tail bats (*Tadarida brasiliensis*) indicated

minimal susceptibility, with viral RNA present in oral secretions, but no transmission nor clinical disease [103,104]. ACE2 residues that are thought to be important in SARS-CoV-2 spike binding [111,112] are more conserved in Egyptian fruit bats (16/20 residues with human), substantially less in big brown bats and Mexican/Brazilian free-tailed bats (11/20 residues), with Jamaican fruit bats intermediate (13/20 residues) (**Table 2.1**). The conservation of these ACE2 residues varies substantially among several horseshoe bat species.

Table 2.1) Alignment of 20 ACE2 residues important for SARS-CoV-2 spike binding (Luan et al. and Wan et al. [cyan]). Residues identical to human are noted in black, whereas differences in red font. Species that are susceptible to SARS-CoV-2 are in red font, not susceptible in blue font, unknown susceptibility in black font.

	ACE2	AA position																				
Common Name	**Species name**	24	27	28	30	31	34	35	37	38	41	42	45	82	83	330	353	354	355	357	393	**ID**
Human	*Homo sapiens*	Q	T	F	D	K	H	E	E	D	Y	Q	L	M	Y	N	K	G	D	R	R	20
Syrian hamster	*Mesocricetus auratus*	Q	T	F	D	K	Q	E	E	D	Y	Q	L	N	Y	N	K	G	D	R	R	18
Deer mouse	*Peromyscus maniculatus*	Q	I	F	D	K	Q	E	E	D	Y	Q	L	N	Y	N	K	G	D	R	R	17
Intermediate horseshoe bat	*Rhinolophus affinis*	R	I	F	D	N	H	E	E	D	Y	Q	L	N	Y	N	K	G	D	R	R	16
Egyptian rousette	*Rousettus aegyptiacus*	L	T	F	E	K	T	E	E	D	Y	Q	L	T	Y	K	K	G	D	R	R	16
Domestic cat	*Felis catus*	L	T	F	E	K	H	E	E	E	Y	Q	L	T	Y	N	K	G	D	R	R	16
Pearson's horseshoe bat	*Rhinolophus pearsonii*	R	T	F	D	K	H	E	E	D	H	E	L	D	Y	N	K	D	D	R	R	15
Least horseshoe bat	*Rhinolophus pusillus*	L	K	F	N	D	S	E	E	D	Y	E	L	N	Y	N	K	G	D	R	R	14
American mink	*Neogale vison*	L	T	F	E	K	Y	E	E	E	Y	Q	L	T	Y	N	K	H	D	R	R	14
Ferret	*Mustela putorius*	L	T	F	E	K	Y	E	E	E	Y	Q	L	T	Y	N	K	R	D	R	R	14
Big-eared horseshoe bat	*Rhinolophus macrotis*	E	K	F	D	K	S	K	E	D	Y	E	L	N	Y	K	K	G	D	R	R	13
Chinese rufous horseshoe bat	*Rhinolophus sinicus*	E	I	F	D	K	T	K	E	D	H	Q	L	N	Y	N	K	G	D	R	R	13
Lander's horseshoe bat	*Rhinolophus landeri*	L	T	F	D	D	S	A	E	N	Y	Q	L	N	F	N	K	G	D	R	R	13
Jamaican fruit bat	*Artibeus jamaicensis*	D	T	F	E	K	T	E	E	E	Y	E	L	A	Y	N	K	N	D	R	R	13
House mouse	*Mus musculus*	N	T	F	N	N	Q	E	E	D	Y	Q	L	S	F	N	H	G	D	R	R	13
Greater horseshoe bat	*Rhinolophus ferrumequinum*	L	K	F	D	D	S	E	E	N	H	Q	L	N	F	N	K	G	D	R	R	12
Halcyon horseshoe bat	*Rhinolophus alcyone*	L	I	F	D	N	S	E	E	N	H	Q	L	K	F	N	K	N	D	R	R	11
Big brown bat	*Eptesicus fuscus*	E	I	F	Q	R	T	E	E	E	H	Q	L	R	Y	N	K	G	D	R	R	11
Brazilian free-tailed bat	*Tadarida brasiliensis*	E	I	F	Q	R	T	E	E	E	H	Q	L	R	Y	N	K	G	D	R	R	11
		24	27	28	30	31	34	35	37	38	41	42	45	82	83	330	353	354	355	357	393	**ID**

It may be that SARS-CoV-2 spike protein, which mediates cellular attachment to ACE2, is substantially different compared to its ancestral virus because of the likely route of passage through one or more intermediate bridge hosts before spillover into humans, and subsequent adaptations as it transmitted among humans. As SARS-CoV-2 has continued to circulate among humans, new variants that have emerged are likely also more divergent from the ancestral virus, such that SARS-CoV-2 may now be more of a human virus than a bat virus. Ideally, the original bat virus that spilled over into the bridge host(s) is required to fully understand the biology of the virus. However, it is unlikely the virus will ever be found because by now it may have gone extinct or has undergone substantial recombination with other sarbecoviruses, a common occurrence of coronaviruses [74,113], such that it no longer exists in nature. The earliest SARS-CoV-2 isolate available to us was WA1, which was isolated from a patient in Washington state, USA. It may be that earlier isolates, such as the initial Wuhan isolates, may have behaved differently in Jamaican fruit bats. Regardless, the results presented here suggest that SARS-CoV-2 has limited ability to bind Jamaican fruit bat ACE2 (AjACE2) (poor susceptibility), which is consistent with a report demonstrating spike binding to AjACE2 [114], it is unable to replicate in Jamaican fruit bat cells (poor permissibility), the innate response controls infection, or a combination of these features.

Several adenovirus serotypes use the coxsackievirus and adenovirus receptor (CAR, *Cxadr*) for cellular entry. We determined that Jamaican fruit bat CAR protein shares 86% identity and 92% similarity with the mouse ortholog, suggesting it could be used for adenovirus transduction of human ACE2. To address this possibility, we adopted an approach previously developed for the assessment of SARS-CoV-1 and SARS-CoV-2 infection of laboratory mice, in which a replication-defective serotype 5 adenovirus (Ad5), which uses CAR for cellular entry, was generated that expresses human ACE2 (Ad5/hACE2) [105-107,115]. Upon transduction of Jamaican

fruit bat primary kidney epithelial (Ajk) cells with Ad5/hACE2/eGFP, sustained fluorescence was observed for several days. However, inoculation of the cells with SARS-CoV-2 did not lead to detectable virus replication, suggesting the cells are not permissive. It is also possible that the cells lacked a suitable protease, such as TMPRSS2, that can facilitate SARS-CoV-2 penetration of the plasma membrane, or that adenovirus transduction activated antiviral pathways in the cells that restricted SARS-CoV-2 replication. Alternatively, SARS-CoV-2 can infect certain cells, such as Vero E6, via endosomal entry where cathepsin L facilitates endosomal escape of the genomic RNA into the cytoplasm [116]. A recent study determined that cell lines from several insectivorous bat species were not permissive to SARS-CoV-2 replication despite expression of endogenous bat ACE2 on some of these cells. One of the cell lines tested was from a patagium biopsy of a greater horseshoe bat (*Rhinolophus ferrumequinum*), a member of the genus that harbors sarbecoviruses [74]; however, it was unclear whether these cells expressed endogenous ACE2, or whether a lack of sufficient RfACE2 binding residues may impair spike binding (12/20 residues, **Table 2.1**), and attempts to transduce this cell line with human ACE2 failed [117]. Transduction of human ACE2 led to low-level, nonproductive SARS-CoV-2 infection in four of the other bat cell lines, but none were of kidney origin like Ajk cells. One of the lines appeared to produce virus particles; however, electron microscopy indicated the viruses were unable to complete exocytosis. The authors postulated that tetherin, which appears to be under strong selective pressure in bats [118], may account for this observation. In the other cells, expression of *Oas1* and *Ifih1* (MDA-5) transcripts were elevated during SARS-CoV-2 infection and may have impaired virus replication. Thus, our results are consistent with these findings.

Despite the discouraging results of the Ajk cells, we proceeded with hACE2 transduction of cells in the lungs of Jamaican fruit bats to determine susceptibility. Transduced bats challenged

with 10^5 $TCID_{50}$ equivalents of SARS-CoV-2 WA1 did not show visual signs of disease and they did not lose weight (**Figure 2.3D**). BALB/c mice similarly transduced with hACE2 and challenged with SARS-CoV-2 exhibited significant weight loss of 10-25% during the first week but recovered thereafter [105]. Viral RNA was only detected early in infection and at low levels (**Figure 2.3B**). This could be a limitation of the Ad5/hACE2 penetrance because lung tissue for RNA extraction was collected from the distal ends. It also could be that this represents residual input virus; Hassan et al. detected low levels of viral RNA in the lungs of SARS-CoV-2 challenged BALB/c mice that had not been transduced with hACE2 [105]. Regardless, clear pathology was present in hACE-transduced and infected bat lungs (**Figure 2.5A**), antigen was readily detected in the main stem bronchi of hACE2 transduced lungs and challenged bats for up to 14 days, but not in the lungs of bats only transduced with hACE2 (**Figure 2.5B**), and clear but low-titer antibody responses occurred beginning on day 4 (**Figure 2.5C, Figure 2.4**). This is consistent with work by us and others showing that bats typically produce low-titer antibody responses to viral infections [101,108,110,119-123]. We cannot exclude the possibility that adenovirus transduction elicited an innate response that could have augmented control of SARS-CoV-2 infection; however, mouse studies have shown innate stimulation from transduction subsides within a day of inoculation with the vector [124].

We also determined that $CD4^+$ helper T cells responded to SARS-CoV-2 infection in the hACE2 bats. Antigen-reactive T cells typically are rare in infected animals, usually fewer than 2% of T cells even days or weeks after infection, making assessment of ex vivo T cell responses challenging. However, because CD154 is an activation marker of helper T cells, its expression can be used in the activation-induced marker (AIM) test [125,126] to identify the rare helper T cells reactive to antigen by flow cytometry. We found a significant increase in CD154 (CD40L) expression on

$CD4^+$ helper T cells when stimulated with a SARS-CoV-2 nucleocapsid peptide library. In humans, abundant $CD4^+/CD154^+$ T cells are associated with severe COVID-19, particularly in T cells producing abundant proinflammatory cytokines, including interferon-γ (IFNγ), tumor necrosis factor, interleukin-2 (IL-2) and/or interleukin-21 (IL-21) [127,128]. In the splenocytes of 3 of 4 bats cultured 24 hours with nucleocapsid peptide library antigen, neither IFNγ nor IL-21 transcripts were elevated, whereas IL-10 and TGFβ were elevated more than two-fold (**Figures 2.9C/D**), despite the low frequency (<2%) of antigen-specific helper T cells in the splenocyte cultures. These two cytokines are typically produced by regulatory T cell subsets that suppress inflammatory responses. Expression of Th1 transcripts IL-2 and IFNγ, Th2 transcripts IL-4 and IL-13, and T follicular helper (Tfh) IL-21 transcripts were lower than basal level expression. Fox-p3 and Cxcr5 expression were not substantially elevated, which could be explained by low levels of expression of this transcription factor and cell surface receptor, respectively, in the few antigen-reactive T cells (i.e., low signal-to-noise ratios). Identification or development of monoclonal antibodies for these bat orthologs could enhance their detection using flow cytometry, particularly to determine whether the Treg-like cells are expressing both IL-10 and TGFβ, or if there are two populations expressing each cytokine. Transcripts of helper T cell markers CD4 and Cxcr4, which is substantially elevated in patients with severe COVID-19 [129], were both elevated, suggesting that Cxcr4 activity may be less in bats compared to humans, or it may have a different role in bats. This study also determined that Treg cell responses during COVID-19 may lead to more severe outcomes in humans, which is seemingly contradictory considering IFNγ- and IL-21-expressing T cells appeared to contribute to immunopathology [128]. Thus, there appear to be similar responses, yet clear differences in helper T cell behaviors in bats and humans infected with SARS-CoV-2. The T cells from bat 3 did not have elevated expression of any gene in the qPCR array (**Figure**

2.9C). Repeated testing of the duplicate samples from this bat yielded similar results; thus, we are confident the RNA was properly extracted. It is also possible that the nucleocapsid peptide library was not added when the splenocytes were plated; however, because each T cell culture from each bat was performed in duplicate we think this is unlikely. It may be that other genes not on the qPCR array were expressed by these T cells; RNA-Seq could help clarify this.

Helper T cells are instrumental for many effector functions and provide the highest level of command and control of immune responses. Indeed, engagement of Th cell CD154 by B cell CD40 leads to T cell help, including IL-21 production from Tfh cells in germinal centers [130], for class switching and somatic hypermutation/affinity maturation. In the present study, we only detected low titer antibody responses in the bats, even at 21 days post infection, and the lack of IL-21 expression may be one reason why antibody titers, which are principally a function of affinity maturation, are poor. In our previous experimental infection studies of Tacaribe virus-infected Jamaican fruit bats, which causes a fatal disease, RNA-Seq analysis identified genes required for somatic hypermutation in spleens, including activation-induced cytidine deaminase; however, they were not differentially expressed in infected bats [109]. Thus, it may be that bats have such robust innate immune responses that they are less dependent on antibody responses. However, prior to this work, no studies have been published describing virus-specific helper or cytotoxic T cells in bats, principally because of a lack of tools for the study of bat adaptive immunity; thus, it is unclear what roles bat T cells play in immunity to viruses. It may be that bats have a greater dependency on regulatory T cells that could temper inflammatory pathology, which is consistent with the observation that bats typically have low or no inflammatory responses during viral infections [108,119,131,132]. This also parallels what occurs in rodent reservoirs of hantaviruses, in which TGFβ-expressing regulatory T cells predominate to what are otherwise innocuous infections

[133,134]. Further studies, including the development of new reagents and methods for bats, will be needed to address these questions, particularly studies for examining individual T cells (e.g., T cell culturing, flow cytometry, single-cell RNA-Seq, etc.).

The findings here also show that serotype 5 adenovirus vectors are important tools for addressing viral infections of bats, including SARS-CoV-2 variants. It is likely that SARS-CoV-2 originated in horseshoe bats, thus it should be possible to address questions of SARS-CoV-2 and other sarbecovirus susceptibility and infection of Jamaican fruit bats transduced with ACE2 from horseshoe bat species. Although work with cells expressing various bat ACE2 proteins have been performed [114], a better understanding of how these viruses behave in bats, particularly adaptive immune responses which require live bats, could shed light on the biology of coronaviruses. A limitation of adenovirus use is that gene transduction is confined to the respiratory tract and not the intestines, where natural bat coronaviruses are typically found. Nonetheless, this approach offers a means to more fully dissect the role of a variety of viral infections of bats and how the adaptive immune system responds to those viruses.

Methods

Jamaican Fruit Bats.

This study was performed with approval from the Colorado State University Institutional Animal Care and Use Committee (protocol 1787). Bats of both sexes were used; however, more males than females were used because the low fecundity (one pup at 6 month intervals for reproductive females). The bat colony is maintained in a free-flight facility; however, Infected bats were confined to bird cages under BSL-3 containment upon challenge with SARS-CoV-2.

Generation of Anti-Jamaican Fruit Bat CD4 Monoclonal Antibody.

The Jamaican fruit bat CD4 protein was submitted to Phyre2 molecular modeling server and the generated structure file provided several candidate solvent-accessible peptides. An extracellular membrane-proximal sequence from residues 236-277 (ENRKVSVVKTRQDRR) with an N-terminal cysteine was generated and covalently linked to KLH (Genscript). BALB/c mice were intraperitoneally-immunized with 25 μg of the KLH-peptide conjugate emulsified in incomplete Freund's adjuvant (IFA) and boosted at 1 month intervals (in IFA) for 3 months. Sera from mice were reactive to Jamaican fruit bat splenocytes. A final boost in PBS was administered and 4 days later splenocytes were fused with Sp2/10 Ag14 cells (ATCC CRL-1581) and cultured overnight prior to concurrent cloning and HAT selection on methylcellulose plates (ClonaCell-HY, StemCell Technologies). After 14 days of incubation at 37°C, clones were picked for expansion. Supernatants were screened by flow cytometry to identify reactive monoclonal antibodies. Several were identified and one, 1-D5 was selected for fluorescent labeling.

Identification of Cross Reactive Anti-CD40 and Anti-CD154 Antibodies: In Silico Protein Homology.

Jamaican fruit bat CD40 (NCBI, XP_037020498) and CD154 (NCBI, XP_037012946) polypeptide sequences were submitted to Phyre2 molecular modeling server to generate PDB files [135]. The generated Jamaican fruit bat protein PDB structures, mouse CD40 (UniProt, P27512), and human CD154 (UniProt, P29965) PDB files were imported into Geneious Prime for the assessment of protein homology by Blocks Substitution Matrix 62 (BLOSUM62) alignment [136]. The three-dimensional structures were then annotated for the transmembrane domains and identical amino

acid residues to identify putative conserved regions to which commercially-available monoclonal antibodies might bind to Jamaican fruit bat orthologs.

Identification of Cross Reactive Anti-CD40 and Anti-CD154 Antibodies: Flow Cytometry.

One naïve male Jamaican fruit bat was euthanized and a single-cell suspension of its spleen was generated by mechanical disassociation in cold 10 ml PBS with 5 mM EDTA by passage through a 70μm cell strainer. Splenocytes were then placed in a 15 ml conical tube and centrifuged at 4°C for 5 minutes at 350 g and supernatant was decanted. Splenocytes were then resuspended in cold 10 ml ammonium chloride solution (150mM NH_4Cl, 10mM $NaHCO_3$, 10mM EDTA in cell culture grade water) and incubated for 10 minutes on an orbital rotator to lyse red blood cells. The cells were washed and resuspended in 10 ml PBS, 5 mM EDTA splenocytes were then counted using a hemocytometer and trypan blue and resuspended in cryopreservation media (90% FBS, 10% DMSO) at $5x10^6$ cells/ml, and 1 ml aliquots dispensed into cryovials. Cryovials were then stored in -80°C for 2 days, then transferred to liquid nitrogen.

One cryovial was removed from liquid nitrogen, thawed in a 37°C water bath, transferred to 15ml conical tube and washed with 10ml PBS, 5 mM EDTA. 10^6 cells were transferred to wells of a 96 well v-bottom plate for the unstained control. Splenocytes were washed and resuspended in 5 ml of a 1:5,000 dilution of primary amine viability dye (Ghost DyeTM Red 780) in PBS with 5 mM EDTA solution and incubated in the dark at 4°C for 30 minutes. Splenocytes were then centrifuged at 4°C for 5 minutes at 350 g and supernatant was decanted. Splenocytes were then washed in 10ml FACS buffer (PBS, 1% BSA, 0.5% sodium azide, 5 mM EDTA) centrifuged at 4°C for 5 minutes at 350 g and supernatant was decanted. Cells were then resuspended in FACS buffer, and 1 million splenocytes were added 96 well v-bottom plate per test sample. Splenocytes

were then centrifuged at 4°C for 3 minutes at 350 g and supernatant was decanted. Splenocytes were then resuspended in 100µl Fc receptor blocker (Innovex, ready-to-use) and incubated for 30 minutes at 4°C in the dark. Splenocytes were then centrifuged at 4°C for 3 minutes at 350g and supernatant was decanted. Test samples were then resuspended in a 1:20 dilution of anti-mouse CD40 PE (Tonbo, clone FGK45), or anti-human CD154 PE (Tonbo, clone 5C8) in FACS buffer and incubated for 30 minutes at 4°C in the dark. Splenocytes were then centrifuged at 4°C for 5 minutes at 350 g and supernatant was decanted. Splenocytes were washed 2x with 150µl FACS buffer centrifuged at 4°C for 5 minutes at 350g and supernatant was decanted each time. Splenocytes were then resuspended in 100µl FACS buffer. A 4 laser Cytek Auora (16V-14B-10YG-8R) cytometer was used to acquire the FCS files. The unmixed FCS files were then analyzed using FlowJo 10.8.1.

SARS-CoV-2 Infections.

The WA1 isolate of SARS-CoV-2 was used for this study and was obtained from BEI Resources and passaged twice in Vero E6 cells to generate a stock. Intranasal inoculations were performed with 3 bats per time point group and one mock control (7 groups, 21 bats total) while holding the bats in a contralateral position to ensure delivery to the trachea and the esophagus (i.e., lungs and GI tracts) with 10^5 $TCID_{50}$ equivalents per bat in 50 µl in sterile PBS. Oral and rectal swabs were collected from bats on days 2, 4, 7, 10, 14 and 21 post-inoculation (PI) for detection of virus by qPCR. Groups of bats were euthanized on days 2, 4, 7, 10, 14 and 21 PI for necropsy with portions of lungs and intestine collected and frozen for viral RNA and virus isolation, and the remaining tissues collected in buffered formalin.

Virus detection. For virus isolation, frozen lungs and intestines were homogenized with a Tissue Lyser II in 10% FBS DMEM, centrifuged at 8,000g for 5 min, then passed through a 0.2 μm filter to remove bacterial contaminants. Log_{10} dilution series were made for each sample and added to replicate 96 wells of Vero E6 cells and scored for CPE 5 days later to calculate $TCID_{50}$. For qPCR, RNA was extracted from frozen tissues (Qiagen RNEasy kit) and $TCID_{50}$ equivalents determined using a SARS-CoV-2 E gene detection kit (Promega) based upon the Berlin primer/probe set [137].

Adenovirus Transduction of Human ACE2.

A serotype 5 defective adenovirus encoding the human ACE2 gene (Ad5CMVhACE2) purchased from the University of Iowa Viral Vector Core was used for this study. The E1 gene is replaced with human ACE2, rendering the virus incapable of replication. For in vitro studies, Jamaican fruit bat Ajk cells were inoculated with 1 MOI of a GFP-expressing virus (Ad5CMVACE2-IRESeGFP) for 1 hour, followed by removal of inoculum and 2x washing in 2% FBS-DMEM. For SARS-CoV-2 challenge, cells were inoculated with virus without GFP (Ad5CMVhACE2) as above and at 48 hours inoculated with 0.1 MOI of SARS-CoV-2. Supernatants were collected at 1 hr and daily thereafter for titration on Vero E6 cells. For in vivo experiments, bats were intranasally inoculated with $2.5x10^8$ pfu in 50 μl of serum-free DMEM. SARS-CoV-2 challenge was performed 5 days later.

Histopathology and Immunohistochemistry.

Tissues and carcasses with open abdomens were collected in 10% neutral buffered formalin for 3 days prior to removal from the BSL-3 and transferred to the Colorado State University Diagnostic Laboratories for trimming. Oral cavity, salivary glands, olfactory bulb, cerebrum, cerebellum, and brain stem were thoroughly inspected for gross lesions. Decalcified skulls and visceral organs were processed, embedded in paraffin wax and 4–5 μm sections were stained with hematoxylin and eosin for blinded evaluation by the pathologist using Nikon i80 microscope (Nikon Microscopy).

Sections were stained using ultraView universal alkaline phosphatase red detection kit. Heat-induced epitope retrieval was performed on a Leica Bond-III IHC automated stainer using Bond Epitope Retrieval solution for 20 minutes. Viral nucleocapsid antigen was detected with a purified rabbit polyclonal antibody. Labeling was performed on an automated staining platform. Fast Red was used as chromogen and slides were counterstained with hematoxylin. Immunoreactions were visualized by a single pathologist in a blinded fashion. In all cases, normal and reactive mouse brain sections incubated with primary antibodies was used as a positive immunohistochemical control. Negative controls were incubated in diluent consisting of Tris-buffered saline with carrier protein and homologous nonimmune sera. All sequential steps of the immunostaining procedure were performed on negative controls following incubation.

Fluorescent Microscopy.

Paraffin embedded tissue sections were stained for SARS-CoV-2 nucleocapsid protein (1:500) using a Leica Bond RXm automated staining instrument following permeabilization using 0.01% Triton X diluted in Tris-buffered saline (TBS). Blocking was performed with 1% donkey serum diluted in TBS. Sections were stained for DAPI (Sigma) and mounted on glass coverslips in ProLong Gold Antifade mounting medium and stored at ambient temperature until imaging. Images were captured using an Olympus BX63 fluorescence microscope equipped with a motorized stage and Hamamatsu ORCA-flash 4.0 LT CCD camera. Images were collected and regions of interest quantified with Olympus cellSens software (v 1.18) using an Olympus X- line apochromat 10X (0.40 N.A.), 20X (0.8 N.A.) or 40X (0.95 N.A.) air objectives, or Uplan Flour X100 oil immersion (1.3 N.A.) objective.

Serum IgG ELISA.

The SARS-CoV-2 spike (S) ectodomain containing the prefusion stabilizing hexapro mutations [138] and a mutated furin cleavage site was produced and purified from Expi293 cells as previously described [139]. The SARS-CoV-2 S protein was diluted to 0.003 mg/mL in PBS and used to coat 384-well Nunc Maxisorp plates (Thermo Fisher) overnight at room temperature. The plates were slapped dry and blocked for 1 hour at 37°C using Casein in PBS (Thermo Fisher). Following blocking, the plates were again slapped dry and sera from infected bats was added to the plates beginning at a 1:30 dilution in TBST followed by a 1:3 serial dilution thereafter. Plates were incubated for 1 hour at 37°C, slapped dry, and washed four times with TBST. Recombinant protein A/G conjugated to HRP (Thermo Fisher) diluted 1:500 in TBST was added each well and the

plates were incubated for 1 hour at 37°C then washed four times with TBST. To measure binding titers, TMB Microwell Peroxidase (Seracare) was added to each well and, after 2 minutes, the reaction was quenched with 1 N HCl. The absorbance at 450 nm was measured using a BioTek Neo2 plate reader and analyzed in GraphPad Prism 9 with ED_{50} values being determined using a four-parameter logistic regression model. Two biological replicates were performed for each sample.

Neutralization Assays.

VSV particles pseudotyped with the SARS-CoV-2 S protein harboring the D614G mutation were produced as previously described [140,141]. To perform the neutralization assays, 20,000 Vero-TMPRSS2 cells were seeded into each well of a 96-well plate and grown overnight until they reached approximately 80-90% confluency. Sera from infected bats were diluted in DMEM (Gibco) beginning at a 1:10 dilution followed by a 1:3 serial dilution thereafter. The diluted sera were then incubated for 30 minutes at room temperature with SARS-CoV-2 S pseudotyped VSV diluted 1:25 in DMEM along with an anti-VSV-G antibody (I1-mouse hybridoma supernatant diluted 1:25, from CRL-2700, ATCC) to block entry of any residual VSV G pseudotyped virus. The Vero-TMPRSS2 cells were washed three times with DMEM and the virus-sera mixture was added to the cells. Two hours after infection, an equal volume of DMEM supplemented with 20% FBS and 2% PenStrep was added to each well. The cells were incubated for 20-24 hours after which ONE-GloEX (Promega) was added to each well and the plates were incubated for 5 minutes. Luminescence values measured in relative light units (RLU) were recorded using a BioTek Neo2 plate reader. The values were normalized in GraphPad Prism 9 with the RLU values from uninfected cells to determine 0% infectivity and the RLU values from cells

infected with pseudovirus only to determine 100% infectivity. ID50 values were determined from the normalized data using a [inhibitor] vs. normalized response – variable slope model. Neutralization assays were performed in duplicate and replicated with two distinct batches of pseudovirus.

Activation-Induced Marker Test.

Five bats were transduced with hACE2 and 5 days later inoculated with SARS-CoV-2. Twelve days later, the bats were euthanized and spleens collected to make single cell suspensions. Red blood cells were lysed with ammonium chloride buffer and 10^6 splenocytes from each bat were cultured with 1 μg of SARS-CoV-2 PepTivator® SARS-CoV-2 Prot_N peptide library (15mers with 12 residue overlaps, Miltenyi) for 6 hours in 5% FBS Clicks medium (Fujifilm/Irvine Scientific) and 1 μg of anti-mouse CD40 monoclonal antibody (FGK45, Tonbo/Cytek, to block CD154 ligation) at 37° C in duplicate. Identical wells were set up in duplicate without peptide library to provide baseline marker levels. Cells were collected, washed and stained with anti-Jamaican fruit bat CD4 and anti-human CD154 (5C8, Tonbo/Cytek). Cells were fixed in paraformaldehyde and examined by flow cytometry. Gating on CD4 was performed and the mean fluorescent intensity (MFI) of CD154 was determined. MFI were evaluated between groups using Wilcoxon signed-rank test.

Immune Gene Expression Profiling.

Identical cultures described in the AIM test were examined for immune gene expression. Splenocytes ($5x10^6$) were cultured in 24 well plates with 5 μg of SARS-CoV-2 PepTivator® SARS-CoV-2 Prot_N peptide library for 24 hours. Identical cultures without peptide library were used to determine baseline gene expression. Duplicate splenocyte cultures were examined for changes in gene expression by SYBR Green qPCR array as previously described [94,134,142]. Briefly, total RNA was extracted from the cells (RNEasy kit, Qiagen) and cDNA produced (QuantiTech RT, Qiagen). Primers for Jamaican fruit bat genes (**Table 2.2**) and qPCR was performed (QuantiTech SYBR Green, Qiagen). Within sample gene normalization was performed on Rps18 (ΔCq), and fold-chage determined by comparing each gene from the peptide-stimulated cells to the unstimulated cells from the same bat (ΔΔCq).

Table 2.2 Immune gene expression primers, 5' to 3'.

Gene	Forward	Reverse
Rps18	GCGAGTACTCAACACCAATA	TTTTGGTGAGGTCGATGTCT
IFNg	CCTTGAAAGACAACCAGAGC	CCTCCATTTTGCTGTTGCTG
IL-2	CGAACTCAACCCTCTGAAGG	GTGCGTTCACTGTGACATTG
IL-4	AGCTCTGGTCTGCTTACTAG	TGGTCTCTTCTAAGGTGAGG
IL-10	TGAAAACAAGAGCAAAGCAG	TGAAAACAAGAGCAAAGCAG
IL-12a	TGCTGGCAGCTATTGATGAG	AGATCCGGTTCTTCAAGGGA
IL-13	CATCCAAAAGACCCAGAGG	ATCACTTCCACTTTGGTGTC
IL-21	AGATAATCAGCCTGCTAACG	CTCTGTTTCTGTCTTCTCCC
IL-27	GACCGTGAGTTTGGATCTCC	TCAGGGAGGTTGAATCCTGT
TGFb	TGTTCTTCAACACGTCGGAG	CGTGCTGTTCCACTTTCAAC
Ebi3	GCCCTACATGCTGAACATCA	TCTGGAGGGTCTGGTTTGAT
IL-27Ra	TGAGTCTTACCTGCCTTCCA	CTTGCTGGAATTGCTGTTGG
gp130	CTGAGTCCTTGAAGGCGTAC	TTCCCCACTTTCTTTGTCCG
Tbx21	CCAAAGGATTCCGGGAGAAC	AATTGACAGTTGGGTCCAGG
Gata3	ACCCCTGACTATGAAGAAGG	CACCTTTTTGCACTTTTTGG
Foxp3	CCAGCTCTGTGATCTGGAAC	AAAGCCTGTTGAGGTCCATC
Cxcr4	GCTCAGGCGACTATGACTCC	TGCCCACTATGCCAGTCAAG
Cxcr5	GGTCAGCCAACCTCATCACA	TAGAGGAAGCGGGAGGTGAA
CD4	CTCATTCCCACTCACCTTCG	CTCATTCCCACTCACCTTCG
CD25	TGTGAGTGCAAGAAAGGCTT	TTTTCCCAGAAAGAGTGGCC

Conflict of Interest

The JAR laboratory received support from Tonix Pharmaceuticals, Xing Technologies and Zoetis, outside of the reported work. JAR is inventor of patents and patent applications on the use of antivirals and vaccines for the treatment and prevention of virus infections, owned by Kansas State University, KS.

Acknowledgments

Funding for this study was provided through grants from the National Institute of Allergy and Infectious Diseases R01 AI140442 (TS, SRW), the National Science Foundation (2033260, TS; 2020297257, BB), National Bio and Agro-Defense Facility (NBAF) Transition Fund from the State of Kansas (JAR), the MCB Core of the Center on Emerging and Zoonotic Infectious Diseases (CEZID) of the National Institutes of General Medical Sciences under award number P20GM130448 (JAR), the NIAID Centers of Excellence for Influenza Research and Surveillance under contract number HHSN 272201400006C (JAR) and the NIAID supported Center of Excellence for Influenza Research and Response (CEIRR) under contract number 75N93021C00016 (JAR). The Schountz's lab, Tjalkens' lab, and others who made significant contributions to this work: Savannah M Rocha, Miles Eckley, Shijun Zha, Clara Reasoner, Amin Addetia, Juliette Lewis, Anna Fagre, Phillida Charley, Juergen A Richt, Susan R Weiss, Ronald B Tjalkens, David Veesler, Tawfik Aboellail and Tony Schountz

CHAPTER 3
DISCRIMINATION OF JAMAICAN FRUIT BAT LEUKOCYTES BY FLOW CYTOMETRY AND THE DISCOVERY OF NOVEL CD19+ T CELLS

Summary

There are over 1,400 species of bats, each providing important ecological roles, including pollination and seed dispersal, and consumption of insects such as crop and forest pests, and mosquitos and midges that spread arthropod-borne diseases [47]. Bats are reservoirs for viruses that are transmissible to humans and livestock, including, henipaviruses, filoviruses, coronaviruses, and lyssaviruses. The causative agent of COVID-19, SARS-CoV-2, likely originated from a horseshoe bat (*Rhinolophus* spp.) reservoir. Despite these facts, bats represent underdeveloped animal models. As such, the immunological selection pressures placed on viruses than can transmit or potentially transmit to humans and livestock are also understudied. The primary limitation to investigating the immune systems and responses of bats is the paucity of bat-specific reagents, such as antibodies to cluster of differentiation (CD) antigens of interest. The establishment of a Jamaican fruit bat *(Artibeus jamaicensis*) breeding colony at Colorado State University has allowed us to begin to identify antibody reagents useful for this species. We have generated an anti-CD3γ monoclonal antibody and validated two commercially-available cross-reactive antibodies that target CD19 and CD3ε. Furthermore, we have discovered a novel $CD19^{+}CD3^{+}$ T cell that is present in the homeostatic immune system of Jamaican fruit bats. These antibodies were identified by pre-screening *in silico* for protein homology, tested and validated by flow cytometry, fluorescent microscopy, and confirmed for gene enrichment by cell sorting $CD3\varepsilon^{+}$, $CD3\gamma^{+}$, $CD3e^{+}CD3\gamma^{+}$, and $CD19^{+}$ populations in conjunction with RT-qPCR. These antibodies will

facilitate detailed examination of lymphocyte responses in bats and may clarify the role for CD19+CD3+ T cells (**Figure 3.1).**

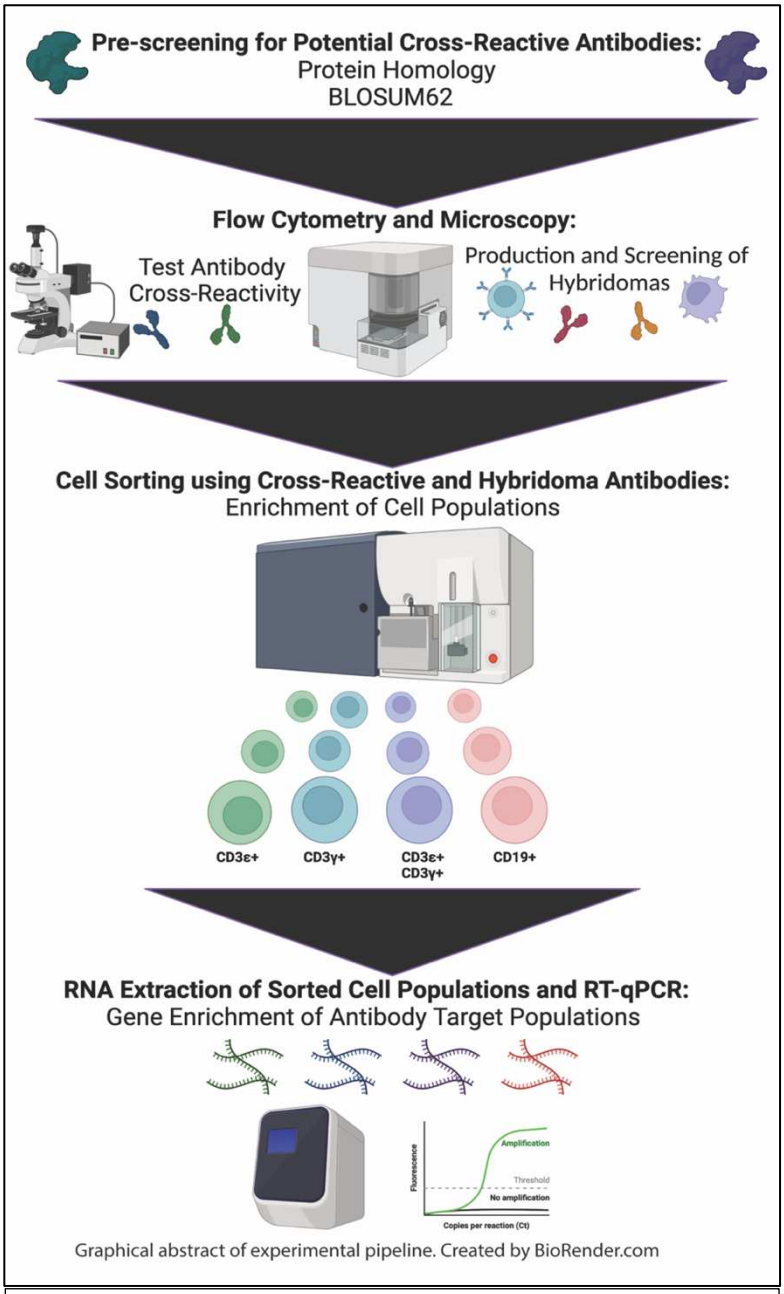

Figure 3.1) Graphical Abstract of Experimental pipeline.

Introduction

There are over 1,400 species of bats, each providing important ecological roles, including pollination and seed dispersal, and consumption of insects such as crop and forest pests, and mosquitos and midges that spread arthropod-borne diseases [47]. Bats represent major reservoir hosts for viruses that are transmissible to humans and livestock, including, henipaviruses, filoviruses, coronaviruses, and lyssaviruses [53]. SARS-CoV2, the etiologic agent of COVID-19, likely originated from a bat reservoir [57]. Moreover, bats are susceptible to other pathogens such as rabies virus and *Pseudogymnoascus destructans*, the causative agent of white nose syndrome (WNS) that has killed millions of North American bats. A recent study has reported that populations of three species of North American bats (*Myotis septentrionalis*, *Myotis lucifugus*, and *Perimyotis subflavus*) have been reduced by more than 90% by WNS [58]. As such, bats interconnect ecological and agricultural importance, and human health.

Human and laboratory mouse immunology provide a foundation to understand bat immune systems and responses; however, clear differences exist between these well understood species and bats. Some bats have a constitutively active innate type I interferon (IFN) system with higher basal expression of the *Ifna* genes, unlike humans and mice [59]. However, constitutive expression of *Ifna* in these bats induces the expression of a subset of IFN-stimulated genes but without chronic inflammatory pathology [60]. Another difference in some bat species may be differences in heavy chain VDJ recombination for immunoglobulins in B cells [62]. Humans have about 40 functional V segments, 24 D

segments, and 6 J segments, giving rise to a potential 5,760 heavy chains by recombination [60]. In contrast, the little brown bat (*Myotis lucifugus*) has 236 V segments, 24 D segments, and 13 J segments giving rise to a potential 73,632 heavy chain combinations [62]. Furthermore, little brown bats may use affinity maturation of antibodies to a lesser degree than humans [62]. The Egyptian fruit bat (*Rousettus aegyptiacus*) has a similar capacity as to humans to perform VDJ recombination, yet the genome denotes an expansion of the KLRC/KLRD family of natural killer (NK) cell receptors, MHC class I genes, and type I interferons [143].

Despite the differences known about the immune system of bats, there is little known about the cellular immune system and subsequent responses to perceived pathogens, principally because of a lack of well-defined reagents to profile leukocytes of bats. Jamaican fruit bats (*Artibeus jamaicensis*) are Central and South American bats that represent an underdeveloped animal model for immunology and infectious disease research. They are a natural reservoir of H18N11 influenza A virus, and a species used to study other viral infections as an experimental surrogate host model, including MERS-CoV, Zika virus and Tacaribe virus [63,65,144].

Immunophenotyping uses antibodies to identify cells based extracellular and/or intracellular antigens or markers. This allows for cell-specific separation based on the labeled cellular characteristics and is the foundation for the use of high throughput technologies such as flow cytometry, cell sorting, and highly quantitative and anatomical data gained from fluorescent microscopy. A lack of reactive antibody reagents limits

investigations of bat immune responses to pathogens. To overcome this limitation three approaches are available: 1) identify commercially available cross-reactive antibodies for other species 2) produce bat specific hybridomas 3) RNA probe-based technologies.

The aim of this work was focused on identifying cross-reactive antibodies and to produce monoclonal antibodies that recognize Jamaican fruit bat-specific antigens for immunophenotyping and validation that target Jamaican fruit bat T and B cell antigens: CD3ε, CD3γ, and CD19. The continued characterization of bat immune responses will provide valuable insight into selection pressures placed on bat-borne viruses driving critical spill-over events. Furthermore, these reagents will clarify how Jamaican fruit bats, and likely other bat species, respond to infections, providing aid to bolster conservation efforts.

Materials and Methods

Animals

All animal work was approved by the Institutional Animal Care and Use Committee (IACUC, Colorado State University). Mice were housed in microinsulator cages (2 animals per cage), with a 12-hour light dark cycle and had access to food and water *ad libitum*. Jamaican fruit bats were housed in a free-flight captive breeding colony room at Colorado State University.

Pre-Screening Antibody Cross-Reactivity

To identify potentially cross-reactive antibodies, protein sequences used to produce the antibody were BLASTed against the Jamaican fruit bat proteome. Alignment scores ≥50-80 were chosen as candidates to screen for cross-reactivity to Jamaican fruit bat splenocytes using flow cytometry. To further assess protein homology, protein sequences were downloaded into Geneious Prime and Geneious Protein Alignment BLOSUM62 analysis was performed for human, mouse (*Mus musculus*), Jamaican fruit bat, common vampire bat (*Desmodus rotundus*), Chinese horseshoe bat (*Rhinolophus sinicus*), greater horseshoe bat (*Rhinolophus ferrumequinum*), Egyptian fruit bat (*Rousettus aegyptiacus*), Indian flying fox (*Pteropus medius,* formerly *Pteropus giganteus*), and black flying fox (*Pteropus alecto*) for all CD3ε, CD3γ, and CD19 protein isoforms [145,146]. BLOSUM62 homology precents were then averaged for CD3ε and CD19. A protein alignment tree was

then generated. Greater than 60% protein homology determined if commercially available mouse and human antibody clones should be screened for cross-reactivity via flow cytometry. Additionally, protein sequences were submitted to the Phyre2 server to generate predicted 3D models of each protein [147]. The PDB files for CD3ε and CD19 were then imported into Geneious Prime where BLOSUM62 alignment was ran with human CD3ε against Jamaican fruit bat CD3ε and murine CD19 against Jamaican fruit bat CD19 to identify identical protein alignment regions. These identical sites were colorimetrically annotated for extracellular regions (red) and transmembrane and intracellular regions (cyan). See **appendix I** for more information about protein homology and cross-reactivity.

Anti-CD3γ Hybridoma Production

Jamaican fruit bat CD3γ protein sequences were submitted to the Phyre2 server to generate predicted 3D models of each protein. PDB files were imported into Geneious Prime, and the solvent-accessible peptide sequence were assessed. Peptide sequence for CD3γ (LKDQNIKWFKDGKEIMTNGNTWKLG) was selected for antigen preparation. Anti-Jamaican fruit bat CD3γ hybridomas were produced by immunizing BALB/c mice intraperitoneally with 25 μg of the CD3γ peptides conjugated to KLH emulsified in incomplete Freund's adjuvant (IFA). Mice were boosted 4 weeks and 8 weeks after initial immunization with peptide-KLH in IFA. Twelve weeks post-initial immunization, mice were boosted with peptide-KLH in PBS and 4 days later were euthanized. Spleens were harvested and processed into a single cell suspension and fused with Sp2/10-Ag14 cells. Fused cells were then cultured overnight for recovery, then plated on 100 mm Petri dishes

with methylcellulose containing HAT medium for concurrent cloning and selection. Two weeks after fusion, clones were picked and placed in 96 well plates and cultured to expand clones. To screen CDγ hybridomas Jamaican fruit bat splenocytes were incubated with hybridoma clone supernatants. Splenocytes were subsequently washed and then stained with a secondary anti-mouse IgG (FITC) antibody. CD3γ hybridomas were analyzed using a 488 Guava easyCyte (data not shown). See **appendix II** for more information about how hybridomas were produced – the same methodology was used.

Tissue Extraction and Fixation

Male and female Jamaican fruit bats were placed under continual isoflurane anesthesia for the entire procedure. Cardiac puncture was performed followed by intra-cardiac perfusion of the whole animal with 60 ml of profusion buffer (1X PBS, 5 mM EDTA, 10 U/ml heparin sulfate). Tissue extraction was rapidly performed after perfusion with subsequent tissue fixation in 4% paraformaldehyde.

Tissue Preparation and Automated High-Throughput Immunofluorescent Staining

Paraffin embedded spleen and intestinal tissue was sectioned at 5µm thickness and mounted onto polyionic slides. Slides were deparaffinized and tissue sections were immunofluorescently labeled on a fully automated Leica Bond RX_m robotic staining system. Epitope retrieval was performed through application of Bond Epitope Retrieval Buffer 1 (ER1) for 20 minutes in conjunction with heat. Sections were then incubated with

antibodies directed toward epitopes of interest that were diluted in 0.1% Triton-X containing phosphate buffered saline (PBS). Antibodies were optimized for fluorescent staining at the following dilutions: CD3γ (1:50), CD3ε (1:100), CD19 (1:500). Sections were stained for DAPI (Sigma) and mounted on glass coverslips with Prolong Gold Anti-fade mounting media. Mounting media was allowed to cure at room temperature in the dark for 24 hours. Sections were stored at 4°C until imaged.

Detection and Quantification of Resident Tissue Immune cells

Full section montage images were acquired on a fully-automated motorized stage VS200 Olympus microscope equipped with a Hamamatsu ORCA-Fusion camera and collected using Olympus CellSens software. Whole tissue section montages were generated by compiling 200X images acquired by using an Olympus UPLX-Apochomat 20X (0.8 N.A.) air objective. Anatomical determination was performed by manual application of regions of interest (ROIs) based on tissue architecture and immunofluorescently labeled cells. High magnification inset images were acquired using an Olympus UPLX-Apochromat 60X oil immersion objective (1.42 N.A.).

Cell Sorting

Two male and two female bats were euthanized, and spleens were removed and processed into a single cell suspension. Splenocytes were then stained with Tonbo Ghost Violet 450 viability dye followed by staining with CD3γ (Clone: XE2, fluorophore: Alexa Fluor 647), CD3ε (Hit3a, FITC), and CD19 (1D3, PE-eFluor610). Cells were then sorted

using a FACS Aria-III. UltraComp eBeads™ Plus Compensation Beads were used for CD3ε (Hit3a, FITC), CD19 (1D3, PE-eFluor610); ArC™ Amine Reactive Compensation Beads were used for Tonbo Ghost Violet 450; splenocytes were used for CD3γ (XE2, Alexa Fluor 647) single color control. FACSDiva Version 6.1.3 was used to calculate compensation. Gates were drawn using fluorescence minus one controls (FMOs). Cells were sorted into six categories by gating strategy: Not sorted (whole spleen), $CD19^+$, $CD3\varepsilon^+$, $CD3\gamma^+$, and $CD3\varepsilon^+$ $CD3\gamma^+$. Sorted cells were then pelleted and supernatant was decanted. RNA was then extracted from the cell pellets using Trizol. RNA yields were determined by NanoDrop UV spectrometry [148,149]. For detailed cell sorting and RNA extraction methods refer to **appendix III** and **appendix IV**.

Post-Hoc Cell Sorting Analysis of $CD19^+$ $CD3^+$ Cells

FCS files generated from cell sorting were analyzed in FlowJo V 10.8.1 Mac OS X 10.8.1. Single color controls as described above were used to calculate compensation matrix in FlowJo V 10.8.1 Mac OS X. FCS files were from all four bats were concatenated to better visualize $CD19^+$ $CD3^+$ cell populations. Gates were drawn using FMOs. Initial gating is as follows: Intact > Single Cells > Live. $CD19^+$ $CD3^+$ cells were then viewed two ways: 1) first gating on $CD3^+$ cells followed by $CD19^+$ cells 2) first gating on $CD19^+$ cells followed by $CD3^+$ cells.

Validation of Antibodies by RT-qPCR

Primer sets were designed targeting *Actb, Rps18, Cd3γ, Cd3ε, Cd4, Cd8a, Cd19, Cd28, and Cd45*. Tonbo Low ROX One-step RT-qPCR kit was used. Primers were optimized and validated using unsorted splenocyte single cell suspension RNA, and the limit of quantification (LOQ) was determined for each primer set. Primer efficiencies were between 92%-105% (**Table 3.1**). CD3ε had the highest LOQ, 11.222 ng of RNA. As such, 11.25 ng was the amount of RNA used for the RT-qPCR assay. RT-qPCR was carried out on each sorted sample using all primer sets in duplicate. Beta actin and RPS18 were used as reference genes. ΔΔCt method was then performed to calculate expression fold-change and data was then normalized to whole spleen control. Statistical analysis was performed using Prism. Two statistical tests were performed: one-way repeated measures ANOVA for pooled data output, and a two-way ANOVA to observe differences between sexes.

Table 3.1) Cell enriched RT-qPCR primer array details.

Primer set for *Beta Actin* (Amplicon 125bp)				
Forward	GCC TGG GAC TGA TTG TAC AT			
Reverse	AGG ACT GGC CCT TCT TAG A			
Annealing	**Efficiency**	**SD of Intercept**	**Limit of Detection (ng)**	**Limit of Quantification (ng)**
64°C	92.70824	0.85440918	**2.819550294**	**8.5440918**
Primer set for *RPS18* (Amplicon 125bp)				
Forward	GCG AGT ACT CAA CAC CAA TA			
Reverse	TTT TGG TGA GGT CGA TGT CT			
Annealing	**Efficiency**	**SD of Intercept**	**Limit of Detection (ng)**	**Limit of Quantification (ng)**
64°C	92.171041	0.11017102	**0.363564366**	**1.1017102**
Primer set for *CD3ε* (Amplicon 125bp)				
Forward	AAG ACC TCT GCC AAC ATT CAC			
Reverse	TGC CTT CCT TTT CCT GCC TA			
Annealing	**Efficiency**	**SD of Intercept**	**Limit of Detection (ng)**	**Limit of Quantification (ng)**
65°C	95.807262	1.122284937	**3.703540291**	**11.22284937**
Primer set for *CD3γ* (Amplicon 125bp)				
Forward	CCC TCT CAT GCA TCC CTC AC			
Reverse	TGG TGT GGC TCA GTA GAT TAA GA			
Annealing	**Efficiency**	**SD of Intercept**	**Limit of Detection (ng)**	**Limit of Quantification (ng)**
64°C	97.931966	1.057407084	**3.489443376**	**10.57407084**
Primer set for *CD4* (Amplicon 125bp)				
Forward	GGA AGG AAG TGG TGC TGA GT			
Reverse	GGC TCT TCC CAG AAT CTT GAT C			
Annealing	**Efficiency**	**SD of Intercept**	**Limit of Detection (ng)**	**Limit of Quantification (ng)**
64°C	105.81623	0.582426613	**1.922007822**	**5.824266126**
Primer set for *CD8a* (Amplicon 125bp)				
Forward	TGG AAA CGA AGG GGA AAT ACT TC			
Reverse	GCG TCT TCG GTT TCT GTA GC			
Annealing	**Efficiency**	**SD of Intercept**	**Limit of Detection (ng)**	**Limit of Quantification (ng)**
62°C	104.55039	0.44484626	**1.467992657**	**4.448462596**
Primer set for *CD19* (Amplicon 125bp)				
Forward	GTA GTG TTG CCA TGG TTA CAG T			
Reverse	AGT GAG GAT GCT TCA GTC AGA			
Annealing	**Efficiency**	**SD of Intercept**	**Limit of Detection (ng)**	**Limit of Quantification (ng)**
62°C	92.888664	1.005285915	**3.317443519**	**10.05285915**
Primer set for *CD28* (Amplicon 125bp)				
Forward	GCA CGA GAC TTT GCA GCC TAC			
Reverse	CCG GCT GAA GAT GAG GCA GTC			
Annealing	**Efficiency**	**SD of Intercept**	**Limit of Detection (ng)**	**Limit of Quantification (ng)**
64°C	104.36115	0.892556744	**2.945437254**	**8.925567436**
Primer set for *CD45* (Amplicon 123bp)				
Forward	GTA CGA CAT CAT TGC CAG CAT			
Reverse	GTG GAA TTC GCC TCC TGT TG			
Annealing	**Efficiency**	**SD of Intercept**	**Limit of Detection (ng)**	**Limit of Quantification (ng)**
64°C	105.50664	0.239286223	**0.789644536**	**2.392862231**

Results

Pre-screening Antibody Cross-Reactivity

Jamaican fruit bat CD3ε protein homology from BLOSUM62 analysis indicated 71.63% homology with human CD3ε and indicated 72% homology with mouse CD19 across all isoforms (**Figure 3.2**). Phylogenetic analysis indicated Jamaican fruit bats were the second closest to human and mouse CD3ε, and Jamaican fruit bats were fourth closest to human and mouse CD19 of the bat species included in the analysis (**Figure 3.3**). Phyre2 protein modeling of human and Jamaican fruit bat CD3ε with a secondary BLOSUM62 analysis between the two proteins extracellular domains identified 48 identical sites or 44.4%, and a homology of 63.9%; the cytoplasmic domains of the two CD3ε proteins had 50 identical sites or 89.3%, and a homology of 89.3% (**Figure 3.4**). Phyre2 protein modeling of CD19 mouse and Jamaican fruit bat CD19 with a secondary BLOSUM62 analysis between the two proteins indicated 137 identical extracellular site or 49.6%, and a homology of 62.3%; the cytoplasmic domains of the two proteins indicated 160 identical sites or 64.0%, and a homology of 71.2% (**Figure 3.5**).

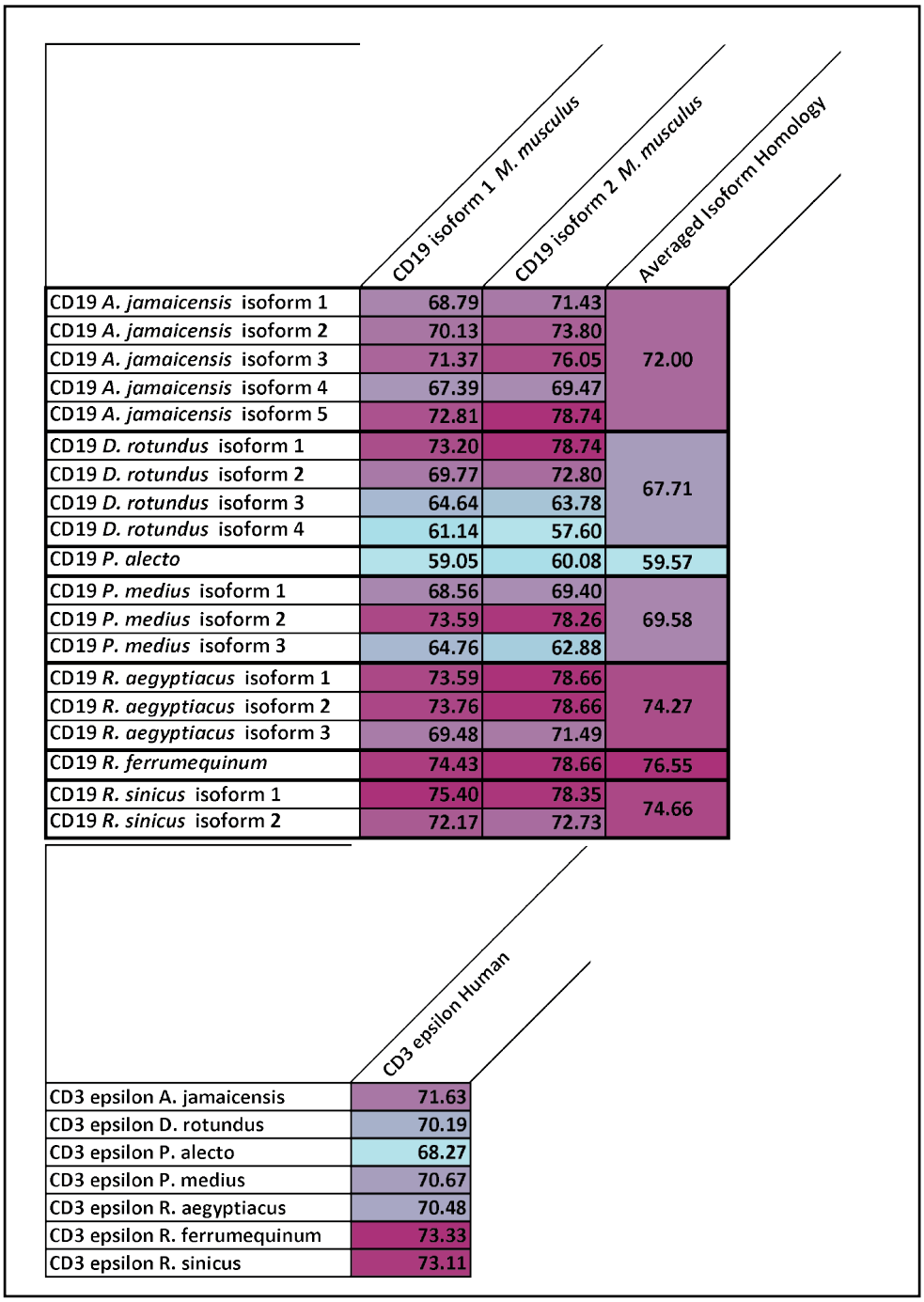

	CD19 isoform 1 *M. musculus*	CD19 isoform 2 *M. musculus*	Averaged Isoform Homology
CD19 *A. jamaicensis* isoform 1	68.79	71.43	72.00
CD19 *A. jamaicensis* isoform 2	70.13	73.80	
CD19 *A. jamaicensis* isoform 3	71.37	76.05	
CD19 *A. jamaicensis* isoform 4	67.39	69.47	
CD19 *A. jamaicensis* isoform 5	72.81	78.74	
CD19 *D. rotundus* isoform 1	73.20	78.74	67.71
CD19 *D. rotundus* isoform 2	69.77	72.80	
CD19 *D. rotundus* isoform 3	64.64	63.78	
CD19 *D. rotundus* isoform 4	61.14	57.60	
CD19 *P. alecto*	59.05	60.08	59.57
CD19 *P. medius* isoform 1	68.56	69.40	69.58
CD19 *P. medius* isoform 2	73.59	78.26	
CD19 *P. medius* isoform 3	64.76	62.88	
CD19 *R. aegyptiacus* isoform 1	73.59	78.66	74.27
CD19 *R. aegyptiacus* isoform 2	73.76	78.66	
CD19 *R. aegyptiacus* isoform 3	69.48	71.49	
CD19 *R. ferrumequinum*	74.43	78.66	76.55
CD19 *R. sinicus* isoform 1	75.40	78.35	74.66
CD19 *R. sinicus* isoform 2	72.17	72.73	

	CD3 epsilon Human
CD3 epsilon A. jamaicensis	71.63
CD3 epsilon D. rotundus	70.19
CD3 epsilon P. alecto	68.27
CD3 epsilon P. medius	70.67
CD3 epsilon R. aegyptiacus	70.48
CD3 epsilon R. ferrumequinum	73.33
CD3 epsilon R. sinicus	73.11

Figure 3.2) BLOSUM62 alignment homology of human, mouse (*Mus musculus*), Jamaican fruit bat, common vampire bat (*Desmodus rotundus*), Chinese horseshoe bat (*Rhinolophus sinicus*), greater horseshoe bat (*Rhinolophus ferrumequinum*), Egyptian fruit bat (*Rousettus aegyptiacus*), Indian flying fox (*Pteropus giganteus*), and black flying fox (*Pteropus alecto*) for all CD3ε, CD3γ, and CD19 protein isoforms. Colorimetric shading indicating high homology (magenta) and low homology (cyan).

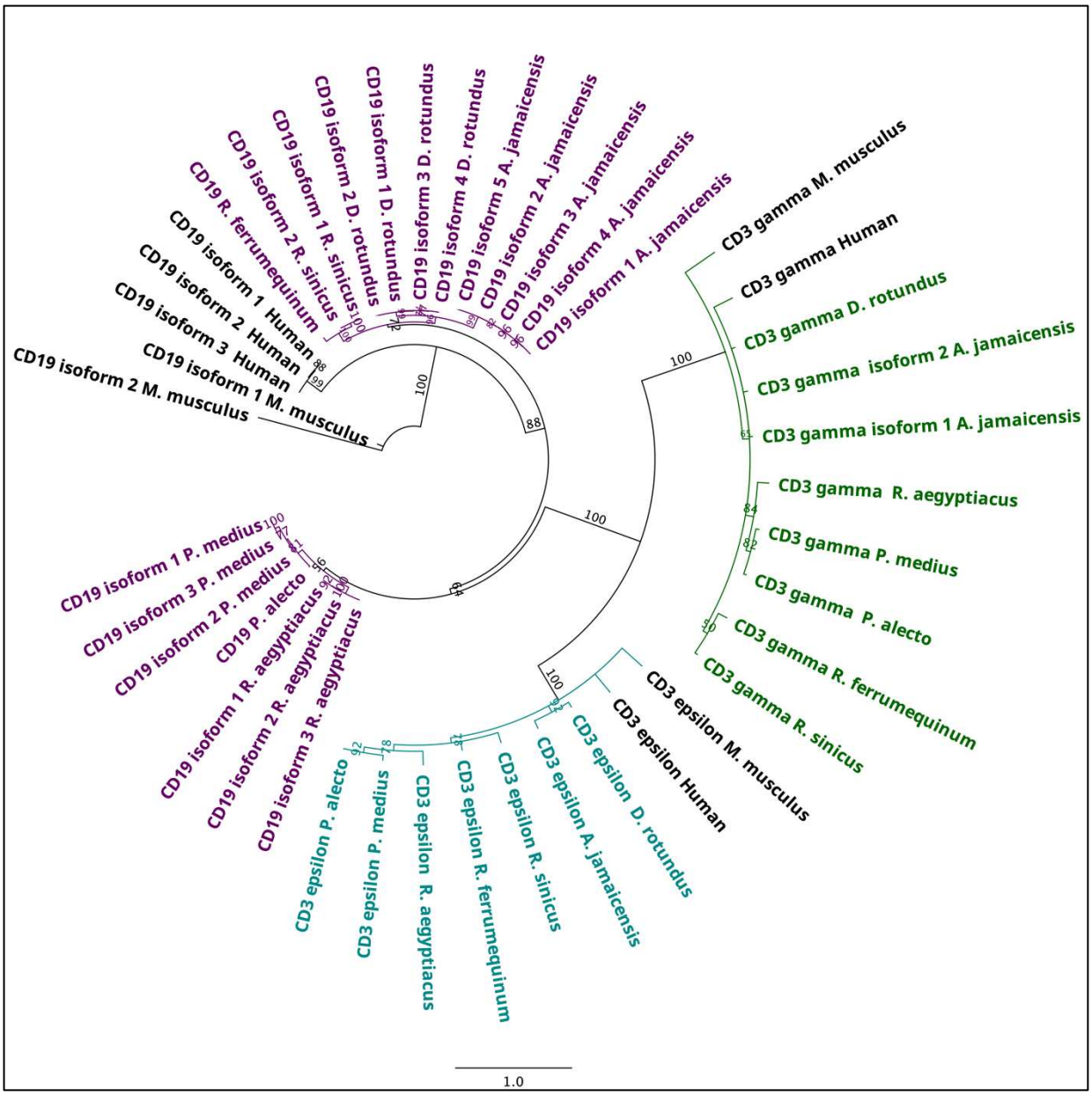

Figure 3.3) Unrooted phylogenetic tree generated from BLOSUM62 alignment of human, mouse (*Mus musculus*), Jamaican fruit bat, common vampire bat (*Desmodus rotundus*), Chinese horseshoe bat (*Rhinolophus sinicus*), greater horseshoe bat (*Rhinolophus ferrumequinum*), Egyptian fruit bat (*Rousettus aegyptiacus*), Indian flying fox (*Pteropus giganteus*), and black flying fox (*Pteropus alecto*) for all CD3ε, CD3γ, and CD19 protein isoforms.

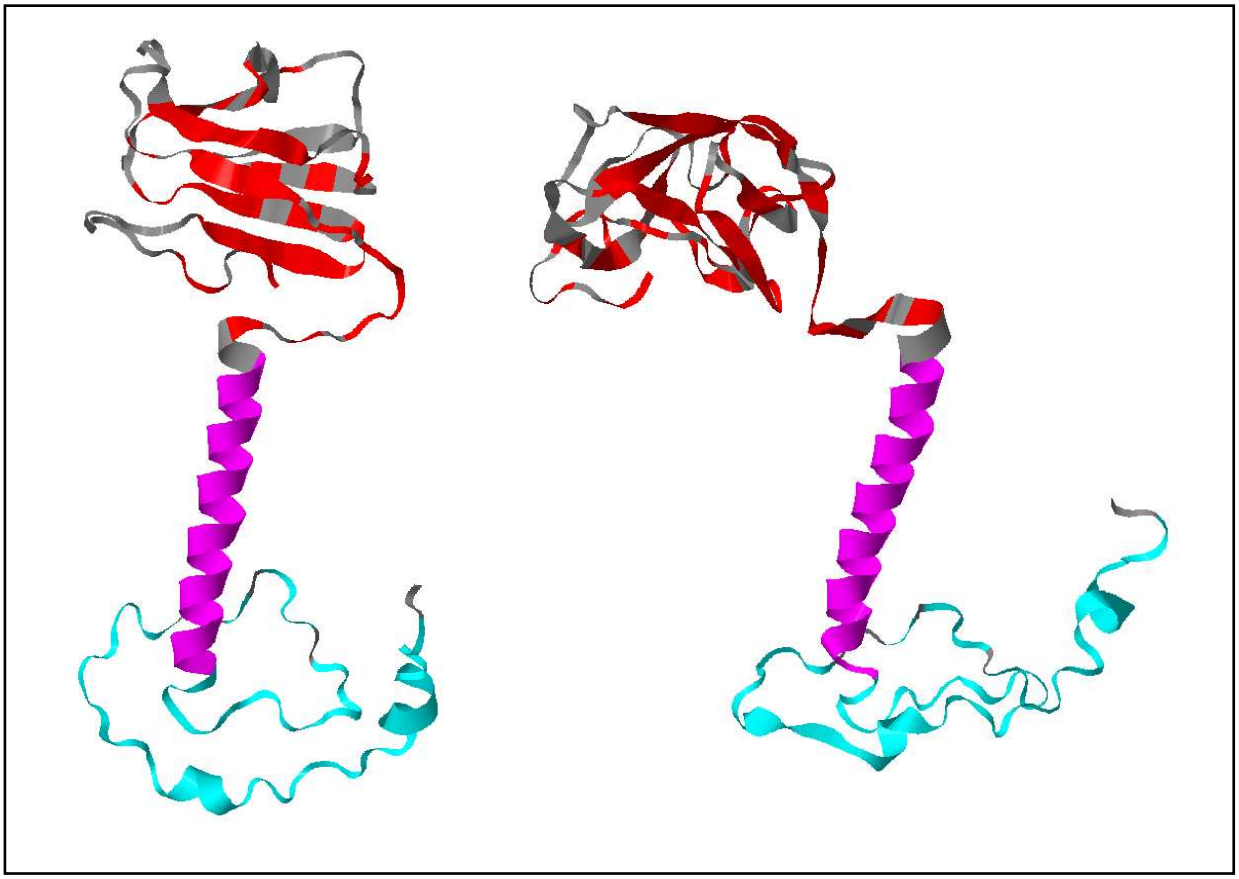

Figure 3.4) Human CD3ε (left) and Jamaican fruit bat CD3ε (right) three-dimensional models and protein homology. Three-dimensional models were generated with PHYR[2]; human (NCBI accession NP_000724) Jamaican fruit bat (NCBI accession XP_037003230). Transmembrane domains (magenta) and signal peptides (removed) were not included in the BLOSUM62 analysis. Human CD3ε and Jamaican fruit bat CD3ε had 48 identical extracellular sites (red) or 44.4% of the extracellular domain, and a homology of 63.9%. There were 50 identical cytoplasmic sites (cyan) or 89.3% of the cytoplasmic domain, and a homology of 89.3%.

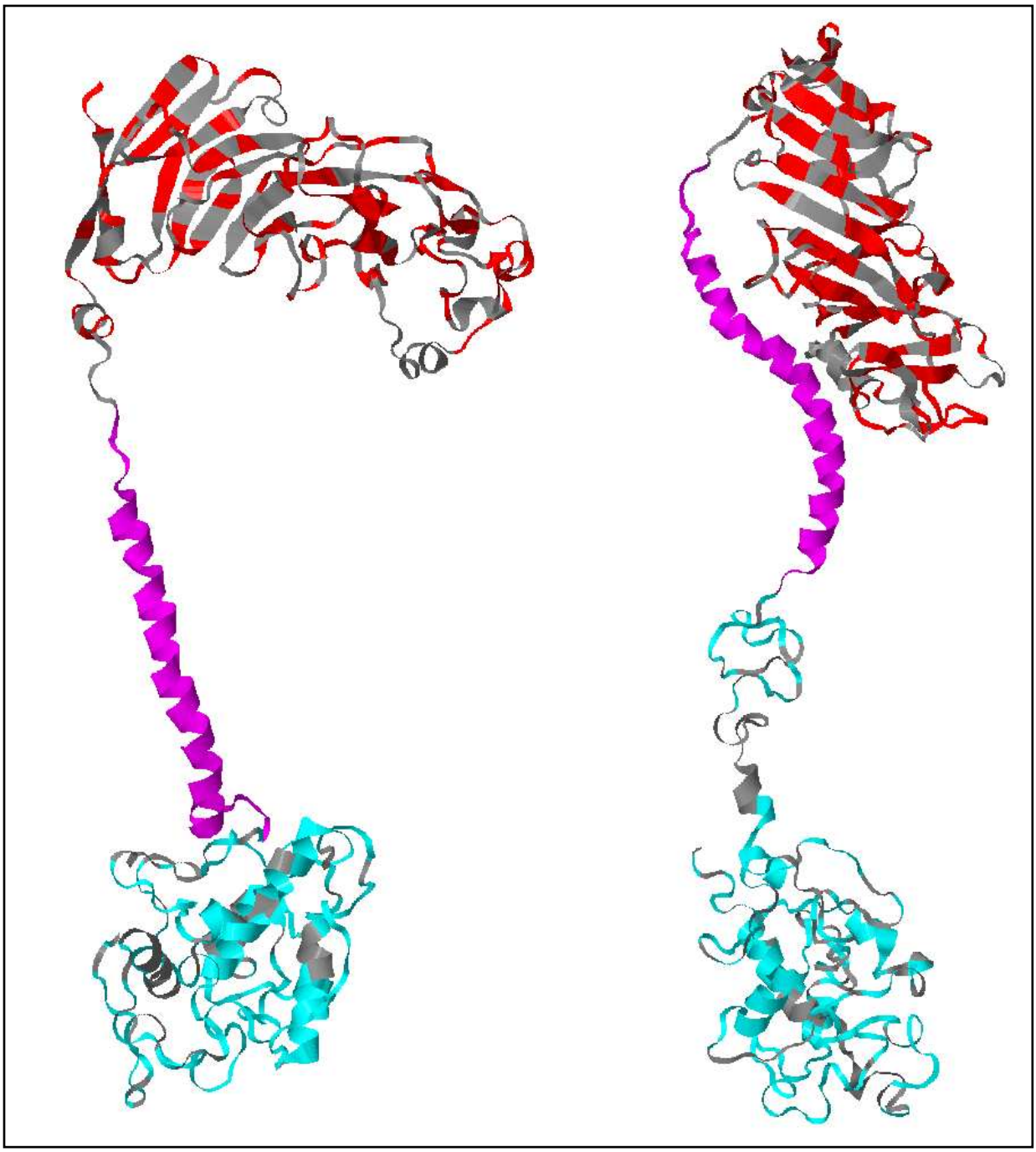

Figure 3.5) Mouse CD19 and Jamaican fruit bat CD19 three-dimensional models and protein homology. Three-dimensional models were generated with PHYR[2]; mouse (NCBI accession AAA37390) Jamaican fruit bat (NCBI accession XP_036995935). Transmembrane domains (magenta) and signal peptides (removed) were not included in the BLOSUM62 analysis. BLOSUM62 analysis between mouse and Jamaican fruit bat CD19 proteins indicated 137 identical extracellular sites (red) or 49.6%, and a homology of 62.3%; the cytoplasmic domains of the two proteins indicated 160 identical sites (cyan) or 64.0%, and a homology of 71.2%.

Immunofluorescent Validation of Antibody Reactivity and Anatomical Mapping of Immune Cells

Montage imaging of entire intestinal sections of Jamaican fruit bats with CD3ε, CD3γ, and CD19 reveals specific populational dynamics and anatomical localization of respective cell types (**Figure 3.6A**). $CD19^{+}$ positive populations within lamina propria, sub-epithelial, and mucosal populations display diffuse staining. Colocalization of cellular staining show unique CD3ε, CD3γ, and CD19 positive cells that are distinct from CD3ε and CD3γ positive cells (**Figure 3.6B-G**).

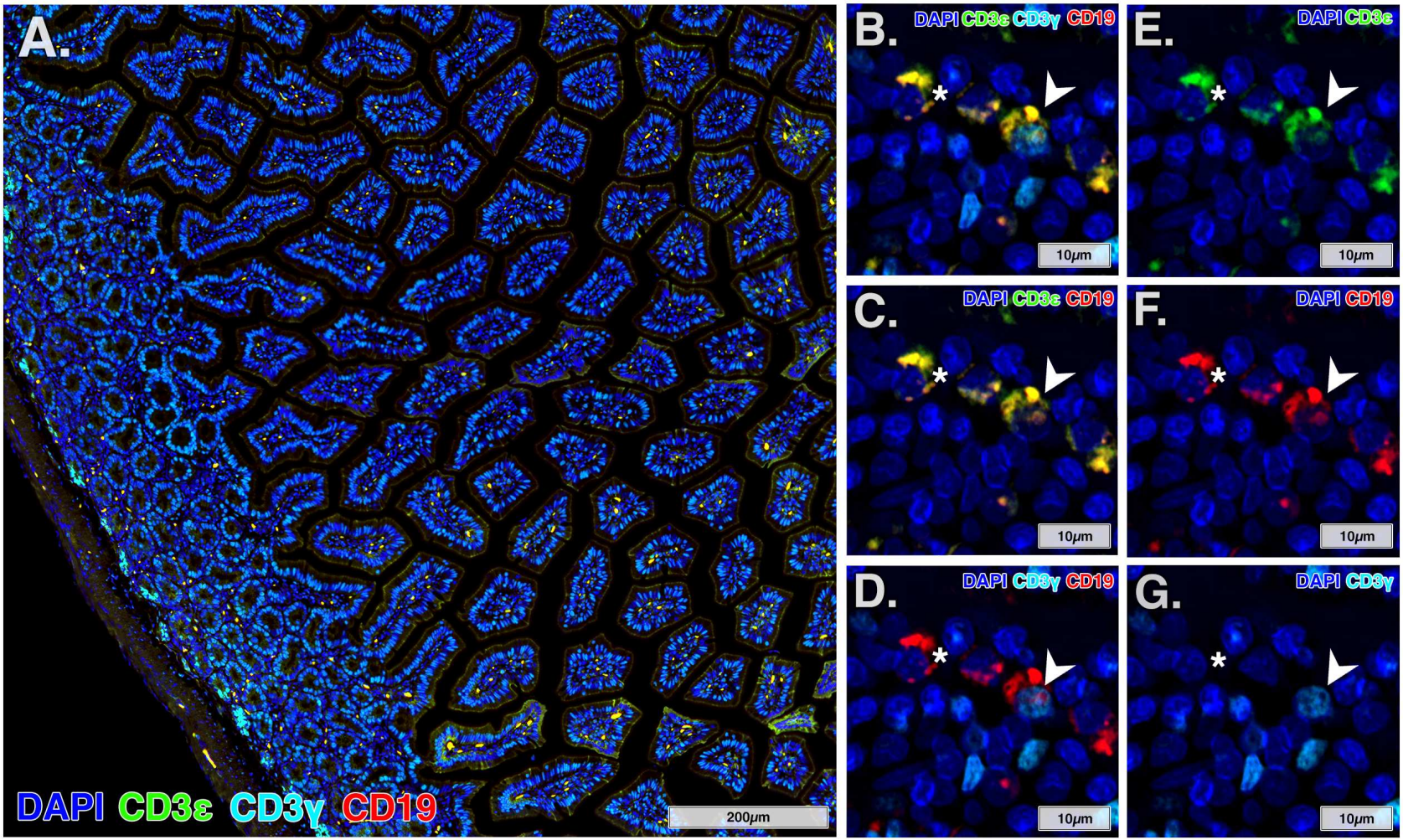

Figure 3.6) Fluorescent immunophenotyping in the small intestine of Jamaican fruit bats. (**A**) Montage imaging of the small intestine of Jamaican fruit bats with CD3ε (green), CD3γ (cyan), and CD19 (red). High magnification imaging showing

Cell Sorting

Cells were enriched by sorting into six categories by a gating strategy (**Figure 3.7**): Not sorted (whole spleen), $CD19^+$, $CD3\varepsilon^+$, $CD3\gamma^+$, and $CD3\varepsilon^+$ $CD3\gamma^+$. Cell counts determined by FACSDiva and RNA yielded by trizol extraction and UV spectrometry for each enriched population can be found in **Table 3.2**. Minimum number of cells sorted was 2,543 and maximum number of cells sorted was 1,243,632. Minimum RNA yield was 245.20 ng and maximum RNA yield was 1,318.15 ng (**Table 3.2**).

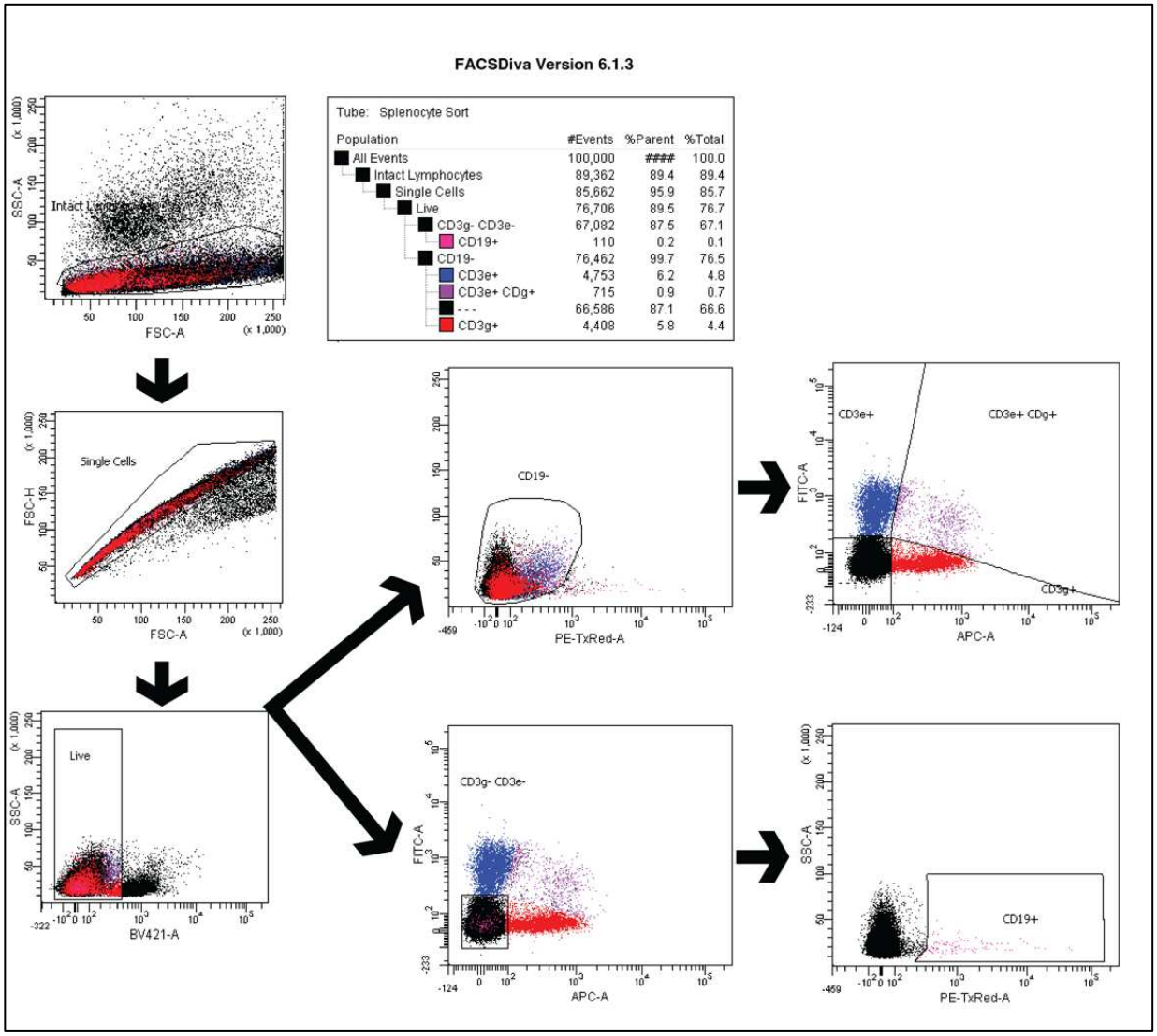

Figure 3.7) Cell Sorting gating strategy. Intact Lymphocytes > Single Cells> Live. Live Cells were then gated for $CD19^{-}$> $CD3\varepsilon^{+}$, $CD3\varepsilon^{+}$ $CD3\gamma^{+}$, $CD3\gamma^{+}$ and $CD3\varepsilon^{-}$ $CD3\gamma^{-}$ > $CD19^{+}$.

Table 3.2) Sorted cell counts and RNA yields.

	Male		**Female**	
	Aj1	**Aj2**	**Aj3**	**Aj4**
Whole Spleen Cells	**~1-2*10^6**	**~1-2*10^6**	**~1-2*10^6**	**~1-2*10^6**
RNA	**892.9ng**	**420.1ng**	**1,318.15ng**	**537.45ng**
CD19+ Cells	**12,538**	**9,432**	**12,056**	**2,543**
RNA	**352.5ng**	**378.8ng**	**256.2ng**	**274.3ng**
CD3ε+ Cells	**442,189**	**776,307**	**1,243,632**	**183,141**
RNA	**748ng**	**246.6ng**	**983.1ng**	**481.4ng**
CD3ε+ Cells	**390,837**	**165,265**	**164,233**	**77,259**
RNA	**382.1ng**	**483.6ng**	**464.9ng**	**914.9ng**
CD3ε+CD3γ+ Cells	**39,035**	**47,138**	**45,730**	**13,452**
RNA	**245.2ng**	**448.7ng**	**574.2ng**	**496.9ng**

Post-Hoc Cell Sorting Analysis

FCS files of *Aj*1-*Aj*4 were concatenated in FlowJo. Concatenated data was gated two ways, either first gating on $CD3\varepsilon^+$, $CD3\gamma^+$, $CD3\varepsilon^+CD3\gamma^+$ followed by CD19 gating, or first gating on $CD19^+$ cells followed by $CD3\varepsilon^+$, $CD3\gamma^+$, and $CD3\varepsilon^+CD3\gamma^+$ gating. This demonstrated that $CD3\varepsilon^+$ cells had minimal $CD19^+$ cells 0.073%. $CD3\varepsilon^+CD3\gamma^+$ cells had 1% $CD19^+$ cells. $CD3\gamma^+$ cells had 17% $CD19^+$ cells. $CD19^+$ cells contained 2.23% $CD3\varepsilon^+$ cells, 3.79% $CD3\varepsilon^+CD3\gamma^+$ cells, 30.1% $CD3\gamma^+$ cells, and 63.8% $CD3\varepsilon^-CD3\gamma^-$ cells (**Figures 3.8 and 3.9**).

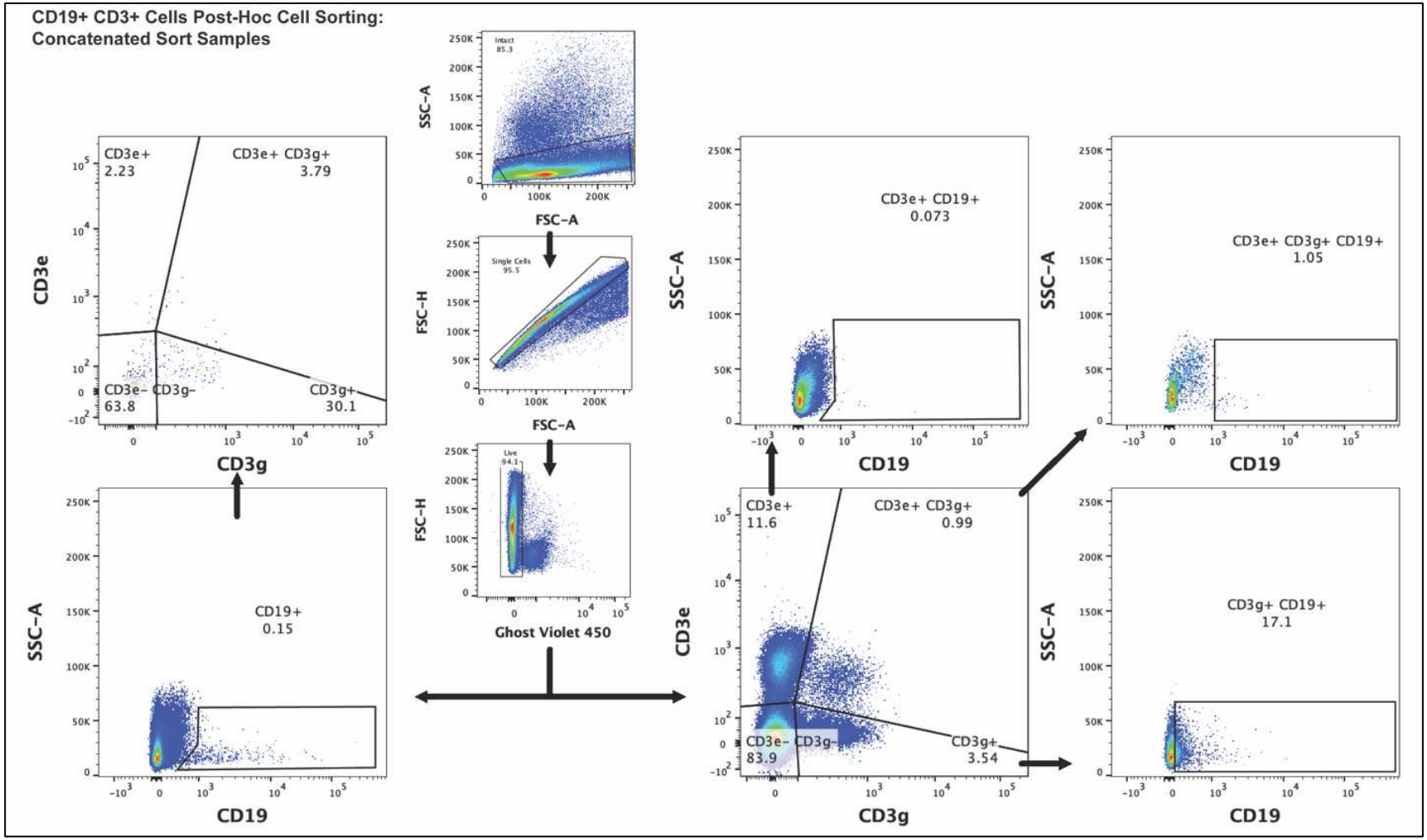

Figure 3.8) Post-hoc $CD19^{+}CD3\varepsilon^{+}$ cells of concatenated sorted FCS files of all 4 bats.

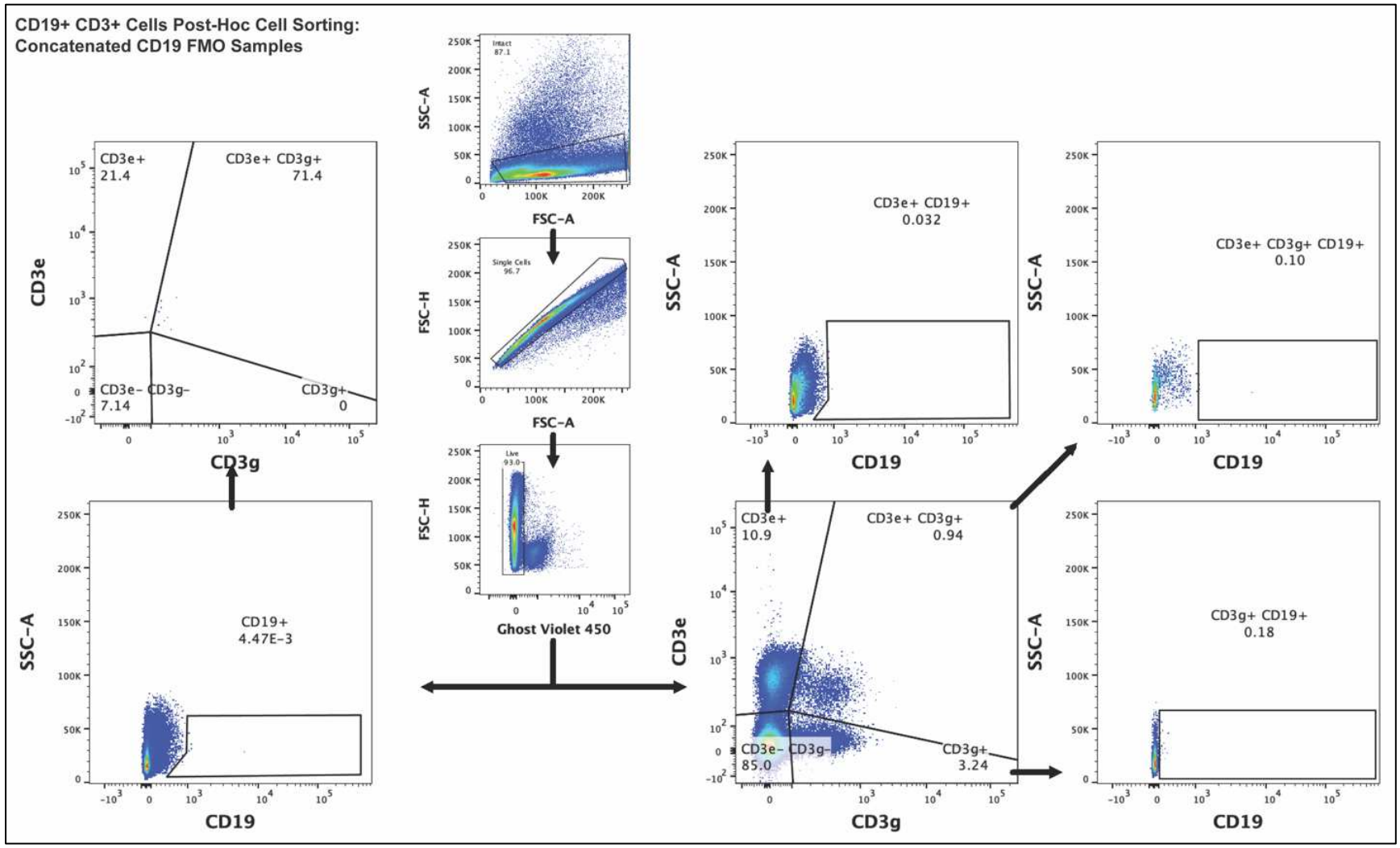

Figure 3.9) Post-hoc $CD19^{+}CD3\varepsilon^{+}$ cells of concatenated CD19 FMO FCS files of all 4 bats.

Validation of Antibodies by RT-qPCR

The CD3ε$^+$ enriched population ordinary one-way ANOVA analysis reported significant increase for *Cd3ε* (p=0.0010), *Cd3γ* (p<0.0001), *Cd4* (p=0.0062), and *Cd28* (p=0.0102) genes. The CD3ε$^+$ enriched population ordinary one-way ANOVA analysis reported significant decrease in *Cd19* (p<0.0001) gene. (**Figure 3.10**). When grouped by sex, the CD3ε$^+$ enriched population showed significant increased gene expression for *Cd3ε*

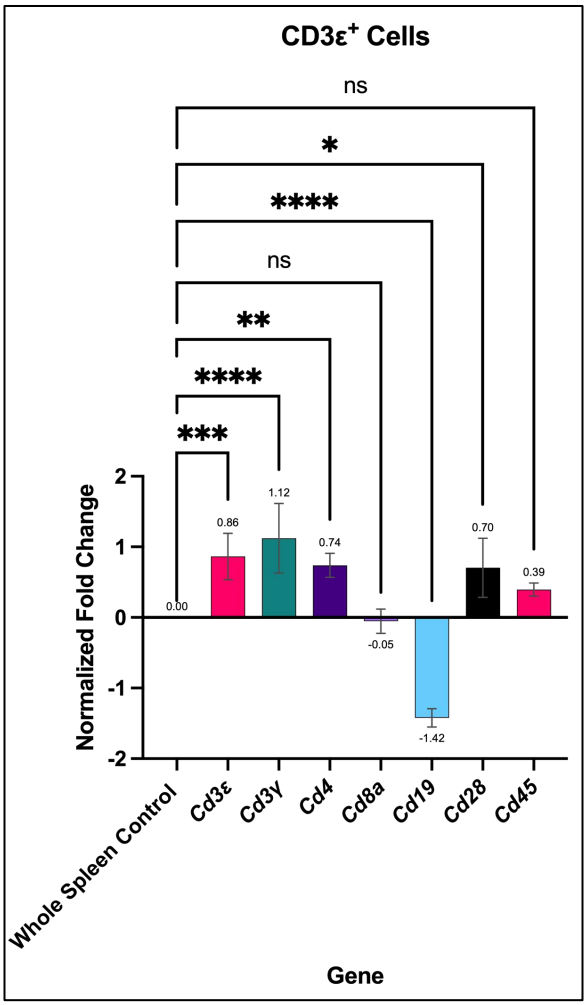

Figure 3.10) Normalized fold change of RT-qPCR array of CD3ε$^+$ sorted cells. Generated by GraphPad Prism V 9.4.1 Ordinary one-way ANOVA V 9.4.1 Ordinary one-way ANOVA.

(♀, p<0.0001), *Cd3γ* (♀, p<0.0001), *Cd4* (♂, p=0.0040), *Cd28* (♀, p<0.0001), *CD45*(♀, p=0.0293) genes, and a significant decreased gene expression for *Cd19* (♂, p<0.0001 and ♀, p<0.0001) (**Figure 3.11**).

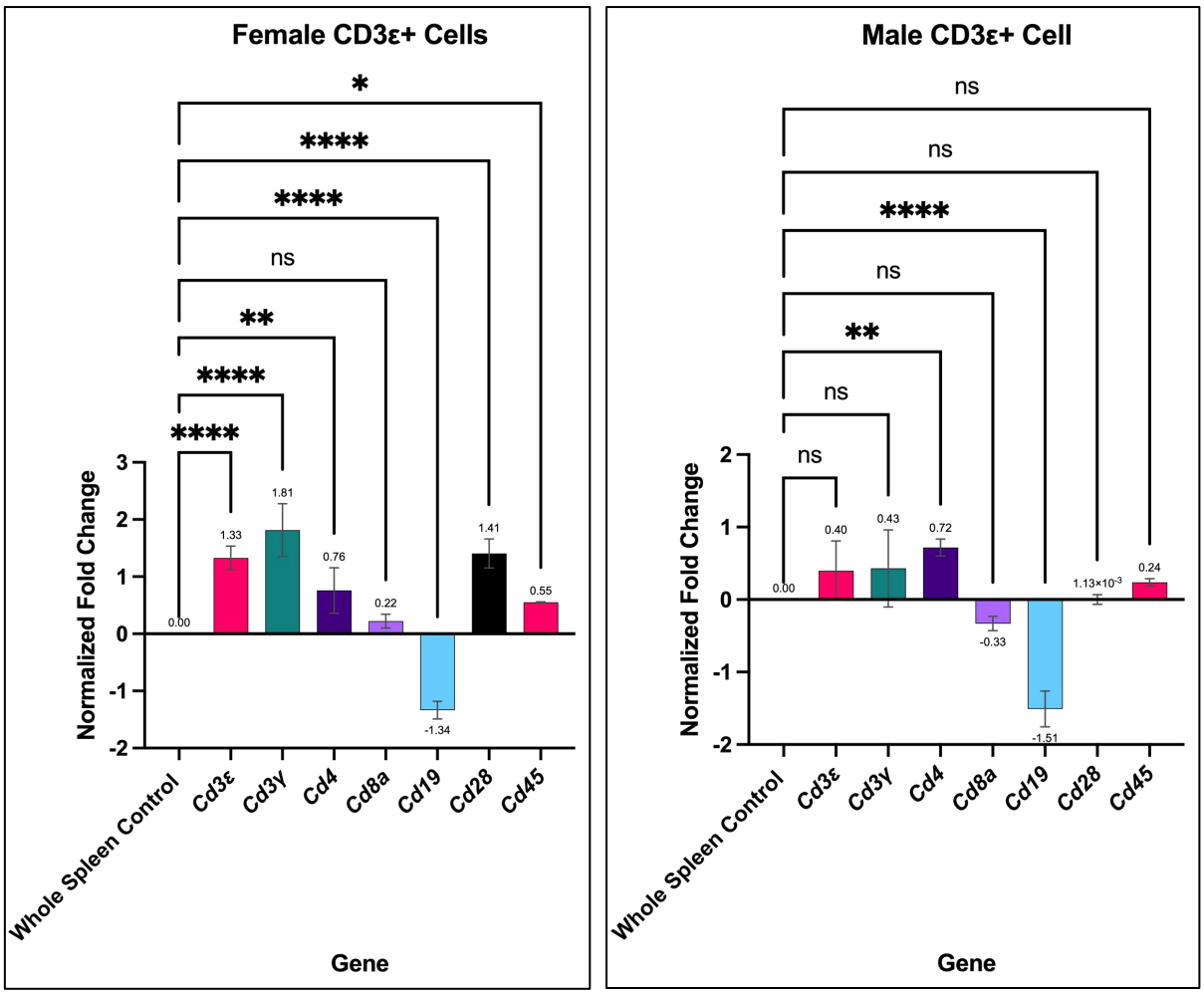

Figure 3.11) Normalized fold change of RT-qPCR array of CD3ε^{+} sorted cells grouped by sex, females (left) males (right). Generated by GraphPad Prism V 9.4.1 Ordinary one-way ANOVA.

The CD3γ$^+$ enriched population ordinary one-way ANOVA analysis reported significant increase for *Cd3ε* (p<0.0001), *Cd3γ* (p<0.0001), *Cd8a* (p=0.0104), and *Cd28* (p<0.0001) genes compared to whole spleen control (**Figure 3.12**). When grouped by sex, the CD3ε$^+$ enriched population showed significant increased gene expression for *Cd3ε* (♂, p<0.0001 and ♀, p=0.0030), *Cd3γ* (♂, p<0.0001 and ♀, p<0.0001), *Cd8α* (♀, p=0.0012), *Cd28* (♂, p<0.0001 and ♀, p<0.0001) genes compared to whole spleen control, and a decreased gene expression trend for *Cd19* (♂) (**Figure 3.13**).

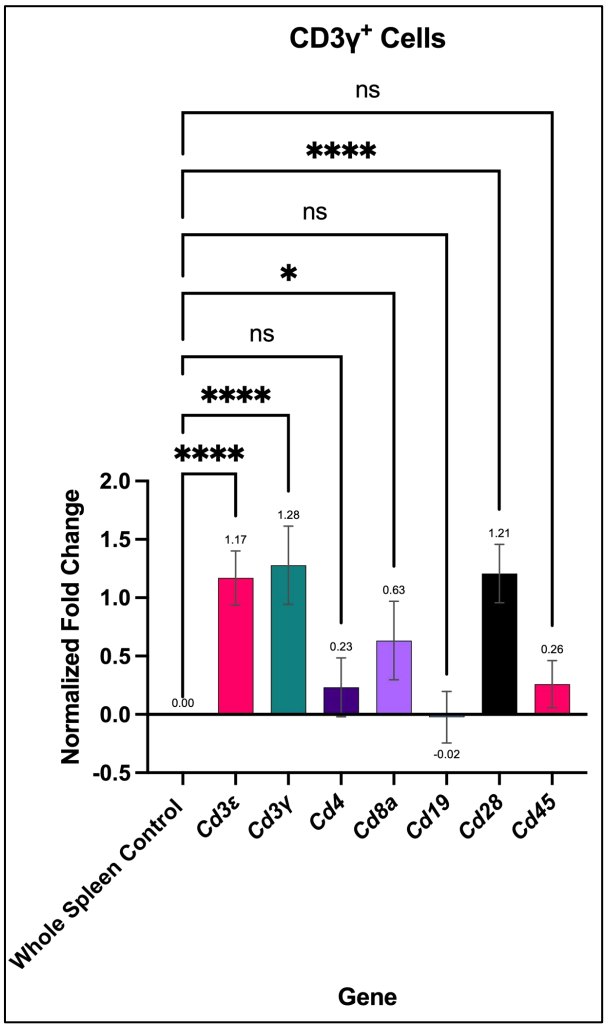

Figure 3.12) Normalized fold change of RT-qPCR array of CD3γ$^+$ sorted cells. Generated by GraphPad Prism V 9.4.1 Ordinary one-way ANOVA.

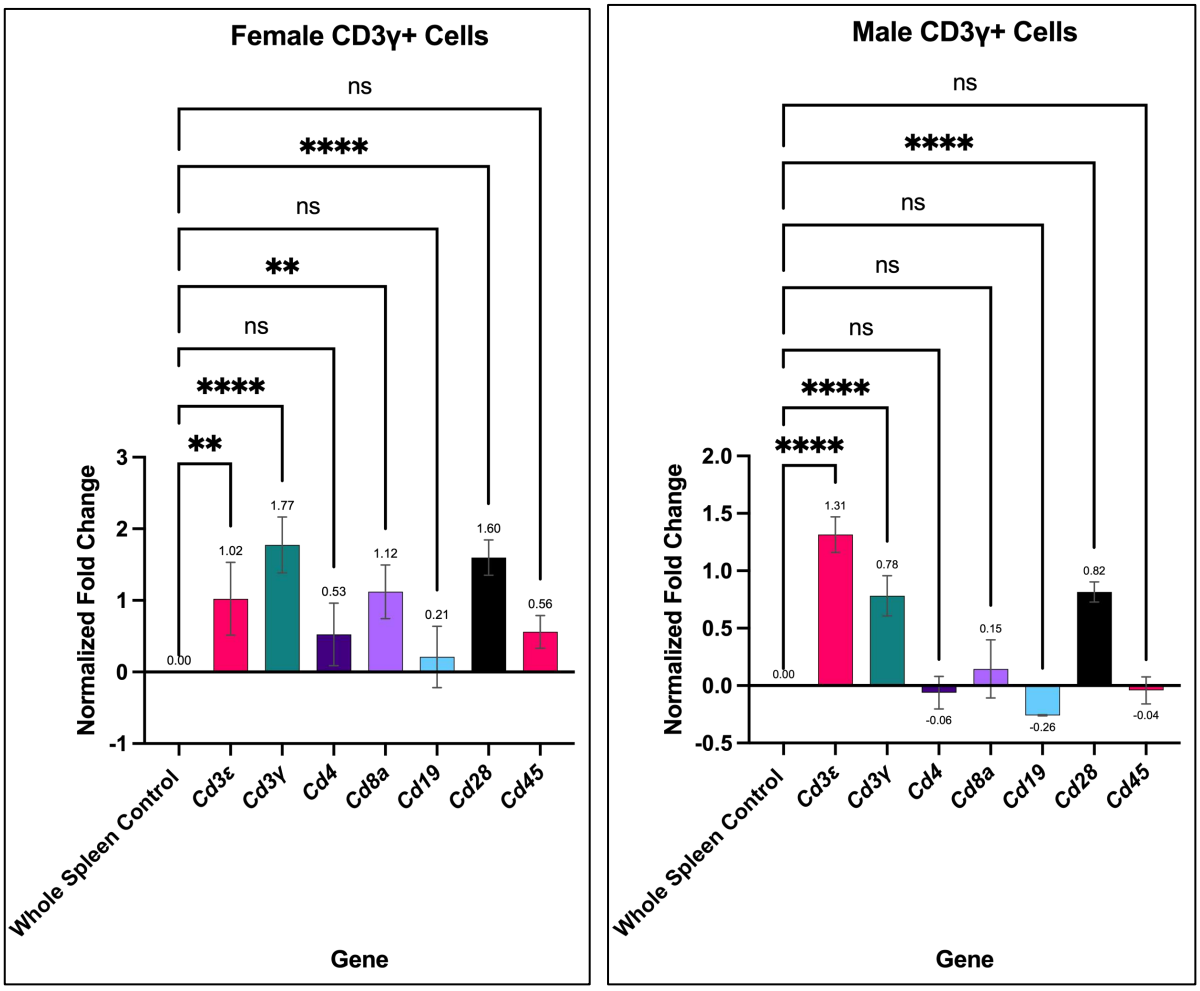

Figure 3.13) Normalized fold change of RT-qPCR array of CD3γ^{+} sorted cells grouped by sex, females (left) males (right). Generated by GraphPad Prism V 9.4.1 Ordinary one-way ANOVA.

The CD3ε$^+$ CD3γ$^+$ enriched population ordinary one-way ANOVA analysis reported significant increase for *Cd3ε* (p<0.0001), *Cd3γ* (p<0.0001), *Cd4* (p<0.0001), *Cd8a* (p<0.0001), *Cd28* (p<0.0001), and *Cd45* (p=0.0057) genes compared to whole spleen control with a decreased gene expression trend for *Cd19*. (**Figure 3.14**). When grouped by sex, the CD3ε$^+$ CD3γ$^+$enriched population showed significant increased gene expression for *Cd3ε* (♂, p<0.0001 and ♀, p<0.0001), *Cd3γ* (♂, p<0.0001 and ♀, p<0.0001), *Cd4* (♂, p<0.0001 and ♀, p<0.0001), *Cd8α* (♂, p<0.0001 and ♀, p<0.0001), *Cd28* (♂, p<0.0001 and ♀, p<0.0001), *CD45* (♂, p=0.0382 and ♀, p<0.0001) genes compared to whole spleen

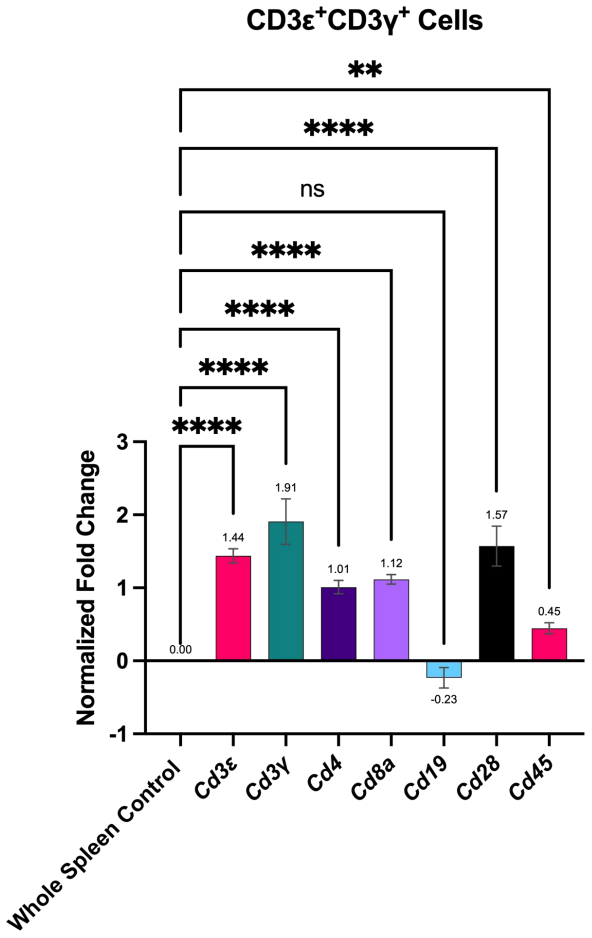

Figure 3.14) Normalized fold change of RT-qPCR array of CD3ε$^+$CD3γ$^+$ sorted cells. Generated by GraphPad Prism V 9.4.1 Ordinary one-way ANOVA.

control, and a significant decreased gene expression for *Cd19* (♂, p=0.0040) compared to whole spleen control (**Figure 3.15**).

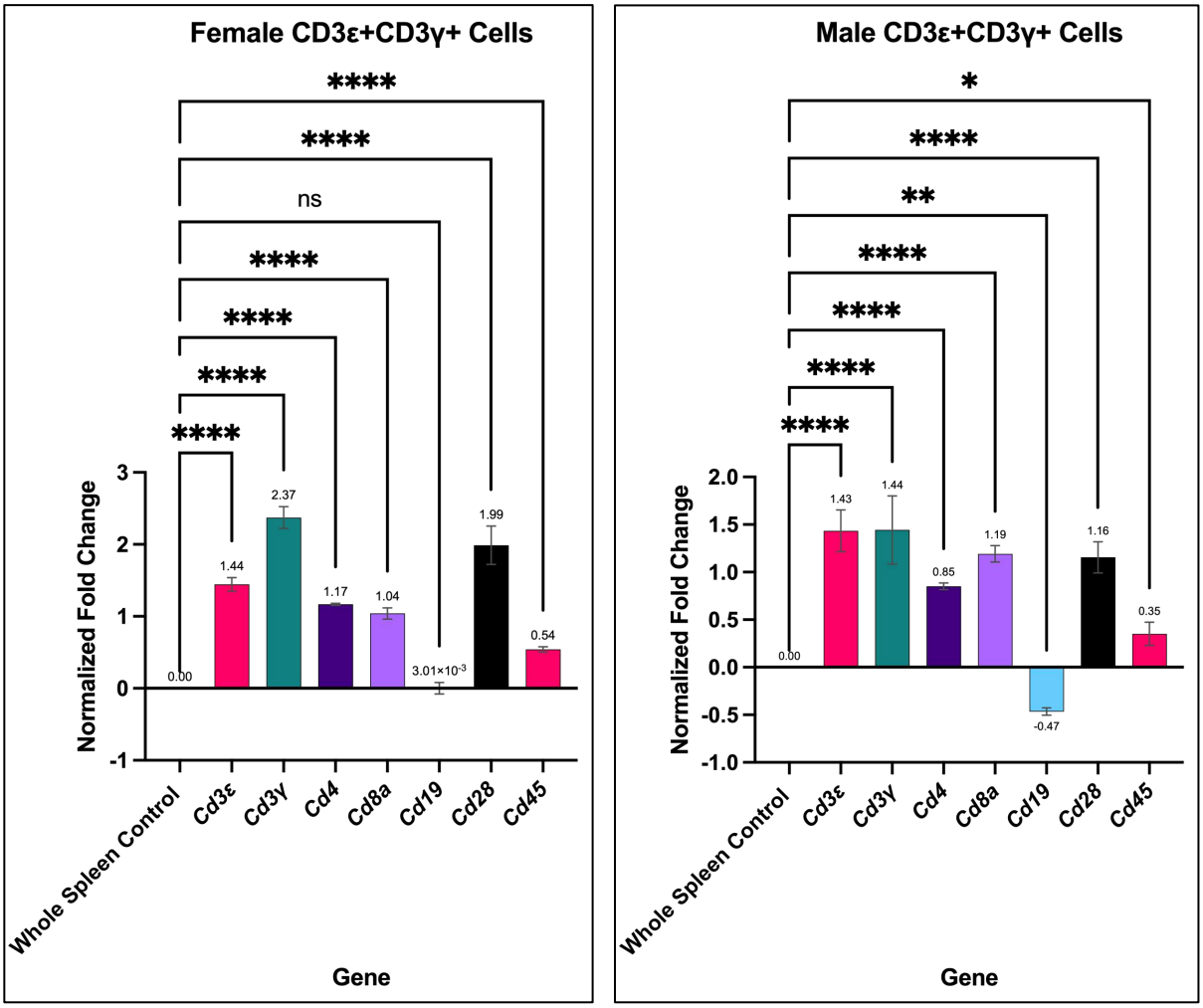

Figure 3.15) Normalized fold change of RT-qPCR array of CD3ε^{+}CD3γ^{+} sorted cells grouped by sex, females (left) males (right). Generated by GraphPad Prism V 9.4.1 Ordinary one-way ANOVA.

The CD19^{+} enriched population ordinary one-way ANOVA analysis reported significant increase for *Cd3ε* (p<0.0001), *Cd3γ* (p<0.0001), *Cd19* (p=0.0020), and *Cd28* (p<0.0001) genes compared to whole spleen control (**Figure 3.16**). When grouped by sex,

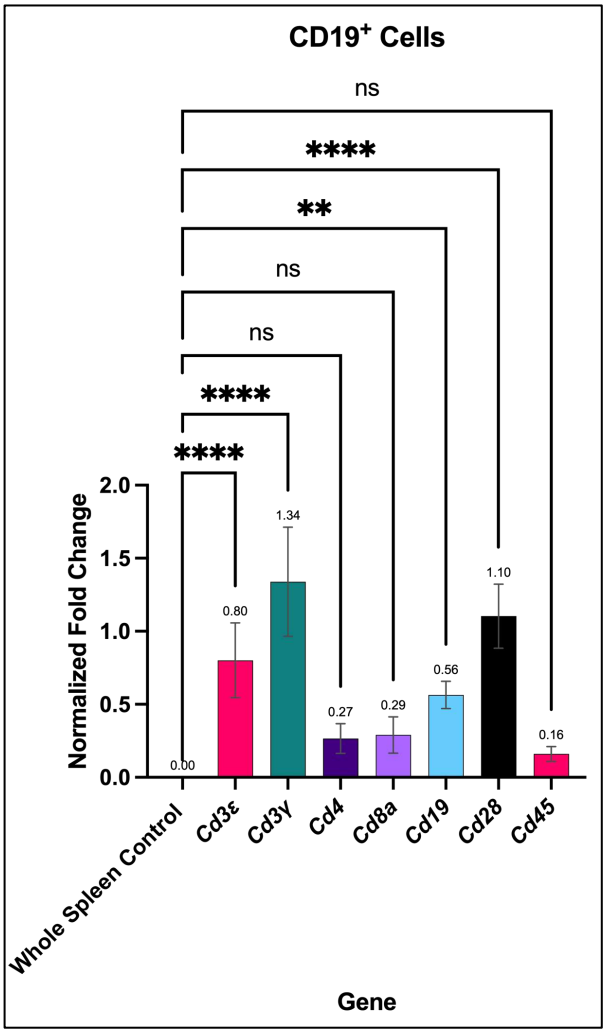

Figure 3.16) Normalized fold change of RT-qPCR array of CD19^{+} sorted cells. Generated by GraphPad Prism V 9.4.1 Ordinary one-way ANOVA.

the CD19^{+} enriched population showed significant increased gene expression for *Cd3ε* (♂, p=0.0097 and ♀, p<0.0001), *Cd3γ* (♂, p=0.0007 and ♀, p<0.0001), *Cd4*(♀, p=0.0025), *Cd8a* (♀, p=0.0022), *Cd19* (♂, p=0.002 and ♀, p=0.0047), and *Cd28* (♂, p=0.0016 and ♀, p<0.0001) genes compared to whole spleen control (**Figure 3.17**).

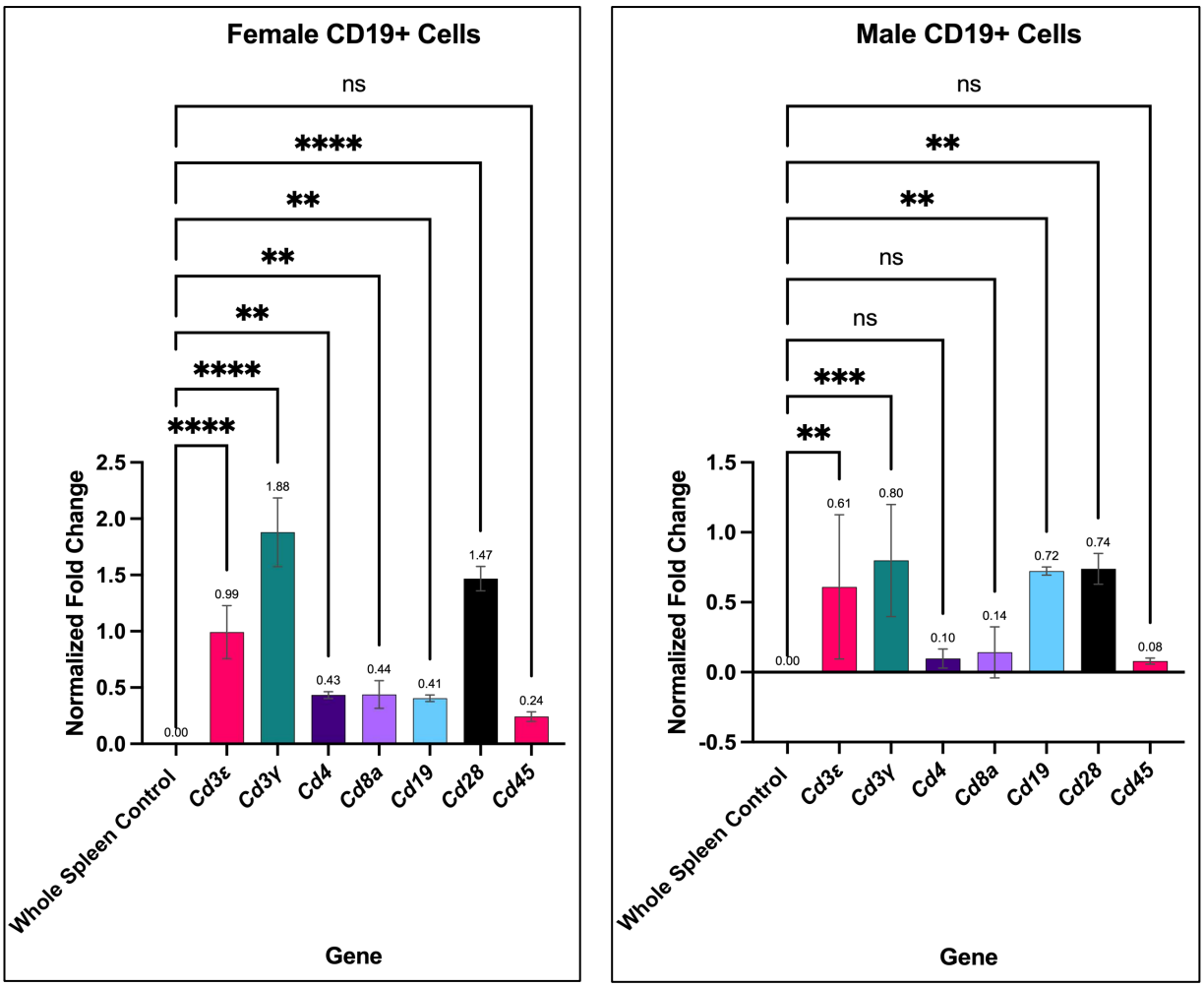

Figure 3.17) Normalized fold change of RT-qPCR array of CD19+ sorted cells grouped by sex, females (left) males (right). Generated by GraphPad Prism V 9.4.1 Ordinary one-way ANOVA.

Discussion

The lack of adequate reagents available to identify immunological cells in bats remains a limiting factor in the proper characterization of these animals. Furthermore, the lack of immunological reagents for bats constrains the use of high throughput technologies such as flow cytometry, cell sorting, and highly quantitative data and anatomical determination from fluorescent microscopy. This impedes an understanding of how bats are capable of hosting viruses that cause a substantial disease burden in humans, such as SARS-CoV-2, Marburg virus and Nipah virus. To begin to address some of these challenges, we established a breeding colony of Jamaican fruit bats (*Artibeus jamaicensis*) for use in the study of bat-borne viral infections. Although many studies of wild and captive bats have shed light on the virology of infection, few have examined bat immune responses to viruses and nearly all of those that did, examined the innate responses *in vitro*. To date, investigations into the adaptive immune systems of bats have not been conducted, principally due to the lack of validated reagents. We have identified and developed such reagents that will permit detailed examination of bat adaptive immune responses to viruses. In this study we have identified commercially available cross-reactive antibodies for the following Jamaican fruit bat epitopes: CD3ε (clones: Hit3a and OKT3), and CD19. These were identified by pre-screening protein homology *in silico* for cross-reactivity potential, tested via flow cytometry and fluorescent microscopy, validated by cell sorting and RT-qPCR, and have demonstrated cross-reactivity with targeted Jamaican fruit bat epitopes. Furthermore, we produced monoclonal antibodies against two Jamaican fruit bat antigens: CD3γ and CD4.

It is interesting that CD3ε$^+$ cells with a significantly higher *Cd4* gene expression in conjunction with significant increases for Cd3ε, Cd3γ, and Cd28 suggests that CD3ε$^+$ cells of Jamaican fruit bats are principally CD4 T helper cells (**Figure 3.10**). In contrast to CD3ε$^+$ cells, CD3γ$^+$ cells had significantly higher *Cd8a* gene expression (**Figure 3.12**). Additionally, CD3γ$^+$ cells, had a significantly higher gene expression of *Cd3ε, Cd3γ,* and *Cd28* implies that CD3γ+ cells are primarily CD8 cytotoxic T cells (**Figure 3.12**). For the CD3ε$^+$ CD3γ$^+$ splenocyte population, RT-qPCR gene expression increases for *Cd3ε*, *Cd3γ*, *Cd4*, *Cd8a*, *Cd28*, and *Cd45* (**Figure 3.14**). As such, CD3ε$^+$ CD3γ$^+$ splenocyte population of Jamaican fruit bat T cells implicate canonical CD4 and CD8 T cell populations.

Normal human spleens contain 31±9% CD3ε$^+$ cells [150] and normal mouse spleens contain roughly 30% CD3ε$^+$ cells [151-153]. CD3ε is commonly a marker for T lymphocyte lineage due to the establishment of the TCRαβ, CD3δε, CD3γε dimer stoichiometry 2(ε)/1(δ)/1(γ) – as such CD3ε is the most abundant CD3 chain [154,155]. Compared to human and mouse spleens, containing roughly 30% CD3ε$^+$ T lymphocytes, the four Jamaican fruit bats averaged 11.6% CD3ε$^+$ T lymphocytes. CD3γ$^+$ T lymphocytes accounted for 3.54% of the concatenated FCS files of the Jamaican fruit bat spleens. CD3ε$^+$, CD3γ$^+$, and CD3ε$^+$ CD3γ$^+$ T lymphocytes totaled and averaged across the four Jamaican fruit bats averaged 16.13% (**Figure 3.8**) – half that observed in human and mouse spleens by flow cytometry. Using a cross-reactive intracellular anti-human CD3ε antibody, black flying fox (*Pteropus alecto*) spleens have roughly 15.6% CD3ε$^+$ cells, but no other CD3 chains were targeted for labeling [70]. As such the established TCRαβ, CD3δε, CD3γε dimer stoichiometry 2(ε)/1(δ)/1(γ) in Jamaican fruit bats, and likely other bat species is questionable. Furthermore, the implication of this study calls for the investigation as to why Jamaican fruit bat T lymphocyte

abundance is nearly half that of human and mouse spleens. This could be due to a unique CD3 dimer stoichiometry specific to these animals. However, it is possible that the Jamaican fruit bat T cell populations cannot be visualized with cell surface staining in its entirety without labeling all three CD3 chains. Given this, the assumption currently made about the dimerization of CD3 chains in bats, being similar to that of humans and mice, may lead to inaccurate populational representations of T cells and T cell subsets. The results herein describe that commonly implemented pan-T cell staining using CD3ε would only account for some T cells, were ~3.54% of $CD3^+$ cells would be missed that only stain positive for CD3γ. Likewise, if identification of T cell populations was solely based upon anti-CD3γ, ~11.6% of $CD3^+$ cells would not be detected that only stain positive for CD3ε. As such, anti-CD3δ, anti-CD3ζ, anti-TCRα, and anti-TCRβ antibodies specific for detection in Jamaican fruit bats is needed to accurately and effectively characterize T lymphocyte and other $CD3^+$ cell populations such as natural killer T cells. Natural killer T cells could be identified with the addition of anti-AGM1 and CD161 antibodies [156-159].

Peculiarly, CD19 enriched cell populations reported significant gene increased for *Cd19,* alongside *Cd3ε*, *Cd3γ*, and *Cd28* (**Figure 3.16**). The cell sorting gating strategy attempted to remove $CD3^+$ $CD19^+$ cells by first gating on $CD3\varepsilon^-$ $CD3\gamma^-$ splenocytes (**Figure 3.7**). $CD19^+$ $CD3^+$ cells continued to be found in immunofluorescent staining for microscopy in the intestines (**Figure 3.6**). In concert, three distinct biochemical and molecular detection-based assays (flow cytometry, fluorescent microscopy, and RT-qPCR) uncovered a novel subset of $CD19^+$ $CD3^+$ cells (**Figure 3.6, 3.7, 3.16, and 3.17**). The exact functionality/physiological role of this distinct cell type will be an important topic of research in future studies. These cells may be a subset of T cells rather than a subset of B cells because these $CD19^+$ cells express CD3 proteins as shown by flow

cytometry and immunofluorescent microscopy in combination with statistically significant increased gene expression of *Cd28*, a T cell specific marker, and CD3ε and CD3γ (**Figures 3.16 and 3.17**). In humans, a case of a novel CD19-expressing T cell lymphoma has been documented in a 29 year old male [160]. Additionally, dual positive $CD19^+$ $CD3^+$ CAR T cells have also been identified (Schultz et al., 2020). As such, there is supporting evidence that CD19 expression can occur on T cells even though CD19 expression on T cells is not typical of a homeostatic immune state of humans. The Jamaican fruit bats in this study did not have any anatomical or pathological abnormalities such as cancer. Additionally, bats are a long-lived species and have low incidences of cancer [161,162]. As such, this evidence suggests that this novel subset of $CD19^+$ $CD3^+$ cells are a part of the Jamaican fruit bat homeostatic immune system. The functionality of these $CD19^+CD3^+$ T cells can only be postulated at the moment. However, CD19 associates with CD21 and CD81 on B cells, and it is known that CD21 binds to complement component CD3dg during the opsonization process [21,163,164]. Therefore, it can be hypothesized that these $CD19^+CD3^+$ T cells can recognize pathogens independent of an antigen presenting cell through complement opsonization.

Furthermore, with antibody clones 1D3 anti-CD19 and Hit3a anti-CD3ε demonstrating cross-reactivity with Jamaican fruit bat epitopes it is likely that these clones will cross-react with other bat species as indicated by BLOSUM62 protein homology (**Figures 3.4 and 3.5**). This work will help provide a framework for other researchers in the field of bat immunology to more rigorously test antibody cross-reactivity and help build a more robust body of literature of cross-reactive antibodies.

When the RT-qPCR data were evaluated by sex, female bats had a greater fold change than males in the primary gene of interest. $CD3e^+$ cells from females had a 1.33-fold

increase in *Cd3ε*, whereas males only had a 0.4-fold increase. CD3γ$^+$ cells form females had a 1.77-fold increase in *Cd3γ*, whereas males only had a 0.78-fold increase. CD3ε$^+$CD3γ$^+$ cells from females had a 1.44 *Cd3ε* and 2.37 *Cd3γ* fold increase, whereas males had a 1.43 CD3ε and *Cd3γ* 1.44-fold increase. However, in CD19$^+$ cells males had a greater fold increase in *Cd19* (0.72) than females (0.41). Other sex differences included a 1.4-fold increase in *Cd28* expression in CD3ε$^+$ cells in females but no change in males. CD3γ$^+$ cells had a *Cd8α* 1.12-fold increase in females but only a trending 0.15-fold increase in males. In CD3ε$^+$CD3γ$^+$ cells, *Cd19* had a 0.447-fold decrease in males but no change in females. CD19$^+$ cells had a *Cd28* 1.47-fold increase in females, but only a 0.74 fold increase in males. As such, these sexual dimorphisms could impact the immune responses of male and female Jamaican fruit bats and thereby could impact viral shedding and transmission.

Conclusions and Future Directions

The paucity of bat specific reagents makes cross-reactive validation studies vital to discover commercially available reagents that can be utilized. This study has demonstrated two commercially available antibodies, CD3ε (clone Hit3a, anti-human) and CD19 (clone 1D3, anti-mouse), that positively cross-react with Jamaican fruit bat epitopes. Validation of these antibodies in fresh and fixed tissue allows for their use, with confidence, in flow cytometry assays and microscopy. Validation also provides additional tools to help elucidate the differences in the Jamaican fruit bat homeostatic immune system and immune responses compared to established animal models and clinical research conducted in humans. However, it is to be noted and warrants further study as to why the Jamaican fruit bat splenic $CD3^+$ T-lymphocyte population is nearly half that of humans and mice. Furthermore, this study highlights the need to develop more Jamaican fruit bat specific reagents as it appears that Jamaican fruit bat CD3 dimer stoichiometry might not follow the established and currently accepted ratios represented in humans and mice. There is a continued need for the production of anti-CD3δ, anti-CD3ζ, anti-TCRα, and anti-TCRβ antibodies specific to Jamaican fruit bats to allow for the enhanced and accurate detection, visualization, and characterization of T-lymphocytes and other $CD3^+$ cell populations.

Validation of cellular markers and reagents is a crucial first step in the investigative process that allows for the generation of informed conclusions, in any study, and hold a higher level of immanent need and accuracy in underdeveloped animal models. This same antibody validation methodology can be used to validate other cross-reactive antibodies across various species of bats. Additionally, this methodology can be applied to in-house

generated antibodies. To reiterate, it is of high importance for bat researchers to more rigorously validate and test cross-reactive antibodies to better advance the field of bat immunology. The identification of novel $CD3^+$ $CD19^+$ cells in the gastrointestinal tract and spleen of the Jamaican fruit bat warrants further scrutiny to determine the physiological function and compounding affects that these cells may impose on the immune responses of Jamaican fruit bats.

CHAPTER 4
ANTI-AGM1 IN VIVO TREATMENT OF JAMAICAN FRUIT BATS FOR AGM1^{+} CELL DEPLETION

Summary

Jamaican fruit bats are an underdeveloped animal model, therefore limited characterization of immunomodulatory techniques has been described. Modulating the immune response allows for hypothesis driven research to be performed to elucidate the functionality of immune cell populations and immunoregulatory pathways. One classical immunological experimental technique is to deplete an immune cell population prior to experimental infection to determine the role of that cell population. If an immune cell population is depleted and the animal model demonstrates worsened pathology, this indicates the depleted immune cell population plays a critical role in controlling the infection. If an immune cell population is depleted and the animal model demonstrated no change in pathology, this indicates the depleted immune cell population does not play a critical role in controlling the infection. If an immune cell population is depleted and the animal model demonstrated improvement in pathology, this indicates the depleted immune cell population is responsible for causing pathology. One such method to deplete an immune cell population is use a depleting antibody. Polyclonal anti-asialo-GM1 (AGM1) antibodies have been used to deplete $AGM1^+$ cells, which are principally natural killer cells *in vivo*. Antibody mediated cellular depletion can occur through multiple pathways: antibody-depended cell cytotoxicity (ADCC), complement-depended cytotoxicity (CDC), or opsonization leading to phagocytosis. In this study we sought to use anti-AGM1 treatment as a reagent to modulate the Jamaican fruit bat immune system. We hypothesized that anti-AGM1 *in vivo* treatment would deplete $AGM1^+$ cells in Jamaican fruit bats. Interestingly, anti-AGM1 treatment demonstrated an expansion of AGM1+ cells in Jamaican fruit bats.

Introduction

Jamaican fruit bats are an underdeveloped animal model with limited reagents that allow for the modulation of the immune system. As such, a paucity of bat specific reagents limits hypothesis driven studies from being performed to determine the role of immunomodulatory molecules and immune cell functions in the Jamaican fruit bat. A method for examining the role of a cellular population is to deplete that population *in vivo* using depleting antibodies to determine the role of that population during experimental infection. Anti-AGM1 antibody treatment is a classic example of an immunomodulatory reagent used to deplete $AGM1^+$ cells, which is principally expressed on the surface of natural killer (NK) cells[156,157]. NK cells are a part of the innate immune system and they play a critical role in early control of viral infections [165]. Egyptian fruit bats (*Rousettus aegyptiacus*) have an expansion of KLRC genes, and KLRC are largely expressed by NK cells [143], suggesting that NK cells play a prominent role in bat immune systems. However, studies need to be performed on more species of bats to determine if this is common among the order of chiroptera and not specific immune characteristic to Egyptian fruit bats. Polyclonal anti-AGM1 antibodies were first produced in 1974, and anti-AGM1 antibodies have been used to deplete $AGM1^+$ cells *in vivo* [157,166,167]. Antibody mediated cellular depletion can occur through multiple pathways: antibody-depended cell cytotoxicity (ADCC), complement-depended cytotoxicity (CDC), or phagocytosis[168]. As such, this study was performed to determine if rabbit polyclonal anti-AGM1 *in vivo* treatment would induce $AGM1^+$ cell depletion. Four tissues were analyzed for AGM1 treatment: splenocytes, PBMCs, gastrointestinal lamina propria fraction, and gastrointestinal intraepithelial fraction.

Methods

Dosing Strategy of Jamaican Fruit Bats with Anti-AGM1 Antibody

Four adult Jamaican fruit bats were used for this study, two males and two females. One male and one female were used as a control group and were mock dosed with 1xPBS equal volume to the treatment group. One male and one female were used as the treatment group and were dosed with 170 µg of rabbit polyclonal anti-AGM1 antibody in a volume of 100 µl. The initial dose was administered at day 0 and a second dose was administered at day 3. Bats were euthanized 24 hours after the second dose (**Figure 4.1**).

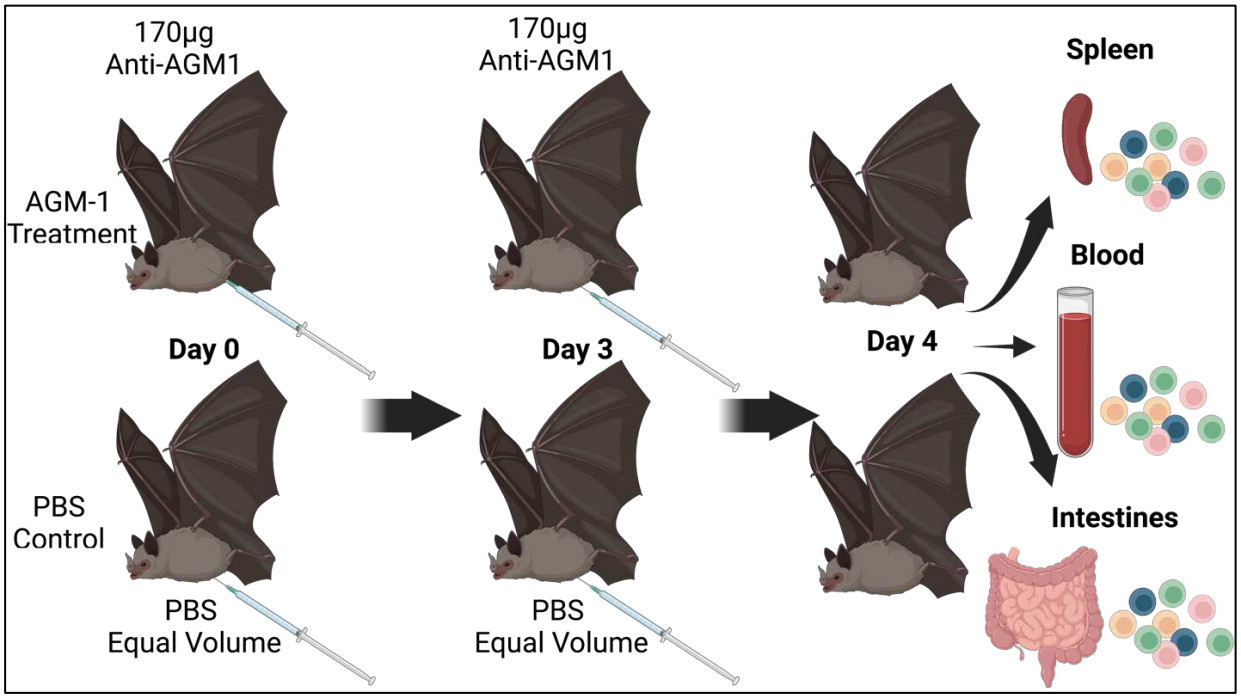

Figure 4.1) Anti-AGM1 dosing strategy of Jamaican fruit bats. Bats were dosed with 170 µg of rabbit polyclonal anti-AGM1 antibody in a volume of 100 µl at day 0, and again at day 3. Mock or PBS control bats were dosed with equal volume of 1xPBS at the same time points. On day 4 bats were euthanized. Blood, spleens, and intestines were harvested and processed into single cell suspensions. Illustration created with BioRender.com.

Flow Cytometry: Tissue Disassociation

Once bats were under general anesthesia, a terminal heart bleed was performed and the blood was incubated in ammonium chloride solution for 10 minutes to lyse red blood cells. Spleens were disassociated through a 70 μm cell strainer. The small and large intestines were processed together using Miltenyi mouse disassociation kit. (Refer to **appendix V** for detailed tissue processing methods used.)

Flow Cytometry: Staining Strategy

Disassociated tissues were first stained with Ghost Red 780 viability stain, followed by Fc block. Then cells were stained with a secondary anti-rabbit IgG (BV421) to determine if $AGM1^+$ cells were depleted. Following the secondary antibody staining, cells were then incubated with primary anti-AGM1 antibody to determine saturation of AGM1 from *in vivo* dosing (**Figure 4.2**). fluorescence minus one (FMO) controls were also stained for each tissue sample, excluding peripheral blood mono nuclear cells (PBMCs) because there was not enough PBMCs for FMOs. (Refer to **appendix V** for detailed staining methods used.)

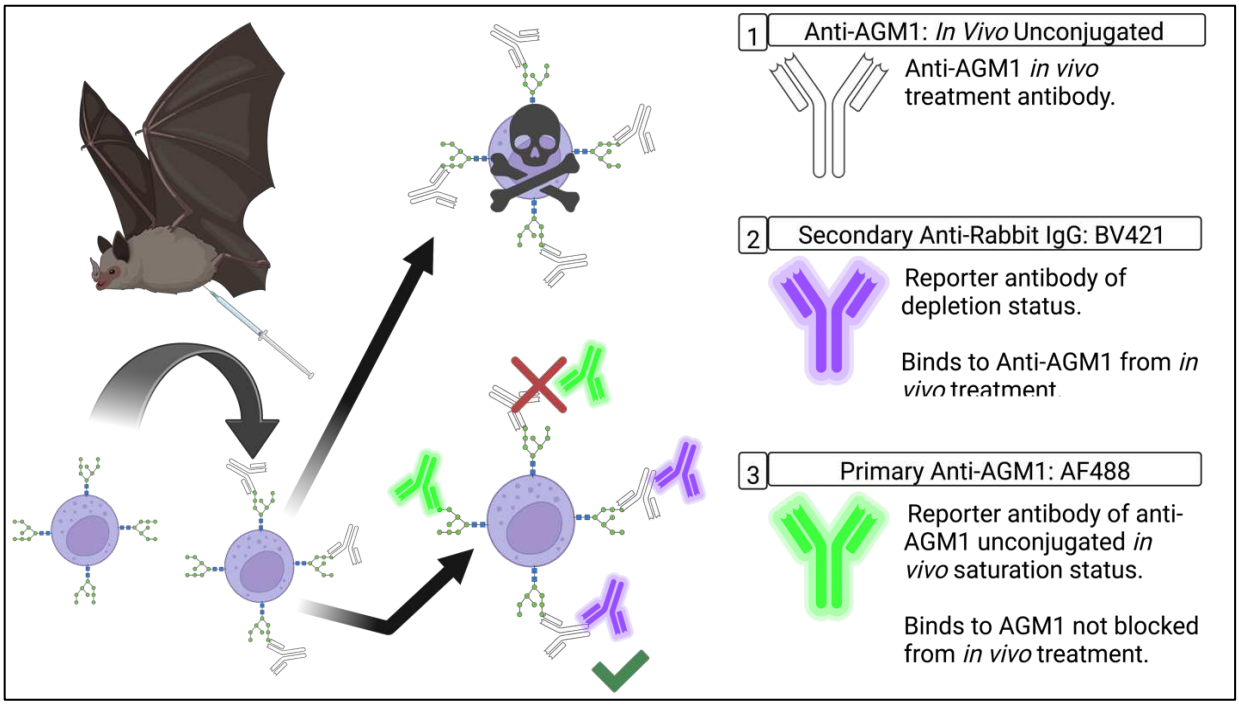

Figure 4.2) Staining strategy of disassociated tissues. Anti-AGM1 antibody binds to AGM-1 *in vivo*, therefore single cell suspensions were first stained with a secondary anti-rabbit IgG (BV421) to assess if cells were depleted. Single cell suspensions were then stained with a primary anti-IgG (AF488) to determine saturation of in vivo anti-AGM1 binding. Created with BioRender.com.

Flow Cytometry: Analytical Methods

Disassociated single cell suspensions were analyzed on a Cytek Aurora 4L 16V-14B-10YG-8R spectral cytometer. Generated FCS files were then analyzed on FlowJo V 10.8.1 Mac OS X. Gates were determined by FMO controls. Anti-AGM1 (AF488) determined $AGM1^+$ cells in mock control group and anti-rabbit IgG (BV421) determined $AGM1^+$ cells in anti-AGM1 treated group.

For statistical analysis of $AGM1^+$ cells comparing each group within tissue types a X^2 test was used. Each tissue was downsized to the smallest number of cells of the parent $AGM1^+$ gate in

FlowJo V 10.8.1 Mac OS X. Samples were downsized to better visualize the X^2 test in a bar graph format by removing sample size bias. Female treated splenocytes was the smallest sample population collected: Intact > Single Cells > Live Cells > AF– (76,649 cells). Therefore, each splenocyte sample population was downsized to 76,649 cells for chi square analysis. Male mock control PBMCs was the smallest sample population collected: Intact > Single Cells > Live Cells > AF– (77,899 cells). Therefore, each splenocyte sample population was downsized to 77,899 cells for chi square analysis. Female treated lamina propria was the smallest sample population collected: Intact > Single Cells > Live Cells > AF– (4,438 cells). Therefore, each lamina propria sample population was downsized to 4,438 cells for X^2 analysis. Male treated intraepithelial small cell population was the smallest population collected: Intact > Single Cells > Live Cells > Small IEL> AF– (16,157 cells). Female mock control large intraepithelial was the smallest sample population collected: Intact > Single Cells > Live Cells > Large IEL> AF– (2,526 cells). Female mock control large granular intraepithelial was the smallest sample population collected: Intact > Single Cells > Live Cells > Large Granular IEL> AF– (7,098 cells).

Results

Anti-AGM1 Treatment in Jamaican Fruit Bats: Splenocytes

Mock treated bats had an average of 5.21% $AGM1^+$ cells. Anti-AGM1 treated bats had an average of 32.95% $AGM1^+$ splenocytes (**Figure 4.3 and 4.4**). X^2 analysis of downsized splenocyte populations – Intact > Single Cells > Live Cells > AF– (76,649 cells) – reported significant increase of $AGM1^+$ splenocytes ($p < 0.0001$) in anti-AGM1 treatment group (**Figure 4.3, 4.5, and Table 4.1**).

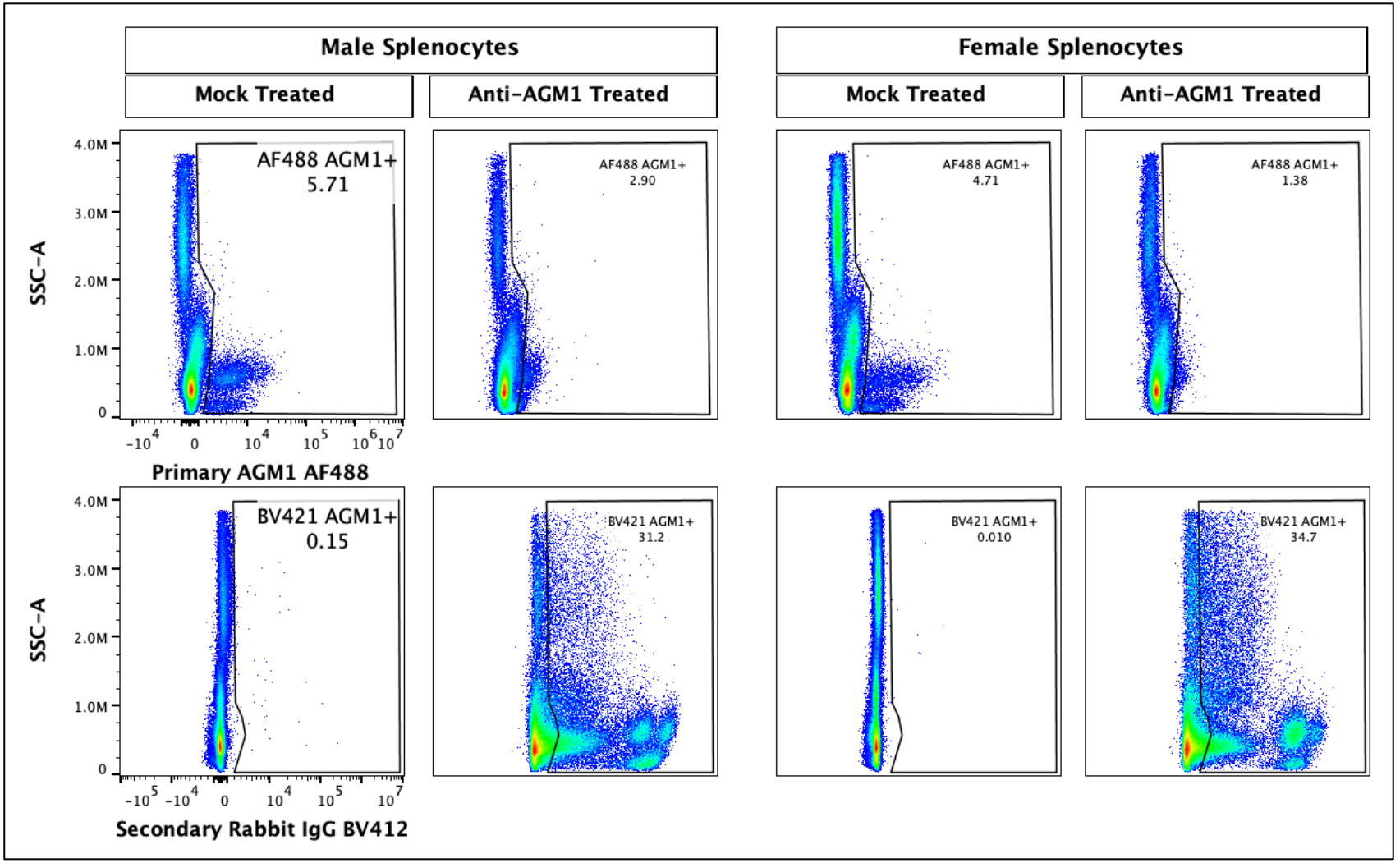

Figure 4.3) Flow cytometry gating of AGM1$^+$ splenocytes. Mock treated bats had an average of 5.21% AGM1$^+$cells. Anti-AGM1 treated bats had an average of 32.95% AGM1$^+$ splenocytes. Splenocytes were then analyzed on a Cytek Aurora 4L 16V-14B-10YG-8R spectral cytometer. FCS files were analyzed in FlowJo V 10.8.1 Mac OS X. Gates were drawn based on FMOs.

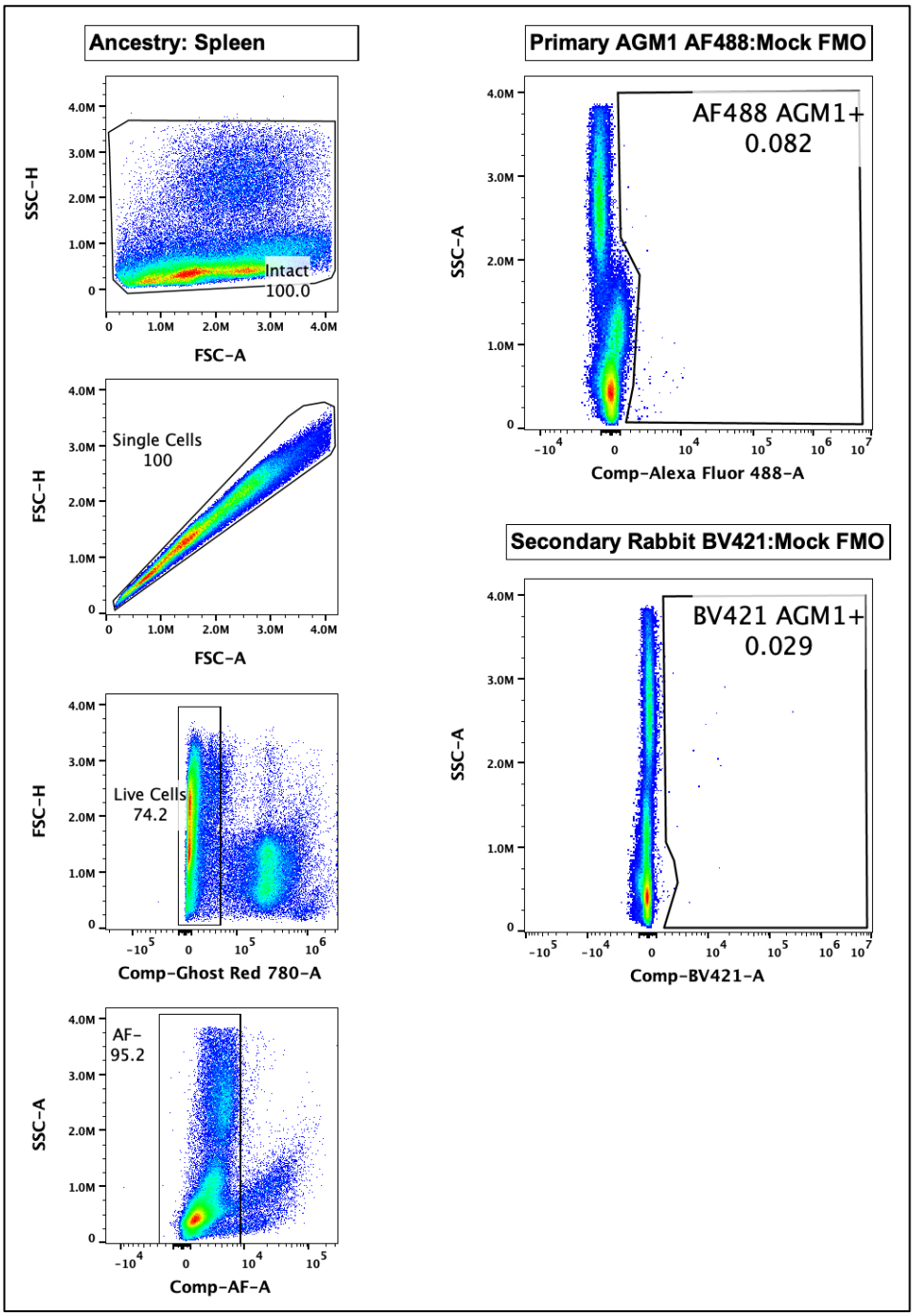

Figure 4.4) Flow cytometry ancestry gating of AGM1^{+} splenocytes. Splenocytes were then analyzed on a Cytek Aurora 4L 16V-14B-10YG-8R spectral cytometer. FCS files were analyzed in FlowJo V 10.8.1 Mac OS X. Gates were drawn based on FMOs.

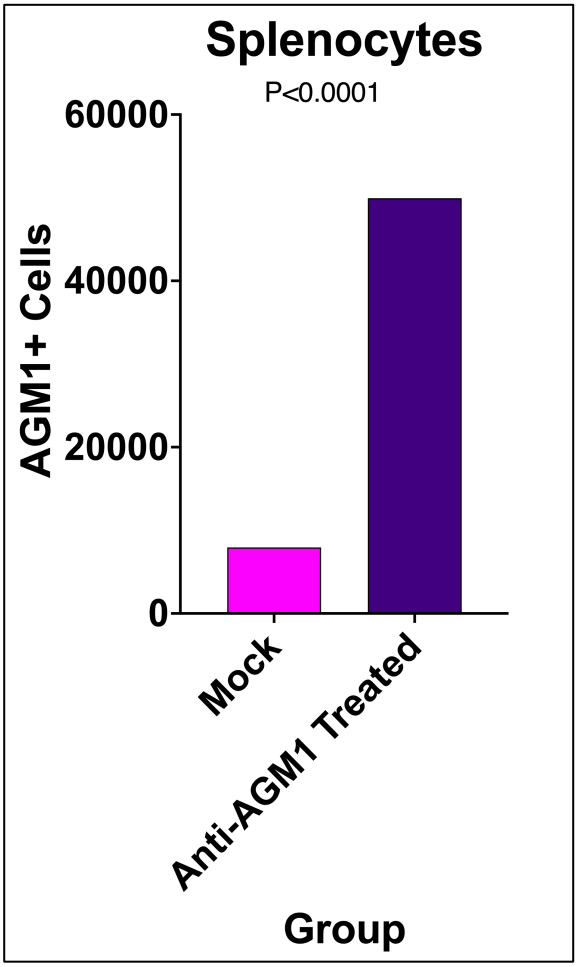

Figure 4.5) AGM1^{+} cell counts of downsized splenocyte FCS files. A X^2 test was performed for statistical analysis with a reported $p<0.0001$.

Table 4.1) X^2 output of $AGM1^+$ cell counts of downsized splenocyte FCS files. P value <0.0001. Generated by GraphPad Prism.

Table Analyzed	**Splenocytes**		
P value and statistical significance			
Test	**Chi-square**		
Chi-square, df	37524, 1		
z	193.7		
P value	<0.0001		
P value summary	****		
One- or two-sided	Two-sided		
Statistically significant (P < 0.05)?	Yes		
Data analyzed	**AGM1-**	**AGM1+**	**Total**
Mock	145348	7950	153298
Anti-AGM1 Treated	103418	49940	153358
Total	248766	57890	306656
Percentage of row total	**AGM1-**	**AGM1+**	
Mock	94.81%	5.19%	
Anti-AGM1 Treated	67.44%	32.56%	
Percentage of column total	**AGM1-**	**AGM1+**	
Mock	58.43%	13.73%	
Anti-AGM1 Treated	41.57%	86.27%	
Percentage of grand total	**AGM1-**	**AGM1+**	
Mock	47.40%	2.59%	
Anti-AGM1 Treated	33.72%	16.29%	

Anti-AGM1 Treatment in Jamaican Fruit Bats: PBMCs

Mock treated bats had an average of 6.72% $AGM1^+$ cells. Anti-AGM1 treated bats had an average of 7.31% $AGM1^+$ PBMCs (**Figures 4.6 and 4.7**). X^2 statistical analysis of downsized PBMC populations Intact > Single Cells > Live Cells > AF– (155,798 cells) reported no significant change in $AGM1^+$ cells (**Figures 4.6, 4.8, and Table 4.2**).

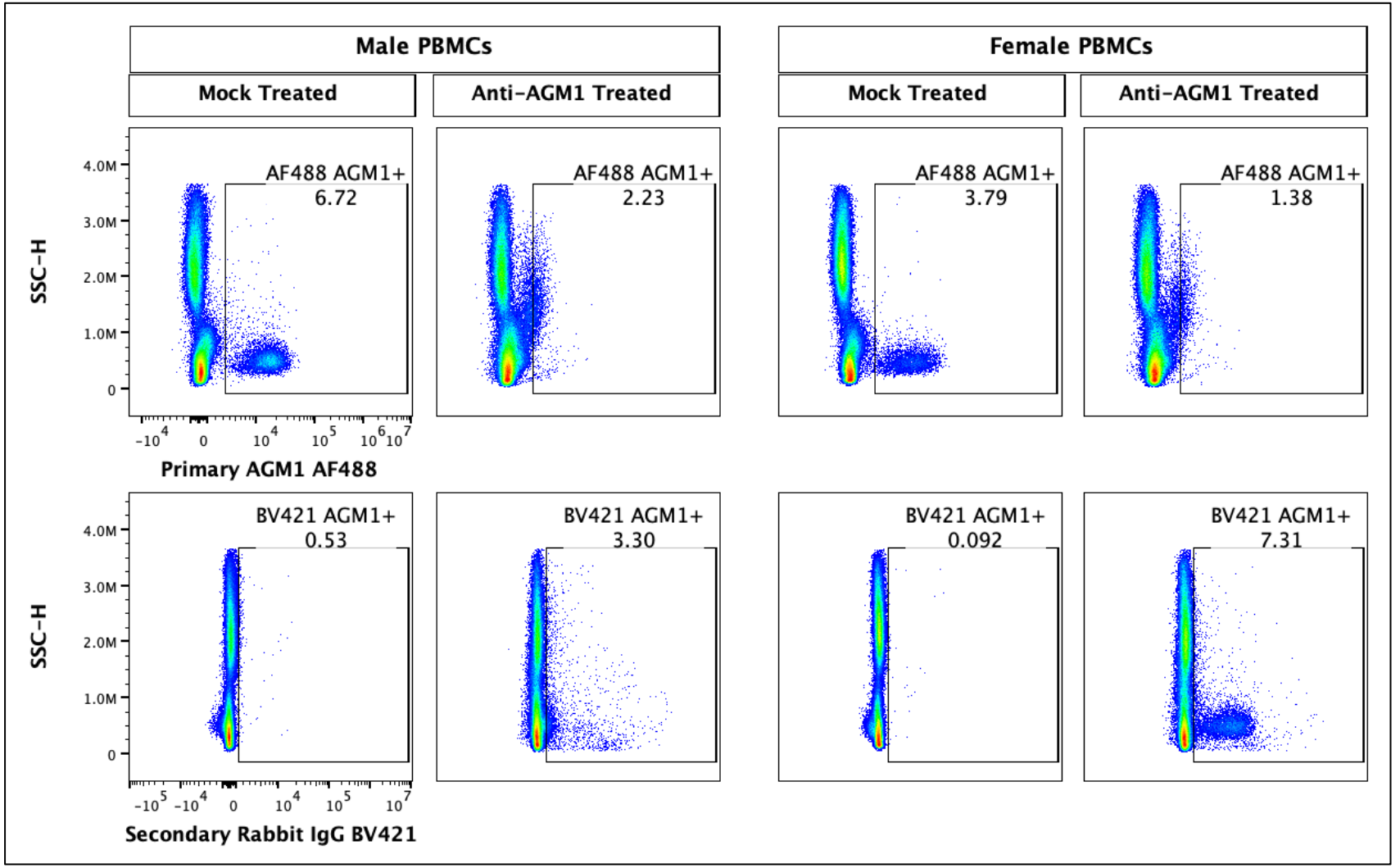

Figure 4.6) Flow cytometry gating of AGM1$^+$ PBMCs. Mock treated bats had an average of 5.21% AGM1$^+$ cells. Anti-AGM1 treated bats had an average of 32.95% AGM1$^+$ PBMCs. PBMC FCS files were then analyzed on a Cytek Aurora 4L 16V-14B-10YG-8R spectral cytometer. FCS files were analyzed in FlowJo V 10.8.1 Mac OS X. Gates were drawn based on FMOs.

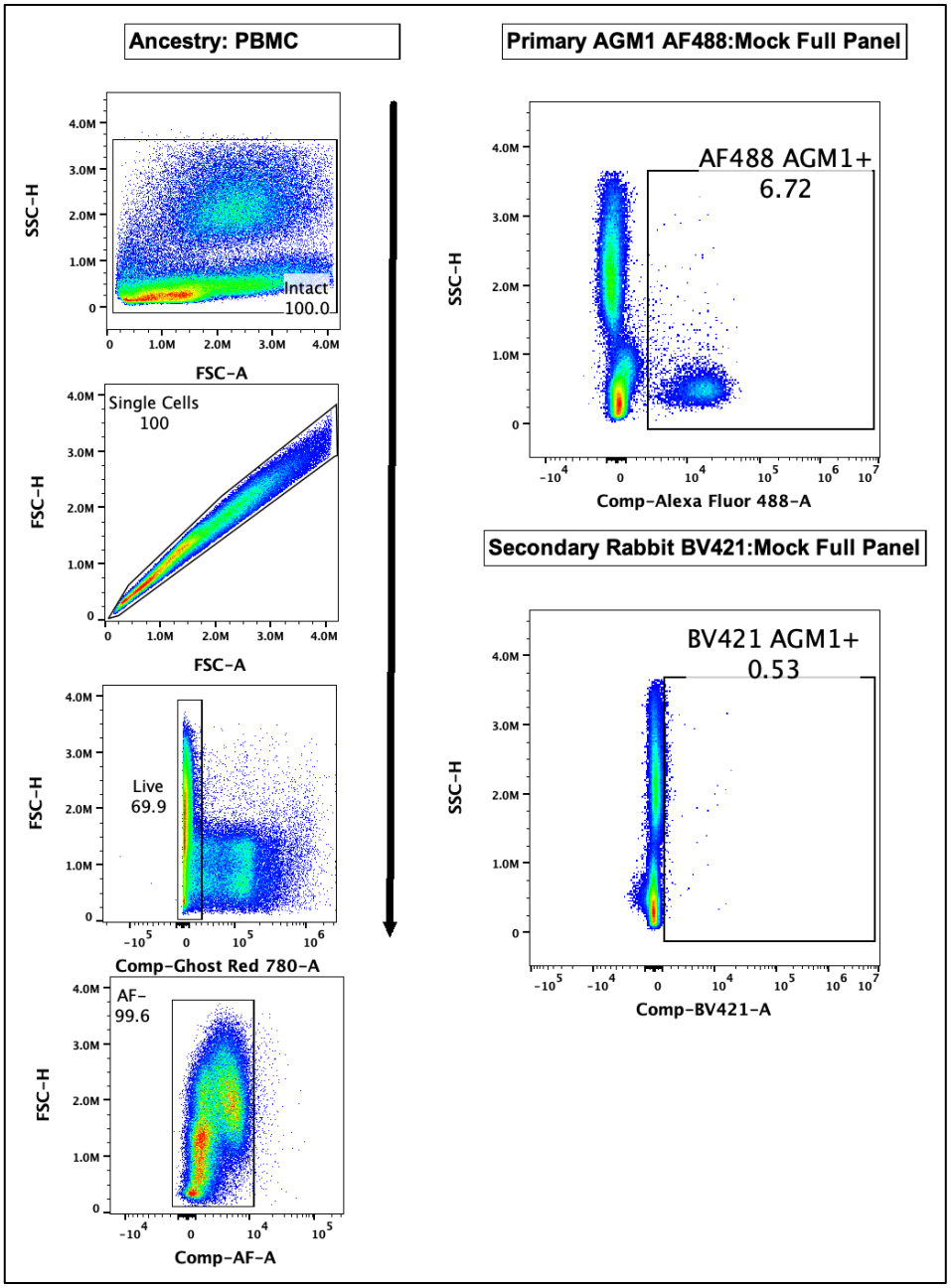

Figure 4.7) Flow cytometry ancestry gating of AGM1^{+} PBMCs. Splenocytes were then analyzed on a Cytek Aurora 4L 16V-14B-10YG-8R spectral cytometer. FCS files were analyzed in FlowJo V 10.8.1 Mac OS X. Gates were drawn based on FMOs.

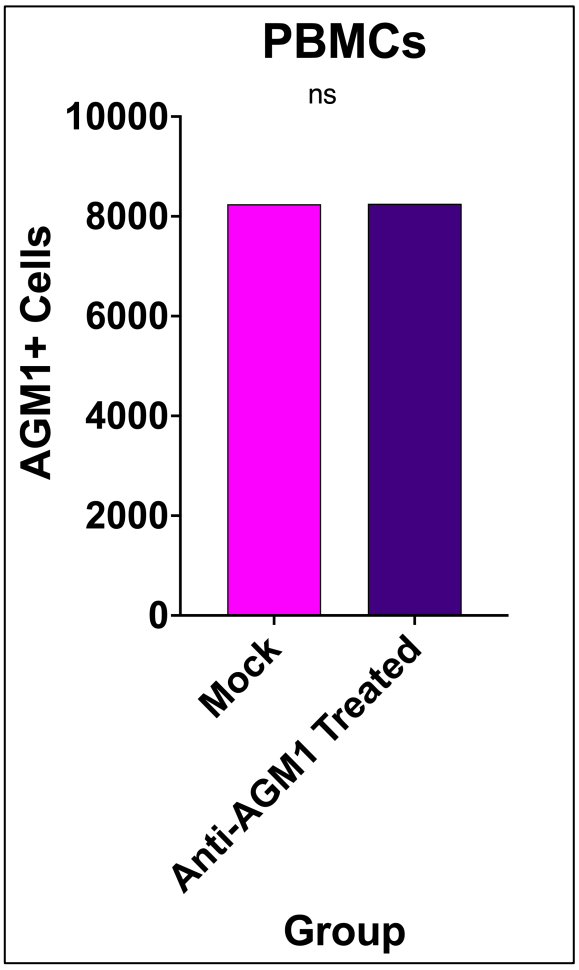

Figure 4.8) AGM1^{+} cell counts of downsized PBMC FCS files. A X^2 test was performed for statistical analysis with a reported nonsignificant P value.

Table 4.2) X^2 output of $AGM1^+$ cell counts of downsized PBMC FCS files. P value 0.9426. Generated by GraphPad Prism V 9.4.1 chi square analysis.

Table Analyzed	**PBMCs**		
P value and statistical significance			
Test	**Chi-square**		
Chi-square, df	0.005184, 1		
z	0.072		
P value	0.9426		
P value summary	ns		
One- or two-sided	Two-sided		
Statistically significant (P < 0.05)?	No		
Data analyzed	**AGM1-**	**AGM1+**	**Total**
Mock	147553	8245	155798
Anti-AGM1 Treated	147544	8254	155798
Total	295097	16499	311596
Percentage of row total	**AGM1-**	**AGM1+**	
Mock	94.71%	5.29%	
Anti-AGM1 Treated	94.70%	5.30%	
Percentage of column total	**AGM1-**	**AGM1+**	
Mock	50.00%	49.97%	
Anti-AGM1 Treated	50.00%	50.03%	
Percentage of grand total	**AGM1-**	**AGM1+**	
Mock	47.35%	2.65%	
Anti-AGM1 Treated	47.35%	2.65%	

Anti-AGM1 Treatment in Jamaican Fruit Bats: Gastrointestinal Lamina Propria Fraction

Mock treated bats had an average of 0.775 % $AGM1^+$ lamina propria cells. Anti-AGM1 treated bats had an average of 3.90 % $AGM1^+$ lamina propria cells (**Figure 4.9 and 4.10**). X^2 analysis of down sized lamina propria populations – Intact > Single Cells > Live Cells > AF– (4,438 cells) – reported significant increase ($p<0.0001$) of $AGM1^+$ cells in the anti-AGM1 treatment group (**Figure 4.9, 4.11 and Table 4.3**).

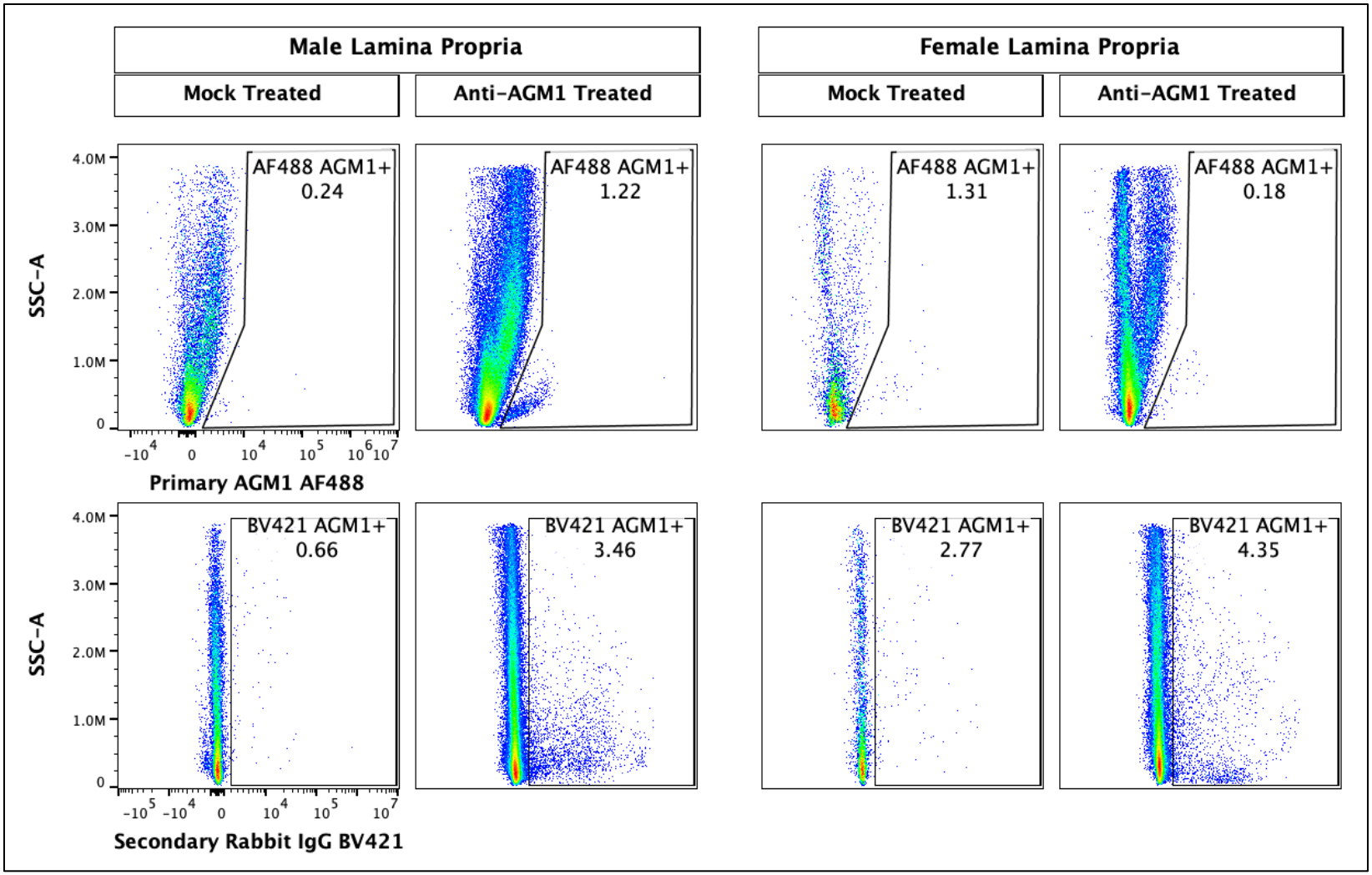

Figure 4.9) Flow cytometry gating of AGM1$^+$ disassociated lamina propria single cell suspension. Mock treated bats had an average of 0.775 % AGM1$^+$ lamina propria cells. Anti-AGM1 treated bats had an average of 3.90 % AGM1$^+$ lamina propria cells. Disassociated lamina propria single cell suspensions were then analyzed on a Cytek Aurora 4L 16V-14B-10YG-8R spectral cytometer. FCS files were analyzed in FlowJo V 10.8.1 Mac OS X. Gates were drawn based on FMOs.

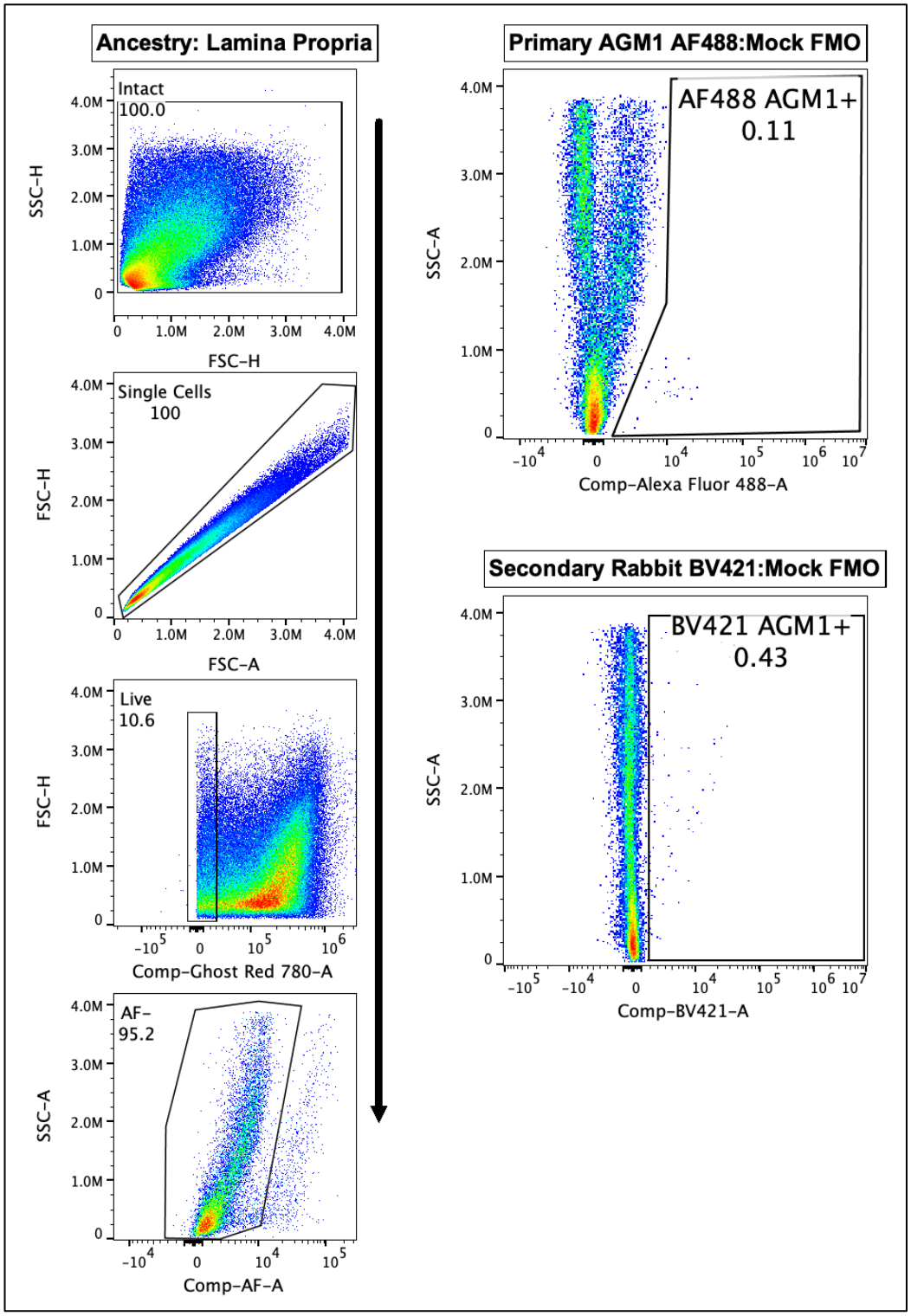

Figure 4.10) Flow cytometry ancestry gating of AGM1^{+} lamina propria. Lamina propria single cell suspensions were then analyzed on a Cytek Aurora 4L 16V-14B-10YG-8R spectral cytometer. FCS files were analyzed in FlowJo V 10.8.1 Mac OS X. Gates were drawn based on FMOs.

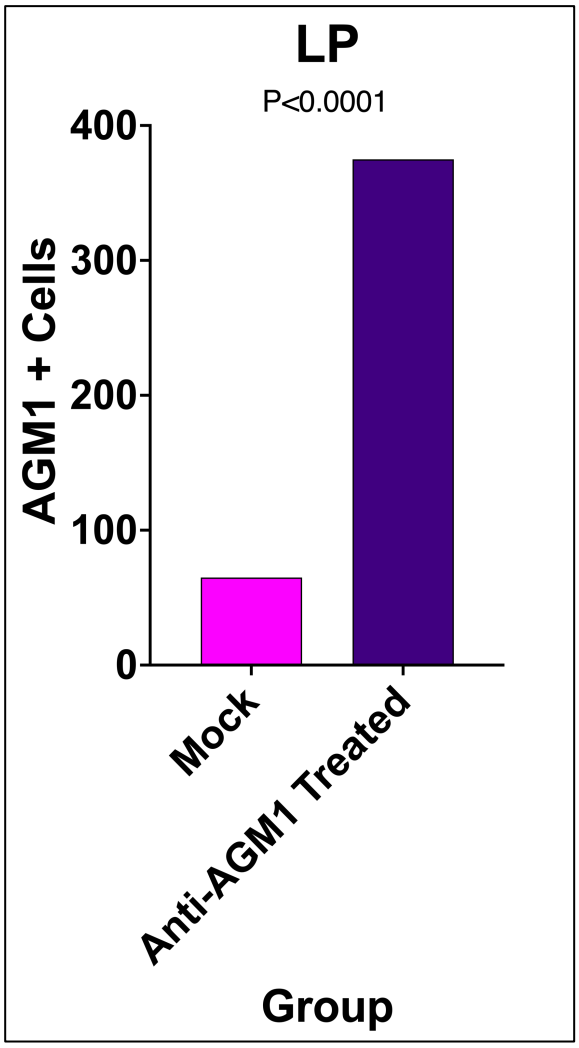

Figure 4.11) AGM1^{+} cell counts of downsized lamina propria (LP) FCS files. A X^2 test reported p <0.0001.

Table 4.3) X^2 output of $AGM1^+$ cell counts of downsized lamina propria (LP) FCS files. P value <0.0001. Generated by GraphPad Prism V 9.4.1 chi square analysis.

Table Analyzed	**LP**		
P value and statistical significance			
Test	**Chi-square**		
Chi-square, df	224.0, 1		
z	14.97		
P value	<0.0001		
P value summary	****		
One- or two-sided	Two-sided		
Statistically significant (P < 0.05)?	Yes		
Data analyzed	**AGM1-**	**AGM1+**	**Total**
Mock	8811	65	8876
Anti-AGM1 Treated	8501	375	8876
Total	17312	440	17752
Percentage of row total	**AGM1-**	**AGM1+**	
Mock	99.27%	0.73%	
Anti-AGM1 Treated	95.78%	4.22%	
Percentage of column total	**AGM1-**	**AGM1+**	
Mock	50.90%	14.77%	
Anti-AGM1 Treated	49.10%	85.23%	
Percentage of grand total	**AGM1-**	**AGM1+**	
Mock	49.63%	0.37%	
Anti-AGM1 Treated	47.89%	2.11%	

Anti-AGM1 Treatment in Jamaican Fruit Bats Gastrointestinal Intraepithelial Fraction: Small Cells

Mock treated bats had an average of 0.11 % $AGM1^+$ small cells. Anti-AGM1 treated bats had an average of 1.575% $AGM1^+$ small cells (**Figures 4.12 and 4.13**). X^2 analysis of downsized intraepithelial small cell populations – Intact > Single Cells > Live Cells > Small IEL> AF– (16,157 cells)– reported a significant increase of $AGM1^+$ cells ($p<0.0001$) in the anti-AGM treatment group (**Figures 4.12, 4.14, and Table 4.4**).

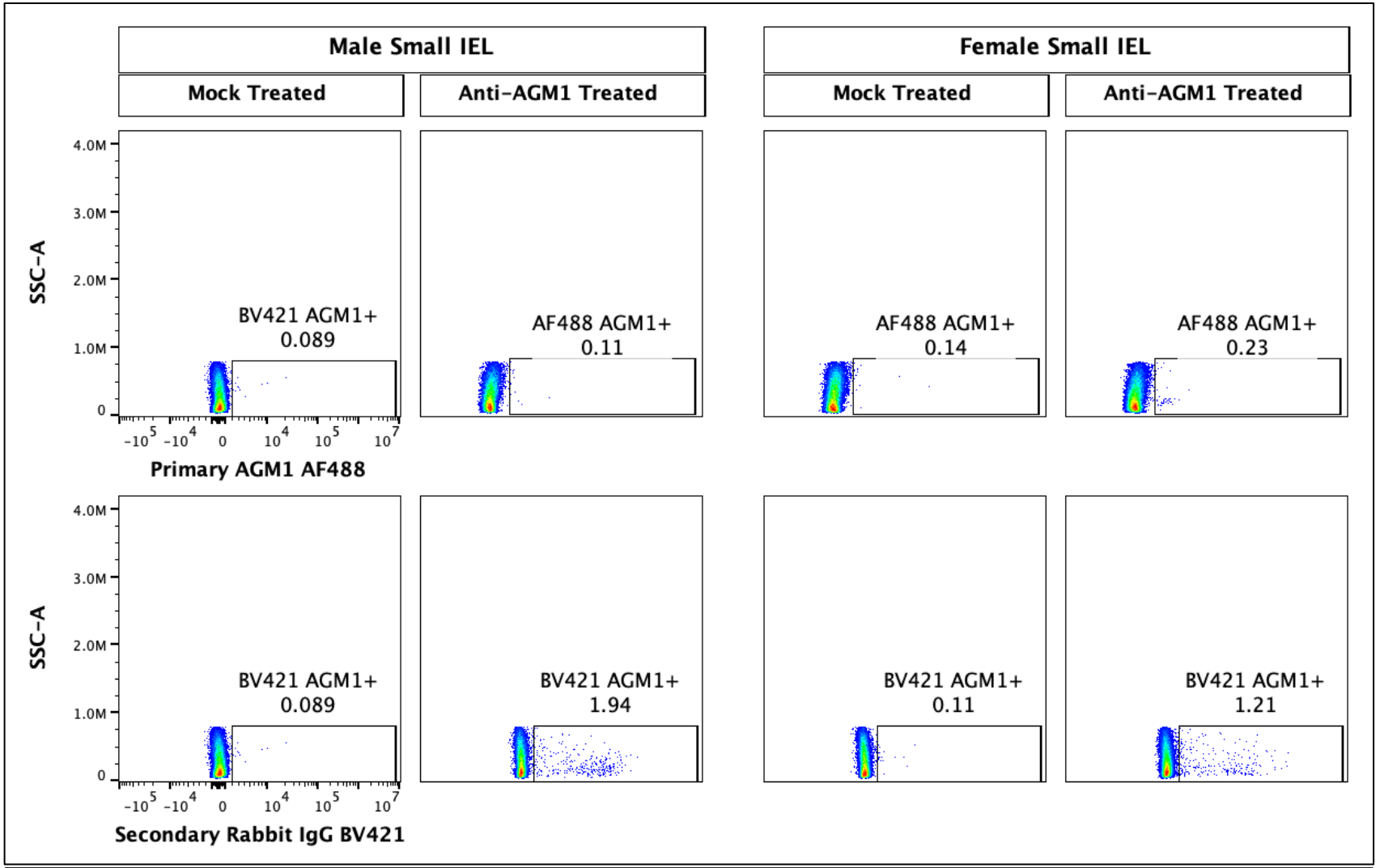

Figure 4.12) Flow cytometry gating of AGM1$^+$ disassociated small intraepithelial single cell suspension. Mock treated bats had an average of 0.11 % AGM1$^+$ small cells. Anti-AGM1 treated bats had an average of 1.575% AGM1$^+$ small cells. Disassociated intraepithelial fractions were analyzed on a Cytek Aurora 4L 16V-14B-10YG-8R spectral cytometer. FCS files were analyzed in FlowJo V 10.8.1 Mac OS X. Gates were drawn based on FMOs.

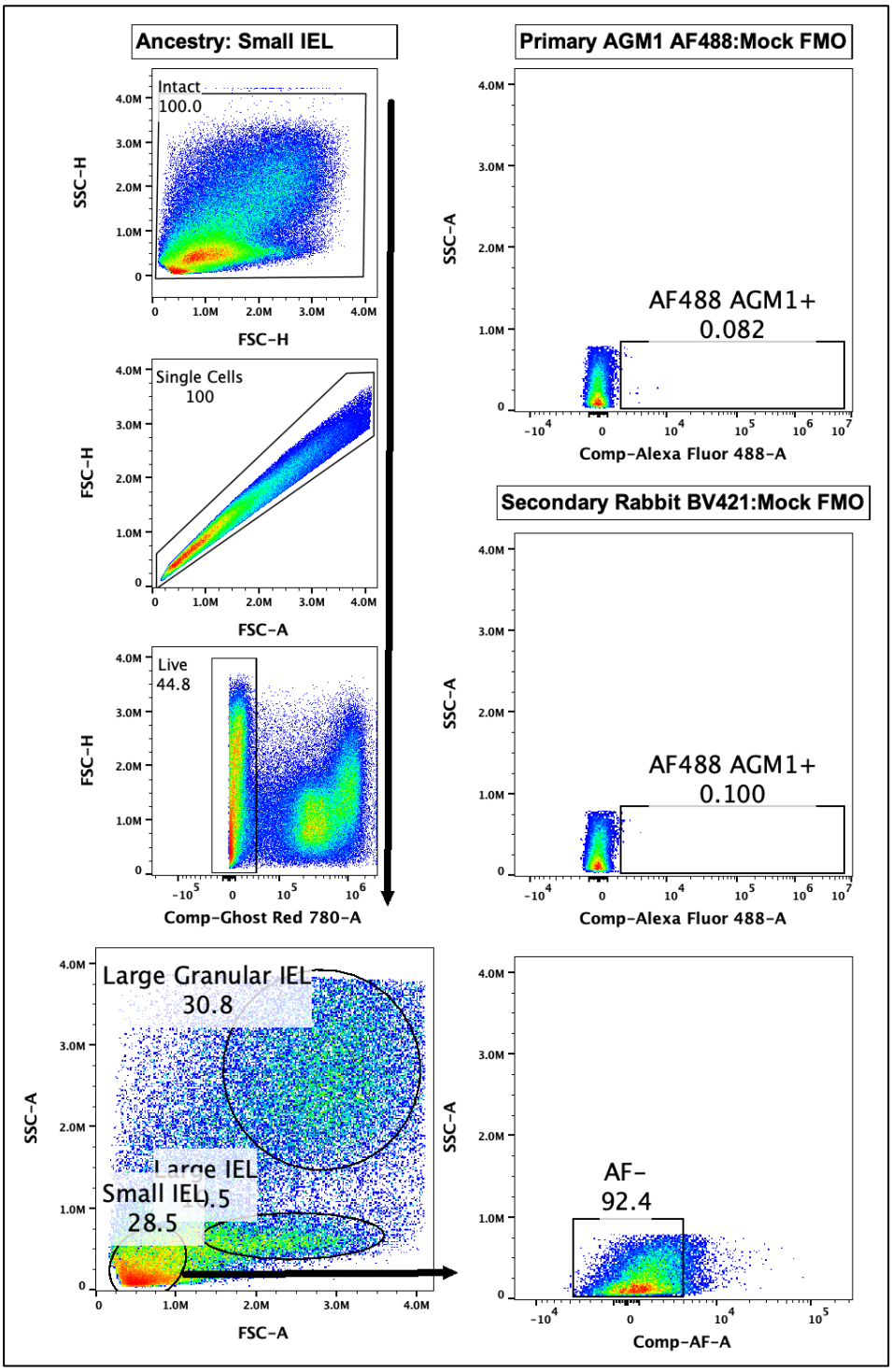

Figure 4.13) Flow cytometry ancestry gating of AGM1^{+} intraepithelial small cells. Disassociated single cell suspensions were than analyzed on a Cytek Aurora 4L 16V-14B-10YG-8R spectral cytometer. FCS files were analyzed in FlowJo V 10.8.1 Mac OS X. Gates were drawn based on FMOs.

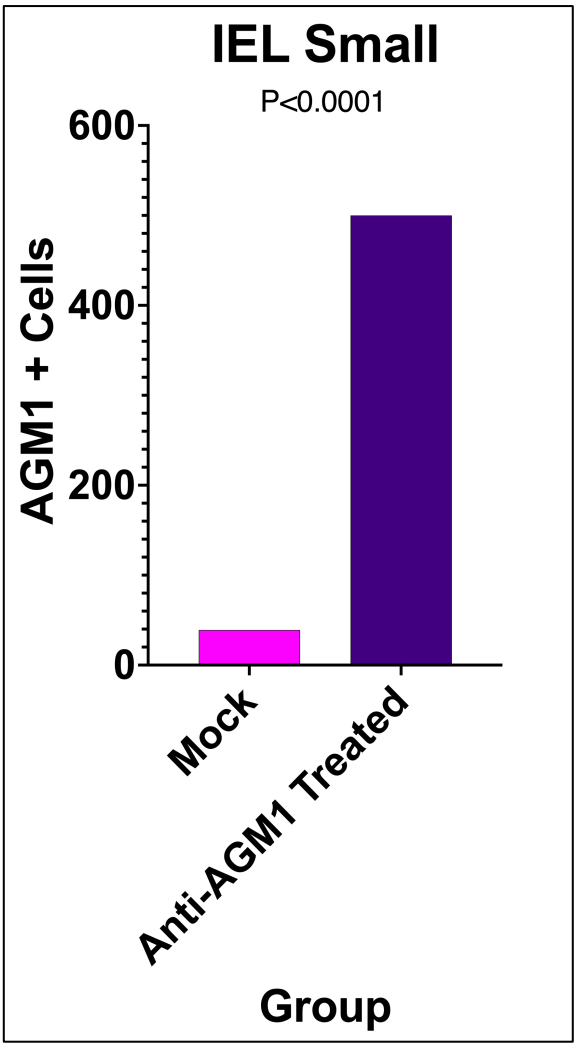

Figure 4.14) AGM1^{+} cell counts of downsized small intraepithelial gastrointestinal FCS files. X^2 test p <0.0001.

Table 4.4) X^2 output of $AGM1^+$ cell counts of downsized intraepithelial small cell (IEL Small) FCS files. P value <0.0001. Generated by GraphPad Prism V 9.4.1 chi square analysis.

Table Analyzed	**IEL Small**		
P value and statistical significance			
Test	**Chi-square**		
Chi-square, df	397.6, 1		
z	19.94		
P value	<0.0001		
P value summary	****		
One- or two-sided	Two-sided		
Statistically significant (P < 0.05)?	Yes		
Data analyzed	**AGM1-**	**AGM1+**	**Total**
Mock	32275	39	32314
Anti-AGM1 Treated	31814	500	32314
Total	64089	539	64628
Percentage of row total	**AGM1-**	**AGM1+**	
Mock	99.88%	0.12%	
Anti-AGM1 Treated	98.45%	1.55%	
Percentage of column total	**AGM1-**	**AGM1+**	
Mock	50.36%	7.24%	
Anti-AGM1 Treated	49.64%	92.76%	
Percentage of grand total	**AGM1-**	**AGM1+**	
Mock	49.94%	0.06%	
Anti-AGM1 Treated	49.23%	0.77%	

Anti-AGM1 Treatment in Jamaican Fruit Bats Gastrointestinal Intraepithelial Fraction: Large Cells

Mock treated bats had an average of 0.525% $AGM1^+$ large cells. Anti-AGM1 treated bats had an average of 2.32% $AGM1^+$ large cells (**Figures 4.15 and 4.16**). X^2 analysis of downsized intraepithelial large cells Intact > Single Cells > Live Cells > Large IEL> AF– (2,526 cells) reported a significant increase of $AGM1^+$ cells ($p<0.0001$) in the anti-AGM1 treated group (**Figures 4.15, 4.17, and Table 4.5**).

Figure 4.15) Flow cytometry gating of AGM1$^+$ disassociated large intraepithelial cells. Mock treated bats had an average of 0.525% AGM1$^+$ large cells. Anti-AGM1 treated bats had an average of 2.32% AGM1$^+$ large cells. Disassociated intraepithelial cell fractions were analyzed on a Cytek Aurora 4L 16V-14B-10YG-8R spectral cytometer. FCS files were analyzed in FlowJo V 10.8.1 Mac OS X. Gates were drawn based on FMOs.

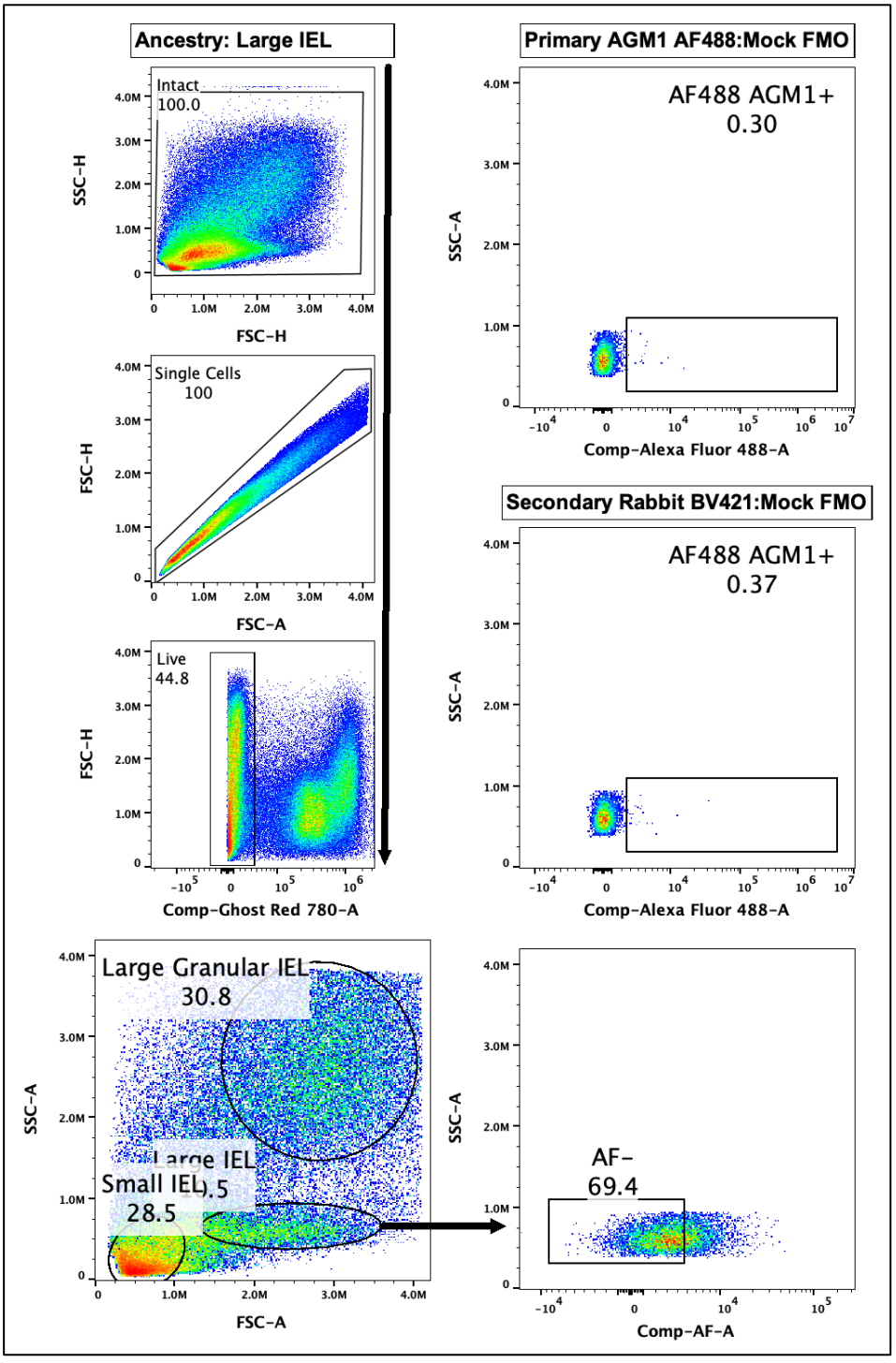

Figure 4.16) Flow cytometry ancestry gating of AGM1^{+} intraepithelial large cells. Disassociated single cell suspensions were than analyzed on a Cytek Aurora 4L 16V-14B-10YG-8R spectral cytometer. FCS files were analyzed in FlowJo V 10.8.1 Mac OS X. Gates were drawn based on FMOs.

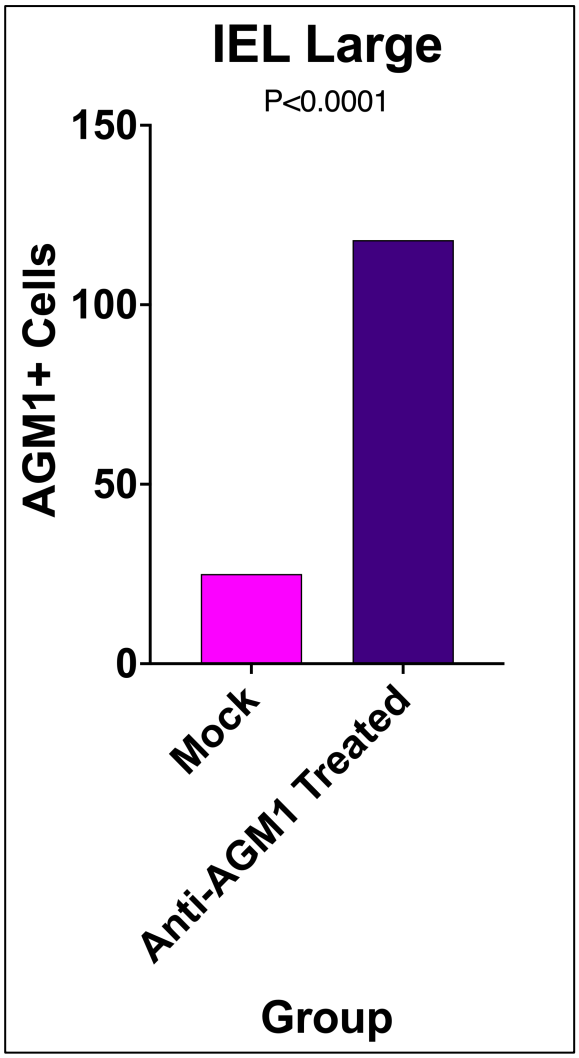

Figure 4.17) $AGM1^+$ cell counts of downsized large intraepithelial gastrointestinal FCS files. A X^2 test was performed for statistical analysis with a reported P value <0.0001.

Table 4.5) X^2 output of $AGM1^+$ cell counts of downsized intraepithelial large cell (IEL Large) FCS files. P value <0.0001. Generated by GraphPad Prism V 9.4.1 chi square analysis.

Table Analyzed	**IEL Large**		
P value and statistical significance			
Test	**Chi-square**		
Chi-square, df	61.35, 1		
z	7.833		
P value	<0.0001		
P value summary	****		
One- or two-sided	Two-sided		
Statistically significant (P < 0.05)?	Yes		
Data analyzed	**AGM1-**	**AGM1+**	**Total**
Mock	5027	25	5052
Anti-AGM1 Treated	4934	118	5052
Total	9961	143	10104
Percentage of row total	**AGM1-**	**AGM1+**	
Mock	99.51%	0.49%	
Anti-AGM1 Treated	97.66%	2.34%	
Percentage of column total	**AGM1-**	**AGM1+**	
Mock	50.47%	17.48%	
Anti-AGM1 Treated	49.53%	82.52%	
Percentage of grand total	**AGM1-**	**AGM1+**	
Mock	49.75%	0.25%	
Anti-AGM1 Treated	48.83%	1.17%	

Anti-AGM1 Treatment in Jamaican Fruit Bats Gastrointestinal Intraepithelial Fraction: Large Granular Cells

Mock treated bats had an average of 3.98% $AGM1^+$ large granular cells. Anti-AGM1 treated bats had an average of 5.165% $AGM1^+$ large granular cells (**Figures 4.18 and 4.19**). X^2 analysis of downsized intraepithelial large granular cells – Intact > Single Cells > Live Cells > Large Granular IEL > AF– (7,098 cells) – reported a significant increase of $AGM1^+$ cells ($p<0.0001$) in the anti-AGM1 treatment group (**Figures 4.18, 4.20, and Table 4.6**).

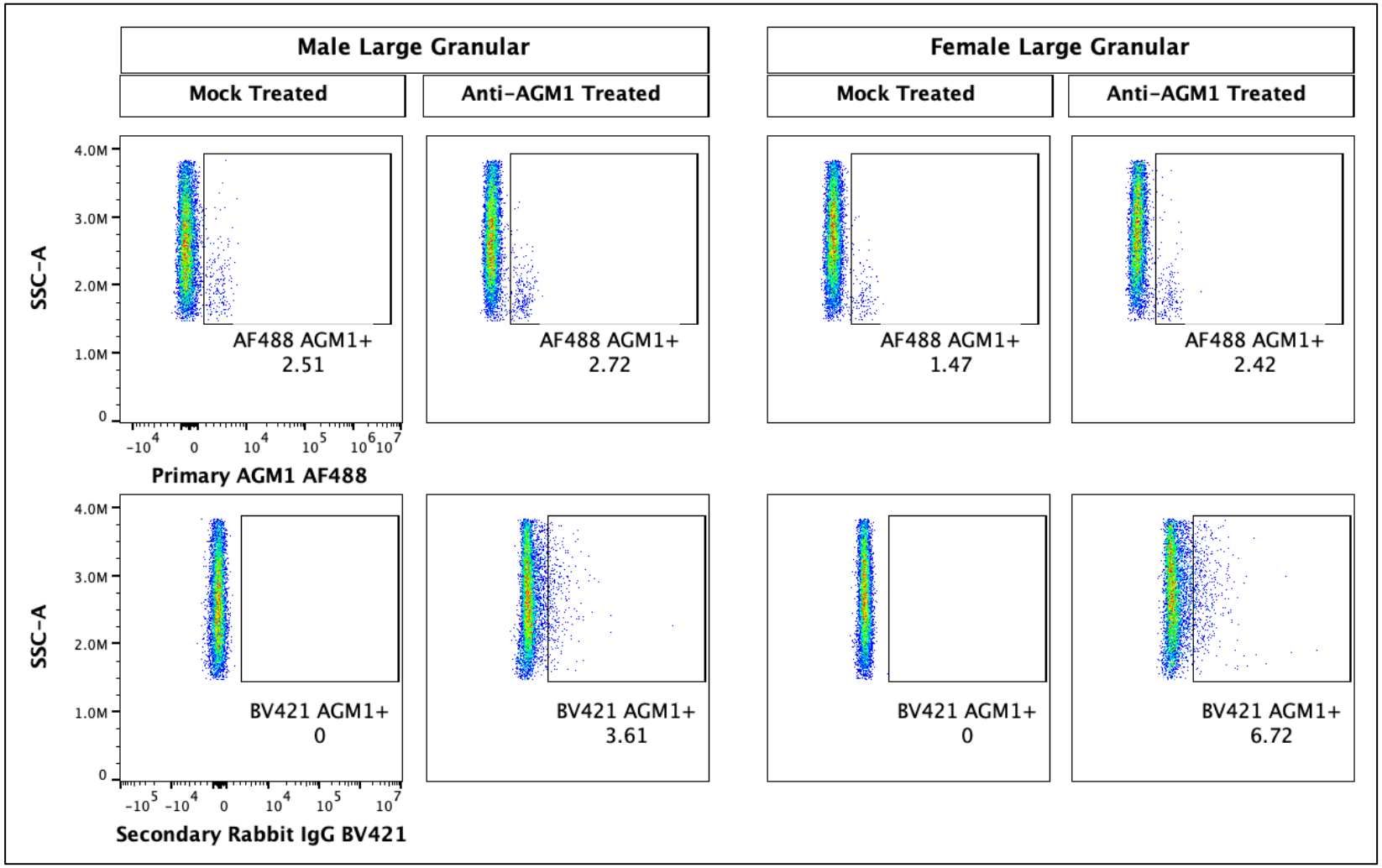

Figure 4.18) Flow cytometry gating of AGM1$^+$ disassociated large granular intraepithelial cells. Mock treated bats had an average of 3.98% AGM1$^+$ large granular cells. Anti-AGM1 treated bats had an average of 5.165% AGM1$^+$ large granular cells. Disassociated intraepithelial cell fractions were analyzed on a Cytek Aurora 4L 16V-14B-10YG-8R spectral cytometer. FCS files were analyzed in FlowJo V 10.8.1 Mac OS X. Gates were drawn based on FMOs.

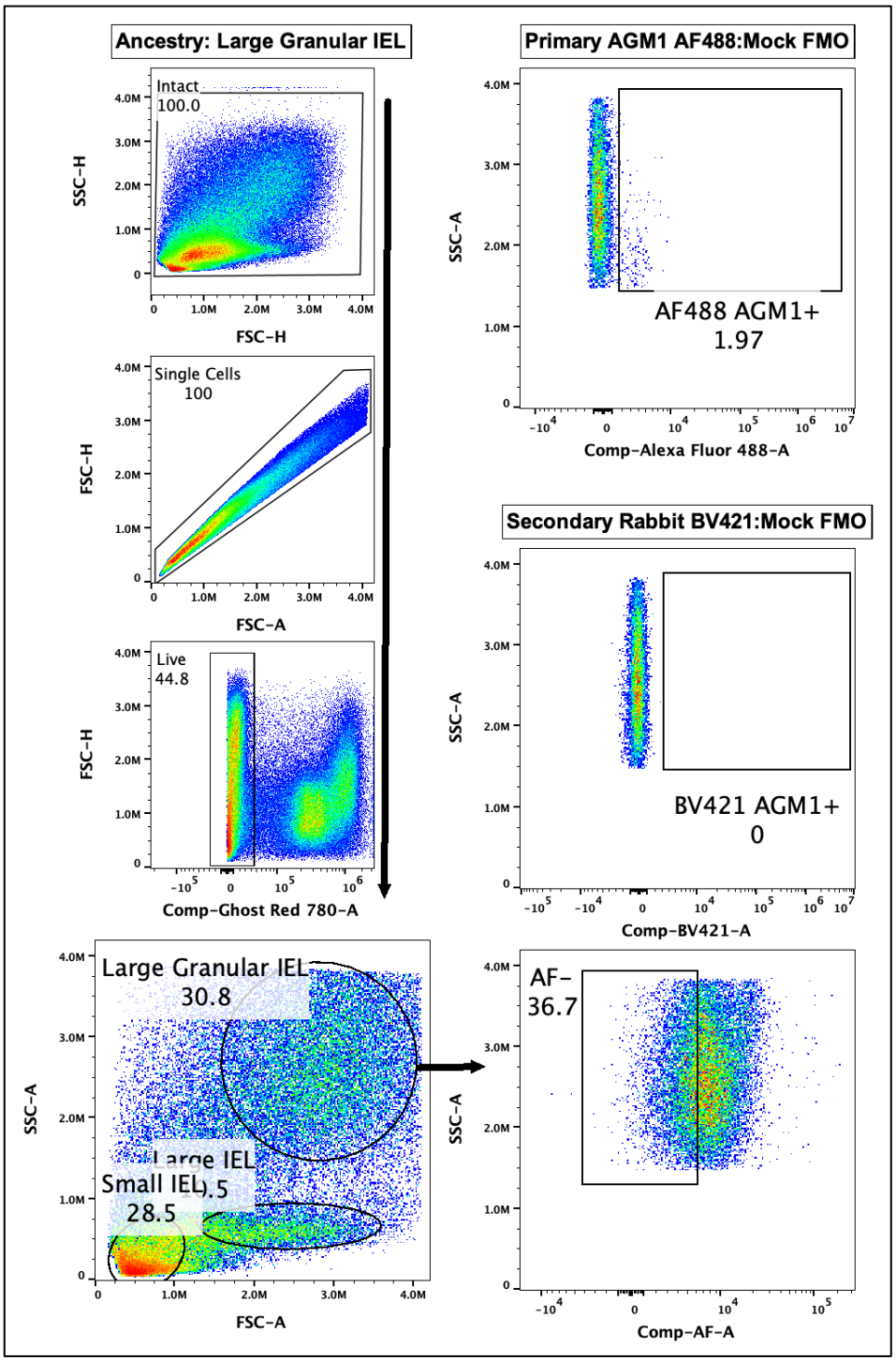

Figure 4.19) Flow cytometry ancestry gating of AGM1^{+} intraepithelial large granular cells. Disassociated single cell suspensions were than analyzed on a Cytek Aurora 4L 16V-14B-10YG-8R spectral cytometer. FCS files were analyzed in FlowJo V 10.8.1 Mac OS X. Gates were drawn based on FMOs.

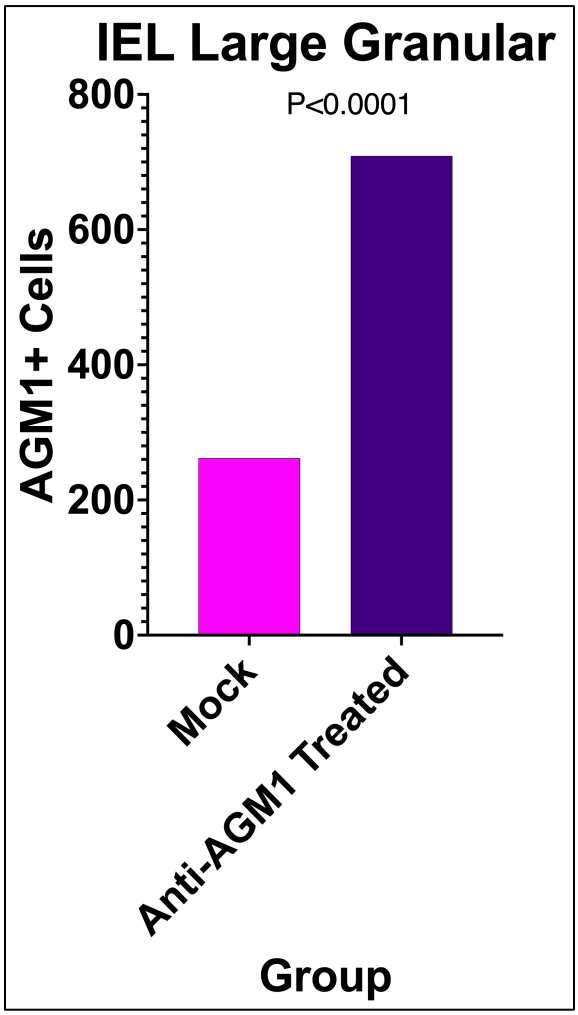

Figure 4.20) AGM1^{+} cell counts of downsized large granular intraepithelial gastrointestinal FCS files. A X^2 test was performed for statistical analysis with a reported P value <0.0001.

Table 4.6) X^2 output of $AGM1^+$ cell counts of downsized intraepithelial large granular cell (IEL Large Granular) FCS files. P value <0.0001. Generated by GraphPad Prism V 9.4.1 chi square analysis.

Table Analyzed	**IEL Large Granular**		
P value and statistical significance			
Test	**Chi-square**		
Chi-square, df	213.1, 1		
z	14.6		
P value	<0.0001		
P value summary	****		
One- or two-sided	Two-sided		
Statistically significant (P < 0.05)?	Yes		
Data analyzed	**AGM1-**	**AGM1+**	**Total**
Mock	13934	262	14196
Anti-AGM1 Treated	13487	709	14196
Total	27421	971	28392
Percentage of row total	**AGM1-**	**AGM1+**	
Mock	98.15%	1.85%	
Anti-AGM1 Treated	95.01%	4.99%	
Percentage of column total	**AGM1-**	**AGM1+**	
Mock	50.82%	26.98%	
Anti-AGM1 Treated	49.18%	73.02%	
Percentage of grand total	**AGM1-**	**AGM1+**	
Mock	49.08%	0.92%	
Anti-AGM1 Treated	47.50%	2.50%	

Discussion and Future Directions

The *in vivo* anti-AGM1 treatment of Jamaican fruit bats depletion of $AGM1^+$ cells hypothesis was not supported. Interestingly, *in vivo* anti-AGM1 treatment demonstrated a significant increase in the number of $AGM1^+$ cells in three tissues, spleen ($p<0.0001$), lamina propria ($p<0.0001$), and intraepithelial fraction across three cell populations: small IEL cells ($p<0.0001$), large IEL cells ($p<0.0001$), and large granular IEL cells ($p<0.0001$). It does not appear that anti-AGM1 treatment induced apoptosis in Jamaican fruit bats. Furthermore, it is possible that Jamaican fruit bat immune systems cannot recognize the Fc portion of rabbit IgG antibodies, and therefore cellular depletion cannot occur through antibody-dependent cell mediated cytotoxicity, nor complement-depended cytotoxicity. Interestingly, Egyptian fruit bats (*Rousettus aegyptiacus*) have an expansion of KLRC genes, which are proteins principally expressed on the surface of NK cells. Six out of ten of these KLRC genes had both activating and inhibitory motifs, three out of ten had inhibitory motifs, and one had an activating motif [143]. A study into Jamaican fruit bat KLRC genes needs to be performed to determine if Jamaican fruit bats have a similar expansion and elucidate these activating and inhibitory motifs. If so, it would suggest that Old World and New World bats have evolved a more robust innate NK cell immune compartment for controlling viral infections. The increased abundance of $AGM1^+$ cells suggests that $AGM1^+$ cells are likely expanding and in an activated state, but proliferation and activation assays need to be performed to determine the physiological effects anti-AGM1 treatment has on $AGM1^+$ cells. Similarly, *in vivo* anti-AGM1 treatment experiments could determine if expansion and activation of $AGM1^+$ cells occur in other bat species. Antibodies to other cluster of differentiation markers need to be identified to better characterize these $AGM1^+$ cells after anti-AGM1 treatment. As described in

appendix I, AGM1$^+$ cells are predominantly CD161$^+$ and CD3γ$^+$, suggesting they are largely natural killer T cells, γδ T cells, tissue resident memory CD8$^+$ T cells, or mucosal-associated invariant T (MAIT) cells [159,169-177]. Developing antibodies targeting Jamaican fruit bat αβ and δγ TCR, CD56, CD16, and CD26 would help to better classify these AGM1$^+$ CD161$^+$ CD3$^+$ cells into NKT (CD56$^+$ or CD16$^+$), αβ CD8$^+$ T (αβ TCR$^+$ CD8$^+$), (γδ T (γδ TCR$^+$), or MAIT (CD26$^+$) classification and to identify what classification is being expanded by anti-AGM1 treatment [159,169-177].

While anti-AGM1 antibody treatment did not deplete AGM1$^+$ cells, anti-AGM1 treatment could be modified by fusing anti-AGM1 antibodies to a toxin, such as diphtheria toxin, as an alternate method to deplete AGM1$^+$ cells *in vivo*. This type of therapy is called immunotoxin therapy and this strategy of targeted cell depletion is being used for cancer treatments [178,179]. However, without fusing diphtheria toxin to anti-AGM1 antibodies can still prove to be a useful tool in the investigation of immune responses of bats to bat borne pathogens. Anti-AGM1 treatment could be used to preemptively expand and activate AGM1$^+$ immune cells before or during experimental infection. However, in this instance, if AGM1$^+$ cells were expanded, and viral infection was better controlled during experimental infection compared to control, it would suggest that AGM1$^+$ cells play an important role in controlling viral infection. If AGM1$^+$ cells were expanded, and viral infection was not changed during experimental viral infection compared to control, it would suggest AGM1$^+$ cells do not play an important role in viral infection. If AGM1$^+$ cells were expanded, and viral infection was exacerbated and pathology was observed during experimental viral infection compared to control, it would suggest AGM1$^+$ cells can induce pathology. Development of methods that permit depletion of specific immune cell populations will

be required to begin to fully understand how bat immune responses control infections, and to determine how they differ from humans and mice.

CHAPTER 5
SYNTHESIS OF JAMAICAN FRUIT BAT GROWTH FACTORS TO CULTURE SELF-REGENERATIVE CRYPT STEM CELLS IN VITRO

Summary

Major limitations for developing the Jamaican fruit bat as an animal model is the paucity of specific reagents and cell lines. While cell lines cannot recapitulate a system of an organism, cell lines used for *in vitro* assays do offer a reasonable representation of the organism from which they are derived. Cell lines are often used to isolate and propagate viruses, which are used as inocula for *in vivo* studies. Propagation of bat H18N11 and H17N10 influenza A viruses (IAVs) highlight and reiterate the importance of producing Jamaican fruit bat cell lines. To date, bat IAVIAVs have been propagated in two canine epithelial cell lines, and passaging more than twice in these cells invariably accumulate mutations resulting in truncated head domain of the neuraminidase-like (NA) protein in viral progeny. Conversely, this does not occur *in vivo* in Jamaican fruit bats, where the wild type NA is maintained. Inoculation of bats with a stop codon prior to the head domain results in reversion to wild-type within one passage in Jamaican fruit bats, demonstrating an essential, but as yet unknown, biological function in bats. Therefore, these studies highlight the need for Jamaican fruit bat cell lines to propagate bat IAVs in cells originating from a natural reservoir host to mitigate such mutations in viral progeny. Given that many bat-borne viruses have a gastrointestinal tropism, including bat IAVs, it is logical to generate gastrointestinal cell lines to study these viruses. This study generated five plasmid constructs that contain Jamaican fruit bat inserts to produce recombinant wnt3a, noggin, R-spondin-2, epidermal growth factor, and gastrin. These growth factors are critical to culture self-regenerative primary crypt stem cells.

Introduction

Many bat viruses infect the gastrointestinal tract of bats such as coronaviruses and bat influenza A viruses (IAVs). IAVs are shed in feces of infected bats like canonical avian IAVs in avian reservoirs[66]. Bat IAVs H18N11 and H17N10 have not been isolated from bats but only generated using infectious clone technology[180]. Currently, these viruses can only be propagated in two canine epithelial cell lines, MDCK-II and RIE 1495 cells [181]. While H18N11 can be propagated in canine cells, it accumulates mutations in the NA gene resulting in a truncated head domain of the neuraminidase-like protein in viral progeny after two passages [66]. Experimental infection of Jamaican fruit bats (*Artibeus jamaicensis*), a natural reservoir host of H18N11, does not result in truncation of the head domain, and H18N11 infects intestinal epithelial cells [66]. Indeed, inoculation of Jamaican fruit bats with H18N11 virus containing a stop codon in the NA gene leads to reversion to wild-type NA within one passage in bats, showing that it plays an as-yet unknown essential function[1].

Sialic acid is used as a receptor for cell entry and neuraminidases are used for viral release by hydrolyzing sialic acid in canonical IAVs. However, bat IAVs use MHC class II for viral entry, and neuraminidase-like proteins of these viruses do not use cleave sialic acids for release from infected cells [182-185]. The function of bat IAV NA is currently unknown for H18N11. Interestingly, N11 is similar in structure to *Staphylococcus aureus* enterotoxin I, which also interacts with MHC-II [186]. As such, the limitation of bat cell lines hinders *in vitro* work of bat-borne viruses. Therefore, generation of cells lines originating from bats is of high importance because cell lines can reduce

the use of bats and cell lines can be readily shared with other researchers. Given that many bat-borne viruses have intestinal tropism, it is necessary to generate gastrointestinal cell lines.

Self-regenerative primary gastrointestinal cells have been generated from murine, porcine, equine, and human tissues [187-191]. The cultured primary cells that are self-renewing are generated from crypt stem cells [187-189]. To culture primary crypt stem cells for long term, five growth factors are needed: wnt3a, noggin, R-spondin-2, epidermal growth factor (EDGF), and gastrin. Wingless integration sites or 'wnt' are proteins critical to stem cell self-renewal [192-194]. R-spondin proteins work synergistically with wnt proteins for stem cell renewal by stimulating the expression of wnt stimulated genes such as *C-MYC*, *CyclinD1*, and *Axin2*[193]. Gastrin is a hormone that promotes intestinal crypt proliferation and regeneration[195-198]. Gastrin promotes proliferation and regeneration by binding with the G-coupled protein receptor CCK2R which then activates cascades such as, PLC/Ca2+/PKC, MAPK, p125fak, Src, and PI3K/AKT[195,199]. EDGF promotes proliferation, survival, and stem cell maintenance through the ErbB pathway[200]. The ErbB pathway promotes stem cell maintenance by activating downstream signaling pathways such as, PI3K-AKT, MAPK, and JAK-STAT[200]. The bone morphogenetic protein (BMP) signaling pathway is a negative regulator of crypt stem cells and noggin is an inhibitor of BMP signaling[201,202]. Therefore, noggin promotes stem cell renewal[198,201]. These five growth factors have been used to culture self-regenerative primary gastrointestinal crypt stem cells[187-189]

Methods

Protein Homology of Human, Mouse, and Rat Growth Factors to Jamaican Fruit Bat Growth Factors

Mouse and human growth factors wnt3a, noggin, and epidermal growth factor were blasted against the Jamaican fruit bat protein sequences. Gastrin protein sequences from human, mouse, and rat were aligned with the Jamaican fruit bat protein sequences. All aligned sequences demonstrated alignment scores, identities, and similarities – except gastrin alignments – that indicate high homology. (**Table 5.1 and Figure 5.1**).

Table 5.1) Mouse, Human, and Rat growth factors' percent identities and similarities to orthologous Jamaican fruit bat growth factors.

Protein	Species	Identity	Similarity
Wnt3a	Mouse	90.45%	94.66%
	Human	92.70%	96.07%
Noggin	Mouse	98.28%	98.71%
	Human	97.84%	98.71%
R-Spondin-2	Mouse	94.37%	96.71%
	Human	86.83%	88.89%
EDGF	Mouse	68.22%	80.44%
	Human	73.55%	84.23%
Gastrin	Mouse	46.04%	51.80%
	Human	49.64%	53.24%
	Rat	42.86%	50.00%

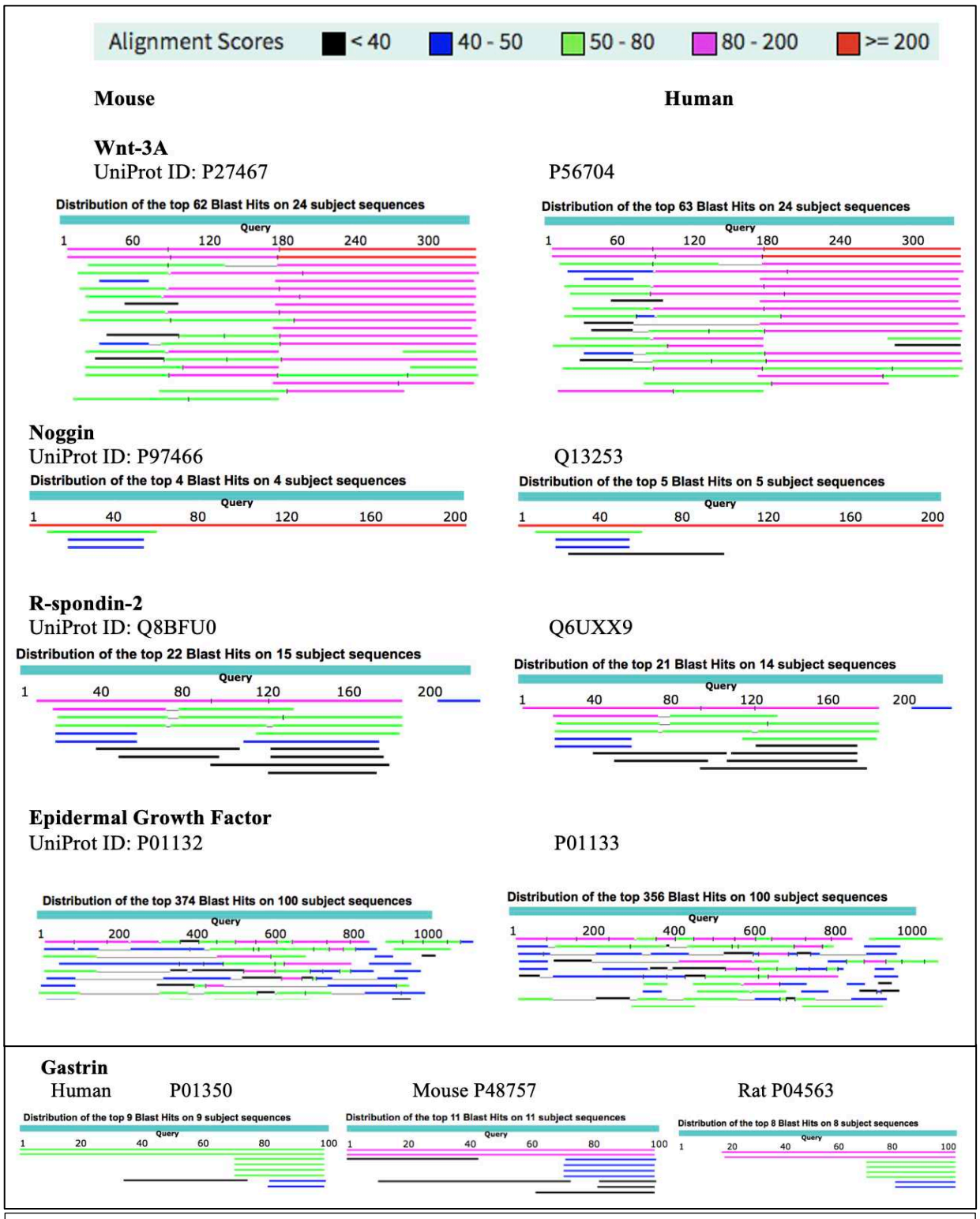

Figure 5.1) NCBI growth factor blast results.Mouse and human growth factors wnt3a, noggin, and epidermal growth factor were BLASTed against the Jamaican fruit bat protein sequences. Gastrin protein sequences from human, mouse, and rat were blasted against the Jamaican fruit bat protein sequences.

Isolation of Jamaican Fruit Bat Intestinal Crypts

Buffer recipes and cell isolation were directly used or modified (as noted below) from previously published methodology [187]. Intestinal crypts were harvested by euthanizing a bat and removing the intestine. Intestines then were cleaned of fecal matter using the back of the forceps. Intestines were then opened to expose the lumen and cut into 5 cm pieces and placed in a 50 ml tube. Intestinal pieces were washed five times using PBS. Intestinal pieces were then placed into 20 ml isolation buffer (5.6 mM/L Na_2HPO_4, 8.0 mM/L KH_2PO_4, 96.2 mM/L NaCl, 1.6 mmol/L KCl, 43.4 mM/L sucrose, and 54.9 mM/L D-sorbitol in cell culture grade water. EDTA 2 mM /ml and DTT 0.5 mM/ml was added to 10 mL isolation buffer immediately before isolation of crypts) and incubated for 1 hour at room temperature. Tubes were shaken by hand forcefully to release crypts, intestinal pieces were allowed to settle, and supernatant was aspirated, washed, and centrifuged (50xg for 3 minutes) two times with PBS. Intestinal pieces were then places into 6 well plates coated with collagen hydrogel (2mg/ml).

Generation of Cloned Plasmids for Chinese Hamster Ovary Cell Transfection

Five plasmid constructs were produced that contain Jamaican fruit bat growth factors: epidermal growth factor, wnt3a, gastrin, R-spondin 2, and noggin. Gene sequences for each growth factor were obtained using the publicly available and annotated genome from the National Center for Biotechnology: *Artibeus jamaicensis (Jamaican fruit-eating bat) GenBank assembly GCA_004027435.1.* After obtaining the sequences, gBlocks (Integrated DNA Technologies, IDT)

of epidermal growth factor, wnt3a, gastrin, R-spondin 2, and noggin, each with a 6X C-terminal end histidine tag, were produced (**Appendix VI**). pcDNA™3.3-TOPO™ TA Cloning™ Kit was used to insert each of the Jamaican fruit bat growth factor vectors (**Figure 5.2**). Following cloning,

Figure 5.2) pcDNA™3.3-TOPO™ TA plasmid vector. gBlock insertion site (magenta).

transformation was carried out using TOP10 chemically competent *Escherichia coli* for each plasmid (**Appendix VII**). To confirm correct insert size of transformed *E. coli.*, whole colony PCR

was performed. Plasmids were sequenced (Genewiz) to identify the inserts in the correct orientation.

Results

We attempted to use human, mouse, and rat growth factors to grow Jamaican fruit bat crypt generated epithelial cells because the initial protein blast sequences appeared to be closely homologous with Jamaican fruit bats. However, the crypt stem cells did not respond to the growth factors. Therefore, Jamaican fruit bat growth factors were generated. The ordered gene blocks of epidermal growth factor, wnt3a, gastrin, R-spondin 2, and noggin, each with a 6X C-terminal end histidine tag from Integrated DNA technologies were cloned into the pcDNA™3.3-TOPO™ TA Cloning™ plasmid. Plasmids with the insert in the proper 5'>3' orientation were identified for each plasmid (**Figures 5.3 - 5.6**).

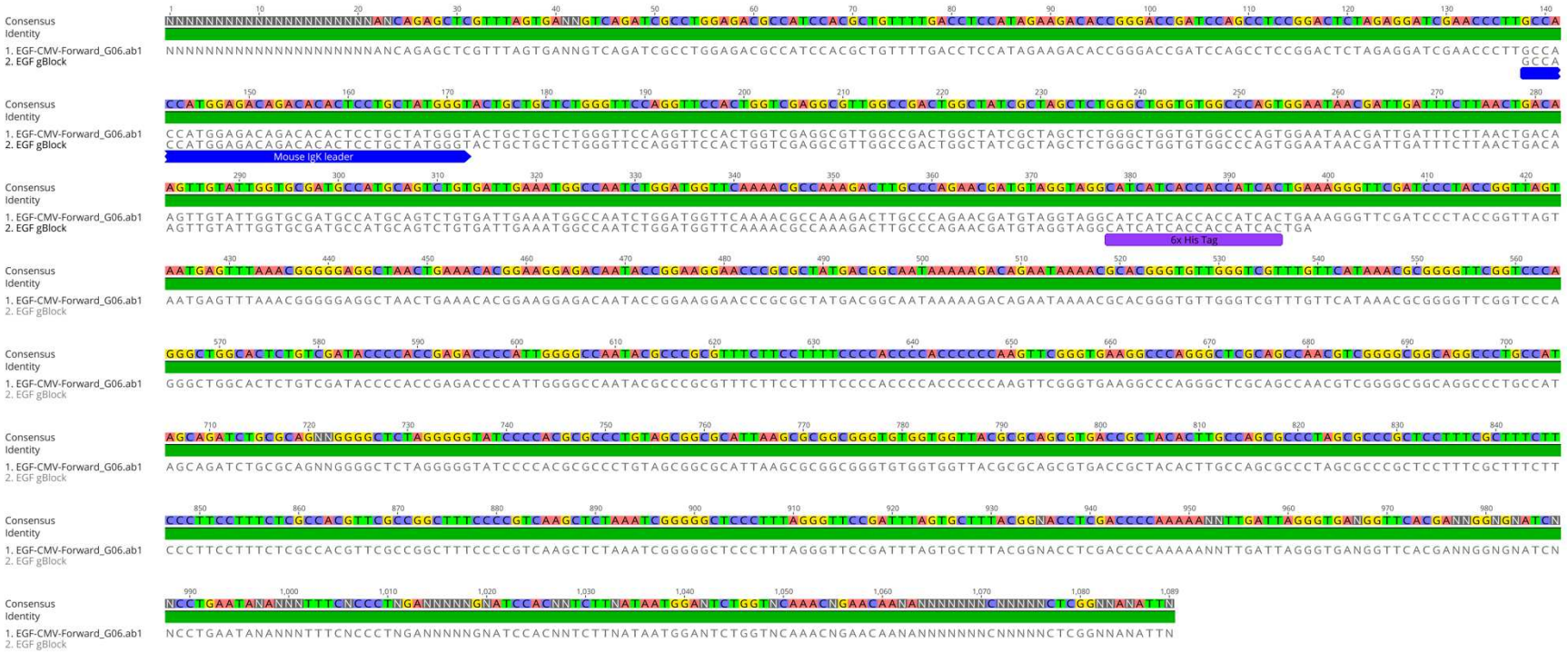

Figure 5.3) Sanger sequencing of Jamaican fruit bat epidermal growth factor plasmid (1). Sanger sequencing demonstrated correct orientation of Jamaican fruit bat epidermal growth factor insert, aligned with gBlock (2).

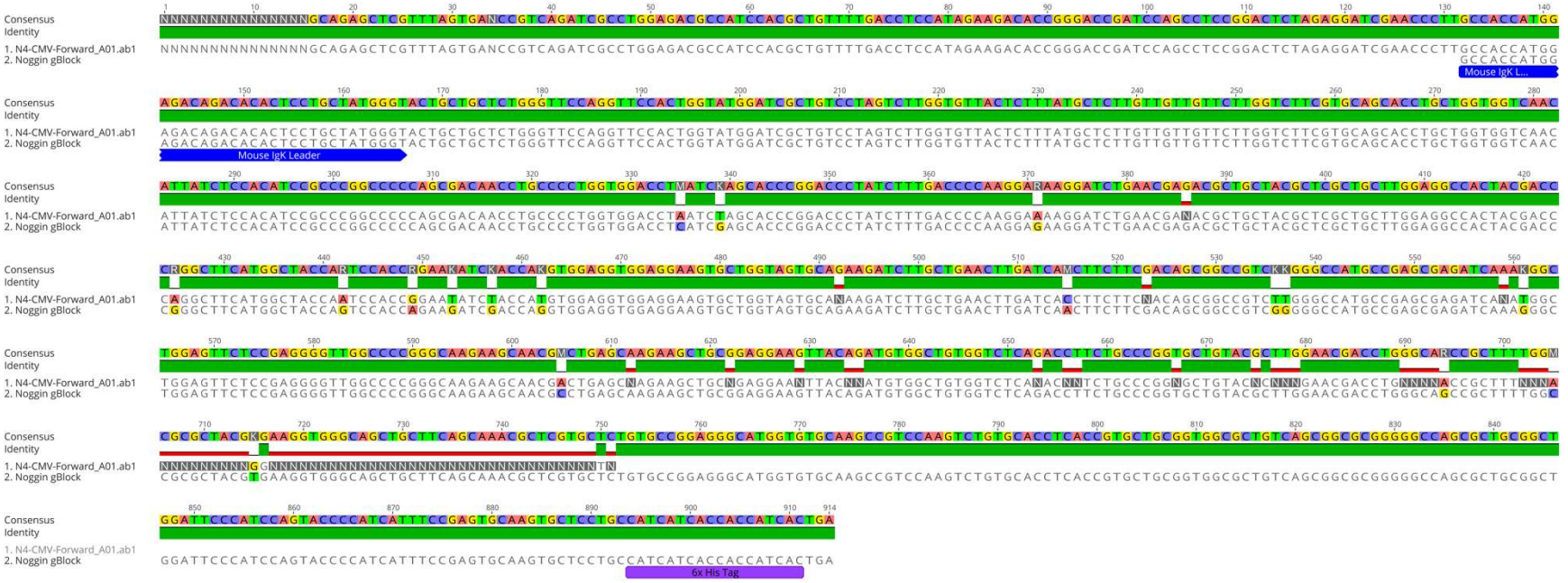

Figure 5.4) Sanger sequencing of Jamaican fruit bat noggin plasmid (1). Sanger sequencing demonstrated correct orientation of Jamaican fruit bat noggin insert, aligned with noggin gBlock (2).

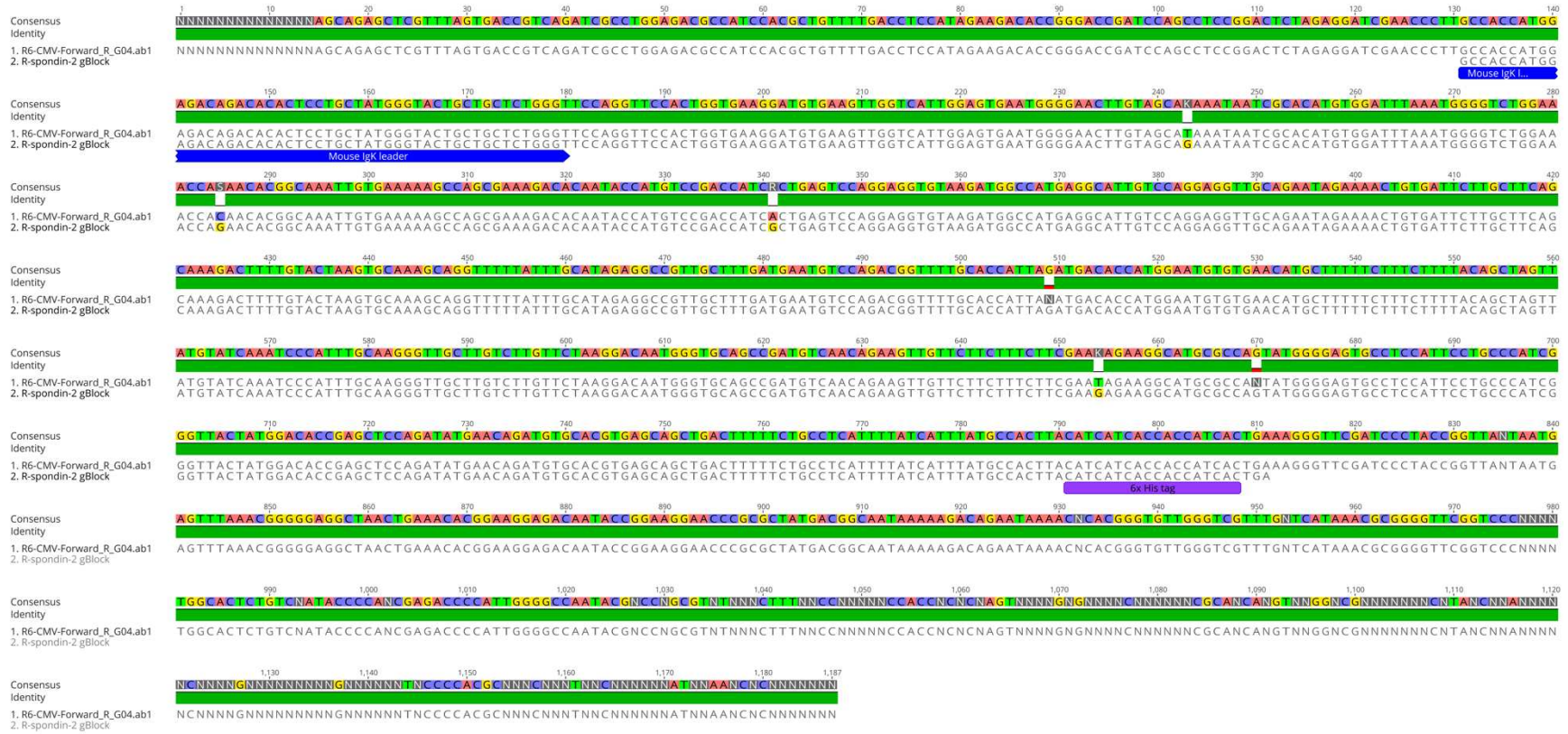

Figure 5.5) Sanger sequencing of Jamaican fruit bat R-spondin 2 plasmid (1). Sanger sequencing demonstrated correct orientation of Jamaican fruit bat noggin insert, aligned with R-spondin 2 gBlock (2).

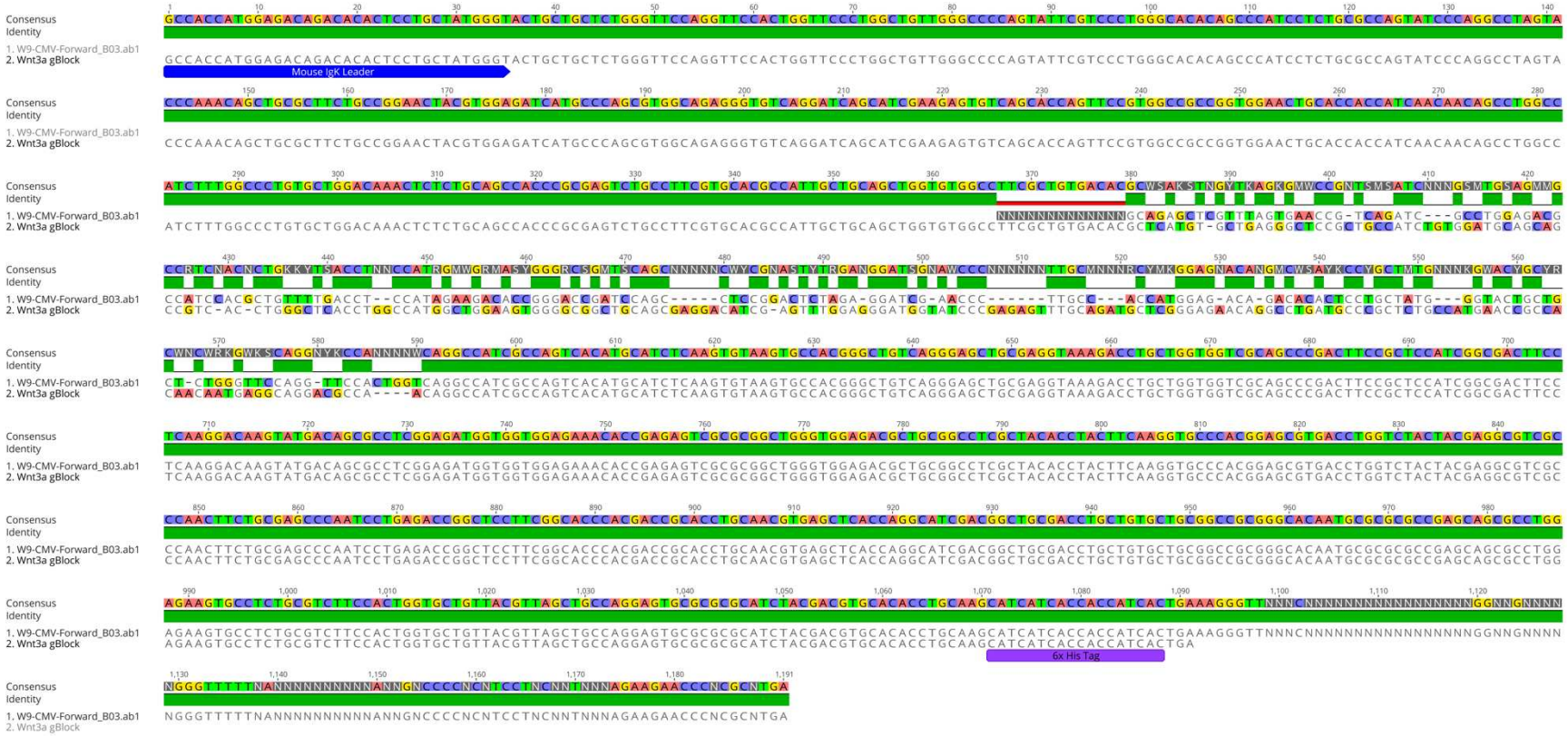

Figure 5.6) Sanger sequencing of Jamaican fruit bat wnt3a plasmid (1). Sanger sequencing demonstrated correct orientation of Jamaican fruit bat noggin insert, aligned with wnt3a gBlock (2).

Discussion and Future Directions

Human, mouse, and rat growth factors, which are commercially available, share a high degree of similarity to Jamaican fruit bat growth factors; however, the bat crypt stem cells did not respond to these growth factors in culture. Therefore, it will be necessary to culture intestinal crypt stem cells with Jamaican fruit bat growth factors. Plasmid constructs were successfully generated for each Jamaican fruit bat epidermal, wnt3a, gastrin, R-spondin 2, and noggin growth factors into pcDNA3.3 vector, which encodes mammalian promoter and polyadenylation sequences. The next step will be to generate transiently or stably transfected Chinese hamster ovary (CHO) cells with the plasmids. CHO cells were chosen to produce the growth factors because it is a well-established protein expression platform that produces mammalian glycolated proteins unlike bacteria and yeast expression platforms[203]. Jamaican fruit bat epidermal, wnt3a, gastrin, R-spondin 2, and noggin growth factors produced from the CHO cells can then be purified using the engineered histidine tags on the C-termini of each protein. Once the growth factors are generated, *in vitro* experimentation on primary Jamaican fruit bat crypt stem cells can be performed. Following the establishment of intestinal crypt stem cell cultures, ratios of growth factors can be altered to differentiate the stem cells into enterocytes. This approach should allow for bat-borne viruses that infect the gastrointestinal tract, such as H17N10 and H18N1, to be propagated without deleterious mutations.

REFERENCES

1. PubChem Identifier: 6450363.

2. Gatsogiannis, C., and Markl, J. (2009). Keyhole Limpet Hemocyanin: 9-angstrom CryoEM Structure and Molecular Model of the KLH1 Didecamer Reveal the Interfaces and Intricate Topology of the 160 Functional Units. Journal of Molecular Biology *385*, 963-983. 10.1016/j.jmb.2008.10.080.

3. The Nobel Prize in Physics 1922. (2023). https://www.nobelprize.org/prizes/physics/1922/summary/.

4. Bohr, N. (1913). I. On the constitution of atoms and molecules. The London, Edinburgh, and Dublin Philosophical Magazine and Journal of Science *26*, 1-25. 10.1080/14786441308634955.

5. Usai, C.a.D., A. (2013). Fluorescence: General Aspects.

6. Drummen, G.P.C. (2012). Fluorescent Probes and Fluorescence (Microscopy) Techniques - Illuminating Biological and Biomedical Research. Molecules *17*, 14067-14090. 10.3390/molecules171214067.

7. Ishikawa-Ankerhold, H.C., Ankerhold, R., and Drummen, G.P.C. (2012). Advanced Fluorescence Microscopy Techniques-FRAP, FLIP, FLAP, FRET and FLIM. Molecules *17*, 4047-4132. 10.3390/molecules17044047.

8. Hertz, H. (1887). Ueber einen Einfluss des ultravioletten Lichtes auf die electrische Entladung. Annalen der Physik *267*, 983-1000. https://doi.org/10.1002/andp.18872670827.

9. Einstein, A. (1905). Über einen die Erzeugung und Verwandlung des Lichtes betreffenden heuristischen Gesichtspunkt. Annalen der Physik *322*, 132-148. 10.1002/andp.19053220607.

10. Prize, T.N. (1921). The Nobel Prize in Physics 1921. https://www.nobelprize.org/prizes/physics/1921/summary/.

11. Burgess, C. (2005). OPTICAL SPECTROSCOPY | Detection Devices. In A.T. Editiors: Paul Worsfold, Colin Poole, ed. Encyclopedia of Analytical Science (Second Edition). Elsevier.

12. Lawrence, W.G., Varadi, G., Entine, G., Podniesinski, E., and Wallace, P.K. (2008). A comparison of avalanche photodiode and photomultiplier tube detectors for flow cytometry. held in San Jose, CA, 2008
Jan 21-23.

13. Song, H.-Z. (2018). Avalanche Photodiode Focal Plane Arrays and Their Application to Laser Detection and Ranging. In Photodetectors [Working Title], (IntechOpen). 10.5772/intechopen.81294.

14. Cheng, Z., Xu, H., and Chen, Y. (2018). Design of low noise silicon reach-through avalanche photodiodes. held in San Diego, CA, 2018
Aug 20-21.

15. Mcintyre, R.J., Webb, P.P., and Dautet, H. (1996). A short-wavelength selective reach-through avalanche photodiode. IEEE Transactions on Nuclear Science *43*, 1341-1346. 10.1109/23.507062.

16. Kaneda, T., Matsumoto, H., and Yamaoka, T. (1976). A model for reach-through avalanche photodiodes (RAPD's). Journal of Applied Physics *47*, 3135-3139. 10.1063/1.323107.

17. Becker, H.N., and Johnston, A.H. (2004). Dark current degradation of near infrared avalanche photodiodes from proton irradiation. Ieee Transactions on Nuclear Science *51*, 3572-3578. 10.1109/tns.2004.839165.

18. The Nobel Prize in Physiology or Medicine 1908. (2023). https://www.nobelprize.org/prizes/medicine/1908/ehrlich/facts/.

19. The Nobel Prize in Physiology or Medicine 1901. (2023). https://www.nobelprize.org/prizes/medicine/1901/behring/article/.

20. Yamada, T. (2011). Therapeutic Monoclonal Antibodies. The Keio Journal of Medicine *60*, 37-46. 10.2302/kjm.60.37.

21. Murphy, K., and Weaver, C. (2017). Janeway's immunobiology, 9th edition. Edition (Garland Science/Taylor & Francis Group, LLC).

22. Grauslund, L.R., Calvaresi, V., Pansegrau, W., Norais, N., and Rand, K.D. (2021). Epitope and Paratope Mapping by HDX-MS Combined with SPR Elucidates the Difference in Bactericidal Activity of Two Anti-NadA Monoclonal Antibodies. Journal of the American Society for Mass Spectrometry *32*, 1575-1582. 10.1021/jasms.0c00431.

23. Hanly, W.C., Artwohl, J.E., and Bennett, B.T. (1995). Review of Polyclonal Antibody Production Procedures in Mammals and Poultry. ILAR journal *37*, 93-118.

24. Van Regenmortel, M.H.V., and Muller, S. (1999, pp.136-138). Synthetic peptides as antigens (Elsevier).

25. The Nobel Prize in Physiology or Medicine 1984. (2023). https://www.nobelprize.org/prizes/medicine/1984/press-release/.

26. Coons, A.H., and Kaplan, M.H. (1950). LOCALIZATION OF ANTIGEN IN TISSUE CELLS. Journal of Experimental Medicine *91*, 1-13. 10.1084/jem.91.1.1.

27. Hopkins, S.J., and Wormall, A. (1933). Phenyl isocyanate protein compounds and their immunological properties. Biochemical Journal *27*, 740-753. 10.1042/bj0270740.

28. Creech, H.J., and Jones, R.N. (1941). Conjugates Synthesized from Various Proteins and the Isocyanates of Certain Aromatic Polynuclear Hydrocarbons. Journal of the American Chemical Society *63*, 1670-1673. 10.1021/ja01851a046.

29. Creech, H.J., and Jones, R.N. (1941). The Conjugation of Horse Serum Albumin with Isocyanates of Certain Polynuclear Aromatic Hydrocarbons. Journal of the American Chemical Society *63*, 1661-1669. 10.1021/ja01851a045.

30. Haugland, R.P. Coupling of Monoclonal Antibodies with Fluorophores. In Monoclonal Antibody Protocols, (Humana Press), pp. 205-222. 10.1385/0-89603-308-2:205.

31. Brinkley, M. (1992). A brief survey of methods for preparing protein conjugates with dyes, haptens and crosslinking reagents. Bioconjugate Chemistry *3*, 2-13. 10.1021/bc00013a001.

32. Oshannessy, D.J., and Quarles, R.H. (1987). LABELING OF THE OLIGOSACCHARIDE MOIETIES OF IMMUNOGLOBULINS. Journal of Immunological Methods *99*, 153-161. 10.1016/0022-1759(87)90120-7.

33. Dennler, P., Fischer, E., and Schibli, R. (2015). Antibody Conjugates: From Heterogeneous Populations to Defined Reagents. Antibodies *4*, 197-224. 10.3390/antib4030197.

34. Fuhrmann, S., Streitz, M., and Kern, F. (2008). How flow cytometry is changing the study of TB immunology and clinical diagnosis. Cytometry Part A *73A*, 1100-1106. 10.1002/cyto.a.20614.

35. Shao, H., Chung, J., Balaj, L., Charest, A., Bigner, D.D., Carter, B.S., Hochberg, F.H., Breakefield, X.O., Weissleder, R., and Lee, H. (2012). Protein typing of circulating microvesicles allows real-time monitoring of glioblastoma therapy. Nature Medicine *18*, 1835-1840. 10.1038/nm.2994.

36. Hoffman, R.A., Maino, V.C., Recktenwald, D.J., and Webster, H.K. (2002). BD Biosciences contributions in CD4 counting and immune status for HIV/AIDS. Cytometry *50*, 129-132. 10.1002/cyto.10095.

37. Clift, I.C. (2015). Diagnostic Flow Cytometry and the AIDS Pandemic. Labmedicine *46*, E59-E64. 10.1309/lmkhw2c86zjdrtfe.

38. Robinson, J.P. (2022). Flow cytometry: past and future. BioTechniques *72*, 159-169. 10.2144/btn-2022-0005.

39. Novo, D., Grégori, G., and Rajwa, B. (2013). Generalized unmixing model for multispectral flow cytometry utilizing nonsquare compensation matrices. Cytometry Part A *83A*, 508-520. 10.1002/cyto.a.22272.

40. Roederer, M. (2002). Compensation in flow cytometry. Current protocols in cytometry *Chapter 1*, Unit 1.14-Unit 11.14. 10.1002/0471142956.cy0114s22.

41. Novo, D. (2022). A comparison of spectral unmixing to conventional compensation for the calculation of fluorochrome abundances from flow cytometric data. Cytometry Part A *101*, 885-891. 10.1002/cyto.a.24669.

42. Fox, A., Dutt, T.S., Karger, B., Obregon-Henao, A., Anderson, G.B., and Henao-Tamayo, M. (2020). Acquisition of High-Quality Spectral Flow Cytometry Data. Current protocols in cytometry *93*, e74. 10.1002/cpcy.74.

43. About HCDM. (2023). https://www.hcdm.org/index.php/about-hcdm.

44. Schmit, T., Klomp, M., and Khan, M.N. (2021). An Overview of Flow Cytometry: Its Principles and Applications in Allergic Disease Research. In Methods in Molecular Biology, (Springer US), pp. 169-182. 10.1007/978-1-0716-1001-5_13.

45. Mccausland, M., Lin, Y.-D., Nevers, T., Groves, C., and Decman, V. (2021). With great power comes great responsibility: high-dimensional spectral flow cytometry to support clinical trials. Bioanalysis *13*, 1597-1616. 10.4155/bio-2021-0201.

46. Mahnke, Y., Chattopadhyay, P., and Roederer, M. (2010). Publication of optimized multicolor immunofluorescence panels. Cytometry Part A *77A*, 814-818. 10.1002/cyto.a.20916.

47. Kunz, T.H., de Torrez, E.B., Bauer, D., Lobova, T., and Fleming, T.H. (2011). Ecosystem services provided by bats. In Year in Ecology and Conservation Biology, R.S. Ostfeld, and W.H. Schlesinger, eds. (Blackwell Science Publ), pp. 1-38. 10.1111/j.1749-6632.2011.06004.x.

48. Nault, L.R., and Ammar, E. (1989). LEAFHOPPER AND PLANTHOPPER TRANSMISSION OF PLANT-VIRUSES. Annual Review of Entomology *34*, 503-529. 10.1146/annurev.en.34.010189.002443.

49. Sick, F., Beer, M., Kampen, H., and Wernike, K. (2019). Culicoides Biting MidgesUnderestimated Vectors for Arboviruses of Public Health and Veterinary Importance. Viruses-Basel *11*, 376. 10.3390/v11040376.

50. Tolle, M.A. (2009). Mosquito-borne diseases. Current problems in pediatric and adolescent health care *39*, 97-140. 10.1016/j.cppeds.2009.01.001.

51. Franklinos, L.H.V., Jones, K.E., Redding, D.W., and Abubakar, I. (2019). The effect of global change on mosquito-borne disease. Lancet Infectious Diseases *19*, E302-E312. 10.1016/s1473-3099(19)30161-6.

52. Mohlmann, T.W.R., Keeling, M.J., Wennergren, U., Favia, G., Santman-Berends, I., Takken, W., Koenraadt, C.J.M., and Brand, S.P.C. (2021). Biting midge dynamics and

bluetongue transmission: a multiscale model linking catch data with climate and disease outbreaks. Scientific Reports *11*, 1892-1892.

53. Calisher, C.H., Childs, J.E., Field, H.E., Holmes, K.V., and Schountz, T. (2006). Bats: Important reservoir hosts of emerging viruses. Clinical Microbiology Reviews *19*, 531-+. 10.1128/cmr.00017-06.

54. Epstein, J.H., Field, H.E., Luby, S., Pulliam, J.R.C., and Daszak, P. (2006). Nipah virus: impact, origins, and causes of emergence. Current infectious disease reports *8*, 59-65. 10.1007/s11908-006-0036-2.

55. Chua, K.B., Goh, K.J., Wong, K.T., Kamarulzaman, A., Tan, P.S.K., Ksiazek, T.G., Zaki, S.R., Paul, G., Lam, S.K., and Tan, C.T. (1999). Fatal encephalitis due to Nipah virus among pig-farmers in Malaysia. Lancet *354*, 1257-1259. 10.1016/s0140-6736(99)04299-3.

56. Rahman, M.A., Hossain, M.J., Sultana, S., Homaira, N., Khan, S.U., Rahman, M., Gurley, E.S., Rollin, P.E., Lo, M.K., Comer, J.A., et al. (2012). Date Palm Sap Linked to Nipah Virus Outbreak in Bangladesh, 2008. Vector-Borne and Zoonotic Diseases *12*, 65-72. 10.1089/vbz.2011.0656.

57. Andersen, K.G., Rambaut, A., Lipkin, W.I., Holmes, E.C., and Garry, R.F. (2020). The proximal origin of SARS-CoV-2. Nature Medicine *26*, 450-452. 10.1038/s41591-020-0820-9.

58. Cheng, T.L., Reichard, J.D., Coleman, J.T.H., Weller, T.J., Thogmartin, W.E., Reichert, B.E., Bennett, A.B., Broders, H.G., Campbell, J., Etchison, K., et al. (2021). The scope and severity of white-nose syndrome on hibernating bats in North America. Conservation Biology *35*, 1586-1597, 1-12. 10.1111/cobi.13739.

59. Zhou, P., Tachedjian, M., Wynne, J.W., Boyd, V., Cui, J., Smith, I., Cowled, C., Ng, J.H.J., Mok, L., Michalski, W.P., et al. (2016). Contraction of the type I IFN locus and unusual constitutive expression of IFN-α in bats. Proc Natl Acad Sci U S A *113*, 2696-2701. 10.1073/pnas.1518240113.

60. Schountz, T., Baker, M.L., Butler, J., and Munster, V. (2017). Immunological Control of Viral Infections in Bats and the Emergence of Viruses Highly Pathogenic to Humans. Front Immunol *8*. 10.3389/fimmu.2017.01098.

61. Max, E., and Fugmann, S. (2013). Fundamental immunology.

62. Bratsch, S., Wertz, N., Chaloner, K., Kunz, T.H., and Butler, J.E. (2011). The little brown bat, M. lucifugus, displays a highly diverse V-H, D-H and J(H) repertoire but little evidence of somatic hypermutation. Developmental and Comparative Immunology *35*, 421-430. 10.1016/j.dci.2010.06.004.

63. Cogswell-Hawkinson, A., Bowen, R., James, S., Gardiner, D., Calisher, C.H., Adams, R., and Schountz, T. (2012). Tacaribe Virus Causes Fatal Infection of An Ostensible

Reservoir Host, the Jamaican Fruit Bat. Journal of Virology *86*, 5791-5799. 10.1128/jvi.00201-12.

64. Malmlov, A., Bantle, C., Aboellail, T., Wagner, K., Campbell, C.L., Eckley, M., Chotiwan, N., Gullberg, R.C., Perera, R., Tjalkens, R., and Schountz, T. (2019). Experimental Zika virus infection of Jamaican fruit bats (Artibeus jamaicensis) and possible entry of virus into brain via activated microglial cells. PLOS Neglected Tropical Diseases *13*, e0007071. 10.1371/journal.pntd.0007071.

65. Munster, V.J., Adney, D.R., van Doremalen, N., Brown, V.R., Miazgowicz, K.L., Milne-Price, S., Bushmaker, T., Rosenke, R., Scott, D., Hawkinson, A., et al. (2016). Replication and shedding of MERS-CoV in Jamaican fruit bats (Artibeus jamaicensis). Scientific Reports *6*, 21878. 10.1038/srep21878.

66. Ciminski, K., Ran, W., Gorka, M., Lee, J., Malmlov, A., Schinkothe, J., Eckley, M., Murrieta, R.A., Aboellail, T.A., Campbell, C.L., et al. (2019). Bat influenza viruses transmit among bats but are poorly adapted to non-bat species. Nature Microbiology *4*, 2298-2309. 10.1038/s41564-019-0556-9.

67. Heinen, P.P., van Nieuwstadt, A.P., de Boer-Luijtze, E.A., and Bianchi, A.T.J. (2001). Analysis of the quality of protection induced by a porcine influenza A vaccine to challenge with an H3N2 virus. Veterinary Immunology and Immunopathology *82*, 39-56. 10.1016/s0165-2427(01)00342-7.

68. Lv, J., Wang, D., Hua, Y.-H., Pei, S.-J., Wang, J., Hu, W.-W., Wang, X.-L., Jia, N., and Jiang, Q.-S. (2014). Pulmonary immune responses to 2009 pandemic influenza A (H1N1) virus in mice. Bmc Infectious Diseases *14*, 197. 10.1186/1471-2334-14-197.

69. Marche, S., van den Berg, T., and Lambrecht, B. (2016). Evaluation of the kinetics of anti-NP and anti-HA antibody after infection of Pekin ducks with low pathogenic avian influenza virus. Veterinary Medicine and Science *2*, 36-46. 10.1002/vms3.18.

70. Periasamy, P., Hutchinson, P.E., Chen, J.M., Bonne, I., Hameed, S.S.S., Selvam, P., Hey, Y.Y., Fink, K., Irving, A.T., Dutertre, C.A., et al. (2019). Studies on B Cells in the Fruit-Eating Black Flying Fox (Pteropus alecto). Frontiers in Immunology *10*, 489. 10.3389/fimmu.2019.00489.

71. Martínez Gómez, J.M., Periasamy, P., Dutertre, C.-A., Irving, A.T., Ng, J.H.J., Crameri, G., Baker, M.L., Ginhoux, F., Wang, L.-F., and Alonso, S. (2016). Phenotypic and functional characterization of the major lymphocyte populations in the fruit-eating bat Pteropus alecto. Scientific Reports *6*, 37796. 10.1038/srep37796.

72. Gamage, A.M., Zhu, F., Ahn, M., Foo, R.J.H., Hey, Y.Y., Low, D.H.W., Mendenhall, I.H., Dutertre, C.-A., and Wang, L.-F. (2020). Immunophenotyping monocytes, macrophages and granulocytes in the Pteropodid bat Eonycteris spelaea. Scientific Reports *10*. 10.1038/s41598-019-57212-1.

73. Burke, B., Rocha, S.M., Zhan, S., Eckley, M., Reasoner, C., Addetia, A., Lewis, J., Fagre, A., Charley, P., Richt, J.A., et al. (2023). Regulatory T Cell-like Response to SARS-CoV-2 in Jamaican Fruit Bats (Artibeus jamaicensis) Transduced with Human ACE2. Cold Spring Harbor Laboratory.

74. Hu, B., Zeng, L.P., Yang, X.L., Ge, X.Y., Zhang, W., Li, B., Xie, J.Z., Shen, X.R., Zhang, Y.Z., Wang, N., et al. (2017). Discovery of a rich gene pool of bat SARS-related coronaviruses provides new insights into the origin of SARS coronavirus. PLoS pathogens *13*, e1006698. 10.1371/journal.ppat.1006698.

75. Zhou, P., Yang, X.L., Wang, X.G., Hu, B., Zhang, L., Zhang, W., Si, H.R., Zhu, Y., Li, B., Huang, C.L., et al. (2020). A pneumonia outbreak associated with a new coronavirus of probable bat origin. Nature *579*, 270-273. 10.1038/s41586-020-2012-7.

76. Zhou, H., Ji, J., Chen, X., Bi, Y., Li, J., Wang, Q., Hu, T., Song, H., Zhao, R., Chen, Y., et al. (2021). Identification of novel bat coronaviruses sheds light on the evolutionary origins of SARS-CoV-2 and related viruses. Cell *184*, 4380-4391 e4314. 10.1016/j.cell.2021.06.008.

77. Worobey, M., Levy, J.I., Malpica Serrano, L., Crits-Christoph, A., Pekar, J.E., Goldstein, S.A., Rasmussen, A.L., Kraemer, M.U.G., Newman, C., Koopmans, M.P.G., et al. (2022). The Huanan Seafood Wholesale Market in Wuhan was the early epicenter of the COVID-19 pandemic. Science *377*, 951-959. 10.1126/science.abp8715.

78. Lau, S.K., Woo, P.C., Li, K.S., Huang, Y., Tsoi, H.W., Wong, B.H., Wong, S.S., Leung, S.Y., Chan, K.H., and Yuen, K.Y. (2005). Severe acute respiratory syndrome coronavirus-like virus in Chinese horseshoe bats. Proceedings of the National Academy of Sciences of the United States of America *102*, 14040-14045.

79. Li, W., Shi, Z., Yu, M., Ren, W., Smith, C., Epstein, J.H., Wang, H., Crameri, G., Hu, Z., Zhang, H., et al. (2005). Bats are natural reservoirs of SARS-like coronaviruses. Science (New York, N.Y.) *310*, 676-679. 10.1126/science.1118391.

80. Poon, L.L., Chu, D.K., Chan, K.H., Wong, O.K., Ellis, T.M., Leung, Y.H., Lau, S.K., Woo, P.C., Suen, K.Y., Yuen, K.Y., et al. (2005). Identification of a novel coronavirus in bats. J Virol *79*, 2001-2009. 10.1128/JVI.79.4.2001-2009.2005.

81. Ge, X.Y., Li, J.L., Yang, X.L., Chmura, A.A., Zhu, G., Epstein, J.H., Mazet, J.K., Hu, B., Zhang, W., Peng, C., et al. (2013). Isolation and characterization of a bat SARS-like coronavirus that uses the ACE2 receptor. Nature *503*, 535-538. 10.1038/nature12711.

82. Delaune, D., Hul, V., Karlsson, E.A., Hassanin, A., Ou, T.P., Baidaliuk, A., Gambaro, F., Prot, M., Tu, V.T., Chea, S., et al. (2021). A novel SARS-CoV-2 related coronavirus in bats from Cambodia. Nat Commun *12*, 6563. 10.1038/s41467-021-26809-4.

83. Wacharapluesadee, S., Tan, C.W., Maneeorn, P., Duengkae, P., Zhu, F., Joyjinda, Y., Kaewpom, T., Chia, W.N., Ampoot, W., Lim, B.L., et al. (2021). Evidence for SARS-

CoV-2 related coronaviruses circulating in bats and pangolins in Southeast Asia. Nat Commun *12*, 972. 10.1038/s41467-021-21240-1.

84. Ruiz-Aravena, M., McKee, C., Gamble, A., Lunn, T., Morris, A., Snedden, C.E., Yinda, C.K., Port, J.R., Buchholz, D.W., Yeo, Y.Y., et al. (2022). Ecology, evolution and spillover of coronaviruses from bats. Nat Rev Microbiol *20*, 299-314. 10.1038/s41579-021-00652-2.

85. Letko, M., Marzi, A., and Munster, V. (2020). Functional assessment of cell entry and receptor usage for SARS-CoV-2 and other lineage B betacoronaviruses. Nat Microbiol *5*, 562-569. 10.1038/s41564-020-0688-y.

86. Munster, V.J., Adney, D.R., van Doremalen, N., Brown, V.R., Miazgowicz, K.L., Milne-Price, S., Bushmaker, T., Rosenke, R., Scott, D., Hawkinson, A., et al. (2016). Replication and shedding of MERS-CoV in Jamaican fruit bats (Artibeus jamaicensis). Sci Rep *6*, 21878. 10.1038/srep21878.

87. van Boheemen, S., de Graaf, M., Lauber, C., Bestebroer, T.M., Raj, V.S., Zaki, A.M., Osterhaus, A.D., Haagmans, B.L., Gorbalenya, A.E., Snijder, E.J., and Fouchier, R.A. (2012). Genomic characterization of a newly discovered coronavirus associated with acute respiratory distress syndrome in humans. mBio *3*. 10.1128/mBio.00473-12.

88. Annan, A., Baldwin, H.J., Corman, V.M., Klose, S.M., Owusu, M., Nkrumah, E.E., Badu, E.K., Anti, P., Agbenyega, O., Meyer, B., et al. (2013). Human betacoronavirus 2c EMC/2012-related viruses in bats, Ghana and Europe. Emerg Infect Dis *19*, 456-459. 10.3201/eid1903.121503.

89. Ithete, N.L., Stoffberg, S., Corman, V.M., Cottontail, V.M., Richards, L.R., Schoeman, M.C., Drosten, C., Drexler, J.F., and Preiser, W. (2013). Close relative of human Middle East respiratory syndrome coronavirus in bat, South Africa. Emerg Infect Dis *19*, 1697-1699. 10.3201/eid1910.130946.

90. Reusken, C.B., Haagmans, B.L., Muller, M.A., Gutierrez, C., Godeke, G.J., Meyer, B., Muth, D., Raj, V.S., Smits-De Vries, L., Corman, V.M., et al. (2013). Middle East respiratory syndrome coronavirus neutralising serum antibodies in dromedary camels: a comparative serological study. Lancet Infect Dis *13*, 859-866. 10.1016/S1473-3099(13)70164-6.

91. Chan, J.F., Zhang, A.J., Yuan, S., Poon, V.K., Chan, C.C., Lee, A.C., Chan, W.M., Fan, Z., Tsoi, H.W., Wen, L., et al. (2020). Simulation of the Clinical and Pathological Manifestations of Coronavirus Disease 2019 (COVID-19) in a Golden Syrian Hamster Model: Implications for Disease Pathogenesis and Transmissibility. Clin Infect Dis *71*, 2428-2446. 10.1093/cid/ciaa325.

92. Oreshkova, N., Molenaar, R.J., Vreman, S., Harders, F., Oude Munnink, B.B., Hakze-van der Honing, R.W., Gerhards, N., Tolsma, P., Bouwstra, R., Sikkema, R.S., et al. (2020). SARS-CoV-2 infection in farmed minks, the Netherlands, April and May 2020. Euro Surveill *25*. 10.2807/1560-7917.ES.2020.25.23.2001005.

93. Sia, S.F., Yan, L.M., Chin, A.W.H., Fung, K., Choy, K.T., Wong, A.Y.L., Kaewpreedee, P., Perera, R., Poon, L.L.M., Nicholls, J.M., et al. (2020). Pathogenesis and transmission of SARS-CoV-2 in golden hamsters. Nature *583*, 834-838. 10.1038/s41586-020-2342-5.

94. Fagre, A., Lewis, J., Eckley, M., Zhan, S., Rocha, S.M., Sexton, N.R., Burke, B., Geiss, B., Peersen, O., Bass, T., et al. (2021). SARS-CoV-2 infection, neuropathogenesis and transmission among deer mice: Implications for spillback to New World rodents. PLoS Pathog *17*, e1009585. 10.1371/journal.ppat.1009585.

95. Griffin, B.D., Chan, M., Tailor, N., Mendoza, E.J., Leung, A., Warner, B.M., Duggan, A.T., Moffat, E., He, S., Garnett, L., et al. (2021). SARS-CoV-2 infection and transmission in the North American deer mouse. Nat Commun *12*, 3612. 10.1038/s41467-021-23848-9.

96. Hale, V.L., Dennis, P.M., McBride, D.S., Nolting, J.M., Madden, C., Huey, D., Ehrlich, M., Grieser, J., Winston, J., Lombardi, D., et al. (2021). SARS-CoV-2 infection in free-ranging white-tailed deer (Odocoileus virginianus). bioRxiv. 10.1101/2021.11.04.467308.

97. van Aart, A.E., Velkers, F.C., Fischer, E.A.J., Broens, E.M., Egberink, H., Zhao, S., Engelsma, M., Hakze-van der Honing, R.W., Harders, F., de Rooij, M.M.T., et al. (2021). SARS-CoV-2 infection in cats and dogs in infected mink farms. Transbound Emerg Dis. 10.1111/tbed.14173.

98. Schountz, T. (2014). Immunology of bats and their viruses: challenges and opportunities. Viruses *6*, 4880-4901. 10.3390/v6124880.

99. Amman, B.R., Jones, M.E., Sealy, T.K., Uebelhoer, L.S., Schuh, A.J., Bird, B.H., Coleman-McCray, J.D., Martin, B.E., Nichol, S.T., and Towner, J.S. (2015). Oral shedding of Marburg virus in experimentally infected Egyptian fruit bats (*Rousettus aegyptiacus*). Journal of wildlife diseases *51*, 113-124. 10.7589/2014-08-198.

100. Foo, R., Hey, Y.Y., Jia Ng, J.H., Chionh, Y.T., Chia, W.N., Kong, P.S., Lee, B.P.Y., Kang, A.E.Z., Borthwick, S.A., Low, D.H.W., et al. (2022). Establishment of a Captive Cave Nectar Bat (Eonycteris spelaea) Breeding Colony in Singapore. J Am Assoc Lab Anim Sci *61*, 344-352. 10.30802/AALAS-JAALAS-21-000090.

101. Schlottau, K., Rissmann, M., Graaf, A., Schon, J., Sehl, J., Wylezich, C., Hoper, D., Mettenleiter, T.C., Balkema-Buschmann, A., Harder, T., et al. (2020). SARS-CoV-2 in fruit bats, ferrets, pigs, and chickens: an experimental transmission study. Lancet Microbe *1*, e218-e225. 10.1016/S2666-5247(20)30089-6.

102. Hall, J.S., Knowles, S., Nashold, S.W., Ip, H.S., Leon, A.E., Rocke, T., Keller, S., Carossino, M., Balasuriya, U., and Hofmeister, E. (2021). Experimental challenge of a North American bat species, big brown bat (Eptesicus fuscus), with SARS-CoV-2. Transbound Emerg Dis *68*, 3443-3452. 10.1111/tbed.13949.

103. Bosco-Lauth, A.M., Porter, S.M., Fox, K.A., Wood, M.E., Neubaum, D., and Quilici, M. (2022). Experimental Infection of Brazilian Free-Tailed Bats (Tadarida brasiliensis) with Two Strains of SARS-CoV-2. Viruses *14*. 10.3390/v14081809.

104. Hall, J.S., Hofmeister, E., Ip, H.S., Nashold, S.W., Leon, A.E., Malave, C.M., Falendysz, E.A., Rocke, T.E., Carossino, M., Balasuriya, U., and Knowles, S. (2022). Experimental infection of Mexican free-tailed bats (*Tadarida brasiliensis*) with SARS-CoV-2. bioRxiv. 10.1101/2022.07.18.500430.

105. Hassan, A.O., Case, J.B., Winkler, E.S., Thackray, L.B., Kafai, N.M., Bailey, A.L., McCune, B.T., Fox, J.M., Chen, R.E., Alsoussi, W.B., et al. (2020). A SARS-CoV-2 Infection Model in Mice Demonstrates Protection by Neutralizing Antibodies. Cell *182*, 744-753 e744. 10.1016/j.cell.2020.06.011.

106. Sun, J., Zhuang, Z., Zheng, J., Li, K., Wong, R.L., Liu, D., Huang, J., He, J., Zhu, A., Zhao, J., et al. (2020). Generation of a Broadly Useful Model for COVID-19 Pathogenesis, Vaccination, and Treatment. Cell *182*, 734-743 e735. 10.1016/j.cell.2020.06.010.

107. Wong, L.R., Li, K., Sun, J., Zhuang, Z., Zhao, J., McCray, P.B., Jr., and Perlman, S. (2020). Sensitization of Non-permissive Laboratory Mice to SARS-CoV-2 with a Replication-Deficient Adenovirus Expressing Human ACE2. STAR Protoc *1*, 100169. 10.1016/j.xpro.2020.100169.

108. Cogswell-Hawkinson, A., Bowen, R., James, S., Gardiner, D., Calisher, C.H., Adams, R., and Schountz, T. (2012). Tacaribe virus causes fatal infection of an ostensible reservoir host, the Jamaican fruit bat. Journal of virology *86*, 5791-5799. 10.1128/JVI.00201-12.

109. Gerrard, D.L., Hawkinson, A., Sherman, T., Modahl, C.M., Hume, G., Campbell, C.L., Schountz, T., and Frietze, S. (2017). Transcriptomic Signatures of Tacaribe Virus-Infected Jamaican Fruit Bats. mSphere *2*. 10.1128/mSphere.00245-17.

110. Malmlov, A., Bantle, C., Aboellail, T., Wagner, K., Campbell, C.L., Eckley, M., Chotiwan, N., Gullberg, R.C., Perera, R., Tjalkens, R., and Schountz, T. (2019). Experimental Zika virus infection of Jamaican fruit bats (Artibeus jamaicensis) and possible entry of virus into brain via activated microglial cells. PLoS Negl Trop Dis *13*, e0007071. 10.1371/journal.pntd.0007071.

111. Luan, J., Jin, X., Lu, Y., and Zhang, L. (2020). SARS-CoV-2 spike protein favors ACE2 from Bovidae and Cricetidae. J Med Virol *92*, 1649-1656. 10.1002/jmv.25817.

112. Wan, Y., Shang, J., Graham, R., Baric, R.S., and Li, F. (2020). Receptor Recognition by the Novel Coronavirus from Wuhan: an Analysis Based on Decade-Long Structural Studies of SARS Coronavirus. Journal of virology *94*. 10.1128/JVI.00127-20.

113. Temmam, S., Vongphayloth, K., Baquero, E., Munier, S., Bonomi, M., Regnault, B., Douangboubpha, B., Karami, Y., Chretien, D., Sanamxay, D., et al. (2022). Bat

coronaviruses related to SARS-CoV-2 and infectious for human cells. Nature *604*, 330-336. 10.1038/s41586-022-04532-4.

114. Yan, H., Jiao, H., Liu, Q., Zhang, Z., Xiong, Q., Wang, B.J., Wang, X., Guo, M., Wang, L.F., Lan, K., et al. (2021). ACE2 receptor usage reveals variation in susceptibility to SARS-CoV and SARS-CoV-2 infection among bat species. Nat Ecol Evol *5*, 600-608. 10.1038/s41559-021-01407-1.

115. Rathnasinghe, R., Strohmeier, S., Amanat, F., Gillespie, V.L., Krammer, F., Garcia-Sastre, A., Coughlan, L., Schotsaert, M., and Uccellini, M.B. (2020). Comparison of transgenic and adenovirus hACE2 mouse models for SARS-CoV-2 infection. Emerg Microbes Infect *9*, 2433-2445. 10.1080/22221751.2020.1838955.

116. Simmons, G., Gosalia, D.N., Rennekamp, A.J., Reeves, J.D., Diamond, S.L., and Bates, P. (2005). Inhibitors of cathepsin L prevent severe acute respiratory syndrome coronavirus entry. Proc Natl Acad Sci U S A *102*, 11876-11881. 10.1073/pnas.0505577102.

117. Aicher, S.M., Streicher, F., Chazal, M., Planas, D., Luo, D., Buchrieser, J., Nemcova, M., Seidlova, V., Zukal, J., Serra-Cobo, J., et al. (2022). Species-Specific Molecular Barriers to SARS-CoV-2 Replication in Bat Cells. J Virol *96*, e0060822. 10.1128/jvi.00608-22.

118. Hayward, J.A., Tachedjian, M., Johnson, A., Irving, A.T., Gordon, T.B., Cui, J., Nicolas, A., Smith, I., Boyd, V., Marsh, G.A., et al. (2022). Unique Evolution of Antiviral Tetherin in Bats. J Virol *96*, e0115222. 10.1128/jvi.01152-22.

119. Halpin, K., Hyatt, A.D., Fogarty, R., Middleton, D., Bingham, J., Epstein, J.H., Rahman, S.A., Hughes, T., Smith, C., Field, H.E., et al. (2011). Pteropid bats are confirmed as the reservoir hosts of henipaviruses: a comprehensive experimental study of virus transmission. Am J Trop Med Hyg *85*, 946-951. 10.4269/ajtmh.2011.10-0567.

120. Paweska, J.T., Jansen van Vuren, P., Masumu, J., Leman, P.A., Grobbelaar, A.A., Birkhead, M., Clift, S., Swanepoel, R., and Kemp, A. (2012). Virological and serological findings in Rousettus aegyptiacus experimentally inoculated with vero cells-adapted hogan strain of Marburg virus. PLoS One *7*, e45479. 10.1371/journal.pone.0045479.

121. Schuh, A.J., Amman, B.R., Sealy, T.K., Spengler, J.R., Nichol, S.T., and Towner, J.S. (2017). Egyptian rousette bats maintain long-term protective immunity against Marburg virus infection despite diminished antibody levels. Sci Rep *7*, 8763. 10.1038/s41598-017-07824-2.

122. Ciminski, K., Ran, W., Gorka, M., Lee, J., Malmlov, A., Schinkothe, J., Eckley, M., Murrieta, R.A., Aboellail, T.A., Campbell, C.L., et al. (2019). Bat influenza viruses transmit among bats but are poorly adapted to non-bat species. Nat Microbiol *4*, 2298-2309. 10.1038/s41564-019-0556-9.

123. Schuh, A.J., Amman, B.R., Sealy, T.K., Kainulainen, M.H., Chakrabarti, A.K., Guerrero, L.W., Nichol, S.T., Albarino, C.G., and Towner, J.S. (2019). Antibody-Mediated Virus

Neutralization Is Not a Universal Mechanism of Marburg, Ebola, or Sosuga Virus Clearance in Egyptian Rousette Bats. J Infect Dis *219*, 1716-1721. 10.1093/infdis/jiy733.

124. Zhang, Y., Chirmule, N., Gao, G.P., Qian, R., Croyle, M., Joshi, B., Tazelaar, J., and Wilson, J.M. (2001). Acute cytokine response to systemic adenoviral vectors in mice is mediated by dendritic cells and macrophages. Mol Ther *3*, 697-707. 10.1006/mthe.2001.0329.

125. Chattopadhyay, P.K., Yu, J., and Roederer, M. (2005). A live-cell assay to detect antigen-specific CD4+ T cells with diverse cytokine profiles. Nat Med *11*, 1113-1117. 10.1038/nm1293.

126. Frentsch, M., Arbach, O., Kirchhoff, D., Moewes, B., Worm, M., Rothe, M., Scheffold, A., and Thiel, A. (2005). Direct access to CD4+ T cells specific for defined antigens according to CD154 expression. Nat Med *11*, 1118-1124. 10.1038/nm1292.

127. Weiskopf, D., Schmitz, K.S., Raadsen, M.P., Grifoni, A., Okba, N.M.A., Endeman, H., van den Akker, J.P.C., Molenkamp, R., Koopmans, M.P.G., van Gorp, E.C.M., et al. (2020). Phenotype and kinetics of SARS-CoV-2-specific T cells in COVID-19 patients with acute respiratory distress syndrome. Sci Immunol *5*. 10.1126/sciimmunol.abd2071.

128. Pusnik, J., Richter, E., Schulte, B., Dolscheid-Pommerich, R., Bode, C., Putensen, C., Hartmann, G., Alter, G., and Streeck, H. (2021). Memory B cells targeting SARS-CoV-2 spike protein and their dependence on CD4(+) T cell help. Cell Rep *35*, 109320. 10.1016/j.celrep.2021.109320.

129. Neidleman, J., Luo, X., George, A.F., McGregor, M., Yang, J., Yun, C., Murray, V., Gill, G., Greene, W.C., Vasquez, J., et al. (2021). Distinctive features of SARS-CoV-2-specific T cells predict recovery from severe COVID-19. Cell Rep *36*, 109414. 10.1016/j.celrep.2021.109414.

130. Zotos, D., Coquet, J.M., Zhang, Y., Light, A., D'Costa, K., Kallies, A., Corcoran, L.M., Godfrey, D.I., Toellner, K.M., Smyth, M.J., et al. (2010). IL-21 regulates germinal center B cell differentiation and proliferation through a B cell-intrinsic mechanism. J Exp Med *207*, 365-378. 10.1084/jem.20091777.

131. Guito, J.C., Prescott, J.B., Arnold, C.E., Amman, B.R., Schuh, A.J., Spengler, J.R., Sealy, T.K., Harmon, J.R., Coleman-McCray, J.D., Kulcsar, K.A., et al. (2021). Asymptomatic Infection of Marburg Virus Reservoir Bats Is Explained by a Strategy of Immunoprotective Disease Tolerance. Curr Biol *31*, 257-270 e255. 10.1016/j.cub.2020.10.015.

132. Kirejczyk, S.G.M., Amman, B.R., Schuh, A.J., Sealy, T.K., Albarino, C.G., Zhang, J., Brown, C.C., and Towner, J.S. (2022). Histopathologic and Immunohistochemical Evaluation of Induced Lesions, Tissue Tropism and Host Responses following Experimental Infection of Egyptian Rousette Bats (Rousettus aegyptiacus) with the Zoonotic Paramyxovirus, Sosuga Virus. Viruses *14*. 10.3390/v14061278.

133. Easterbrook, J.D., Zink, M.C., and Klein, S.L. (2007). Regulatory T cells enhance persistence of the zoonotic pathogen Seoul virus in its reservoir host. Proceedings of the National Academy of Sciences of the United States of America *104*, 15502-15507. 10.1073/pnas.0707453104.

134. Schountz, T., Prescott, J., Cogswell, A.C., Oko, L., Mirowsky-Garcia, K., Galvez, A.P., and Hjelle, B. (2007). Regulatory T cell-like responses in deer mice persistently infected with Sin Nombre virus. Proceedings of the National Academy of Sciences of the United States of America *104*, 15496-15501. 0707454104 [pii] 10.1073/pnas.0707454104.

135. Kelley, L.A., Mezulis, S., Yates, C.M., Wass, M.N., and Sternberg, M.J. (2015). The Phyre2 web portal for protein modeling, prediction and analysis. Nat Protoc *10*, 845-858. 10.1038/nprot.2015.053.

136. Henikoff, S., and Henikoff, J.G. (1992). Amino acid substitution matrices from protein blocks. Proceedings of the National Academy of Sciences of the United States of America *89*, 10915-10919. 10.1073/pnas.89.22.10915.

137. Corman, V.M., Landt, O., Kaiser, M., Molenkamp, R., Meijer, A., Chu, D.K., Bleicker, T., Brunink, S., Schneider, J., Schmidt, M.L., et al. (2020). Detection of 2019 novel coronavirus (2019-nCoV) by real-time RT-PCR. Euro Surveill *25*. 10.2807/1560-7917.ES.2020.25.3.2000045.

138. Hsieh, C.L., Goldsmith, J.A., Schaub, J.M., DiVenere, A.M., Kuo, H.C., Javanmardi, K., Le, K.C., Wrapp, D., Lee, A.G., Liu, Y., et al. (2020). Structure-based design of prefusion-stabilized SARS-CoV-2 spikes. Science *369*, 1501-1505. 10.1126/science.abd0826.

139. Walls, A.C., Park, Y.J., Tortorici, M.A., Wall, A., McGuire, A.T., and Veesler, D. (2020). Structure, Function, and Antigenicity of the SARS-CoV-2 Spike Glycoprotein. Cell *181*, 281-292 e286. 10.1016/j.cell.2020.02.058.

140. McCallum, M., Bassi, J., De Marco, A., Chen, A., Walls, A.C., Di Iulio, J., Tortorici, M.A., Navarro, M.J., Silacci-Fregni, C., Saliba, C., et al. (2021). SARS-CoV-2 immune evasion by the B.1.427/B.1.429 variant of concern. Science *373*, 648-654. 10.1126/science.abi7994.

141. McCallum, M., Walls, A.C., Sprouse, K.R., Bowen, J.E., Rosen, L.E., Dang, H.V., De Marco, A., Franko, N., Tilles, S.W., Logue, J., et al. (2021). Molecular basis of immune evasion by the Delta and Kappa SARS-CoV-2 variants. Science *374*, 1621-1626. 10.1126/science.abl8506.

142. Oko, L., Aduddell-Swope, B., Willis, D., Hamor, R., Coons, T.A., Hjelle, B., and Schountz, T. (2006). Profiling helper T cell subset gene expression in deer mice. BMC Immunol *7*, 18.

143. Pavlovich, S.S., Lovett, S.P., Koroleva, G., Guito, J.C., Arnold, C.E., Nagle, E.R., Kulcsar, K., Lee, A., Thibaud-Nissen, F., Hume, A.J., et al. (2018). The Egyptian

Rousette Genome Reveals Unexpected Features of Bat Antiviral Immunity. Cell. *173*, 1098-1110.e1018. 10.1016/j.cell.2018.03.070.

144. Malmlov, A., Bantle, C., Aboellail, T., Wagner, K., Campbell, C.L., Eckley, M., Chotiwan, N., Gullberg, R.C., Perera, R., Tjalkens, R., and Schountz, T. (2019). Experimental Zika virus infection of Jamaican fruit bats (Artibeus jamaicensis) and possible entry of virus into brain via activated microglial cells. Plos Neglected Tropical Diseases *13*, e0007071. 10.1371/journal.pntd.0007071.

145. Geneious Prime 2022.2.1 (https://www.geneious.com).

146. Henikoff, S., and Henikoff, J.G. (1992). AMINO-ACID SUBSTITUTION MATRICES FROM PROTEIN BLOCKS. Proceedings of the National Academy of Sciences of the United States of America *89*, 10915-10919. 10.1073/pnas.89.22.10915.

147. Kelley, L.A., Mezulis, S., Yates, C.M., Wass, M.N., and Sternberg, M.J.E. (2015). The Phyre2 web portal for protein modeling, prediction and analysis. Nature Protocols *10*, 845-858. 10.1038/nprot.2015.053.

148. JA, L., J, S., K, B., J, C., N, C., M, D., J, F., M, G., M, G., EM, G., et al. (2008). MIFlowCyt: The Minimum Information About a Flow Cytometry Experiment. Cytometry. Part A : the journal of the International Society for Analytical Cytology *73*. 10.1002/cyto.a.20623.

149. Spidlen, J., Breuer, K., and Brinkman, R. (2012). Preparing a Minimum Information about a Flow Cytometry Experiment (MIFlowCyt) compliant manuscript using the International Society for Advancement of Cytometry (ISAC) FCS file repository (FlowRepository.org). Current protocols in cytometry *Chapter 10*, Unit 10.18-Unit 10.18. 10.1002/0471142956.cy1018s61.

150. Colovai, A.I., Giatzikis, C., Ho, E.K., Farooqi, M., Suciu-Foca, N., Cattoretti, G., and Orazi, A. (2004). Flow cytometric analysis of normal and reactive spleen. Modern Pathology *17*, 918-927. 10.1038/modpathol.3800141.

151. Nemoto, S., Mailloux, A.W., Kroeger, J., and Mule, J.J. (2016). OMIP-031: Immunologic Checkpoint Expression on Murine Effector and Memory T-Cell Subsets. Cytometry Part A *89A*, 427-429. 10.1002/cyto.a.22808.

152. Dusoswa, S.A., Verhoeff, J., and Garcia-Vallejo, J.J. (2019). OMIP-054: Broad Immune Phenotyping of Innate and Adaptive Leukocytes in the Brain, Spleen, and Bone Marrow of an Orthotopic Murine Glioblastoma Model by Mass Cytometry. Cytometry Part A *95A*, 422-426. 10.1002/cyto.a.23725.

153. Natalini, A., Simonetti, S., Favaretto, G., Peruzzi, G., Antonangeli, F., Santoni, A., Munoz-Ruiz, M., Hayday, A., and Di Rosa, F. (2021). OMIP-079: Cell cycle of CD4(+) and CD8(+) naive/memory T cell subsets, and of Treg cells from mouse spleen. Cytometry Part A *99*, 1171-1175. 10.1002/cyto.a.24509.

154. Punt, J.A., Roberts, J.L., Kearse, K.P., and Singer, A. (1994). STOICHIOMETRY OF THE T-CELL ANTIGEN RECEPTOR (TCR) COMPLEX - EACH TCR/CD3 COMPLEX CONTAINS ONE TCR-ALPHA, ONE TCR-BETA, AND 2 CD3-EPSILON CHAINS. Journal of Experimental Medicine *180*, 587-593. 10.1084/jem.180.2.587.

155. Delahera, A., Muller, U., Olsson, C., Isaaz, S., and Tunnacliffe, A. (1991). STRUCTURE OF THE T-CELL ANTIGEN RECEPTOR (TCR) - 2 CD3-EPSILON SUBUNITS IN A FUNCTIONAL TCR/CD3 COMPLEX. Journal of Experimental Medicine *173*, 7-17. 10.1084/jem.173.1.7.

156. Kasai, M., Yoneda, T., Habu, S., Maruyama, Y., Okumura, K., and Tokunaga, T. (1981). INVIVO EFFECT OF ANTI-ASIALO GM1 ANTIBODY ON NATURAL-KILLER ACTIVITY. Nature *291*, 334-335. 10.1038/291334a0.

157. Kasai, M., Iwamori, M., Nagai, Y., Okumura, K., and Tada, T. (1980). A GLYCOLIPID ON THE SURFACE OF MOUSE NATURAL-KILLER CELLS. European Journal of Immunology *10*, 175-180. 10.1002/eji.1830100304.

158. Kurioka, A., Cosgrove, C., Simoni, Y., van Wilgenburg, B., Geremia, A., Bjoerkander, S., Sverremark-Ekstrom, E., Thurnheer, C., Guenthard, H.F., Khanna, N., et al. (2018). CD161 Defines a Functionally Distinct Subset of Pro-Inflammatory Natural Killer Cells. Frontiers in Immunology *9*, 486. 10.3389/fimmu.2018.00486.

159. Fergusson, J.R., Huehn, M.H., Swadling, L., Walker, L.J., Kurioka, A., Llibre, A., Bertoletti, A., Hollaender, G., Newell, E.W., Davis, M.M., et al. (2016). CD161(int)CD8+T cells: a novel population of highly functional, memory CD8+T cells enriched within the gut. Mucosal Immunology *9*, 401-413. 10.1038/mi.2015.69.

160. Rizzo, K., Stetler-Stevenson, M., Wilson, W., and Yuan, C.M. (2009). Novel CD19 Expression in a Peripheral T Cell Lymphoma: A Flow Cytometry Case Report with Morphologic Correlation. Cytometry Part B-Clinical Cytometry *76B*, 142-149. 10.1002/cyto.b.20442.

161. Bradford, C., Jennings, R., and Ramos-Vara, J. (2010). Gastrointestinal leiomyosarcoma in an Egyptian fruit bat (Rousettus aegyptiacus). Journal of Veterinary Diagnostic Investigation *22*, 462-465. 10.1177/104063871002200324.

162. McLelland, D.J., Dutton, C.J., and Barker, I.K. (2009). Sarcomatoid carcinoma in the lung of an Egyptian fruit bat (Rousettus aegyptiacus). Journal of Veterinary Diagnostic Investigation *21*, 160-163. 10.1177/104063870902100129.

163. Barclay, A.N., Birkeland, L.M., Brown, H.M., Beyers, D.A., Davis, J.S., Somoza, C., and Williams, F.A. (1993). The Leucocyte antigen factsbook (Academic Press).

164. Kovacs, K.G., Macsik-Valent, B., Matko, J., Bajtay, Z., and Erdei, A. (2021). Revisiting the Coreceptor Function of Complement Receptor Type 2 (CR2, CD21); Coengagement With the B-Cell Receptor Inhibits the Activation, Proliferation, and Antibody Production of Human B Cells. Frontiers in Immunology *12*, 620427. 10.3389/fimmu.2021.620427.

165. Brandstadter, J.D., and Yang, Y. (2011). Natural Killer Cell Responses to Viral Infection. Journal of Innate Immunity *3*, 274-279. 10.1159/000324176.

166. Zhou, G., Juang, S.W.W., and Kane, K.P. (2013). NK cells exacerbate the pathology of influenza virus infection in mice. European Journal of Immunology *43*, 929-938. 10.1002/eji.201242620.

167. Naiki, M., Marcus, D.M., and Ledeen, R. (1974). PROPERTIES OF ANTISERA TO GANGLIOSIDE GM1 AND ASIALO GM1. Journal of Immunology *113*, 84-93.

168. Deligne, C., Milcent, B., Josseaume, N., Teillaud, J.-L., and Siberil, S. (2017). Impact of Depleting Therapeutic Monoclonal Antibodies on the Host Adaptive Immunity: A Bonus or a Malus? Frontiers in Immunology *8*, 950. 10.3389/fimmu.2017.00950.

169. Kreslavsky, T., Gleimer, M., Garbe, A.I., and Von Boehmer, H. (2010). αβ versus γδ fate choice: counting the T-cell lineages at the branch point. Immunological Reviews *238*, 169-181. 10.1111/j.1600-065x.2010.00947.x.

170. Dusseaux, M., Martin, E., Serriari, N., Peguillet, I., Premel, V., Louis, D., Milder, M., Le Bourhis, L., Soudais, C., Treiner, E., and Lantz, O. (2011). Human MAIT cells are xenobiotic-resistant, tissue-targeted, CD161(hi) IL-17-secreting T cells. Blood *117*, 1250-1259. 10.1182/blood-2010-08-303339.

171. Sharma, P.K., Wong, E.B., Napier, R.J., Bishai, W.R., Ndung'U, T., Kasprowicz, V.O., Lewinsohn, D.A., Lewinsohn, D.M., and Gold, M.C. (2015). High expression of CD26 accurately identifies human bacteria-reactive MR1-restricted MAIT cells. Immunology *145*, 443-453. 10.1111/imm.12461.

172. Meermeier, E.W., Laugel, B.F., Sewell, A.K., Corbett, A.J., Rossjohn, J., Mccluskey, J., Harriff, M.J., Franks, T., Gold, M.C., and Lewinsohn, D.M. (2016). Human TRAV1-2-negative MR1-restricted T cells detect S. pyogenes and alternatives to MAIT riboflavin-based antigens. Nature Communications *7*, 12506. 10.1038/ncomms12506.

173. Eberhard, J.M., Hartjen, P., Kummer, S., Schmidt, R.E., Bockhorn, M., Lehmann, C., Balagopal, A., Hauber, J., Van Lunzen, J., and Zur Wiesch, J.S. (2014). CD161+ MAIT Cells Are Severely Reduced in Peripheral Blood and Lymph Nodes of HIV-Infected Individuals Independently of Disease Progression. PLoS ONE *9*, e111323. 10.1371/journal.pone.0111323.

174. Trambley, J., Bingaman, A.W., Lin, A., Elwood, E.T., Waitze, S.Y., Ha, J.W., Durham, M.M., Corbascio, M., Cowan, S.R., Pearson, T.C., and Larsen, C.P. (1999). Asialo GM1(+) CD8(+) T cells play a critical role in costimulation blockade-resistant allograft rejection. Journal of Clinical Investigation *104*, 1715-1722. 10.1172/jci8082.

175. Karunathilaka, A., Halstrom, S., Price, P., Holt, M., Lutzky, V.P., Doolan, D.L., Kupz, A., Bell, S.C., Thomson, R.M., Miles, J.J., and Ratnatunga, C.N. (2022). CD161 expression defines new human γδ T cell subsets. Immunity & Ageing *19*. 10.1186/s12979-022-00269-w.

176. Dintwe, O., Rohith, S., Schwedhelm, K.V., Mcelrath, M.J., Andersen-Nissen, E., and De Rosa, S.C. (2019). OMIP-056: Evaluation of Human Conventional T Cells, Donor-Unrestricted T Cells, and NK Cells Including Memory Phenotype by Intracellular Cytokine Staining. Cytometry Part A *95*, 722-725. 10.1002/cyto.a.23753.

177. Bartolomé-Casado, R., Landsverk, O.J.B., Chauhan, S.K., Richter, L., Phung, D., Greiff, V., Risnes, L.F., Yao, Y., Neumann, R.S., Yaqub, S., et al. (2019). Resident memory CD8 T cells persist for years in human small intestine. Journal of Experimental Medicine *216*, 2412-2426. 10.1084/jem.20190414.

178. Pastan, I., Hassan, R., FitzGerald, D.J., and Kreitman, R.J. (2006). Immunotoxin therapy of cancer. Nature Reviews Cancer *6*, 559-565. 10.1038/nrc1891.

179. Frankel, A.E., Woo, J.H., Ahn, C., Foss, F.M., Duvic, M., Neville, P.H., and Neville, D.M. (2015). Resimmune, an anti-CD3 epsilon recombinant immunotoxin, induces durable remissions in patients with cutaneous T-cell lymphoma. Haematologica *100*, 794-800. 10.3324/haematol.2015.123711.

180. Zhou, B., Ma, J., Liu, Q., Bawa, B., Wang, W., Shabman, R.S., Duff, M., Lee, J., Lang, Y., Cao, N., et al. (2014). Characterization of Uncultivable Bat Influenza Virus Using a Replicative Synthetic Virus. In PLoS Pathog. 10.1371/journal.ppat.1004420.

181. Moreira É, A., Locher, S., Kolesnikova, L., Bolte, H., Aydillo, T., García-Sastre, A., Schwemmle, M., and Zimmer, G. (2016). Synthetically derived bat influenza A-like viruses reveal a cell type- but not species-specific tropism. Proc Natl Acad Sci U S A *113*, 12797-12802. 10.1073/pnas.1608821113.

182. Tong, S., Zhu, X., Li, Y., Shi, M., Zhang, J., Bourgeois, M., Yang, H., Chen, X., Recuenco, S., Gomez, J., et al. (2013). New world bats harbor diverse influenza A viruses. PLoS Pathog *9*, e1003657. 10.1371/journal.ppat.1003657.

183. Zhu, X., Yang, H., Guo, Z., Yu, W., Carney, P.J., Li, Y., Chen, L.-M., Paulson, J.C., Donis, R.O., Tong, S., et al. (2012). Crystal structures of two subtype N10 neuraminidase-like proteins from bat influenza A viruses reveal a diverged putative active site. 10.1073/pnas.1212579109.

184. Li, Q., Sun, X., Li, Z., Liu, Y., Vavricka, C.J., Qi, J., and Gao, G.F. (2012). Structural and functional characterization of neuraminidase-like molecule N10 derived from bat influenza A virus. 10.1073/pnas.1211037109.

185. Tong, S., Zhu, X., Li, Y., Shi, M., Zhang, J., Bourgeois, M., Yang, H., Chen, X., Recuenco, S., Gomez, J., et al. (2013). New World Bats Harbor Diverse Influenza A Viruses. In PLoS Pathog. 10.1371/journal.ppat.1003657.

186. A, W., and S, W. (2015). Using Common Spatial Distributions of Atoms to Relate Functionally Divergent Influenza Virus N10 and N11 Protein Structures to Functionally Characterized Neuraminidase Structures, Toxin Cell Entry Domains, and Non-Influenza Virus Cell Entry Domains. PloS one *10*. 10.1371/journal.pone.0117499.

187. Wang, Y., DiSalvo, M., Gunasekara, D.B., Dutton, J., Proctor, A., Lebhar, M.S., Williamson, I.A., Speer, J., Howard, R.L., Smiddy, N.M., et al. (2017). Self-renewing Monolayer of Primary Colonic or Rectal Epithelial Cells. In Cell Mol Gastroenterol Hepatol, pp. 165-182 e167. 10.1016/j.jcmgh.2017.02.011.

188. Sato, T., Stange, D.E., Ferrante, M., Vries, R.G.J., van Es, J.H., van den Brink, S., van Houdt, W.J., Pronk, A., van Gorp, J., Siersema, P.D., and Clevers, H. (2011). Long-term Expansion of Epithelial Organoids From Human Colon, Adenoma, Adenocarcinoma, and Barrett's Epithelium. Gastroenterology *141*, 1762-1772. 10.1053/j.gastro.2011.07.050.

189. Stewart, A.S., Freund, J.M., Blikslager, A.T., and Gonzalez, L.M. (2018). Intestinal Stem Cell Isolation and Culture in a Porcine Model of Segmental Small Intestinal Ischemia. Jove-Journal of Visualized Experiments, e57647. 10.3791/57647.

190. Stewart, A.S., Freund, J.M., and Gonzalez, L.M. (2018). Advanced three-dimensional culture of equine intestinal epithelial stem cells. Equine Veterinary Journal *50*, 241-248. 10.1111/evj.12734.

191. Gonzalez, L.M., Williamson, I., Piedrahita, J.A., Blikslager, A.T., and Magness, S.T. (2013). Cell Lineage Identification and Stem Cell Culture in a Porcine Model for the Study of Intestinal Epithelial Regeneration. Plos One *8*, e66465. 10.1371/journal.pone.0066465.

192. Nusse, R., and Varmus, H. (2012). Three decades of Wnts: a personal perspective on how a scientific field developed. Embo Journal *31*, 2670-2684. 10.1038/emboj.2012.146.

193. Morgan, R.G., Mortensson, E., and Williams, A.C. (2018). Targeting LGR5 in Colorectal Cancer: therapeutic gold or too plastic? British Journal of Cancer *118*, 1410-1418. 10.1038/s41416-018-0118-6.

194. Schuijers, J., and Clevers, H. (2012). Adult mammalian stem cells: the role of Wnt, Lgr5 and R-spondins. Embo Journal *31*, 2685-2696. 10.1038/emboj.2012.149.

195. Sheng, W.W., Malagola, E., Nienhuser, H., Zhang, Z.Y., Kim, W., Zamechek, L., Sepulveda, A., Hata, M., Hayakawa, Y., Zhao, C.M., et al. (2020). Hypergastrinemia Expands Gastric ECL Cells Through CCK2R(+) Progenitor Cells via ERK Activation. Cellular and Molecular Gastroenterology and Hepatology *10*, 434-+. 10.1016/j.jcmgh.2020.04.008.

196. Zhang, Z.L., and Chen, W.W. (2002). Proliferation of intestinal crypt cells by gastrin-induced ornithine decarboxylase. World Journal of Gastroenterology *8*, 183-187. 10.3748/wjg.v8.i1.183.

197. Ottewell, P.D., Duckworth, C.A., Varro, A., Dimaline, R., Wang, T.C., Watson, A.J.M., Dockray, G.J., and Pritchard, D.M. (2006). Gastrin increases murine intestinal crypt regeneration following injury. Gastroenterology *130*, 1169-1180. 10.1053/j.gastro.2005.12.033.

198. Simmini, S., Bialecka, M., Huch, M., Kester, L., van de Wetering, M., Sato, T., Beck, F., van Oudenaarden, A., Clevers, H., and Deschamps, J. (2014). Transformation of intestinal stem cells into gastric stem cells on loss of transcription factor Cdx2. Nature Communications *5*, 5728. 10.1038/ncomms6728.

199. Zeng, Q., Ou, L., Wang, W., and Guo, D.Y. (2020). Gastrin, Cholecystokinin, Signaling, and Biological Activities in Cellular Processes. Frontiers in Endocrinology *11*, 112. 10.3389/fendo.2020.00112.

200. Abud, H.E., Chan, W.H., and Jarde, T. (2021). Source and Impact of the EGF Family of Ligands on Intestinal Stem Cells. Frontiers in Cell and Developmental Biology *9*, 685665. 10.3389/fcell.2021.685665.

201. Qi, Z., Li, Y.H., Zhao, B., Xu, C., Liu, Y., Li, H.N., Zhang, B.J., Wang, X.Q., Yang, X., Xie, W., et al. (2017). BMP restricts stemness of intestinal Lgr5(+) stem cells by directly suppressing their signature genes. Nature Communications *8*, 13824. 10.1038/ncomms13824.

202. Clevers, H. (2013). The Intestinal Crypt, A Prototype Stem Cell Compartment. Cell *154*, 274-284. 10.1016/j.cell.2013.07.004.

203. Demain, A.L., and Vaishnav, P. (2009). Production of recombinant proteins by microbes and higher organisms. Biotechnology Advances *27*, 297-306. 10.1016/j.biotechadv.2009.01.008.

204. Kishimoto, T., kikutani, H., von dem Borne, A.E.G., Kr., Goyert, S.G., Mason, D.Y., Miyasaka, M., Moretta, Lorenzo, Okumura, K., et al. (1998). Leucocyte typing VI : white cell differentiation antigens : proceedings of the sixth international workshop and conference held in Kobe, Japan, 10-14 November 1996 (Garland Pub.).

205. Zola, H., Swart, B., Nicholson, I., and Voss, E. (2007). Leukocyte and stromal cell molecules : the CD markers (Wiley-Liss).

206. Civin, C.I., Strauss, L.C., Brovall, C., Fackler, M.J., Schwartz, J.F., and Shaper, J.H. (1984). ANTIGENIC ANALYSIS OF HEMATOPOIESIS .3. A HEMATOPOIETIC PROGENITOR-CELL SURFACE-ANTIGEN DEFINED BY A MONOCLONAL-ANTIBODY RAISED AGAINST KG-1A CELLS. Journal of Immunology *133*, 157-165.

207. Sidney, L.E., Branch, M.J., Dunphy, S.E., Dua, H.S., and Hopkinson, A. (2014). Concise Review: Evidence for CD34 as a Common Marker for Diverse Progenitors. Stem Cells *32*, 1380-1389. 10.1002/stem.1661.

208. Kishimoto, T., kikutani, H., von dem Borne, A.E.G., Kr., Goyert, S.G., Mason, D.Y., Miyasaka, M., Moretta, Lorenzo, Okumura, K., et al. (1998). Leucocyte typing VI : white cell differentiation antigens : proceedings of the sixth international workshop and conference held in Kobe, Japan, 10-14 November 1996 (Garland Pub.).

209. Jalkanen, S., Jalkanen, M., Bargatze, R., Tammi, M., and Butcher, E.C. (1988). BIOCHEMICAL-PROPERTIES OF GLYCOPROTEINS INVOLVED IN LYMPHOCYTE RECOGNITION OF HIGH ENDOTHELIAL VENULES IN MAN. Journal of Immunology *141*, 1615-1623.

210. Bourguignon, L.Y.W., and Jin, H.T. (1995). IDENTIFICATION OF THE ANKYRIN-BINDING DOMAIN OF THE MOUSE T-LYMPHOMA CELL INOSITOL 1,4,5-TRISPHOSPHATE (IP3) RECEPTOR AND ITS ROLE IN THE REGULATION OF IP3-MEDIATED INTERNAL CA2+ RELEASE. Journal of Biological Chemistry *270*, 7257-7260. 10.1074/jbc.270.13.7257.

211. Tsukita, S., Oishi, K., Sato, N., Sagara, J., and Kawai, A. (1994). ERM FAMILY MEMBERS AS MOLECULAR LINKERS BETWEEN THE CELL-SURFACE GLYCOPROTEIN CD44 AND ACTIN-BASED CYTOSKELETONS. Journal of Cell Biology *126*, 391-401. 10.1083/jcb.126.2.391.

212. Trowbridge, I.S., and Thomas, M.L. (1994). CD45 - AN EMERGING ROLE AS A PROTEIN-TYROSINE-PHOSPHATASE REQUIRED FOR LYMPHOCYTE-ACTIVATION AND DEVELOPMENT. Annual Review of Immunology *12*, 85-116. 10.1146/annurev.immunol.12.1.85.

213. Basadonna, G.P., Auersvald, L., Khuong, C.Q., Zheng, X.X., Kashio, N., Zekzer, D., Minozzo, M., Qian, H.Y., Visser, L., Diepstra, A., et al. (1998). Antibody-mediated targeting of CD45 isoforms: A novel immunotherapeutic strategy. Proceedings of the National Academy of Sciences of the United States of America *95*, 3821-3826. 10.1073/pnas.95.7.3821.

214. Zola, H. (2007). Leukocyte and stromal cell molecules : the CD markers (Wiley-Liss).

215. Graves, C.L., Harden, S.W., LaPato, M., Nelson, M., Amador, B., Sorenson, H., Frazier, C.J., and Wallet, S.M. (2014). A method for high purity intestinal epithelial cell culture from adult human and murine tissues for the investigation of innate immune function. Journal of Immunological Methods *414*, 20-31. 10.1016/j.jim.2014.08.002.

216. Ieguchi, K., Fujita, M., Ma, Z., Davari, P., Taniguchi, Y., Sekiguchi, K., Wang, B., Takada, Y.K., and Takada, Y. (2010). Direct Binding of the EGF-like Domain of Neuregulin-1 to Integrins (alpha v beta 3 and alpha 6 beta 4) Is Involved in Neuregulin-1/ErbB Signaling. Journal of Biological Chemistry *285*, 31388-31398. 10.1074/jbc.M110.113878.

217. Fujita, M., Ieguchi, K., Davari, P., Yamaji, S., Taniguchi, Y., Sekiguchi, K., Takada, Y.K., and Takada, Y. (2012). Cross-talk between Integrin alpha 6 beta 4 and Insulin-like Growth Factor-1 Receptor (IGF1R) through Direct alpha 6 beta 4 Binding to IGF1 and Subsequent alpha 6 beta 4-IGF1-IGF1R Ternary Complex Formation in Anchorage-independent Conditions. Journal of Biological Chemistry *287*, 12491-12500. 10.1074/jbc.M111.304170.

218. Prieto, D.M.C., Cheng, Y., Chang, C.-C., Yu, J., Takada, Y.K., and Takada, Y. (2017). Direct integrin binding to insulin-like growth factor-2 through the C-domain is required for insulin-like growth factor receptor type 1 (IGF1R) signaling. Plos One *12*, e0184285. 10.1371/journal.pone.0184285.

219. Sun, Y., Malaer, J.D., and Mathew, P.A. (2019). Lectin-like transcript 1 as a natural killer cell-mediated immunotherapeutic target for triple negative breast cancer and prostate cancer. Journal of cancer metastasis and treatment *2019*. 10.20517/2394-4722.2019.29.

220. Rosen, D.B., Bettadapura, Y., Alsharifi, M., Mathew, P.A., Warren, H.S., and Lanier, L.L. (2005). Cutting edge: Lectin-like transcript-1 is a ligand for the inhibitory human NKR-P1A receptor. Journal of Immunology *175*, 7796-7799. 10.4049/jimmunol.175.12.7796.

221. Aldemir, H., Prod'homme, V., Dumaurier, M.J., Retiere, C., Poupon, G., Cazareth, J., Bih, F., and Braud, V.M. (2005). Cutting edge: Lectin-like transcript 1 is a ligand for the CD161 receptor. Journal of Immunology *175*, 7791-7795. 10.4049/jimmunol.175.12.7791.

222. Mathew, S.O., Chaudhary, P., Powers, S.B., Vishwanatha, J.K., and Mathew, P.A. (2016). Overexpression of LLT1 (OCIL, CLEC2D) on prostate cancer cells inhibits NK cell-mediated killing through LLT1-NKRP1A (CD161) interaction. Oncotarget *7*, 68650-68661. 10.18632/oncotarget.11896.

223. Marrufo, A.M., Chaudhary, P., Mathew, S.O., Malaer, J.D., Vishwanatha, J.K., and Mathew, P.A. (2018). Blocking LLT1 (CLEC2D, OCIL)-NKRP1A (CD161) interaction enhances natural killer cell-mediated lysis of triple-negative breast cancer cells. American Journal of Cancer Research *8*, 1050-1063.

224. Wyrozemski, L., and Qiao, S.-W. (2021). Immunobiology and conflicting roles of the human CD161 receptor in T cells. Scandinavian Journal of Immunology *94*, e13090. 10.1111/sji.13090.

225. Duurland, C.L., Brown, C.C., O'Shaughnessy, R.F.L., and Wedderburn, L.R. (2017). CD161(+) Tconv and CD161(+) Treg Share a Transcriptional and Functional Phenotype despite Limited Overlap in TCR beta Repertoire. Frontiers in Immunology *8*, 103. 10.3389/fimmu.2017.00103.

226. Kuttruff, S., Koch, S., Kelp, A., Pawelec, G., Rammensee, H.-G., and Steinle, A. (2009). NKp80 defines and stimulates a reactive subset of CD8 T cells. Blood *113*, 358-369. 10.1182/blood-2008-04-145615.

227. Welte, S., Kuttruff, S., Waldhauer, I., and Steinle, A. (2006). Mutual activation of natural killer cells and monocytes mediated by NKp80-AICL interaction. Nature Immunology *7*, 1334-1342. 10.1038/ni1402.

228. Bartel, Y., Bauer, B., and Steinle, A. (2013). Modulation of NK cell function by genetically coupled C-type lectin-like receptor/ligand pairs encoded in the human natural killer gene complex. Frontiers in Immunology *4*, 362. 10.3389/fimmu.2013.00362.

229. Van Regenmortel, M.H.V., and Muller, S. (1999). Synthetic peptides as antigens (Elsevier).

APPENDIX I

IN SILICO PROTEIN HOMOLOGY OF JAMAICAN FRUIT BAT CLUSTERS OF DIFFERENTIATION AND OTHER IMMUNE CELL MARKERS TO IDENTIFY CROSS-REACTIVE ANTIBODIES

Asialo GM1

Asialo GM1 (AGM1) is a glycosphingolipid (**Figure I.1**) [1]. AGM1 glycosphingolipid is expressed on natural killer cells and some subsets of cytotoxic T cells [157,174]. Polyclonal anti-AGM1 antibodies were first made in 1974 [167]. Classically, anti-AGM1 antibodies have been used to deplete natural killer cells *in vivo* [157,166].

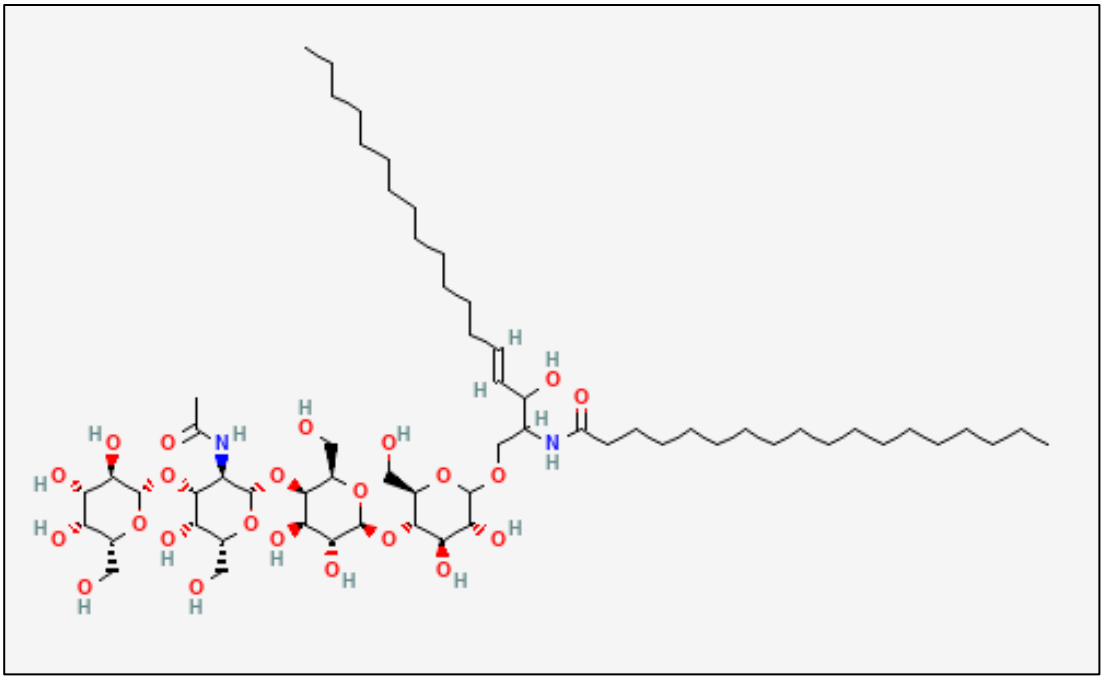

Figure I.1) Structure of glycosphingolipid asialo GM1. [1]

Reactivity of Polyclonal Anti-Asialo GM1 with Jamaican Fruit Bat Splenocytes

There are a variety of glycosphingolipids but established antibodies that bind to specific glycosphingolipids do not have the complication of homology like proteins do. The predominant question is if the glycosphingolipid AGM1 is expressed by Jamaican fruit bats at detectable levels, and the identification of those cell types. Polyclonal anti-AGM1 primary antibody binds to Jamaican fruit bat splenocytes (**Figure I.2**). Refer to CD161 for further characterization of $AGM1^{+}$ cells.

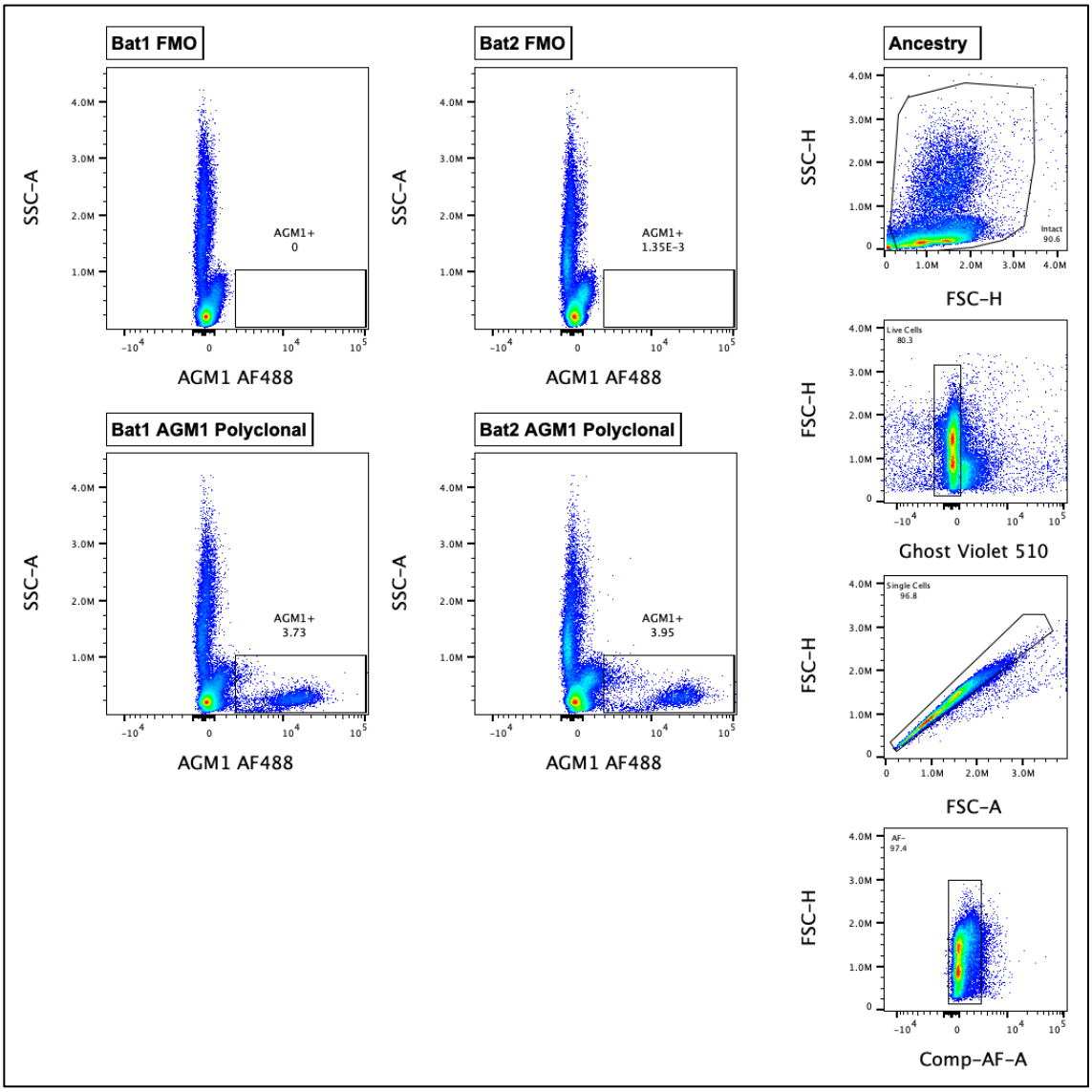

Figure I.2) Anti-AGM1 polyclonal antibody staining of Jamaican fruit bat splenocytes. Panel: Anti-AGM-1 (FITC), primary amine viability (Ghost Violet 510). Acquired using a Cytek Aurora 4L 16V-14B-10YG-8R cytometer.

CD3ε

CD3ε is one chain that is a part of the T cell receptor complex (TCR). The TCR is comprised of two CD3 heterodimers, CD3ε : CD3δ and CD3ε : CD3γ, and one TCR hetero dimer α:β (**Figure I.3**) [21,204]. Each CD3 chain has an immunoreceptor tyrosine-based activation motif (ITAM) to transude activation signals [21]. CD3 chains also associate with γδ heterodimers of the TCR [204]. CD3ε is a marker for T lymphocyte lineage due to the establishment of the TCRαβ, CD3δε, CD3γε dimer stoichiometry 2(ε)/1(δ)/1(γ) and therefore CD3ε is the most abundant CD3 chain [154,155].

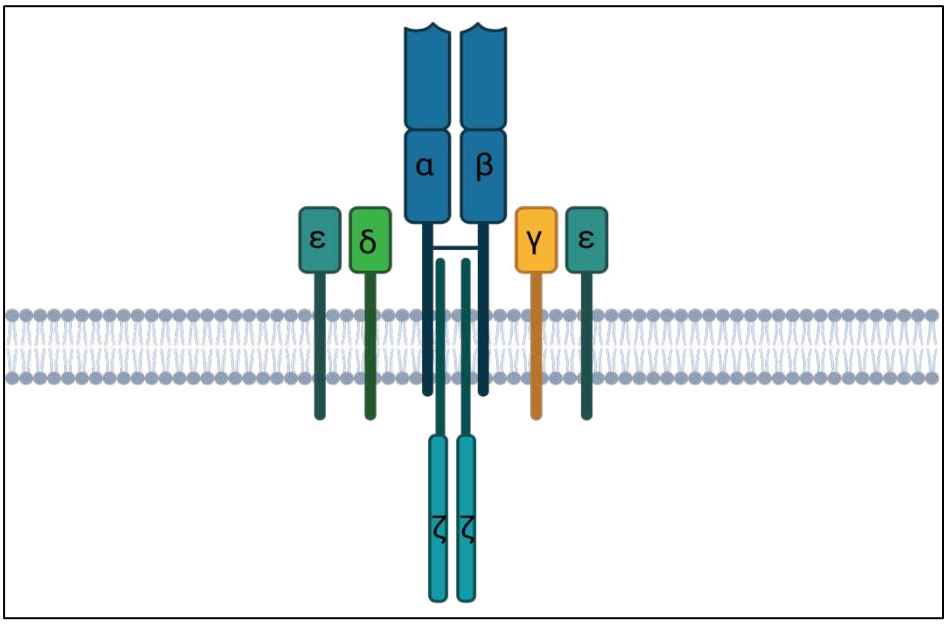

Figure I.3) The T cell receptor complex (TCR). The TCR is comprised of one TCRα:β heterodimer, and two CD3 heterodimers CD3ε : CD3δ and CD3ε : CD3γ. Along with two ζ chains. Created with BioRender.com

Human and Jamaican Fruit Bat CD3ε Protein Homology

Two anti-CD3ε human reactive antibody clones (Hit3a and OKT3) were identified to cross react with Jamaican fruit bat splenocytes (**Figure I.4**) and disassociated lamina propria of the gastrointestinal tract (**Figure I.5**). To further assess protein homology of human and Jamaican fruit bat CD3ε, CD3ε protein sequences were downloaded into Geneious Prime from NCBI: human (NCBI accession NP_000724) Jamaican fruit bat (NCBI accession XP_037003230). Protein sequences were then aligned in Geneious Prime using BLOSUM62 [145,146]. CD3ε protein sequences were used to generate three-dimensional models with PHYR^2 (**Figure I.6**). Transmembrane domains (magenta) and signal peptides (removed) were not included in the BLOSUM62 analysis. The BLOSUM62 protein homology analysis of human CD3ε and Jamaican fruit bat CD3ε identified 48 identical extracellular sites or 44.4% of the extracellular domain, and 50 identical cytoplasmic sites or 89.3% of the cytoplasmic domain. Accounting for peptides that are not identical but had similar properties in conjunction with identical sites the extracellular domain had a BLOSUM62 value of 63.9% homology, and the cytoplasmic domain had a BLOSUM62 value of 72.6% homology. The combined extracellular and cytoplasmic domains had 98 identical sites or 59.8%, and a BLOSUM62 value of 72.6% homology.

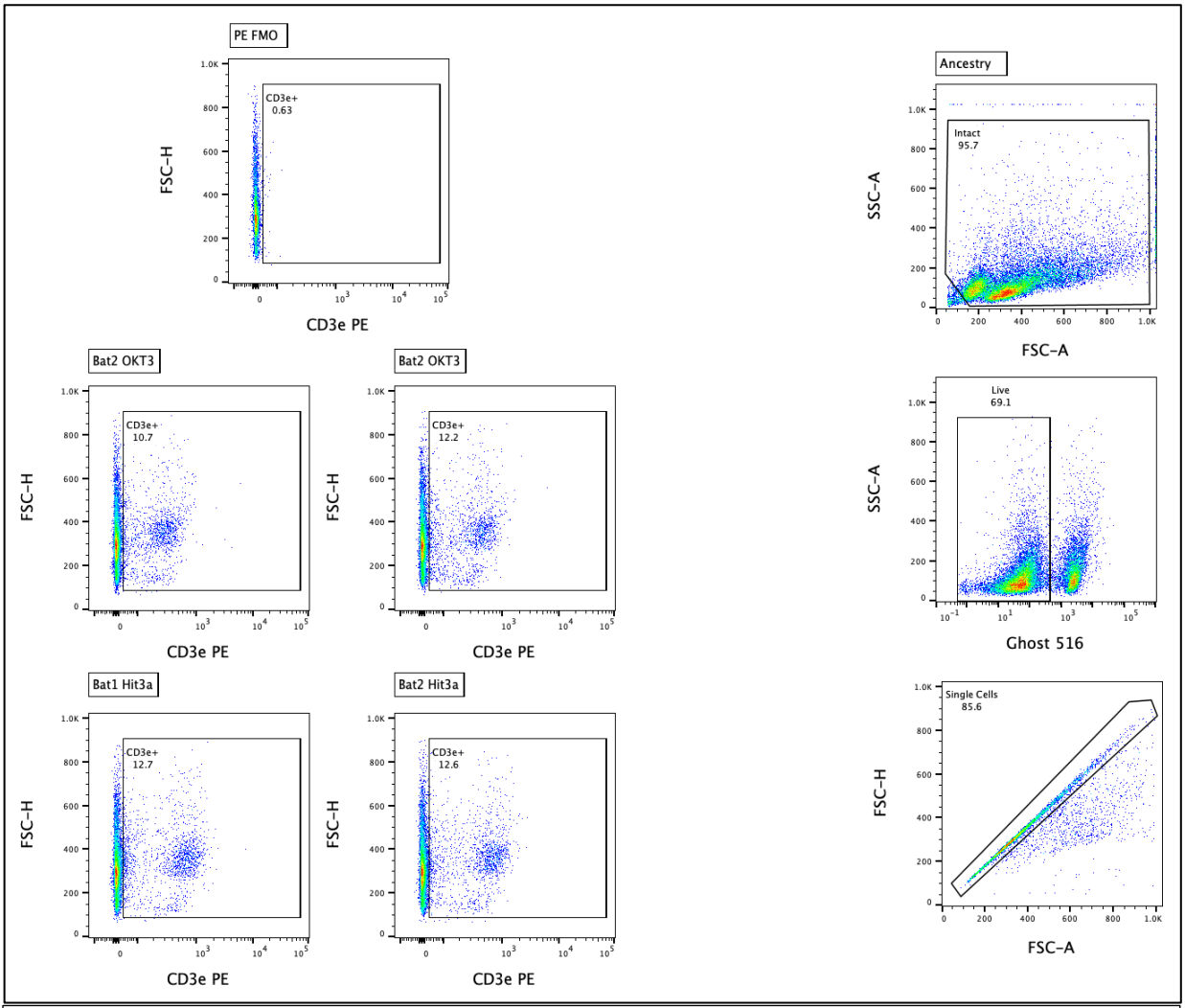

Figure I.4) Anti-CD3ε clones Hit3a and OKT3 staining of Jamaican fruit bat splenocytes from two bats. Gating strategy: ancestry gates (right) Intact > Live > Single Cells . $CD3\varepsilon^{+}$ gate determined by FMO (top left). Clones OKT3 and Hit3a demonstrate similar reactivity. $CD3\varepsilon^{+}$ splenocytes averaged 12.05%. Panel: CD3ε (FITC), primary amine viability (Ghost Blue 516).

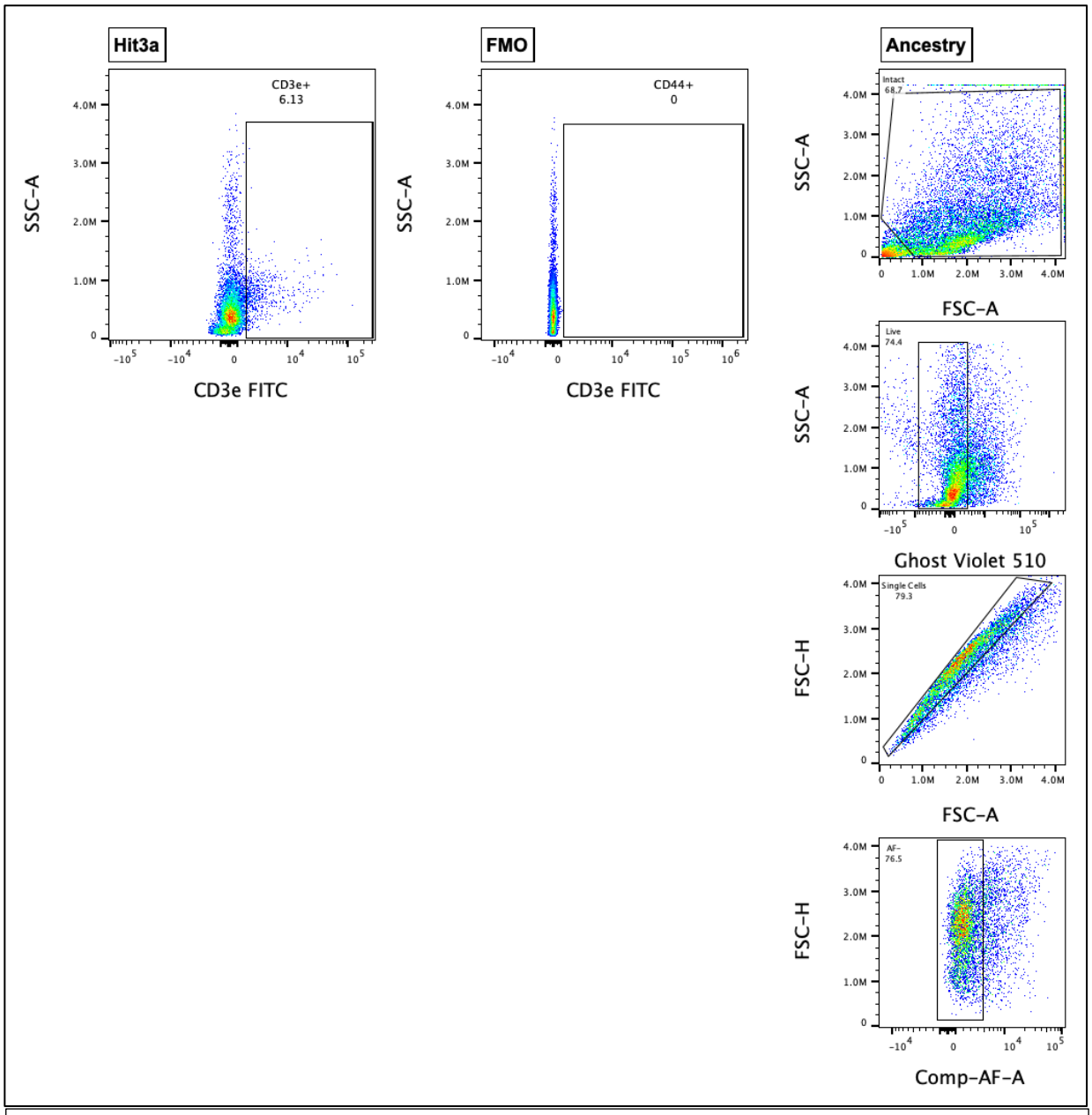

Figure I.5) Anti-CD3ε clone Hit3a staining of Jamaican fruit bat disassociated lamina propria of the gastrointestinal tract of one bat. Gating strategy: ancestry gates (right) Intact > Live > Single Cells > Auto-florescence (AF)$^{-}$. CD3ε^{+} gate determined by FMO (top left). CD3ε^{+} 6.13%. Panel: CD3ε (FITC), primary amine viability (Ghost Violet 510). Analyzed in FlowJo V 10.8.1 Mac OS X. Gates were drawn based on FMOs.

Cross-Reactive Clone	Hit3a, OKT3 (Extracellular)		
Domain	Extracellular (Red)	Cytoplasmic (Cyan)	Combined
Identical Sites	48 (44.4%)	50 (89.3%)	98 (59.8%)
BLOSUM62	63.9%	89.3%	72.6%

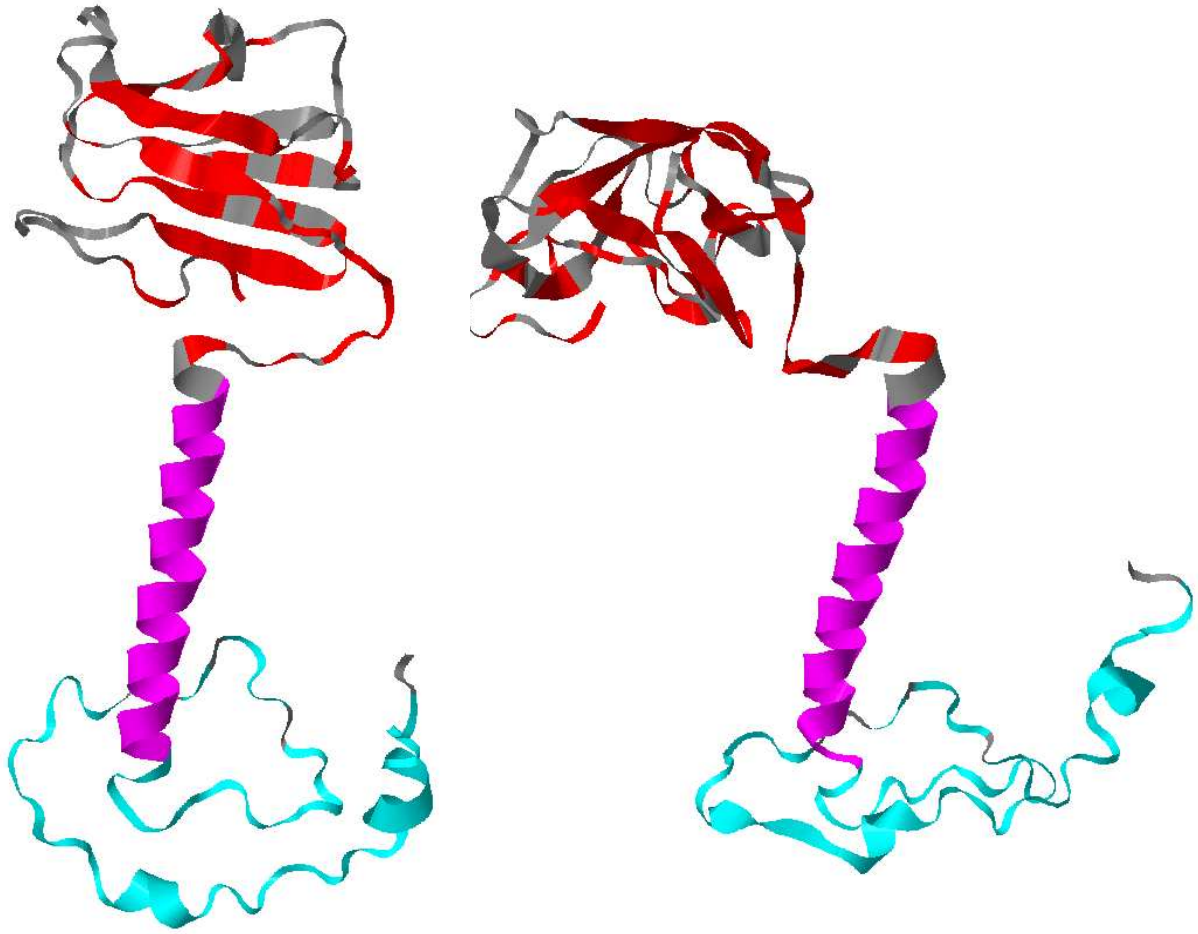

Figure I.6) Human CD3ε (right) and Jamaican fruit bat CD3ε (left) three-dimensional models and protein homology. Three-dimensional models were generated with PHYR[2]; human (NCBI accession NP_000724) Jamaican fruit bat (NCBI accession XP_037003230). Transmembrane domains (magenta) and signal peptides (removed) were not included in the BLOSUM62 analysis. Human CD3ε and Jamaican fruit bat CD3ε had 48 identical extracellular sites (red) or 44.4% of the extracellular domain, there were 50 identical cytoplasmic sites (cyan) or 89.3%. Accounting for peptides that are not identical but had similar properties and identical sites the extracellular domain had a BLOSUM62 value of 63.9% homology, the cytoplasmic domain had a BLOSUM62 value of 72.6% homology. The combined extracellular and cytoplasmic domains had 98 identical sites or 59.8%, and a BLOSUM62 value of 72.6% homology.

CD8α

CD8 is a co-receptor expressed on cytotoxic lymphocytes, γδ T cells, and natural killer cells that recognizes MHC-I molecules for activation (**Figure I.7**). CD8 is a heterodimer composed of a covalently linked α chain and a β chain. Additionally, a variant form of CD8 exists as a homodimer of two α chains. The αβ CD8 heterodimer is expressed by naïve CD8 T cells. The αα CD8 homodimer is found on activated effector and memory T cells, mucosal associated invariant T cells, γδ T cells, and natural killer cells [21,204].

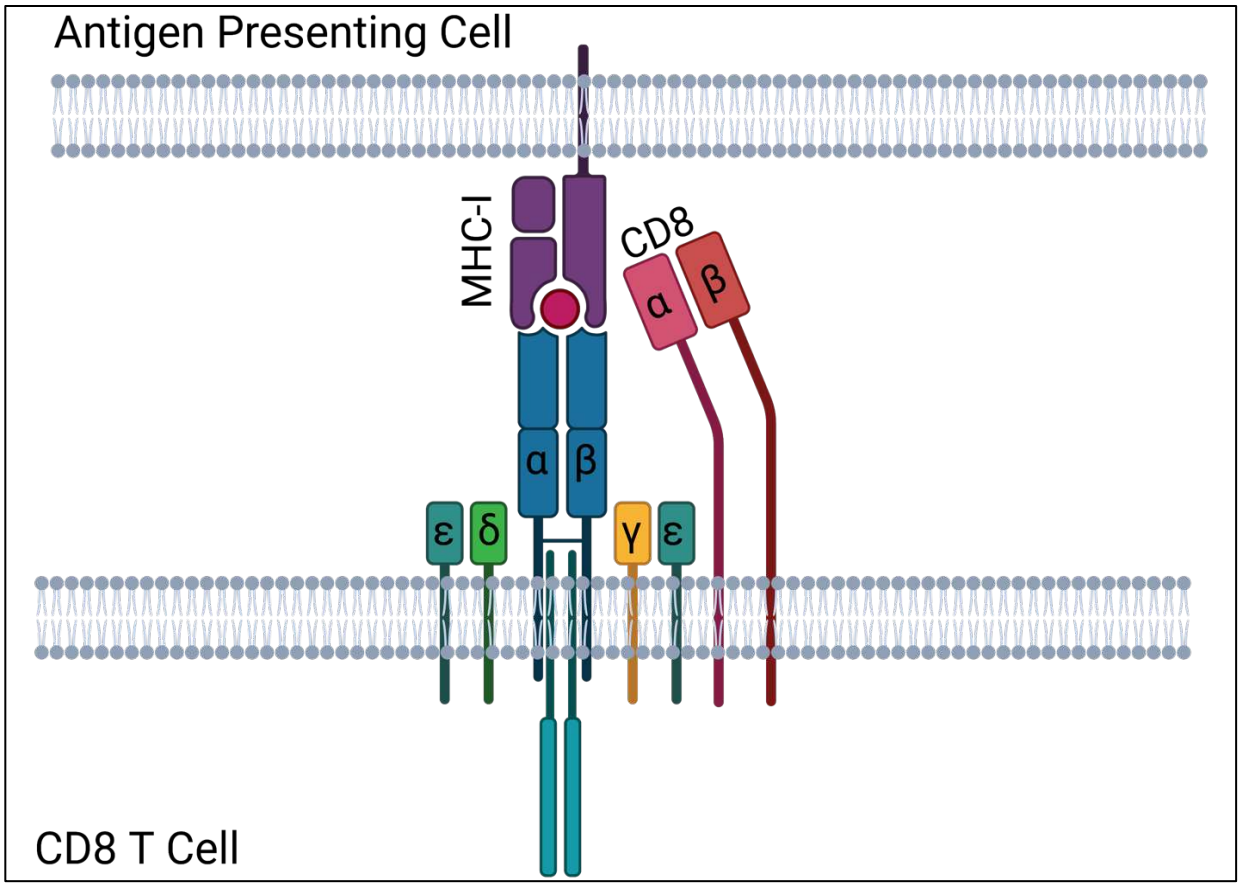

Figure I.7) T cell receptor complex (TCR) with CD8 heterodimer. TCR complex with CD8 co-receptor binding to MHC-I presenting a peptide. Created with BioRender.com.

Pig and Jamaican Fruit Bat CD8α Protein Homology

One anti-CD8α pig reactive antibody was identified to cross-react with Jamaican fruit bat splenocytes (**Figure I.8**) and disassociated lamina propria of the gastrointestinal tract (**Figure I.9**). To further assess protein homology of pig (UniProt A0A5G2Q9C5) and Jamaican fruit bat (NCBI accession XP_036981493, 3-D model generated by PHYRE^2) CD8α three-dimensional models, and peptide sequences were downloaded into Geneious Prime. Protein sequences were then aligned in Geneious Prime using BLOSUM62 (**Figure I.10)** [145,146]. The BLOSUM62 protein alignment analysis of pig CD8α and Jamaican fruit bat CD8α identified 74 identical extracellular sites or 64.2% of the extracellular domain and identified 23 identical cytoplasmic sites or 78.8% of the cytoplasmic domain. Accounting for peptides that were not identical but had similar properties in combination with identical sites the extracellular domain had a BLOSUM62 value of 64.9% homology, and the cytoplasmic domain had a BLOSUM62 value of 78.8% homology. In conjunction the extracellular and cytoplasmic domains had 97 identical sites or 49.7%, and a BLOSUM62 value of 66.7% homology.

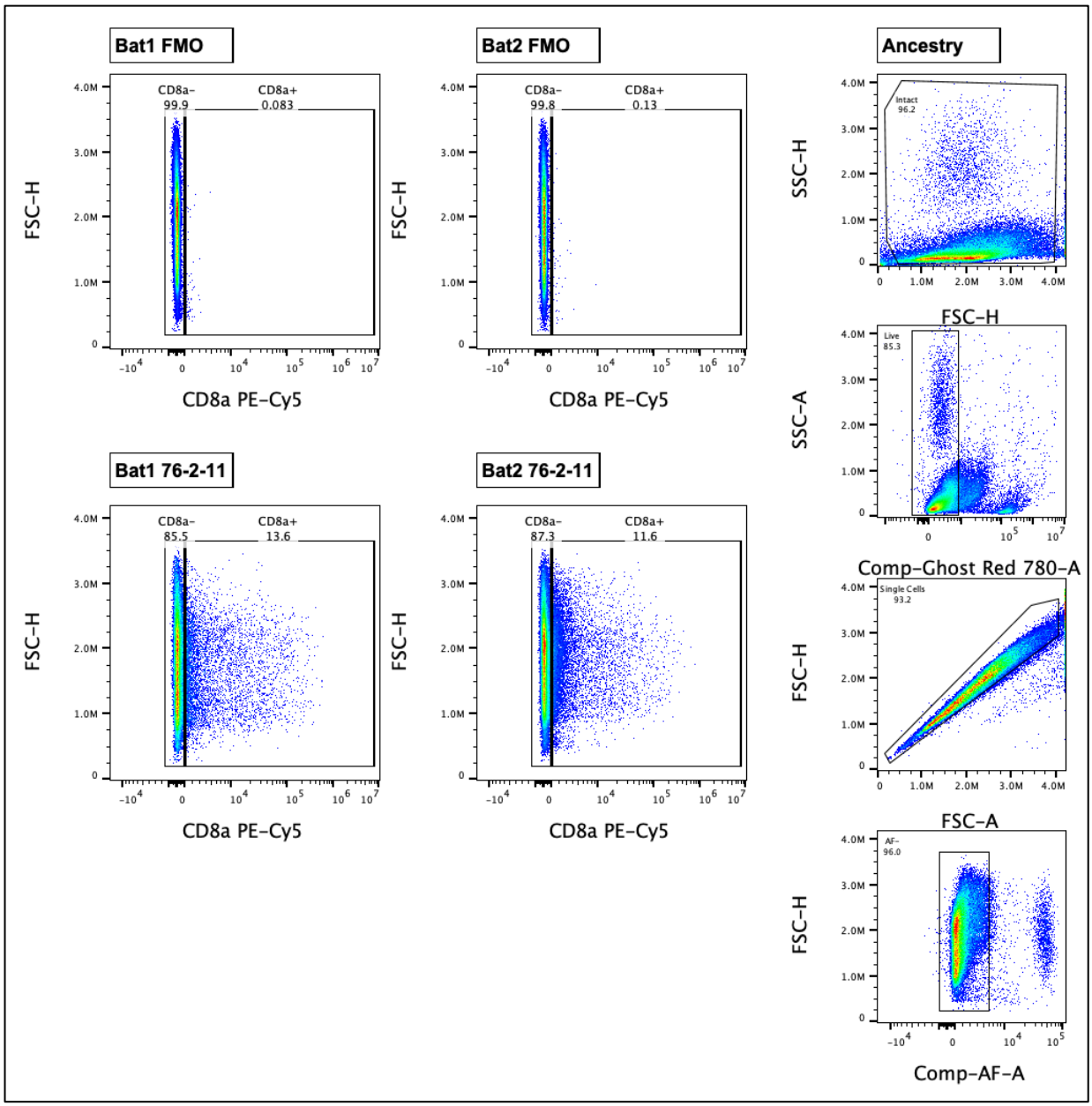

Figure I.8) Anti-CD8α clone 76-2-11 staining of Jamaican fruit bat splenocytes from two bats. Gating strategy: ancestry gates (right) Intact > Live > Single Cells > Auto-florescence $(AF)^-$. $CD8\alpha^+$ gate determined by FMO (top). $CD8a^+$ splenocytes averaged 12.6%. Panel: CD8α (PE-Cy5), primary amine viability (Ghost Red 780). Analyzed in FlowJo V 10.8.1 Mac OS X. Gates were drawn based on FMOs.

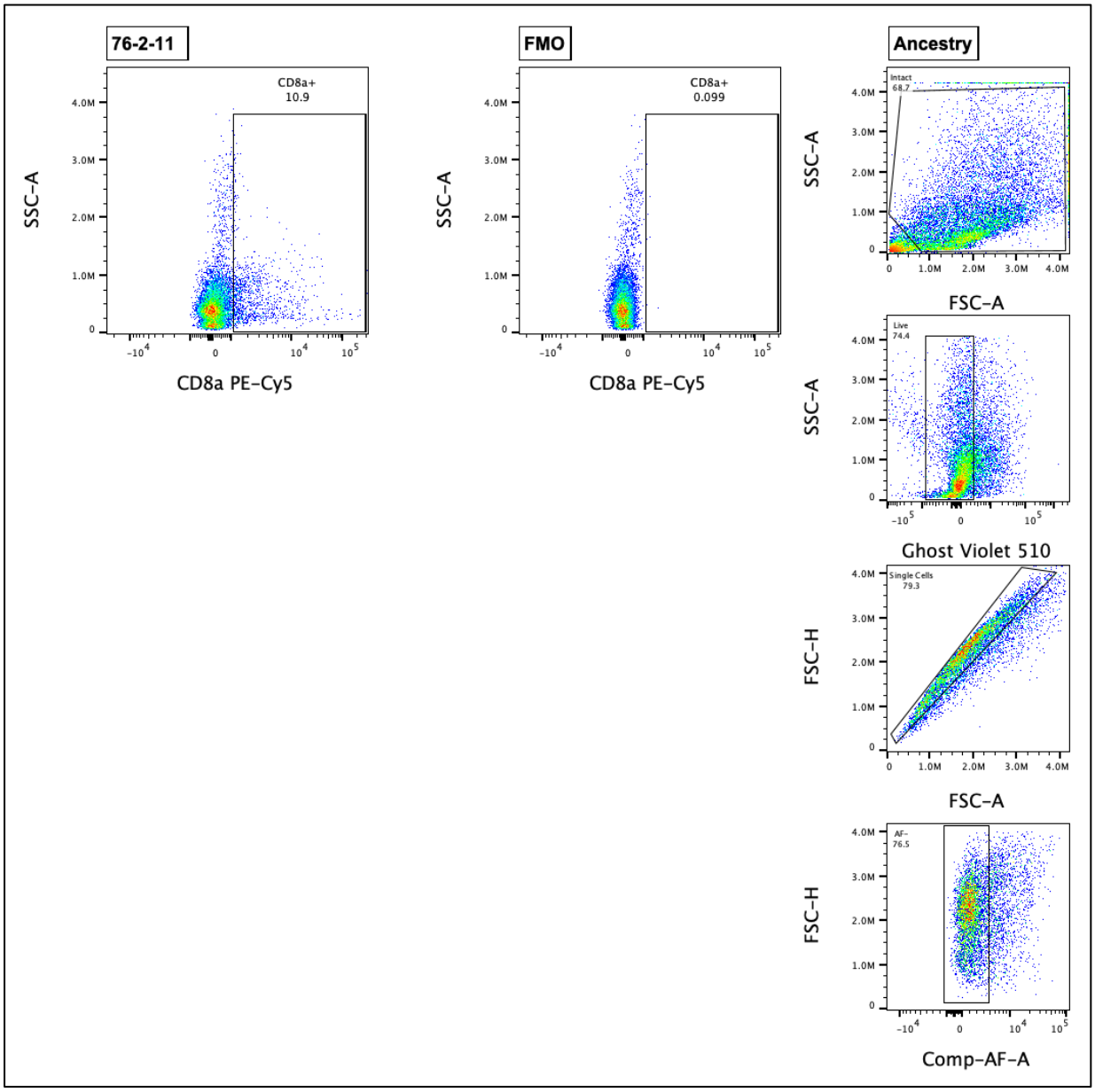

Figure I.9) Anti-CD8α clone 76-2-11 staining of Jamaican fruit bat disassociated lamina propria from the gastrointestinal tract from one bat. Gating strategy: ancestry gates (right) Intact > Live > Single Cells > Auto-florescence (AF)$^{-}$. CD8α^{+} gate determined by FMO (top). CD8a^{+} disassociated lamina propria averaged 10.9%. Panel: CD8α (PE-Cy5), primary amine viability (Ghost Violet). Analyzed in FlowJo V 10.8.1 Mac OS X. Gates were drawn based on FMOs.

Cross-Reactive Clone	76-2-11 (Extracellular)		
Domain	Extracellular (Red)	Cytoplasmic (Cyan)	Combined
Identical Sites	74 (45.7%)	23 (69.7%)	97 (49.7%)
BLOSUM62	64.2%	78.8%	66.7%

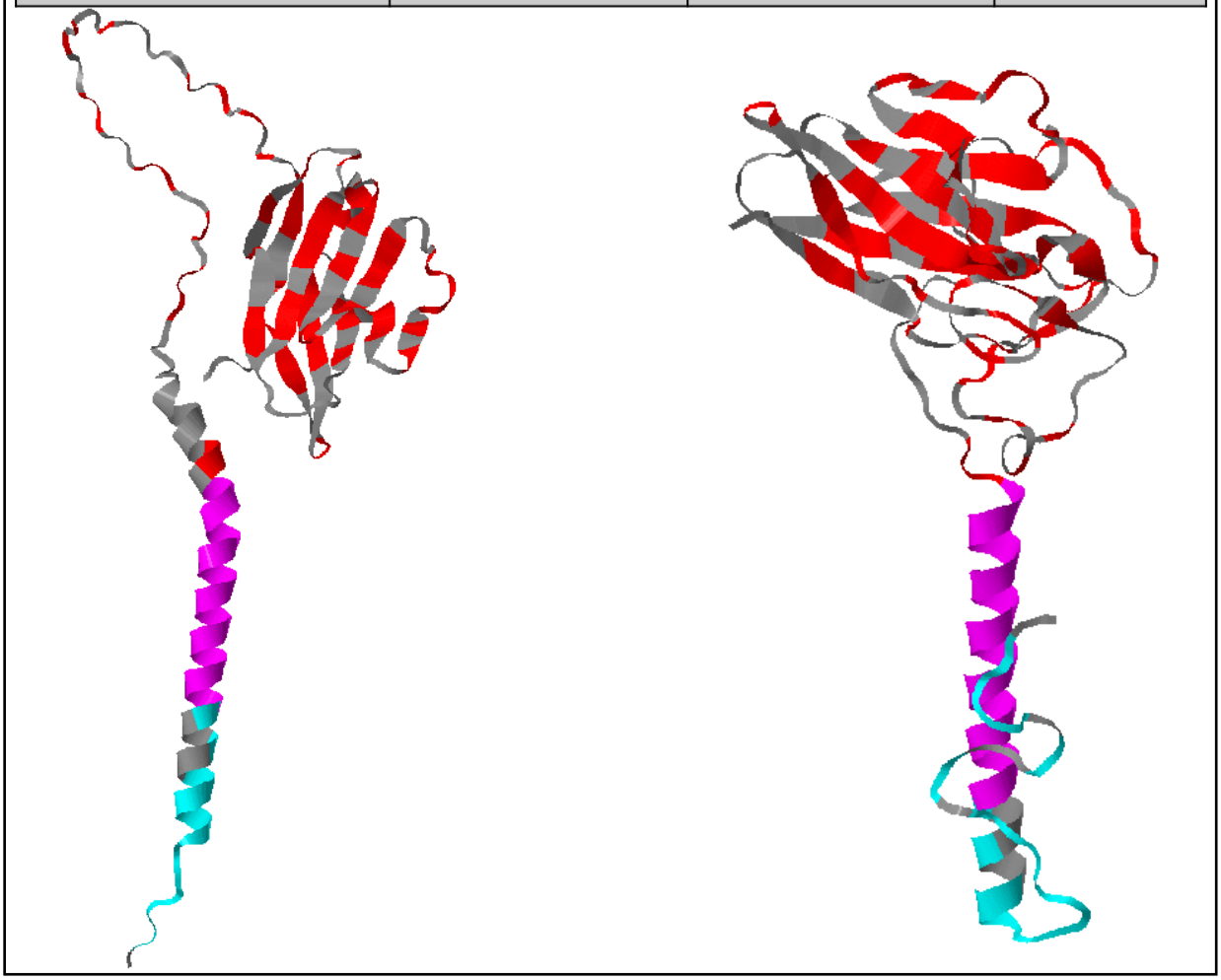

Figure I.10) Pig CD8α (right) and Jamaican fruit bat CD8α (left) three-dimensional models and protein homology. Pig CD8α three-dimensional model was pulled from UniProt (UniProt A0A5G2Q9C5). Jamaican fruit bat CD8α was generated using PHYR^2 (NCBI accession XP_036981493). Transmembrane domains (magenta) and signal peptides (removed) were not included in the BLOSUM62 analysis. Transmembrane domains of each protein are highlighted in magenta. Pig CD8α and Jamaican fruit bat CD8α had 74 identical extracellular sites (red) or 64.2% of the extracellular domain, there were 23 identical cytoplasmic sites (cyan) or 78.8%. Accounting for peptides that are not identical but had similar properties and identical sites the extracellular domain had a BLOSUM62 value of 64.9% homology, the cytoplasmic domain had a BLOSUM62 value of 78.8% homology. The combined extracellular and cytoplasmic domains had 97 identical sites or 49.7%, and a BLOSUM62 value of 66.7% homology.

CD19

CD19 along with CD21 and CD81 form what is known as the B cell co-receptor complex (**Figure I.11**). The B cell co-receptor complex enhances B cell receptor (BCR) signaling transduction [21,163]. In short, CD21 binding to antigens tagged by the complement component C3dg results in the cross-linking of BCR co-receptor with the antigen bound BCR causing phosphorylation of the ITAM domain of the BCR Igα and Igβ [21,163,164]. Phosphorylation of the cytoplasmic tail of CD19 also occurs in this process. Additionally, CD21 is the receptor for Epstein-Barr virus [21,163,204]. CD19 expression on B cells is found on nearly every stage of B cells: early pro-B, late pro-B, large pre-B, small pre-B, immature B, mature naïve B, lymphoblast B, and

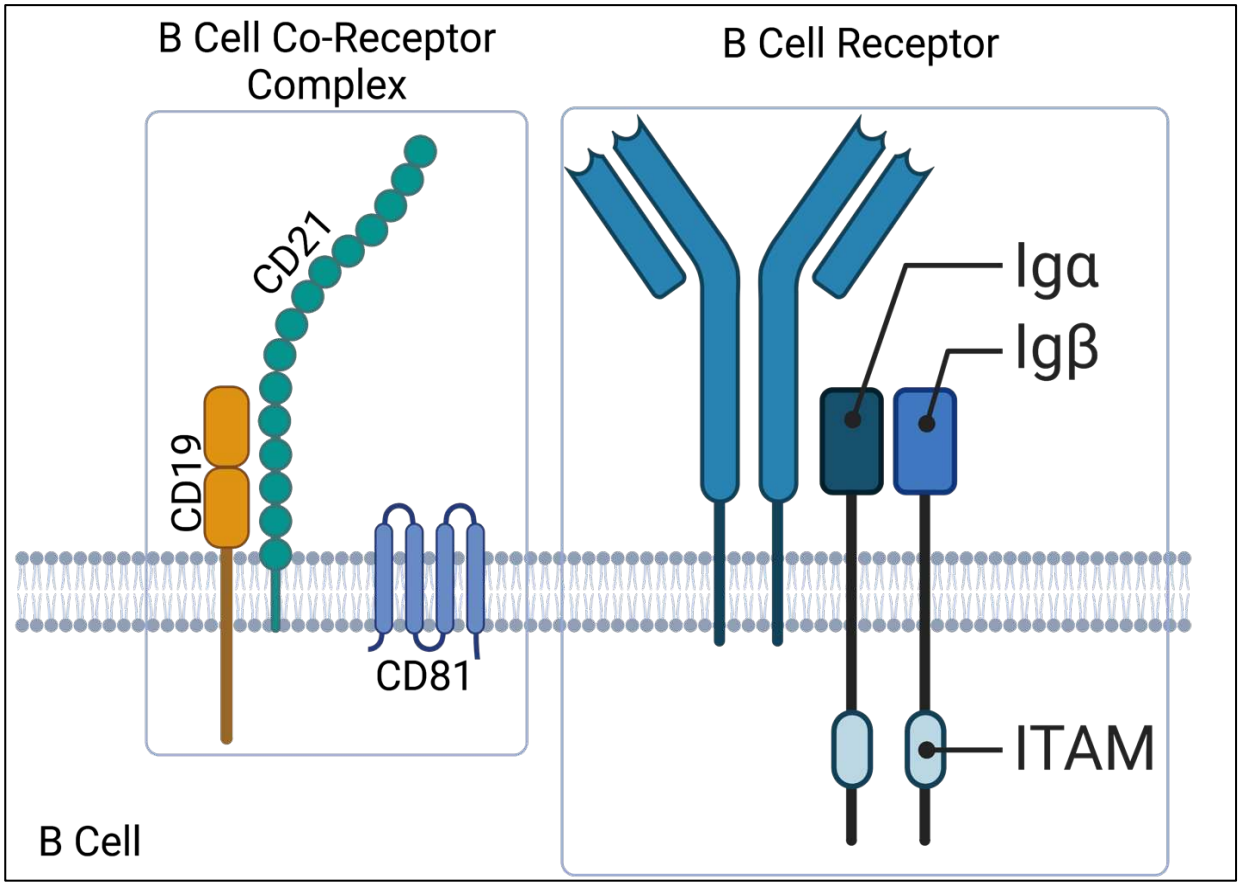

Figure I.11) B cell receptor and B cell co-receptor complex. Created with BioRender.com.

memory B cells [21,163,204]. As such, CD19 can be considered a pan-B cell marker excluding plasma blasts and plasma cells.

Mouse and Jamaican Fruit Bat CD19 Protein Homology

One anti- CD19 mouse reactive antibody clone (1D3) was identified to cross-react with Jamaican fruit bat splenocytes (**Figure I.12**) and disassociated lamina propria of the gastrointestinal tract (**Figure I.13**). To further assess protein homology of mouse (NCBI accession AAA37390) and Jamaican fruit bat (NCBI accession XP_036995935), CD19 peptide sequences were downloaded into Geneious Prime. Protein sequences were then aligned in Geneious Prime using BLOSUM62 [145,146]. Three-dimensional models were generated with PHYR^2 (**Figure I.14**). The aligned polypeptide sequences of mouse CD19 and Jamaican fruit bat CD19 had 137 identical extracellular sites or 62.3% of the extracellular domain, and 160 identical cytoplasmic sites or 71.2% of the cytoplasmic domain. Furthermore, the BLOSUM62 analysis accounting for peptides that were not identical but had similar properties in conjunction with identical sites reported that the extracellular domain had a BLOSUM62 value of 62.3% homology. The cytoplasmic domain of the BLOSUM62 analysis had a BLOSUM62 value of 71.2% homology. The combined extracellular and cytoplasmic domains had 297 identical sites or 56.5%, and a BLOSUM62 value of 66.5% homology.

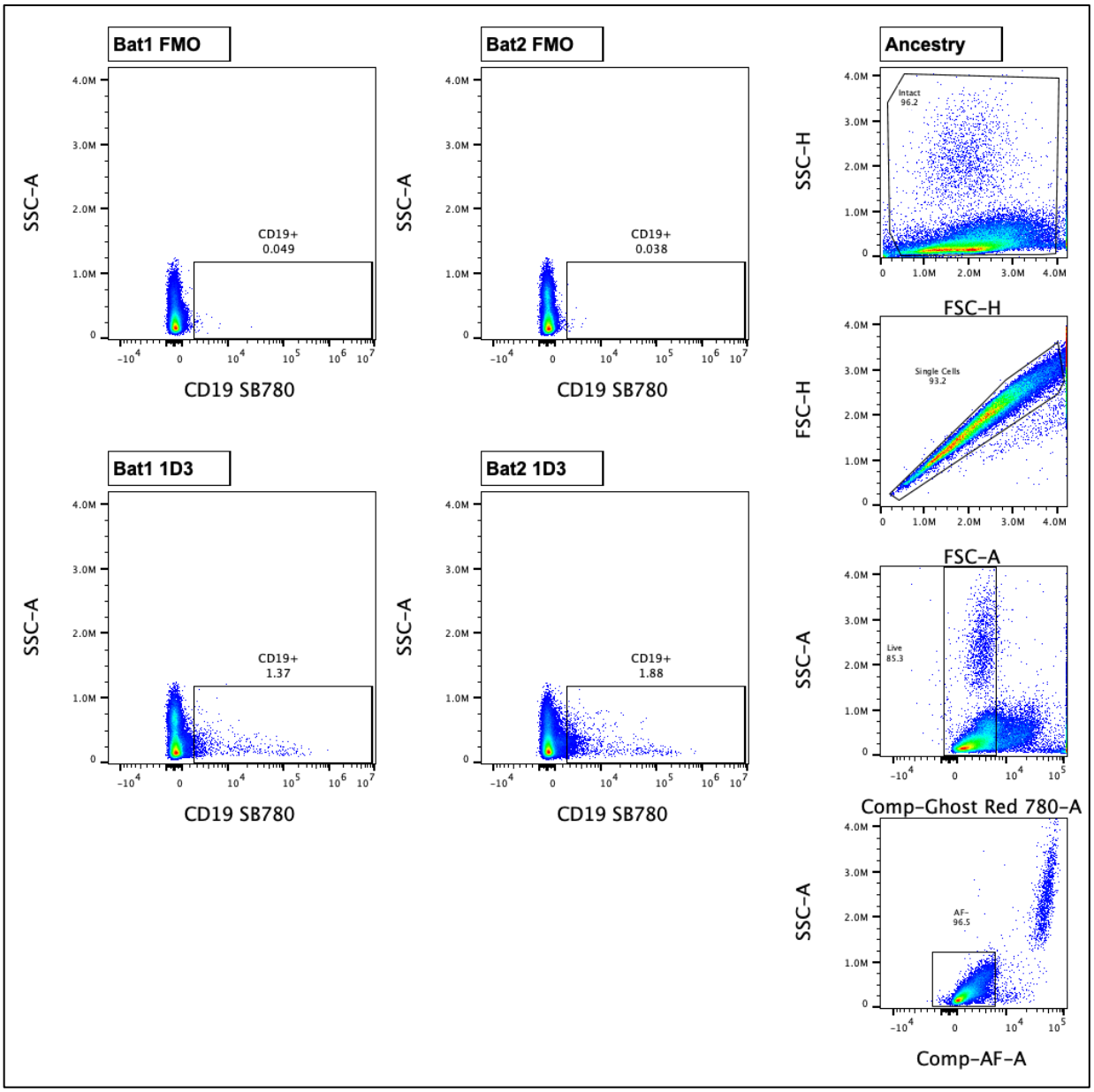

Figure I.12) Anti-CD19 clone 1D3 staining of Jamaican fruit bat splenocytes from two bats. Gating strategy: ancestry gates (right) Intact > Live > Single Cells > Auto-florescence $(AF)^{-}$. $CD19^{+}$ gate determined by FMO (top). $CD19^{+}$ splenocytes averaged 1.625%. Panel: CD19 (Super Bright 780), primary amine viability (Ghost Red 780). Analyzed in FlowJo V 10.8.1 Mac OS X. Gates were drawn based on FMOs.

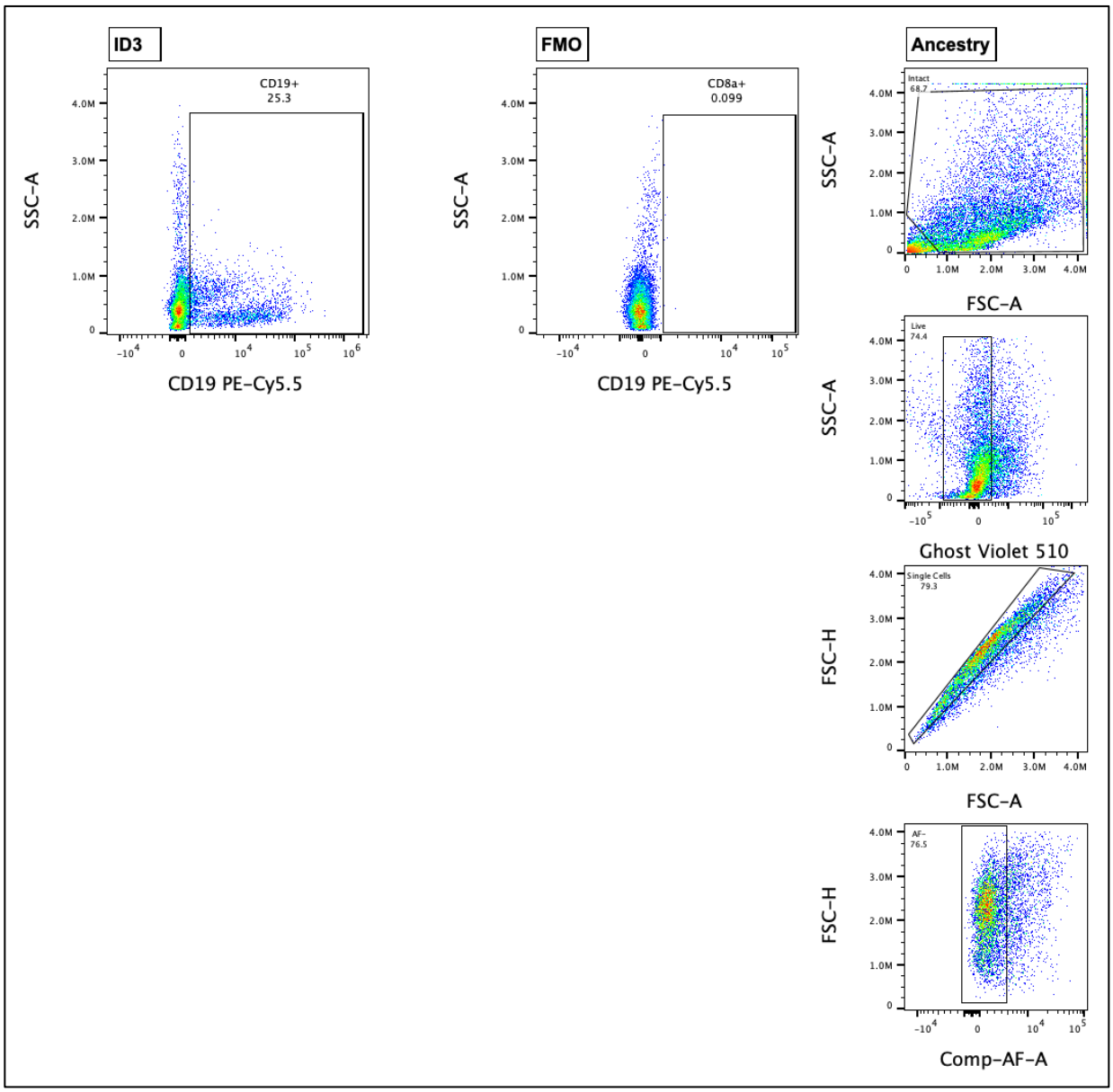

Figure I.13) Anti-CD19 clone 1D3 staining of Jamaican fruit bat disassociated lamina propria from the gastrointestinal tract. Gating strategy: ancestry gates (right) Intact > Live > Single Cells > Auto-florescence $(AF)^{-}$. $CD19^{+}$ gate determined by FMO (top). $CD19^{+}$ disassociated lamina propria averaged 25.3%. Panel: CD19 (PE-Cy5.5), primary amine viability (Ghost Violet 510). Analyzed in FlowJo V 10.8.1 Mac OS X. Gates were drawn based on FMOs.

Cross-Reactive Clone	1D3 (Extracellular)		
Domain	Extracellular (Red)	Cytoplasmic (Cyan)	Combined
Identical Sites	137 (49.6%)	160 (64.0%)	297 (56.5%)
BLOSUM62	62.3%	71.2%	66.5%

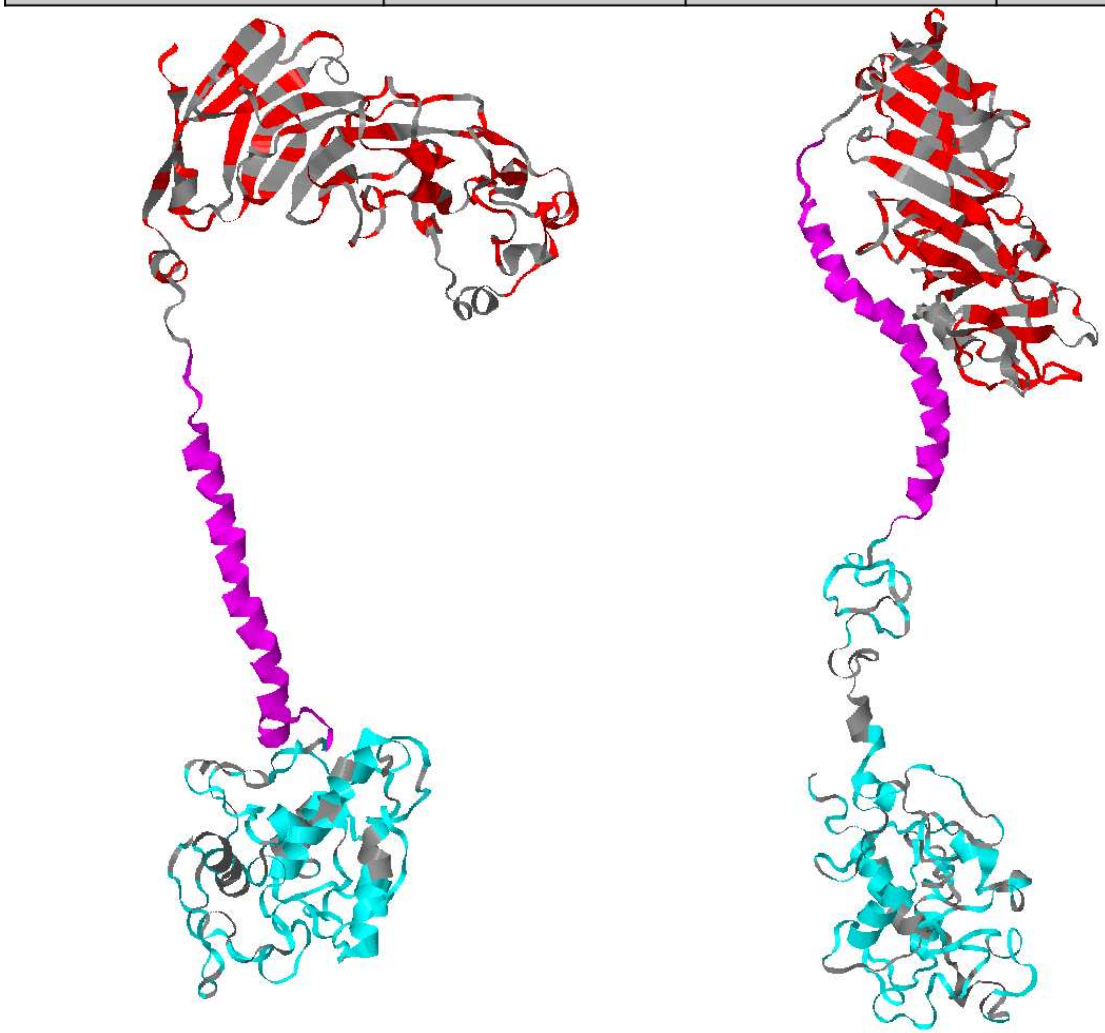

Figure I.14) Mouse CD19 (right) and Jamaican fruit bat CD19 (left) three-dimensional models and protein homology. Three-dimensional models were generated with PHYR[2]; mouse (NCBI accession AAA37390) Jamaican fruit bat (NCBI accession XP_036995935). Transmembrane domains (magenta) and signal peptides (removed) were not included in the BLOSUM62 analysis. Mouse CD19 and Jamaican fruit bat CD19 had 137 identical extracellular sites (red) or 62.3% of the extracellular domain, there are 160 identical cytoplasmic sites (cyan) or 71.2%. Accounting for peptides that were not identical but had similar properties and identical sites the extracellular domain had a BLOSUM62 value of 62.3% homology, the cytoplasmic domain had a BLOSUM62 value of 71.2% homology. The combined extracellular and cytoplasmic domains had 297 identical sites or 56.5%, and a BLOSUM62 value of 66.5% homology.

CD34

CD34 is an addressin, an adhesion molecule, and its ligand is CD62L (L-selectin) (**Figure I.15**) [21,205]. CD34 (My10) was first described in 1984 on hemopoietic stem and progenitor cells [206]. However, since it's first description, CD34 has been found on many other cell types: mesenchymal stromal cells, muscle satellite cells, corneal keratocytes, interstitial cells, epithelial progenitors, and vascular endothelial progenitors [207]. To date, a definable shared function across cell types that express CD34 has yet to be established. CD34 is largely used to mark stem cells and stem cell enrichment [204,205].

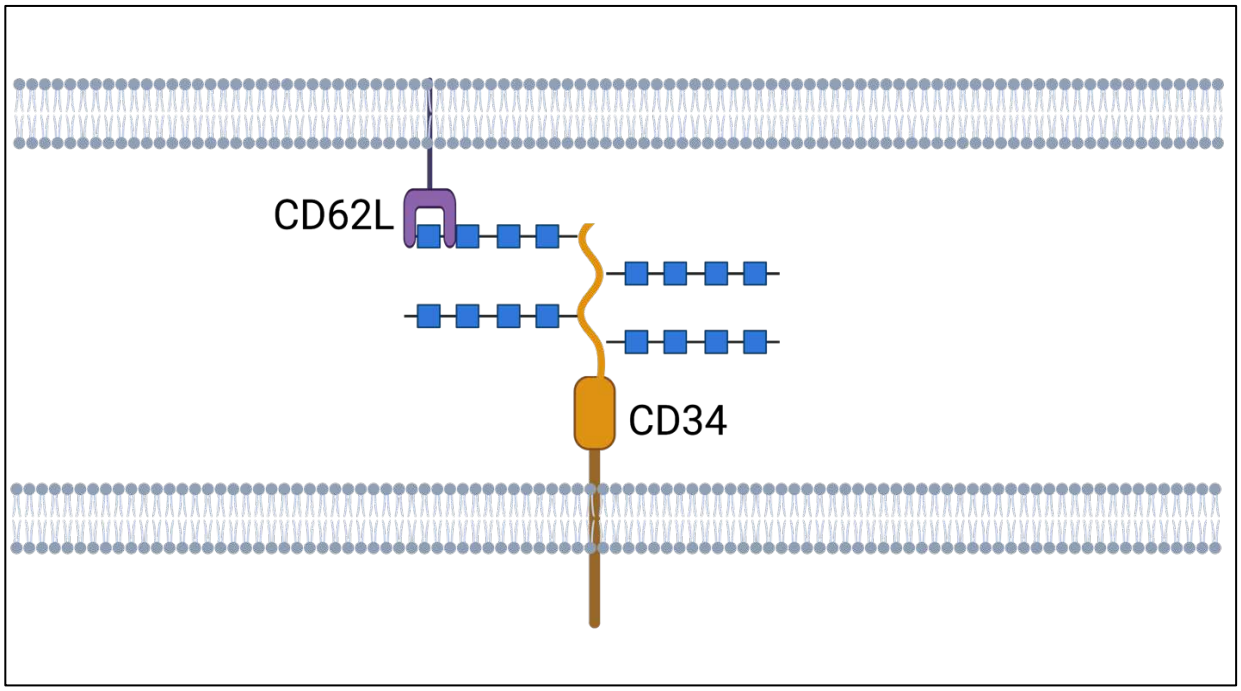

Figure I.15) CD34 binding to its ligand CD62L (L- selectin). Created with BioRender.com.

Mouse and Jamaican Fruit Bat CD34 Protein Homology

One anti- CD34 mouse reactive antibody clone (Hm34) was identified to cross-react with Jamaican fruit bat bone marrow single cell suspension (**Figure I.16**) and disassociated lamina propria of the gastrointestinal tract (**Figure I.17**). To further assess protein homology of mouse and Jamaican fruit bat CD34 three-dimensional models and peptide sequences were downloaded into Geneious Prime (UniProt Q64314) (**Figure I.18**). Jamaican fruit bat CD34 was downloaded into Geneious Prime (NCBI accession XP_037012880), and the three-dimensional model was generated with PHYR^2 (**Figure I.18**). Protein sequences were then aligned in Geneious Prime using BLOSUM62 [145,146]. The BLOSUM62 alignment of mouse CD34 and Jamaican fruit bat CD34 denoted 154 identical extracellular sites or 70.7% of the extracellular domain, and 70 identical cytoplasmic sites or 97.3% of the cytoplasmic domain. Additionally, when accounting for peptides that are not identical but had similar properties in conjunction with identical sites, the BLOSUM62 analysis reported the extracellular domain had 70.7% homology, and the cytoplasmic domain had 97.3% homology. The combined extracellular and cytoplasmic domains had 215 identical sites or 65.2%, and a BLOSUM62 value of 76.7% homology.

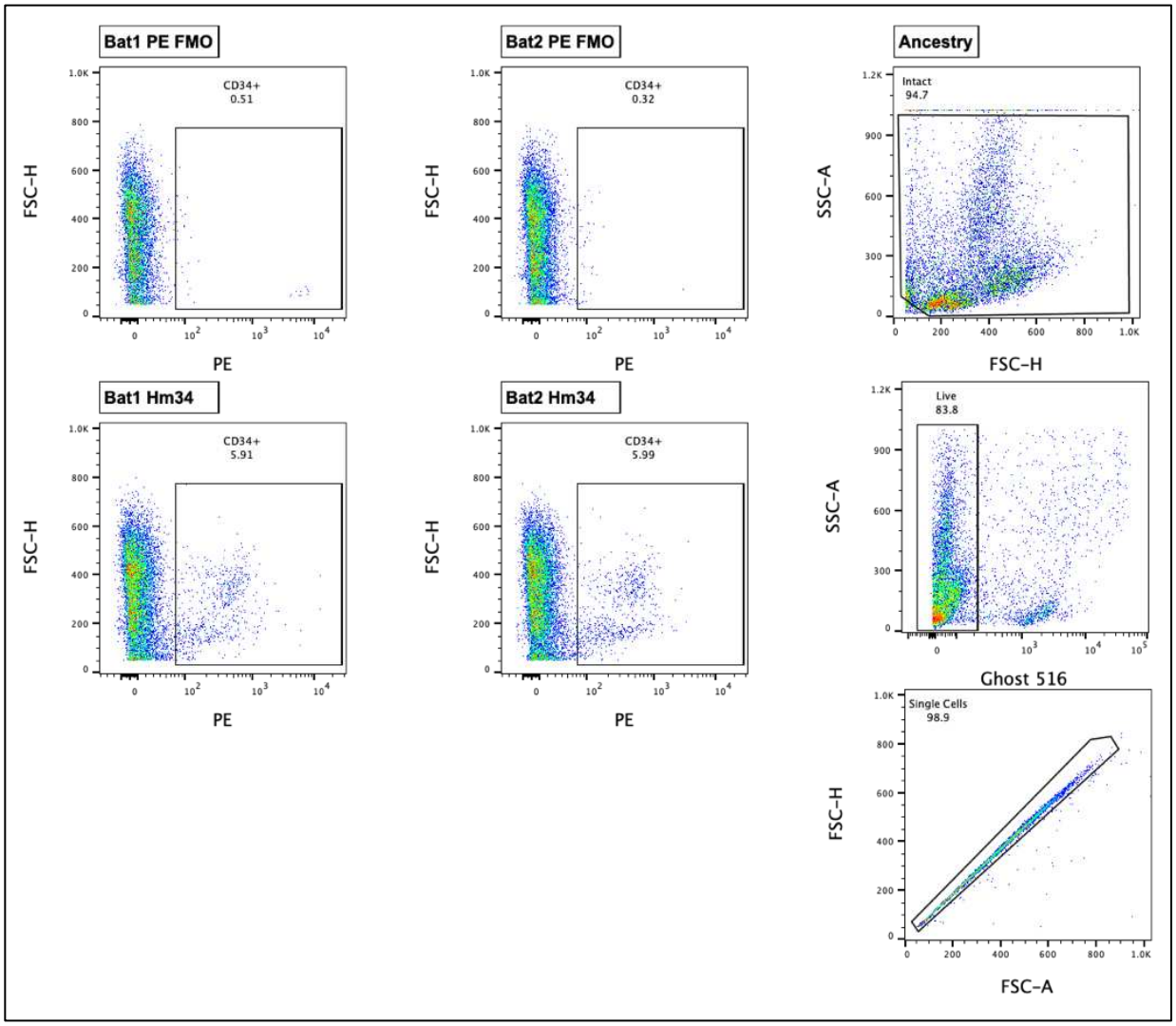

Figure I.16) Anti-CD34 clone Hm34 staining of Jamaican fruit bat bone marrow single cell suspension from two bats. Gating strategy: ancestry gates (right) Intact > Live > Single Cells > Auto-florescence $(AF)^-$. $CD34^+$ gate determined by FMO (top). $CD34^+$ splenocytes averaged 5.95%. Panel: CD34 (PE), primary amine viability (Ghost Blue 516). Analyzed in FlowJo V 10.8.1 Mac OS X. Gates were drawn based on FMOs.

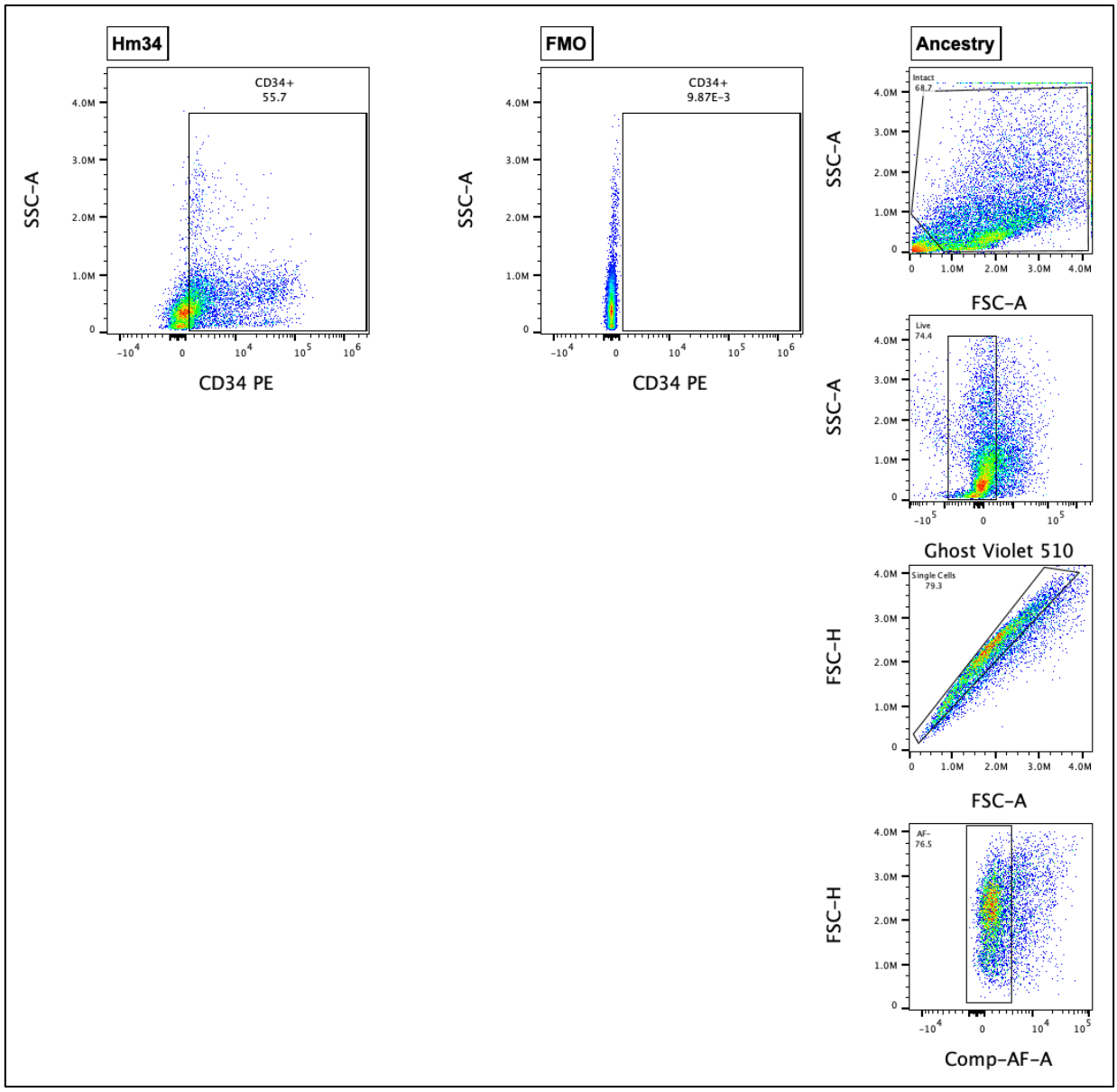

Figure I.17) Anti-CD34 clone Hm34 staining of Jamaican fruit bat lamina propria disassociate single cell suspension from one bat. Gating strategy: ancestry gates (right) Intact > Live > Single Cells > Auto-florescence (AF)$^{-}$. CD34^{+} gate determined by FMO (top). CD34^{+} lamina propria averaged 55.7%. Panel: CD34 (PE), primary amine viability (Ghost Violet 510). Analyzed in FlowJo V 10.8.1 Mac OS X. Gates were drawn based on FMOs.

Cross-Reactive Clone	Hm34 (Extracellular)		
Domain	Extracellular (Red)	Cytoplasmic (Cyan)	Combined
Identical Sites	154 (56.6%)	70 (94.6%)	215 (65.2%)
BLOSUM62	70.7%	97.3%	76.7%

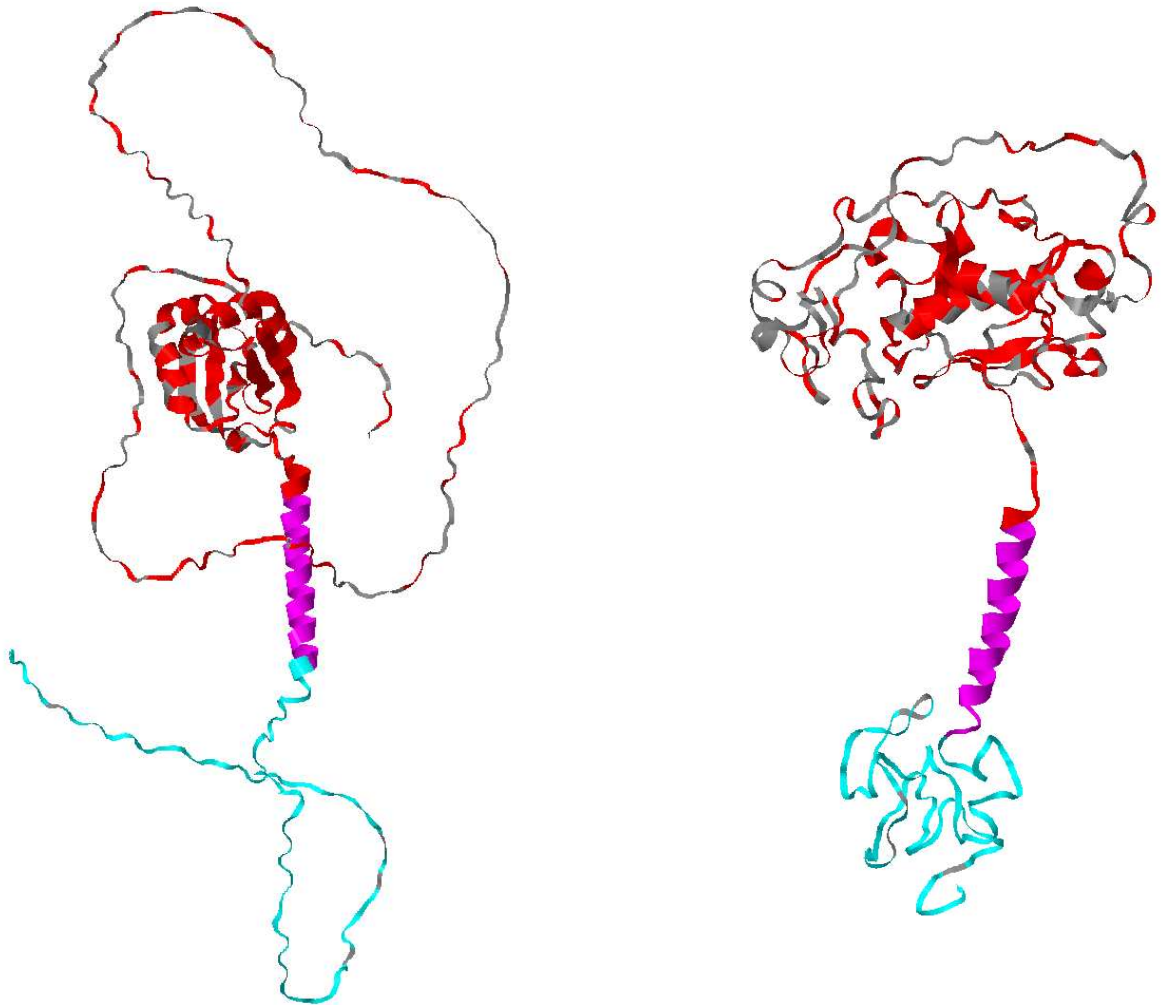

Figure I.18) Mouse CD34 (right) and Jamaican fruit bat CD34 (left) three-dimensional models and protein homology. Mouse CD34 three-dimensional model was pulled from UniProt (UniProt Q64314). Jamaican fruit bat CD34 three-dimensional model was generated using PHYR[2] (NCBI accession XP_037012880). Transmembrane domains (magenta) and signal peptides (removed) were not included in the BLOSUM62 analysis. Mouse CD19 and Jamaican fruit bat CD34 had 154 identical extracellular sites (red) or 70.7% of the extracellular domain, there were 70 identical cytoplasmic sites (cyan) or 97.3%. Accounting for peptides that were not identical but had similar properties and identical sites the extracellular domain had a BLOSUM62 value of 70.7% homology, the cytoplasmic domain had a BLOSUM62 value of 97.3% homology. The combined extracellular and cytoplasmic domains had 215 identical sites or 65.2%, and a BLOSUM62 value of 76.7% homology.

CD40

CD40 is expressed on B cells, macrophages, dendritic cells, and basal epithelial cells. CD154 (CD40L) is the ligand for CD40, and both are trimers (**Figure I.19**). CD40 stimulation provides a co-stimulatory signal for B cells for growth, differentiation, class switching, and aids in germinal center formation and development of plasma and memory B cells [21,205,208]. As such, CD40 is critical for T-cell-depended antibody responses and CD40 is considered a pan-B cell marker [204]. Additionally, CD40 promotes cytokine production by dendritic cells and macrophages when stimulated. Stimulation of CD40 on macrophages sensitizes macrophages to IFN-γ as such they work in concert to activate a macrophage [21].

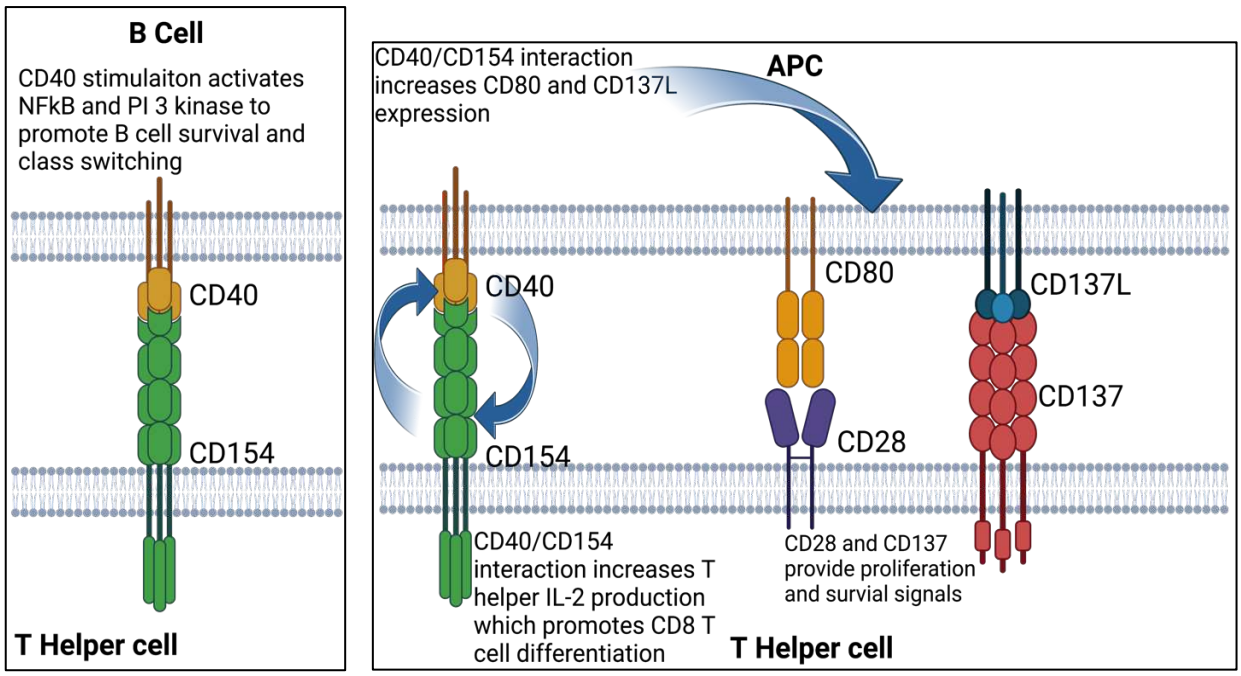

Figure I.19) CD40 binding to its ligand CD154 (CD40L). In B cells, when CD40 is stimulated by CD154 on helper T cell it activates NFkB and PI 3 kinase to promote B cell survival and class switching. When CD40 is stimulated on APCs by T helper cells it increases CD80 and CD137L expression. CD80 will then bind to CD28, and CD137L will bind to CD137 which will provide proliferation and survival signals to T cells. Furthermore, CD154 and CD40 interaction increases IL-2 production which promotes CD8 T cell differentiation. Created with BioRender.com.

Mouse and Jamaican Fruit bat CD40 Protein Homology

One anti-CD40 mouse reactive antibody clone (FGK45) was identified to cross react with Jamaican fruit bat splenocytes (**Figure I.20**). To further assess protein homology of mouse and Jamaican fruit bat CD40, protein sequences were downloaded into Geneious Prime from UniProt and NCBI: mouse (UniProt P27512) Jamaican fruit bat (NCBI accession XP_037020498). Protein sequences were then aligned in Geneious Prime using BLOSUM62 [145,146]. Mouse CD40 three-dimensional model was pulled from UniProt (UniProt P27512) and Jamaican fruit bat CD40 three-dimensional model was generated using PHYR^2 (NCBI accession XP_037020498) (**Figure I.21**). Alignment with BLOSUM62 mouse CD40 and Jamaican fruit bat CD40 identified 90 identical extracellular sites or 70.8% of the extracellular domain, and 39 identical cytoplasmic sites or 61.9% of the cytoplasmic domain. Accounting for peptides that are not identical but had similar properties and identical sites, the BLOSUM62 analysis reported the extracellular domain had 70.8% homology, and the cytoplasmic domain had 73.0% homology. The combined extracellular and cytoplasmic domains had 129 identical sites or 55.8%, and a BLOSUM62 value of 71.4% homology.

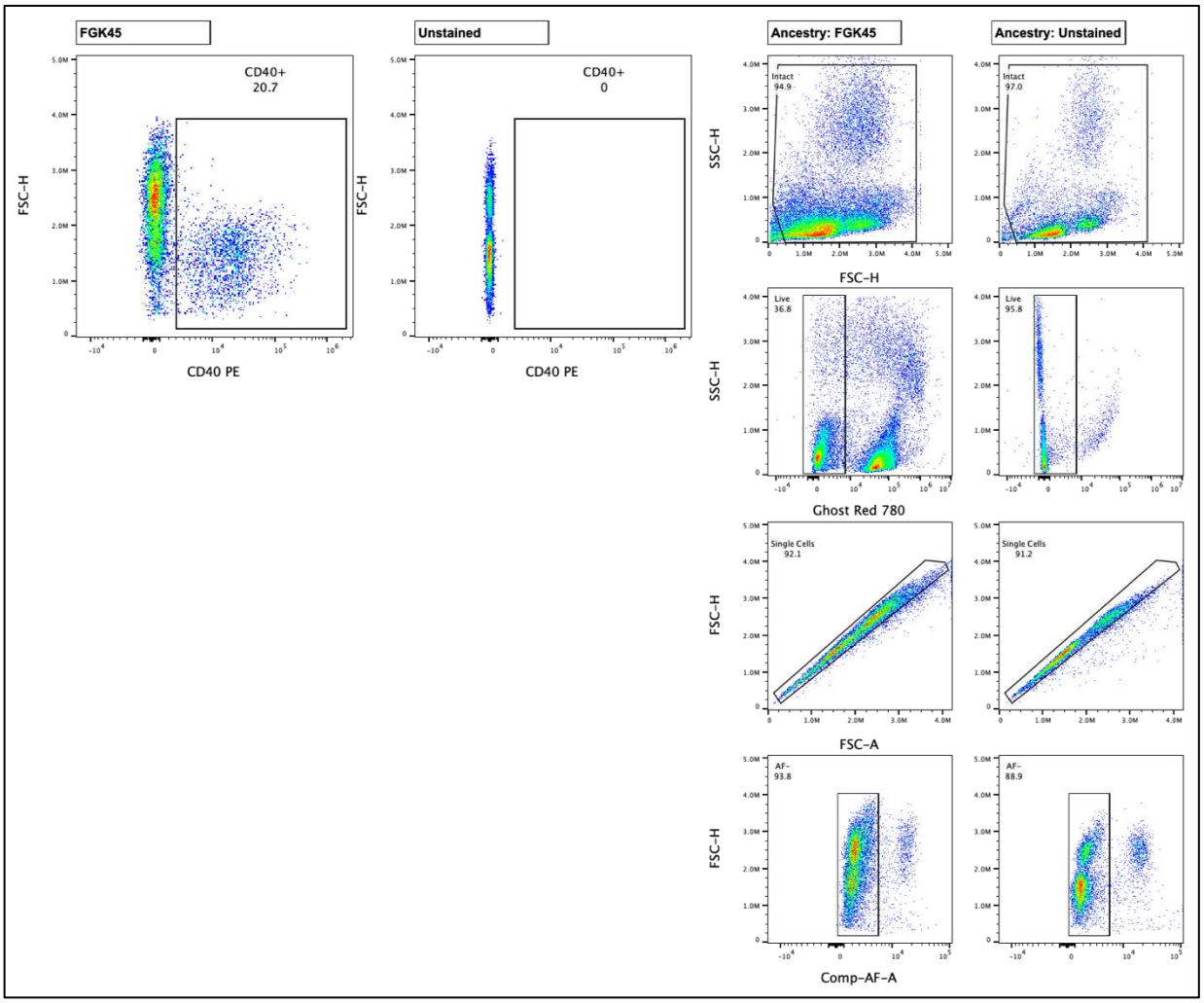

Figure I.20) Anti-CD40 clone FGK45 staining of Jamaican fruit splenocytes from one bat. Gating strategy: ancestry gates (right) Intact > Live > Single Cells > Auto-florescence $(AF)^{-}$. $CD40^{+}$ gate determined by unstained control (top). $CD40^{+}$ splenocytes averaged 20.7%. Panel: CD40 (PE), primary amine viability (Ghost Red 780). Analyzed in FlowJo V 10.8.1 Mac OS X V 10.8.1 Mac OS X. Gates were drawn based on FMOs.

Cross-Reactive Clone	FGK45 (Extracellular)		
Domain	Extracellular (Red)	Cytoplasmic (Cyan)	Combined
Identical Sites	90 (53.6%)	39 (61.9%)	129 (55.8%)
BLOSUM62	70.8%	73.0%	71.4%

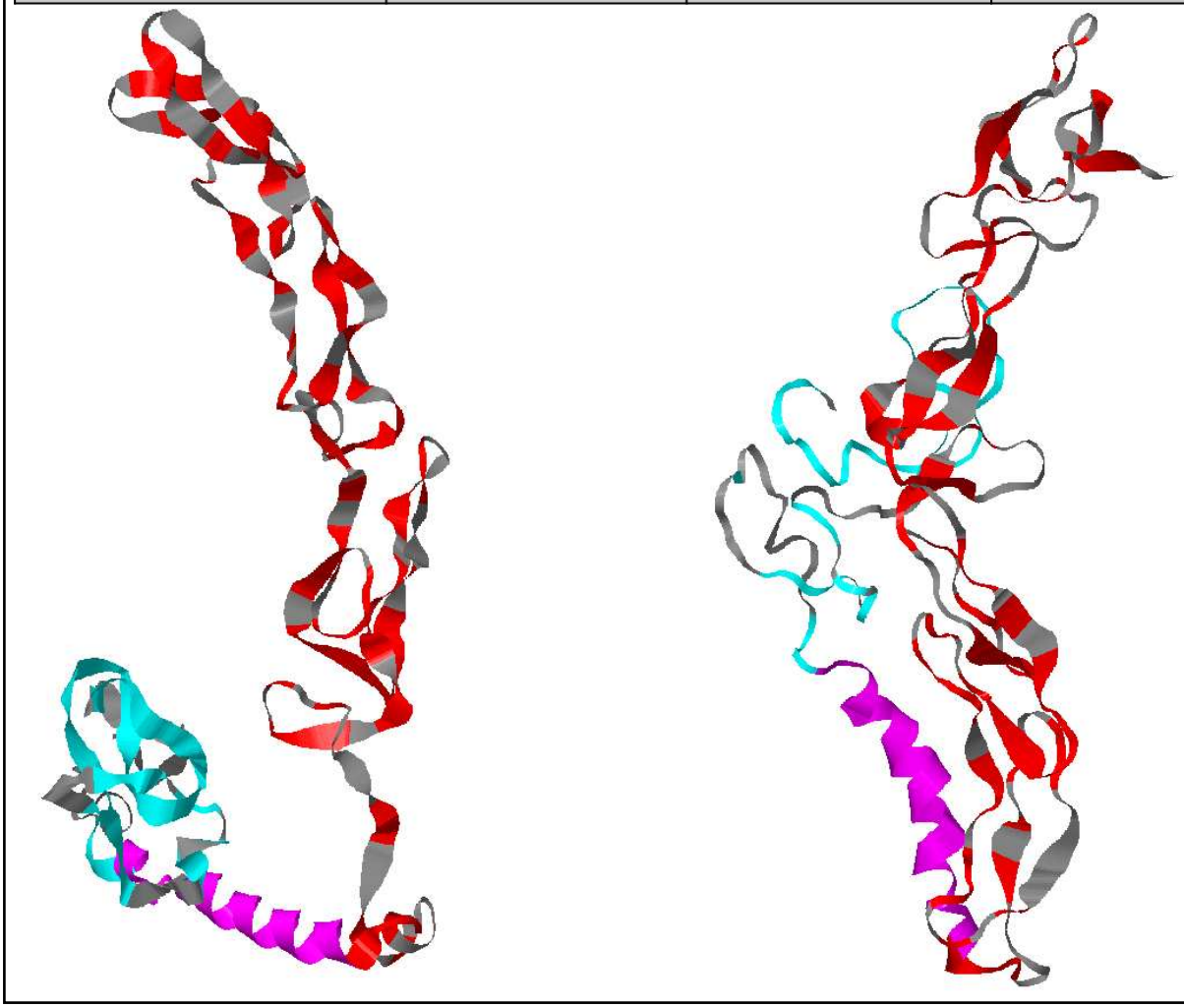

Figure I.21) Mouse CD40 (right) and Jamaican fruit bat CD40 (left) three-dimensional models and protein homology. Mouse CD40 three-dimensional model was pulled from UniProt (UniProt P27512). Jamaican fruit bat CD40 three-dimensional model was generated using PHYR^2 (NCBI accession XP_037020498). Transmembrane domains (magenta) and signal peptides (removed) were not included in the BLOSUM62 analysis. Mouse CD40 and Jamaican fruit bat CD40 had 90 identical extracellular sites (red) or 70.8% of the extracellular domain, there are 39 identical cytoplasmic sites (cyan) or 61.9%. Accounting for peptides that are not identical but had similar properties and identical sites the extracellular domain had a BLOSUM62 value of 70.8% homology, the cytoplasmic domain had a BLOSUM62 value of 73.0% homology. The combined extracellular and cytoplasmic domains had 129 identical sites or 55.8%, and a BLOSUM62 value of 71.4% homology.

CD44

CD44 was first described as an adhesion molecule to mediate cell adhesion and migration – hence the alias name Hermes-1 evoking the mythology of the messenger god Hermes [209]. CD44 is expressed on nearly every cell type [204]. CD44 binds to hyaluronic acid and CD44 interacts with cytoskeletal proteins ankyrin and ezrin/radixin/moesin proteins (**Figure I.22**) [204,205,210,211]. CD44 plays an important role for leucocytes to be homed to peripheral lymphoid organs and sites of inflammation by attachment to and rolling on endothelial cells [204,205]. Effector and memory T cells display a high expression of CD44, and when CD44 is used in conjunction with CD4, CD8, and

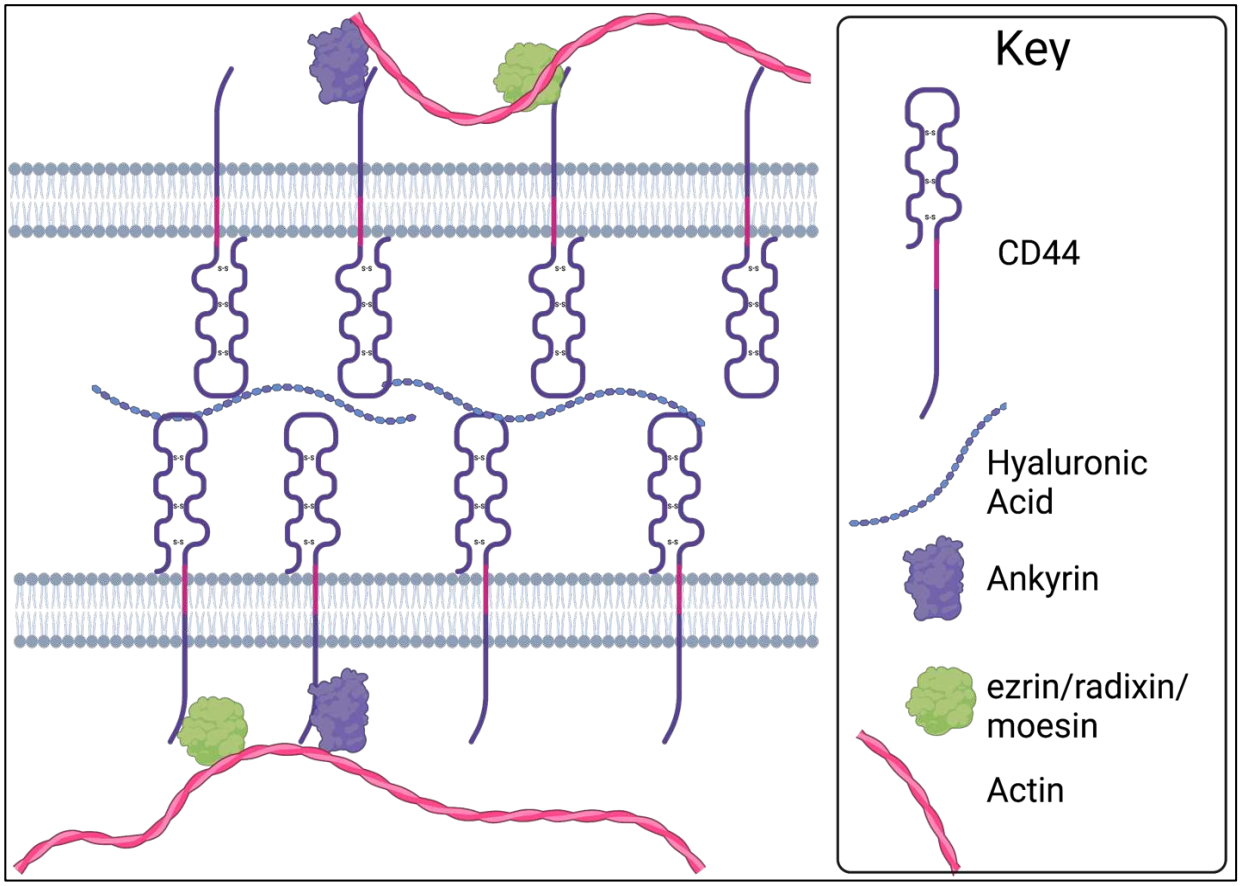

Figure I.22) CD44 binding to Hyaluronic acid. CD44 binding to hyaluronic acid causes CD44 cytoplasmic domain to interact with ankyrin and ezrin/radixin/moesin proteins to cause cytoskeletal changes. Created with BioRender.com.

CD62L, T cells can be classified into T helper and cytotoxic T: naïve (CD44 $^{int/low}$ CD62L^{+}), central memory (CD44 ^{high} CD62L^{+}), effector memory (CD44^{high} CD62L^{-}), and terminally differentiated effector memory (CD44 $^{int/low}$CD62L^{-}) [21,153].

Mouse and Jamaican Fruit Bat CD44 Protein Homology

One anti-CD44 mouse reactive antibody clone (IM7) was identified to cross-react with Jamaican fruit bat splenocytes (**Figure I.23**) and disassociated lamina propria single cell suspension of the gastrointestinal tract (**Figure I.24**). Clone IM7 recognizes all isoforms of mouse CD44. To further assess CD44 protein homology of mouse (UniProt P15379) and Jamaican fruit bat (NCBI accession XP_036984120). peptide sequences were downloaded into Geneious Prime. Protein sequences were then aligned in Geneious Prime using BLOSUM62 [145,146]. Mouse CD44 three-dimensional model was downloaded from UniProt (P15379) and Jamaican fruit bat CD44 three-dimensional model was generated with PHYR^2 using the NCBI peptide sequence (accession XP_036984120) (**Figure I.25**). The protein alignment of mouse CD44 and Jamaican fruit bat CD44 identified 360 identical extracellular sites or 54.3% of the extracellular domain, and 62 identical cytoplasmic sites or 90.3% of the cytoplasmic domain. When peptides with similar properties and identical sites were accounted for in the BLOSUM62 alignment, the extracellular domain had 62.3% homology, and the cytoplasmic domain had 90.3% homology. The combined

extracellular and cytoplasmic domains had 422 identical sites or 57.4%, and a BLOSUM62 value of 65.0% homology.

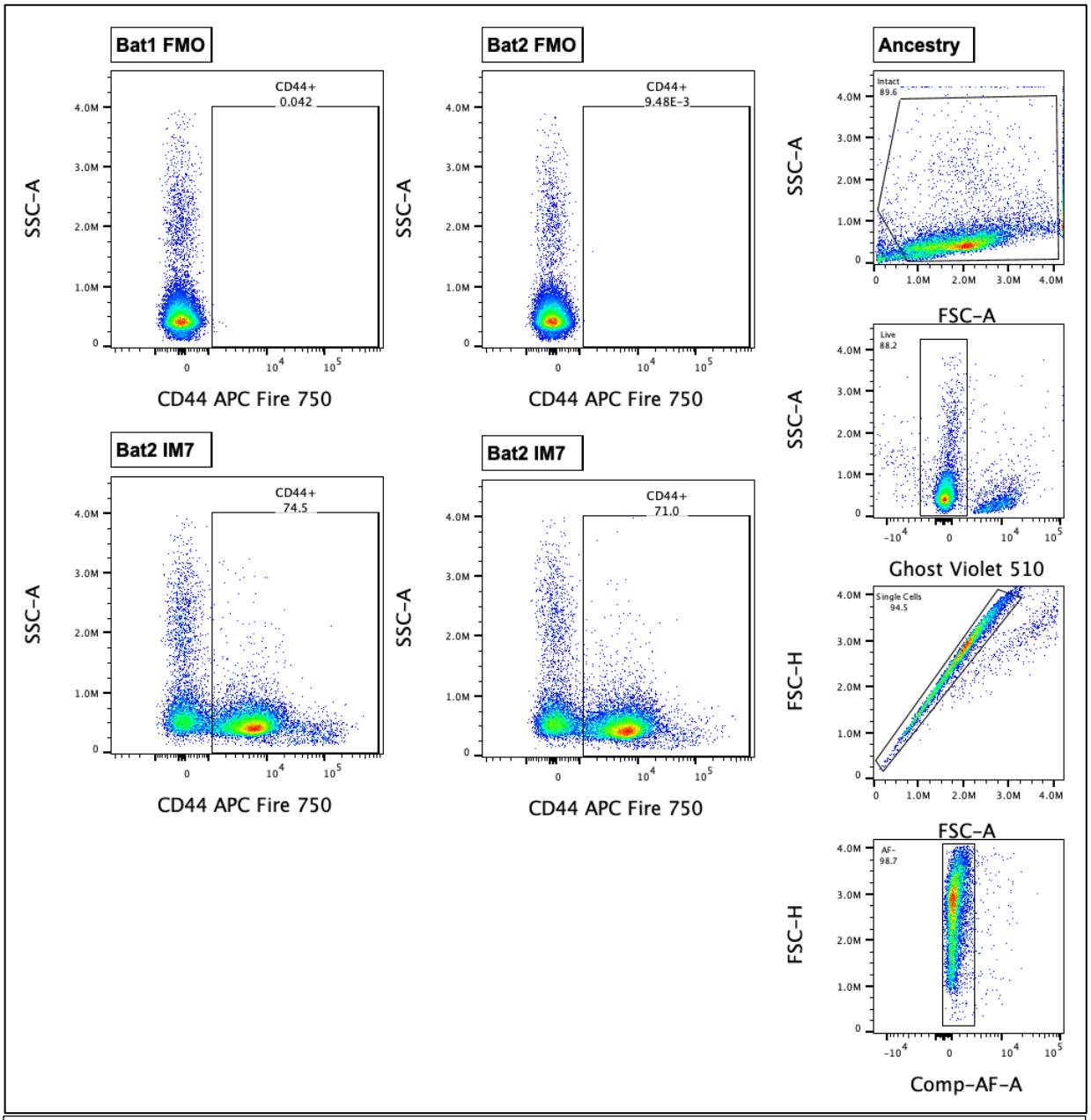

Figure I.23) Anti-CD44 clone IM7 staining of Jamaican fruit splenocytes from two bats. Gating strategy: ancestry gates (right) Intact > Live > Single Cells > Auto-florescence $(AF)^{-}$. $CD44^{+}$ gate determined by FMO control (top). $CD40^{+}$ splenocytes averaged 72.75%. Panel: CD44 (APC-Fire750), primary amine viability (Ghost Violet 510). Analyzed in FlowJo V 10.8.1 Mac OS X. Gates were drawn based on FMOs.

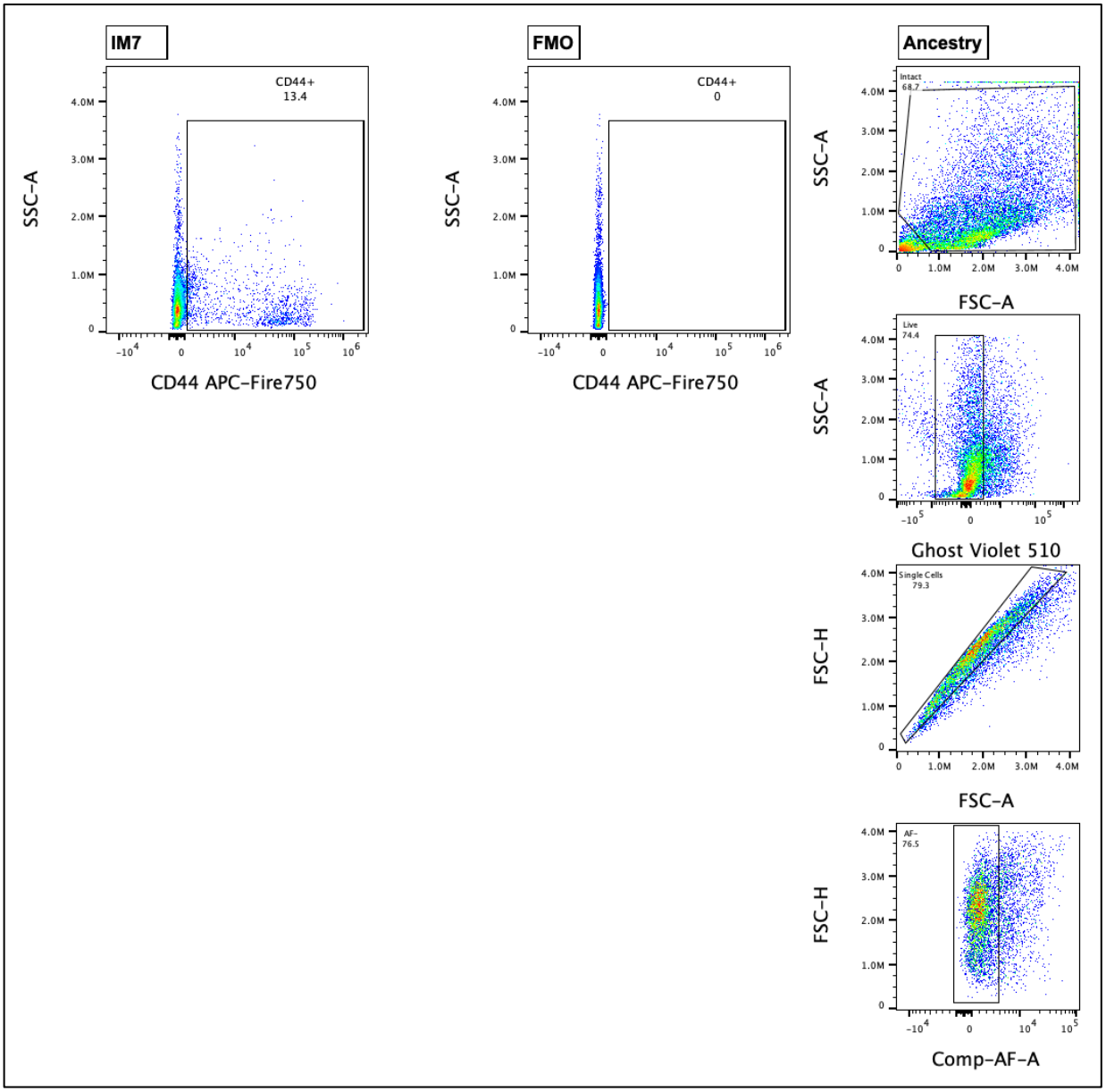

Figure I.24) Anti-CD44 clone IM7 staining of Jamaican fruit bat disassociated lamina propria single cell suspension from one bat. Gating strategy: ancestry gates (right) Intact > Live > Single Cells > Auto-florescence $(AF)^-$. $CD44^+$ gate determined by FMO control (top). $CD40^+$ splenocytes averaged 13.4%. Panel: CD44 (APC-Fire750), primary amine viability (Ghost Violet 510). Analyzed in FlowJo V 10.8.1 Mac OS X. Gates were drawn based on FMOs.

Cross-Reactive Clone	IM7 (Extracellular)		
Domain	Extracellular (Red)	Cytoplasmic (Cyan)	Combined
Identical Sites	360 (54.3%)	(86.1%)	422 (57.4%)
BLOSUM62	62.3%	90.3%	65.0%

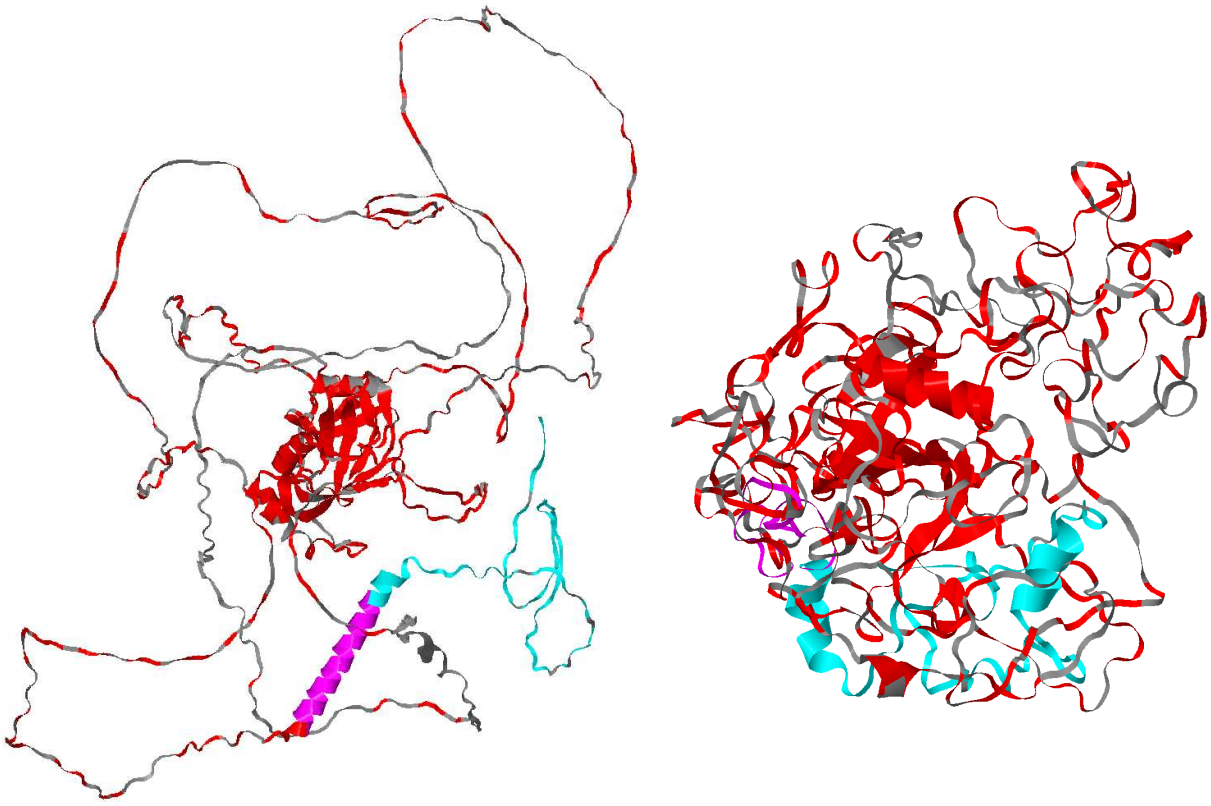

Figure I.25) Mouse CD44 (right) and Jamaican fruit bat CD44 (left) three-dimensional models and protein homology. Mouse CD44 three-dimensional model was pulled from UniProt (UniProt P15379). Jamaican fruit bat CD44 three-dimensional model was generated using PHYR[2] (NCBI accession XP_036984120). Transmembrane domains (magenta) and signal peptides (removed) were not included in the BLOSUM62 analysis. Mouse CD44 and Jamaican fruit bat CD44 had 360 identical extracellular sites (red) or 54.3% of the extracellular domain, there were 62 identical cytoplasmic sites (cyan) or 90.3%. Accounting for peptides that were not identical but had similar properties and identical sites the extracellular domain had a BLOSUM62 value of 62.3% homology, the cytoplasmic domain has a BLOSUM62 value of 90.3% homology. The combined extracellular and cytoplasmic domains had 422 identical sites or 57.4%, and a BLOSUM62 value of 65.0% homology.

CD45 (B220)

CD45, also known as common leukocyte antigen or protein tyrosine phosphatase receptor type C is a protein expressed in many isoforms exclusively by hemopoietic cells. CD45 is involved with the regulation of Scr-kinases which are involved with TCR and BCR signal transduction for cellular activation [204,205]. These isoforms are generated by alternate splicing of exons 4 through 6, frequently referred to as A, B, and C (**Figure I.26**) [205,212,213]. CD45 RABC is the largest isoform containing exons A, B, and C [213].

Mouse and Jamaican Fruit Bat CD45 Protein Homology

One mouse reactive anti-CD45RA antibody clone (RA3-6B2) cross-reacted with Jamaican fruit bat splenocytes (**Figure I.27**) and disassociated lamina propria of the gastrointestinal tract (**Figure I.28**). RA3-6B2 is an A restricted antibody meaning the antibody binds only to CD45 isoforms that contain exon A (**Figure I.26**). Hence the name anti-CD45"RA" meaning restricted to exon A and should not be confused with only binding to CD45 A. In mice, RA3-6B2 predominantly binds to the longest form of CD45RA (CD45ABC) and is largely found on B cells and naïve T cells [21,213].

To assess protein homology of mouse and Jamaican fruit bat CD45 the largest isoform of CD45 of each species was downloaded into Geneious Prime for BLOSUM62 protein alignment: Mouse CD45 (UniProt P06800), and Jamaican fruit bat (NCBI accession XP_037006826). For the three-dimensional modeling, Mouse CD45 was downloaded from UniProt (P06800), and Jamaican fruit bat CD45 was generated using PHYR^2 using the NCBI sequence (NCBI accession XP_037006826) (**Figure I.29**). Transmembrane domains (magenta) and signal peptides (removed) were not included in the BLOSUM62 analysis. The BLOSUM62 protein alignment of mouse CD45 and Jamaican fruit bat CD45 identified 182 identical extracellular sites or 45.6% of the extracellular domain, and 566 identical cytoplasmic sites or 88.1% of the cytoplasmic domain. For BLOSUM62 percent similarity, which accounted for peptides that were not identical but had similar properties and identical sites, the extracellular domain had 45.6% homology, and the

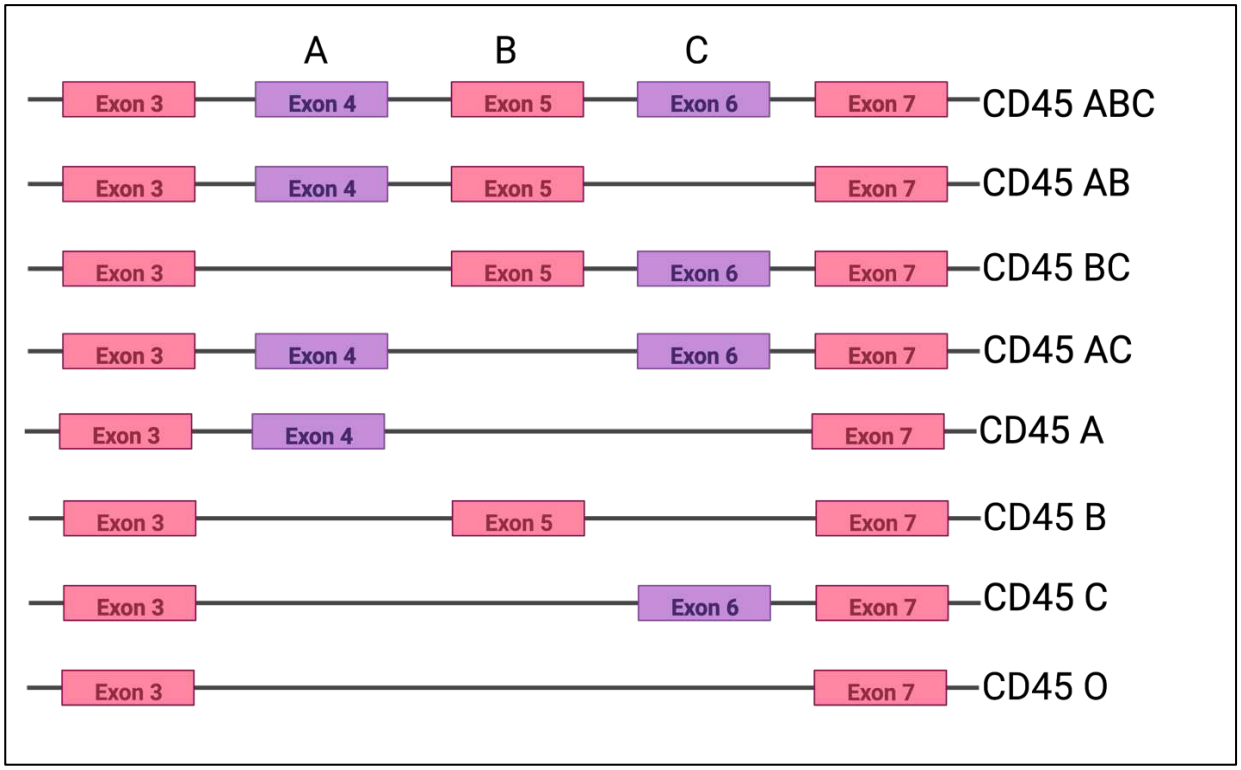

Figure I.26) CD45 exon splice variants. Exons 4, 5, and 6 are the variable regions of CD45 which create various isoforms of CD45. Created with BioRender.com.

cytoplasmic domain had 88.1% homology. The combined extracellular and cytoplasmic domains had 748 identical sites or 57.9%, and a BLOSUM62 value of 68.9% homology.

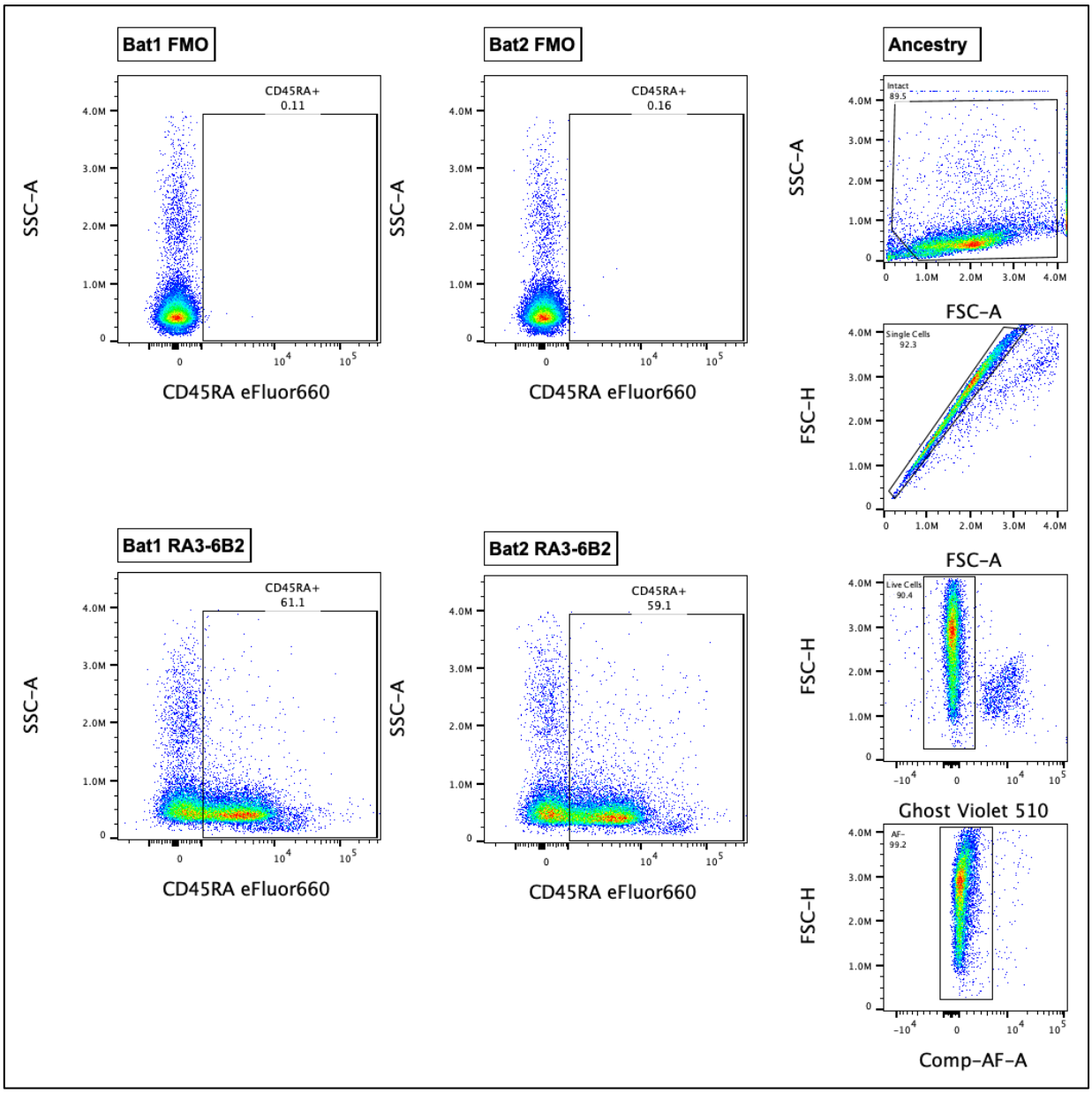

Figure I.27) Anti-CD45RA clone RA3-6B2 staining of Jamaican fruit splenocytes from two bats. Gating strategy: ancestry gates (right) Intact > Live > Single Cells > Auto-florescence $(AF)^-$. $CD45RA^+$ gate determined by FMO control (top). $CD45RA^+$ splenocytes averaged 60.1%. Panel: CD44 (eFluor660), primary amine viability (Ghost Violet 510). Analyzed in FlowJo V 10.8.1 Mac OS X. Gates were drawn based on FMOs.

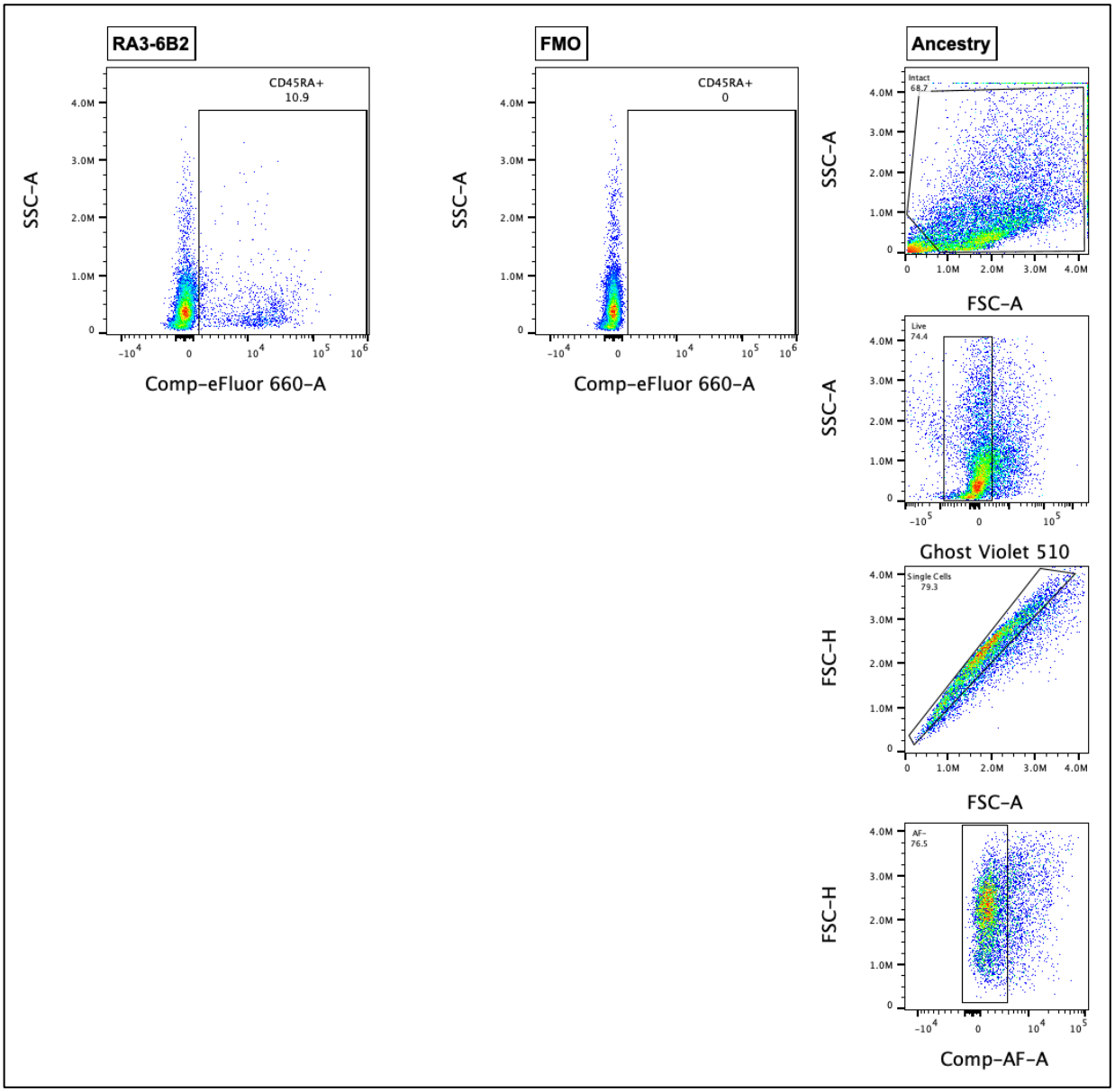

Figure I.28) Anti-CD45RA clone RA3-6B2 staining of Jamaican fruit disassociated lamina propria single cell suspension from one bat. Gating strategy: ancestry gates (right) Intact > Live > Single Cells > Auto-florescence $(AF)^{-}$. $CD45RA^{+}$ gate determined by FMO control (top). $CD40^{+}$ splenocytes averaged 10.9%. Panel: CD45RA (eFluor660), primary amine viability (Ghost Violet 510). Analyzed in FlowJo V 10.8.1 Mac OS X. Gates were drawn based on FMOs.

Cross-Reactive Clone	RA3-6B2 (Extracellular)		
Domain	Extracellular (Red)	Cytoplasmic (Cyan)	Combined
Identical Sites	182 (31.1%)	566 (80.1%)	748 (57.9%)
BLOSUM62	45.6%	88.1%	68.9%

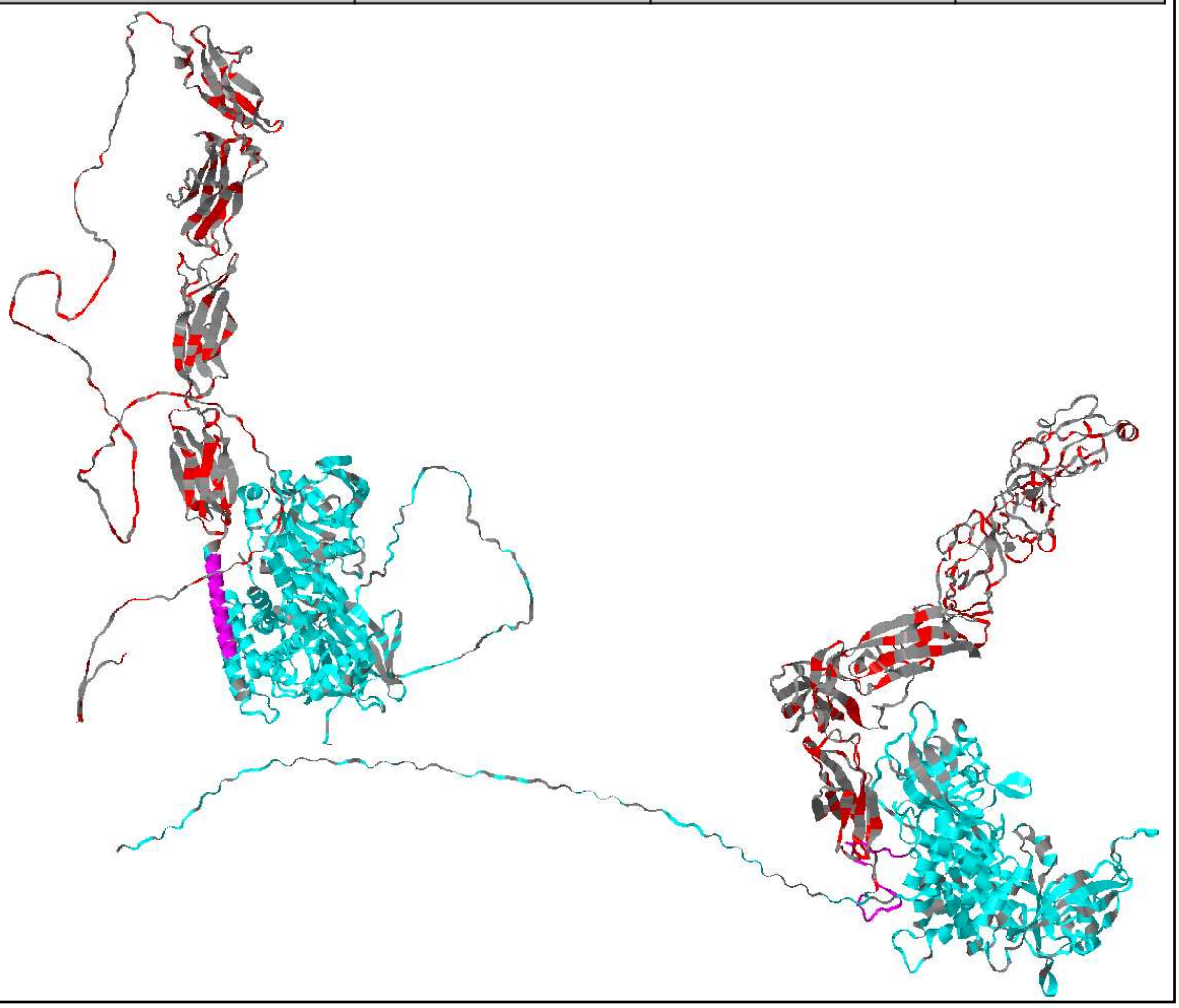

Figure I.29) Mouse CD45 (right) and Jamaican fruit bat CD45 (left) three-dimensional models and protein homology. Mouse CD45 three-dimensional model was pulled from UniProt (UniProt P06800). Jamaican fruit bat CD45 three-dimensional model was generated using PHYR[2] (NCBI accession XP_037006826). Transmembrane domains (magenta) and signal peptides (removed) were not included in the BLOSUM62 analysis. Mouse CD45 and Jamaican fruit bat CD45 had 182 identical extracellular sites (red) or 45.6% of the extracellular domain, there were 566 identical cytoplasmic sites (cyan) or 88.1%. Accounting for peptides that were not identical but had similar properties and identical sites the extracellular domain had a BLOSUM62 value of 45.6% homology, the cytoplasmic domain had a BLOSUM62 value of 88.1% homology. The combined extracellular and cytoplasmic domains had 748 identical sites or 57.9%, and a BLOSUM62 value of 68.9% homology.

CD80

CD80, also known as B7, is a homodimer and its ligand is CD28 (**Figure I.30**). CD80 is expressed on antigen presenting cells, activated B and T cells [21,204,205]. Stimulation of an MHC molecule presenting an antigen with the co-stimulation of CD80 and secreted cytokines from an antigen presenting cell such as IL-4, IL-6, IL-12, and IL-23 work in concert to activate a T cell (**Figure I.30**) [21,204,205]. This activation allows for T cell clonal expansion and differentiation. CD80 binding to CD28 causes the phosphorylation of the cytoplasmic domain of CD28 which activates PI 3-kinase. This results in several signaling pathways for the outcome of producing IL-2. IL-2 is a vital cytokine for T cell proliferation and differentiation into effector T cells [21]. Activated T cells upregulate CD152, also known as CXCR-4, which has a higher affinity for CD80 outcompeting CD28 which negatively regulates activated T cells [21,204,205].

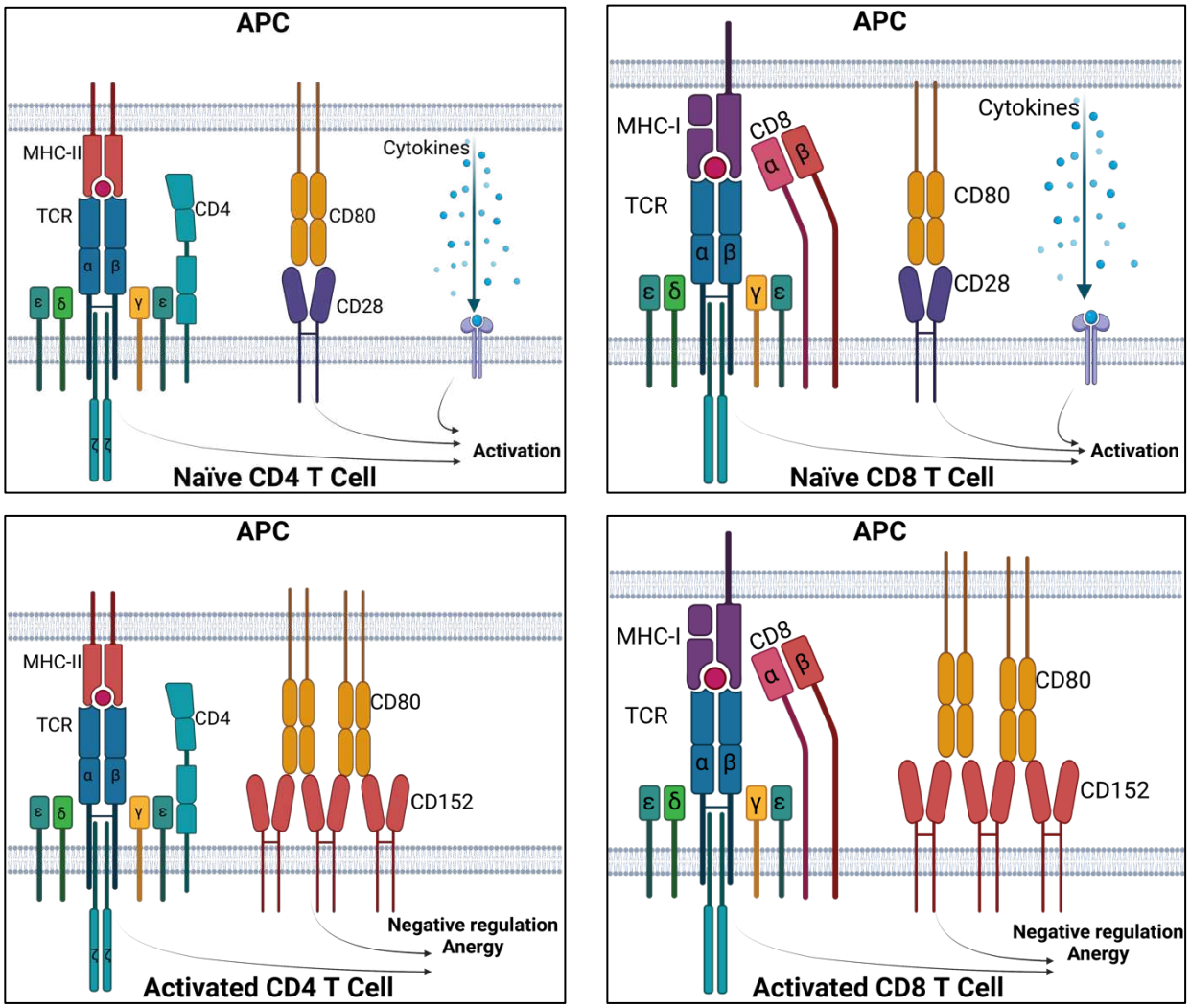

Figure I.30) CD80 and its dual role in activation and negative regulation of T cells. CD80 stimulation with MHC antigen presentation in concert with cytokines activate naïve T cells for clonal expansion and differentiation. Activated T cells up regulate CD152 or CTLA-4 which out competes CD28 and negatively regulates activated T Cells. Created with BioRender.com.

Mouse and Jamaican Fruit Bat CD80 Protein Homology

One mouse anti-CD80 reactive antibody clone (16-10A1) cross-reacted with Jamaican fruit bat splenocytes (**Figure I.31**) and disassociated lamina propria single cell suspension (**Figure I.32**). Mouse CD80 (UniProt Q00609) and Jamaican fruit bat CD80 (NCBI accession XP_037014596) protein sequences were downloaded into Geneious Prime for protein alignment and annotation. Mouse CD80 three-dimensional model was downloaded from UniProt (UniProt Q00609) and Jamaican fruit bat CD80 three-dimensional model was generated using PHYR^2 (NCBI accession XP_037014596) (**Figure I.33**). Transmembrane domains (magenta) and signal peptides (removed) were not included in the BLOSUM62 analysis. The BLOSUM62 alignment of mouse CD80 and Jamaican fruit bat CD80 identified 119 identical extracellular sites or 55.3% of the extracellular domain, and 9 identical cytoplasmic sites or 30.8% of the cytoplasmic domain. When peptides that are not identical but had similar properties were accounted for in conjunction with identical sites, the extracellular domain had 68.8% BLOSUM62 homology, and the cytoplasmic domain had 30.8% BLOSUM62 homology. The combined extracellular and cytoplasmic domains had 128 identical sites or 50.4%, and a BLOSUM62 value of 63.0% homology.

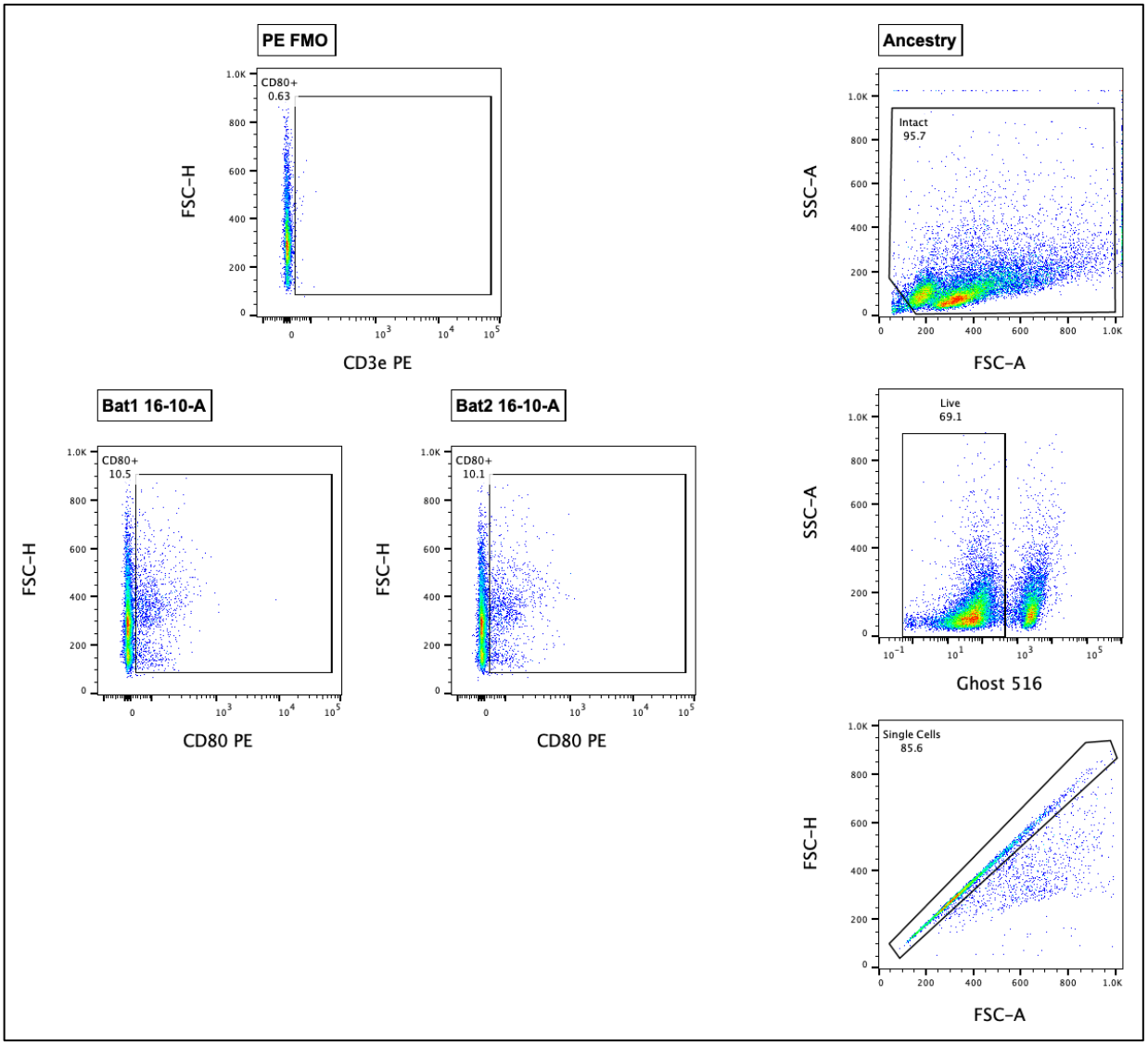

Figure I.31) Anti-CD80 clone 16-10-A staining of Jamaican fruit splenocytes from two bats. Gating strategy: ancestry gates (right) Intact > Live > Single Cells > Auto-florescence $(AF)^-$. $CD80^+$ gate determined by FMO control (top). $CD80^+$ splenocytes averaged 10.3%. Panel: CD80 (PE), primary amine viability (Ghost Blue 516). Analyzed in FlowJo V 10.8.1 Mac OS X. Gates were drawn based on FMOs.

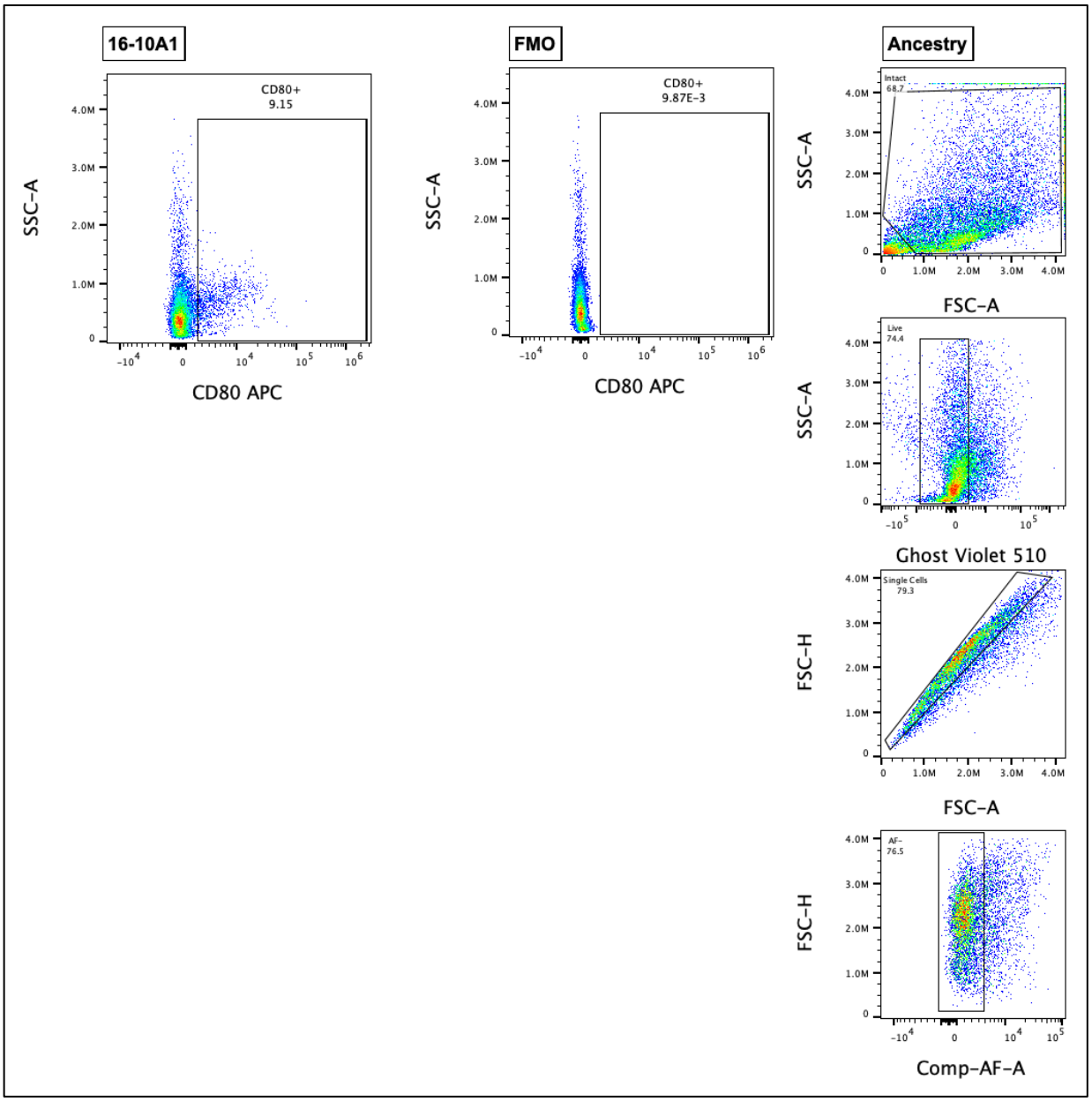

Figure I.32) Anti-CD80 clone 16-10A1 staining of Jamaican fruit disassociated lamina propria single cell suspension from one bat. Gating strategy: ancestry gates (right) Intact > Live > Single Cells > Auto-florescence $(AF)^{-}$. $CD80^{+}$ gate determined by FMO control (top). $CD80^{+}$ splenocytes averaged 9.15%. Panel: CD80 (APC), primary amine viability (Ghost Violet 510). Analyzed in FlowJo V 10.8.1 Mac OS X. Gates were drawn based on FMOs.

Cross-Reactive Clone	16-10A1 (Extracellular)		
Domain	Extracellular (Red)	Cytoplasmic (Cyan)	Combined
Identical Sites	119 (55.3%)	9 (23.1%)	128 (50.4%)
BLOSUM62	68.8%	30.8%	63.0%

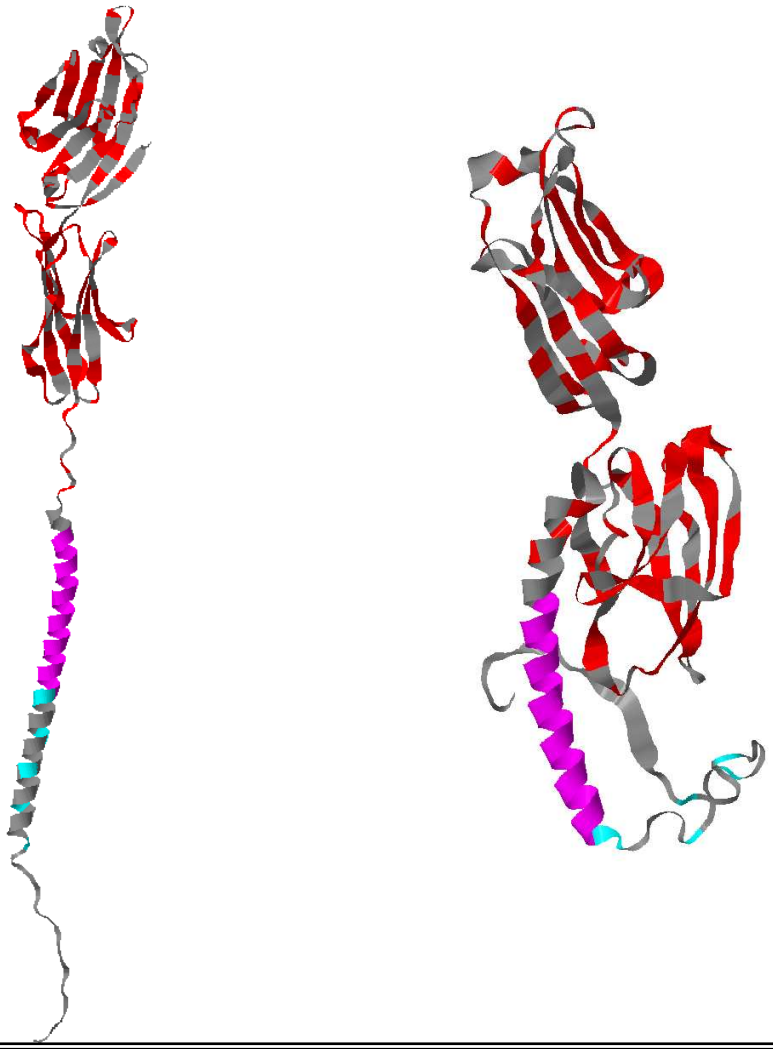

Figure I.33) Mouse CD80 (right) and Jamaican fruit bat CD80 (left) three-dimensional models and protein homology. Mouse CD80 three-dimensional model was pulled from UniProt (UniProt Q00609). Jamaican fruit bat CD80 three-dimensional model was generated using PHYR[2] (NCBI accession XP_037014596). Three-dimensional models represent proteins with signal peptides removed and transmembrane domains (magenta). Mouse CD80 and Jamaican fruit bat CD80 had 119 identical extracellular sites (red) or 55.3% of the extracellular domain, there were 9 identical cytoplasmic sites (cyan) or 30.8%. Accounting for peptides that were not identical but had similar properties and identical sites the extracellular domain had a BLOSUM62 value of 68.8% homology, the cytoplasmic domain had a BLOSUM62 value of 30.8% homology. The combined extracellular and cytoplasmic domains had 128 identical sites or 50.4%, and a BLOSUM62 value of 63.0% homology.

CD104

CD104, also known as Integrin beta 4, non-covalently associates with CD69f and binds laminins (**Figure I.34**) [21,208,214]. CD104 is expressed by double-negative thymocytes, monocytes, neurons, epithelial cells, endothelial cells, Schwan cells, and trophoblasts [21,208,215]. CD104:CD49f binds predominantly to laminins, but can also bind to neuregulin-1, insulin-like growth factor-1, and insulin-like growth factor-2 [21,205,208,216-218]. CD104 binding of thymocytes

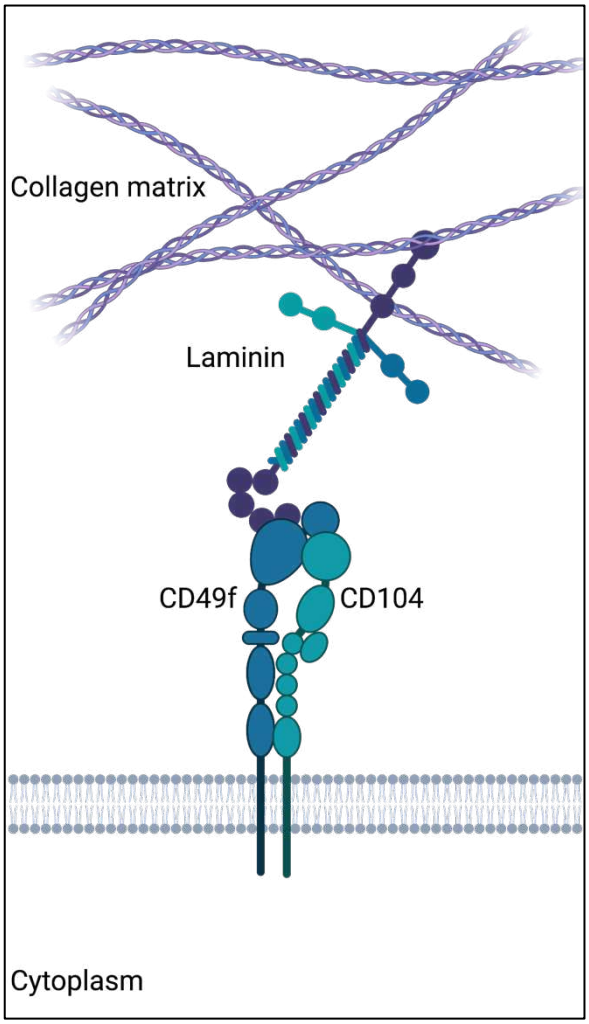

Figure I.34) CD104 associating with CD49f non-covalently binding to laminin bound to collagen matrix. Created with BioRender.com.

contribute to thymocyte differentiation and migration [208]. Interestingly, anti-CD104 antibodies bind weakly to natural killer cells, and bind to T helper cells *in vitro* upon activation by phytohemagglutinin [208].

Mouse and Jamaican Fruit Bat CD104 Protein Homology

Two mouse reactive anti-CD104 antibody clones (H8XB4, and 345-11A) reacted with Jamaican fruit bat disassociated lamina propria fraction of the gastrointestinal tract (**Figure I.35**). To further assess protein homology CD104 peptide sequences from mouse (UniProt A2A863) and Jamaican fruit bat (NCBI accession XP_037013824) were downloaded into Geneious Prime for BLOSUM62 protein alignment. Only mouse CD104 three-dimensional model was downloaded into Geneious Prime from Uniprot (A2A863) and the model represents CD104 with the signal peptide removed (**Figure I.36**). PHYR2 cannot produce three-dimensional models of protein sequences longer than 1,200 peptides and CD104 is 1,824 peptides. The BLOSUM62 protein alignment of mouse CD104 and Jamaican fruit bat CD104 identified 589 identical extracellular sites or 85.7% of the extracellular domain, and 934 identical cytoplasmic sites or 85.2% of the cytoplasmic domain. BLOSUM62 percent similarity of the two CD104 proteins reported the extracellular domain had a 92.0% BLOSUM62 homology, and the cytoplasmic

domain had a 91.1% BLOSUM62 homology. The combined extracellular and cytoplasmic domains had 1,523 identical sites or 85.4%, and a BLOSUM62 value of 91.4% homology.

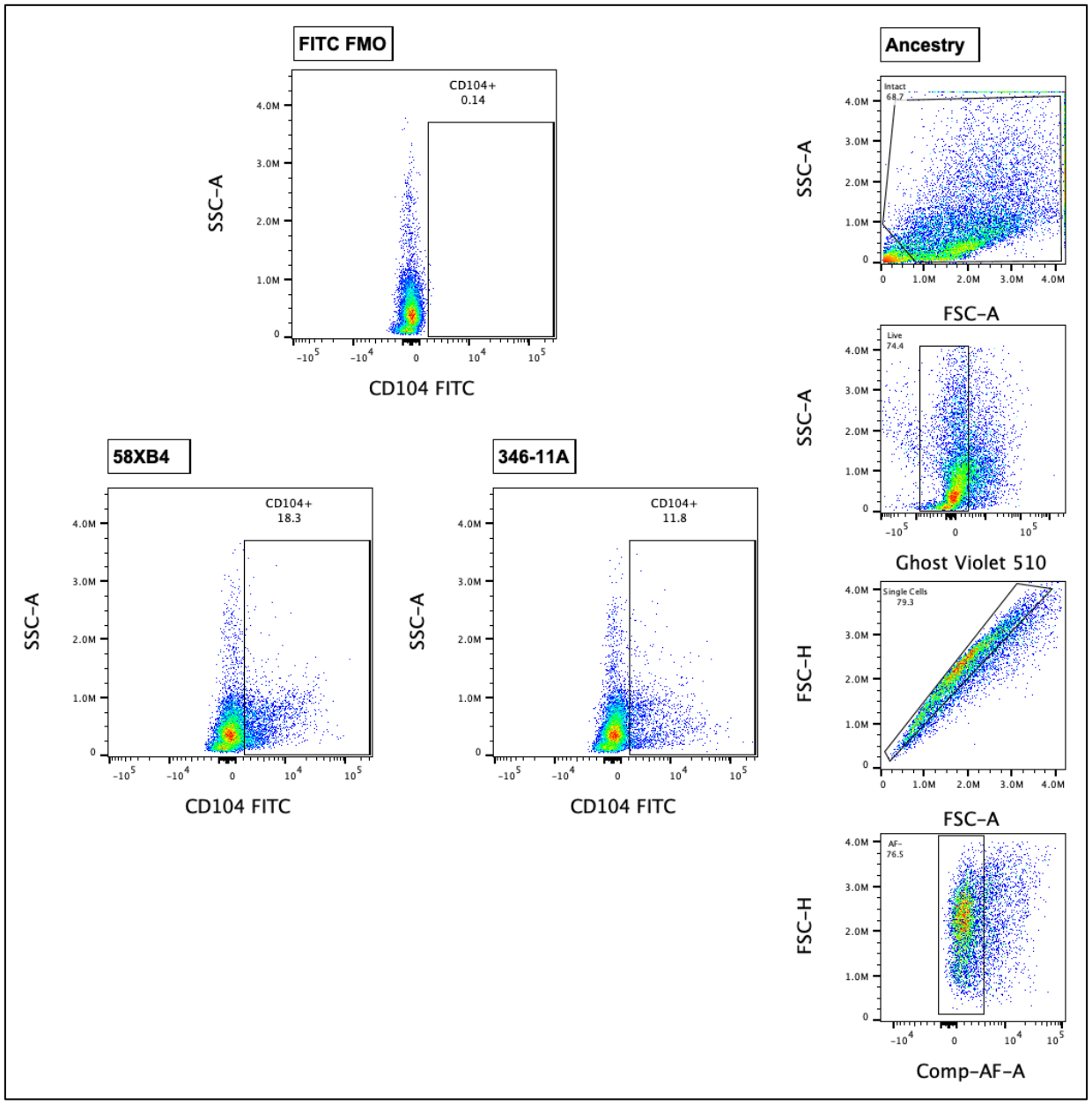

Figure I.35) Anti-CD104 clones 58XB4 and 346-11A staining of Jamaican fruit disassociated lamina propria single cell suspension from one bat. Gating strategy: ancestry gates (right) Intact > Live > Single Cells > Auto-florescence $(AF)^{-}$. $CD104^{+}$ gate determined by FMO control (top). $CDCD104^{+}$ disassociated lamina propria clone 58XB4 averaged 18.3%, and clone 346-11A averaged 11.8% . Panel: CD104 (FITC), primary amine viability (Ghost Violet 510). Analyzed in FlowJo V 10.8.1 Mac OS X. Gates were drawn based on FMOs.

Cross-Reactive Clone	346-11A, 58xB4 (Extracellular)		
Domain	Extracellular (Red)	Cytoplasmic (Cyan)	Combined
Identical Sites	589 (85.7%)	934 (85.2%)	1,523 (85.4%)
BLOSUM62	92.0%	91.1%	91.4%

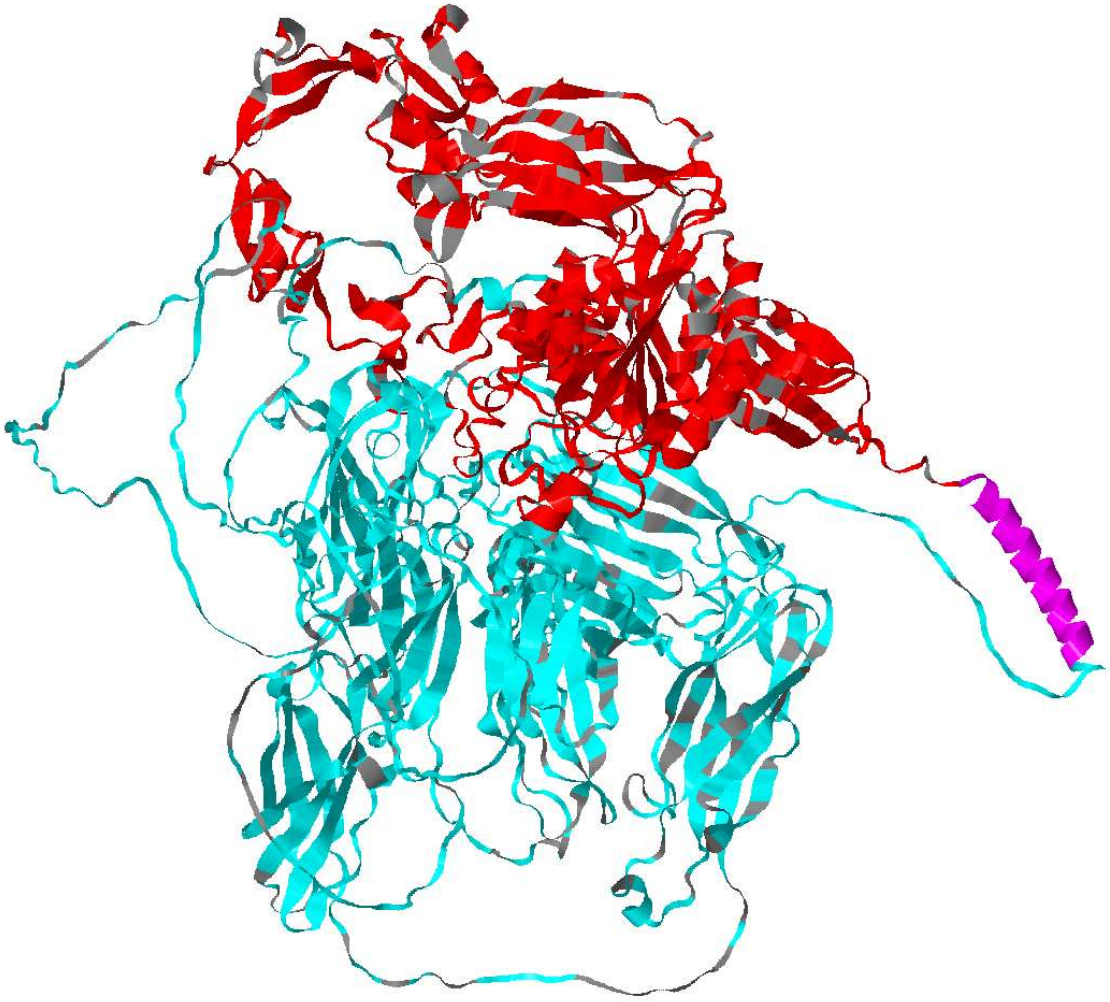

Figure I.36) Mouse CD104 three-dimensional model and Jamaican fruit bat CD104 protein homology. Mouse CD104 three-dimensional model was pulled from UniProt (UniProt A2A863). Jamaican fruit bat CD104 (NCBI accession XP_037013824) was used for protein homology analysis. Three-dimensional model represents CD104 with signal peptides removed and transmembrane domains (magenta). Mouse CD104 and Jamaican fruit bat CD104 had 589 identical extracellular sites (red) or 85.7% of the extracellular domain, there are 934 had cytoplasmic sites (cyan) or 85.2%. Accounting for peptides that were not identical but had similar properties and identical sites the extracellular domain had a BLOSUM62 value of 92.0% homology, the cytoplasmic domain had a BLOSUM62 value of 91.1% homology. The combined extracellular and cytoplasmic domains had 1,523 identical sites or 85.4%, and a BLOSUM62 value of 91.4% homology.

CD154

CD154 is a trimer expressed on activated T helper cells and its ligand is CD40 (**Figure I.19**). CD154 is expressed predominantly on activated T helper cells, however it is also expressed on cytotoxic T lymphocytes but at lesser levels than activated CD4 T cells [208]. CD154 provides a co-stimulatory signal for B cells via binding of CD40 for growth, differentiation, immunoglobulin class switching, and aids in germinal center formation and development of plasma and memory B cells [205,208]. When CD154 is nonfunctional it causes what is known as hyper IgM syndrome because elevated levels of IgM are found in serum with trace or no measurable amounts of IgG, IgA and IgE due to the critical need of functional CD154 for B cells to class switch [204,205]. Additionally, CD154 binding to CD40 promotes cytokine production by dendritic cells and macrophages. CD154 stimulation of CD40 on macrophages sensitizes macrophages to IFN-γ. As such, CD154, CD40, and IFN-γ work in concert to activate a macrophage [21].

Human and Jamaican Fruit Bat CD154 Protein Homology

One human reactive CD154 antibody clone (5C8) cross reacted with Jamaican fruit bat splenocytes (**Figure I.37**). To further assess protein homology of human (UniProt P29965) and Jamaican fruit bat (NCBI accession XP_037012946) CD154 peptide sequences were downloaded into Geneious Prime for BLOSUM62 protein alignment. CD154 three-dimensional models human (UniProt P29965) and Jamaican fruit bat (NCBI accession XP_037012946) (**Figure I.38**). Jamaican fruit bat CD154 three-dimensional model was generated using PHYR^2. BLOSUM62

analysis of human CD154 and Jamaican fruit bat CD154 had 190 identical extracellular sites or 88.4% of the extracellular domain, and 18 identical cytoplasmic sites or 72.0% of the cytoplasmic domain. When peptides that were not identical but had similar properties in conjunction with identical sites the extracellular domain had a 92.1% BLOSUM62 homology, and the cytoplasmic domain had 84.0% BLOSUM62 homology. The combined extracellular and cytoplasmic domains had 208 identical sites or 86.7%, and a BLOSUM62 value of 91.3% homology.

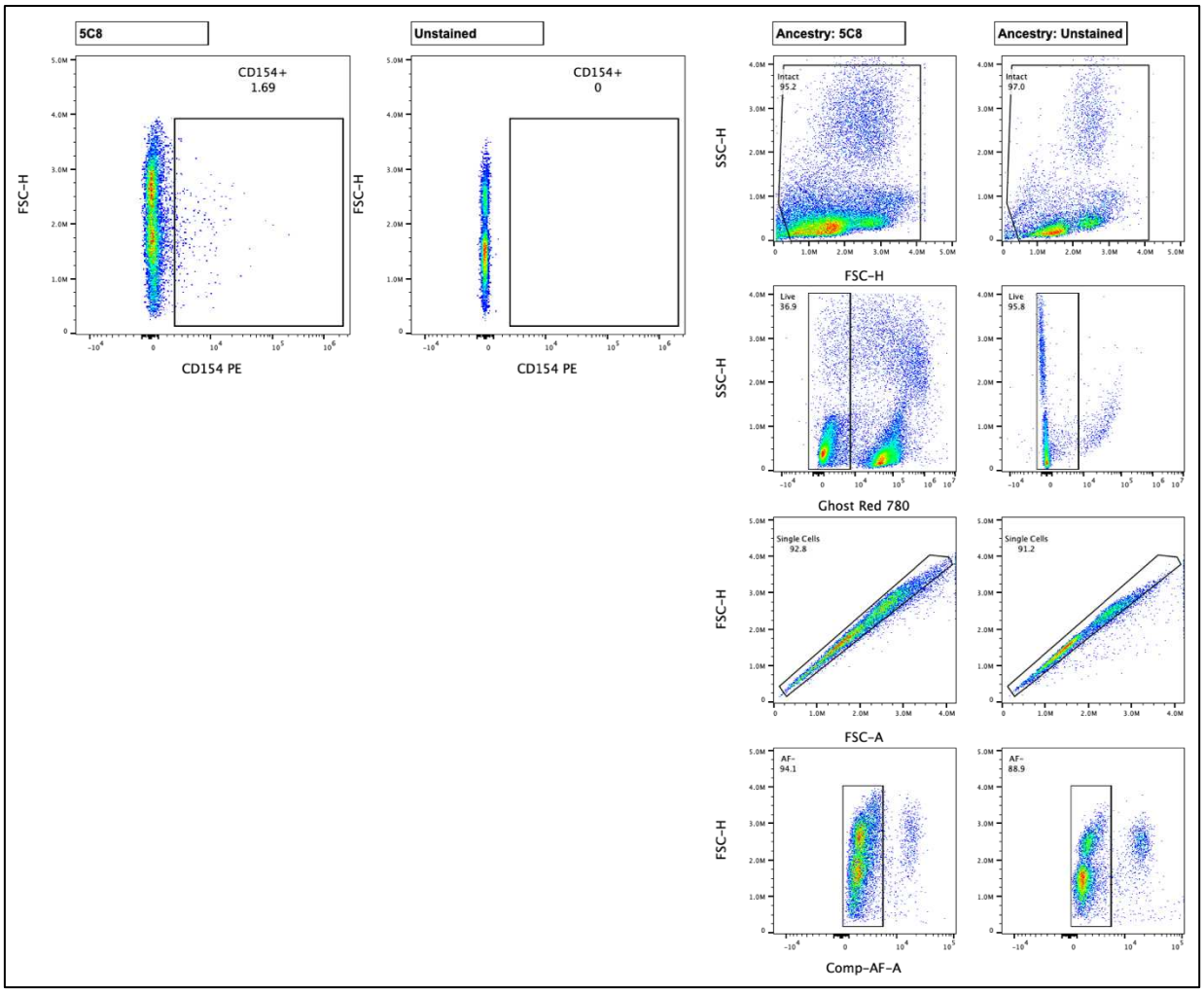

Figure I.37) Anti-CD154 clone 5C8 staining of Jamaican fruit splenocytes from one bat. Gating strategy: ancestry gates (right) Intact > Live > Single Cells > Auto-florescence $(AF)^{-}$. $CD154^{+}$ gate determined by unstained control (top). $CD154^{+}$ splenocytes averaged 1.69%. Panel: CD154 (PE), primary amine viability (Ghost Red 780). Analyzed in FlowJo V 10.8.1 Mac OS X. Gates were drawn based on FMOs.

Cross-Reactive Clone	5C8 (Extracellular)		
Domain	Extracellular (Red)	Cytoplasmic (Cyan)	Combined
Identical Sites	190 (88.4%)	18 (72.0%)	208 (86.7%)
BLOSUM62	92.1%	84.0%	91.3%

Figure I.38) Human CD154 (right) and Jamaican fruit bat CD154 (left) three-dimensional models and protein homology. Human CD154 three-dimensional model was pulled from UniProt (UniProt P29965). Jamaican fruit bat CD154 three-dimensional model was generated using PHYR[2] (NCBI accession XP_037012946). Three-dimensional models represent proteins with signal peptides removed and transmembrane domains (magenta). Human CD154 and Jamaican fruit bat CD154 had 190 identical extracellular sites (red) or 88.4% of the extracellular domain, there were 18 identical cytoplasmic sites (cyan) or 72.0%. Accounting for peptides that were not identical but had similar properties and identical sites the extracellular domain had a BLOSUM62 value of 92.1% homology, the cytoplasmic domain had a BLOSUM62 value of 84.0% homology. The combined extracellular and cytoplasmic domains had 208 identical sites or 86.7%, and a BLOSUM62 value of 91.3% homology.

Mouse CD161 and Jamaican Fruit Bat KLRF1

CD161 is a lectin protein heterodimer preferentially expressed on natural killer cells, but is also expressed on memory T helper and memory cytotoxic T cells [204]. Lectin-like transcript factor 1 is a ligand for CD161, when CD161 binds to lectin like transcription factor 1 it provides an inhibitory signal to natural killer cells (**Figure I.39**) [219,220]. It has been demonstrated that CD161 engagement with lectin-like transcription factor 1 inhibited natural killer cell cytotoxicity and IFN-γ production [220-223]. CD161 expressed on T cells has conflicting and no clear function on T cells [224]. However, memory $CD161^+$ CD4 T cells trend in higher production of IFN-γ than memory $CD161^-$ CD4 T cells [225]. Similarly, $CD161^+$ CD8 T cells have been shown to produce significantly more IFN-γ compared to memory $CD161^-$ CD8 T cells [159]. Three CD161 genes have been identified in mice, and only one gene in humans [204]. KLRF1 is expressed on natural killer cells and subsets of cytotoxic T cells [226]. KLRF1 binds to AICL, or C-type lectin domain family 2 member B, KLRF stimulation promotes effector functions of natural killer cells and effector functions of cytotoxic T cells (**Figure I.39**) [226-228].

The annotation of *Artibeus jamaicensis* on NCBI was released on October 30, 2020, and even with the release of the annotations more work needs to be carried out. Prior to the release of annotations, known sequences of a well annotated species such as mouse or human were used to blast against the Jamaican fruit bat genome, transcriptome, or proteome to identify the similar sequences. Surprisingly after the release of annotations, mouse CD161 aligned with Jamaican fruit bat KRLF1. Interestingly, it has been demonstrated that Egyptian fruit bats (*Rousettus aegyptiacus*) have an expansion of KLRC genes. Six out of ten of these KLRC genes had both

activating and inhibitory motifs, three out of ten had inhibitory motifs, and one had an activating motif [143]. A study into Jamaican fruit bat and other bat species' KLRC genes need to be carried out to better understand if this is a common occurrence across bat species.

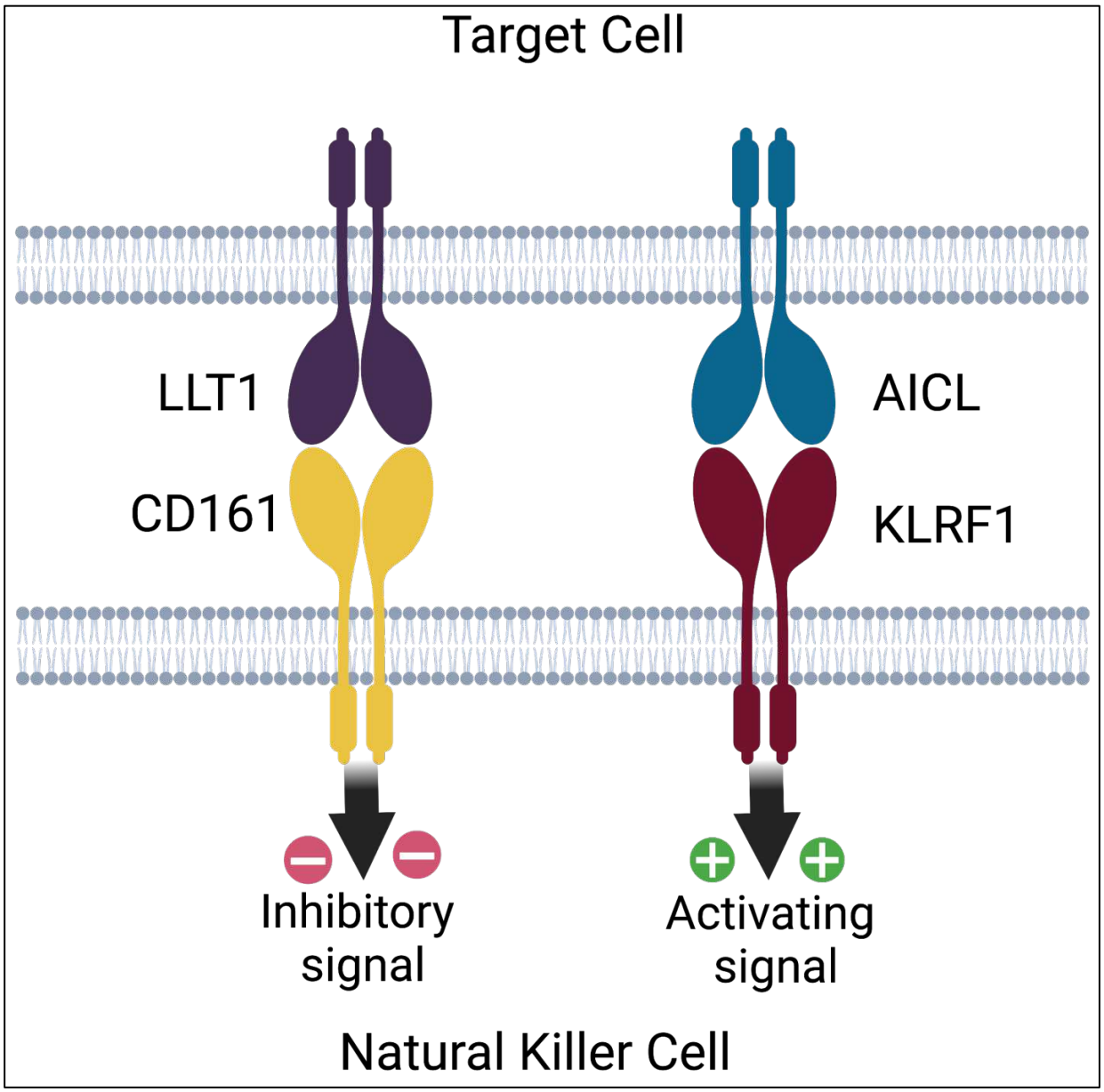

Figure I.39) CD161 and KLRF1 binding to their ligands lectin-like transcription factor 1 and C-type lectin domain family 2 member B (AICL). Stimulation of CD161 provides an inhibitory signal to natural killer cells. Stimulation of KLRF1 provides an activating signal to natural killer cells. Created with BioRender.com.

Protein Homology of Mouse CD161 and Jamaican Fruit Bat KLRF1

One mouse anti-CD161 antibody clone (PK136), that reacts with KLRB1B and KLRB1C in mice, cross-reacted with Jamaican fruit bat splenocytes (**Figures I.40-I.43**) and PBMCs (**Figures I.44 and I.45**). However, to what Jamaican fruit bat antigen antibody clone PK136 is binding to remains in question. To better understand if the cross-reactive anti-CD161 antibody is binding to natural killer cells and natural killer T cells, Jamaican fruit bat splenocytes were analyzed via flow cytometry using anti-CD161 (PE), in conjunction with anti-AGM1 (FITC) and anti-CD3γ(AF647, clone X-E2) (**Figures I.40-I.45**). The same samples were analyzed on two different cytometers, a FACSAria-III (**Figure I.40, I.41, and I.44**) and a Cytek Aurora 4L 16V-14B-10YG-8R cytometer (**Figure I.42, I.43, and I.45**) to better understand the resolution difference between the two cytometers, and the impact of highly autofluorescent cells on flow cytometry data. The data suggests that the majority of $CD161^+AGM1^+$ and $AGM1^+$ cells in spleen and circulating PBMCs are natural killer T cells as these cells ≥83.4% were $CD3\gamma^+$. $CD161^+$ splenocytes only had 21.7% (FACSAria-II) or 41.3% $CD3\gamma^+$ (Cytek 4L). $CD161^+$ PBMCs were 3.94% (FACSAria-II) or 16.9% $CD3\gamma^+$ (**Figure I.46).** As such, the data indicates that the majority of $CD161^+$ cells are natural killer cells. However, further analysis of these cell types needs to be carried out to elucidate their lineage and functionality.

While the data is only an N of one, but are the same sample acquired by two different cytometers, this highlights a potential difference in reported population proportions and abundance in the literature. The Cytek 4L Aurora is a spectral cytometer with the ability to identify highly autofluorescent cells allowing for them to be gated out. It is worth noting that there were differences in population percentages when there is the ability to remove highly autofluorescent

cells. Most notably, splenocyte $CD161^+$cells increased from 1.16% (FACSAria-III) to 5.62% (Cytek 4L), $AGM1^+CD161^+$ decreased from 4.9% (FACSAria-III) to 3.2%(Cytek 4L), and $CD161^+$ $CD3\gamma^+$ cells increased from 21.1% (FACSAria-III) to 41.3% (Cytek 4L) (**Figure I.46**). Similarly, PBMC $CD161^+$ cells increased from 3.68% (FACSAria-III) to 7.34% (Cytek 4L), and $CD161^+CD3\gamma^+$ cells increased from 3.94% (FACSAria-III) to 16.9% (Cytek 4L) (**Figure I.46)**. As such, the type of cytometer and gating strategy (i.e. removal of autofluorescent cells) can impact the data.

The *in silico* analysis suggests antibody clone PK136 is cross-reacting with Jamaican fruit bat KLRF1. To further assess protein homology of mouse KLRB1B (UniProt P27812) and KLRB1C (KLRB1C UniProt P27814) with Jamaican fruit bat KLRF (NCBI accession XP_037023746) were downloaded into Geneious prime for BLOSUM62 protein alignment. Additionally three-dimensional models of mouse KLRB1B (UniProt P27812) and KLRB1C (KLRB1C UniProt P27814) were downloaded into Geneious prime. The three-dimensional model for Jamaican fruit bat KLRF (NCBI accession XP_037023746) was generated with $PHYR^2$ and then downloaded into Geneious Prime. The BLOSUM62 protein alignment of mouse CD161(KLRB1B and KLRB1C) and Jamaican fruit bat KLRF1 identified 58 identical extracellular sites or 32.2% of the extracellular domain, and 4 identical cytoplasmic sites or 35.1% of the cytoplasmic domain. When non-identical peptides with similar properties were accounted for in conjunction with identical sites the extracellular domain had 61.9% BLOSUM62 homology, and the cytoplasmic domain had a 35.1% BLOSUM62 homology. The combined extracellular and cytoplasmic domains had 62 identical sites or 56.9%, and a BLOSUM62 value of 56.9% homology.

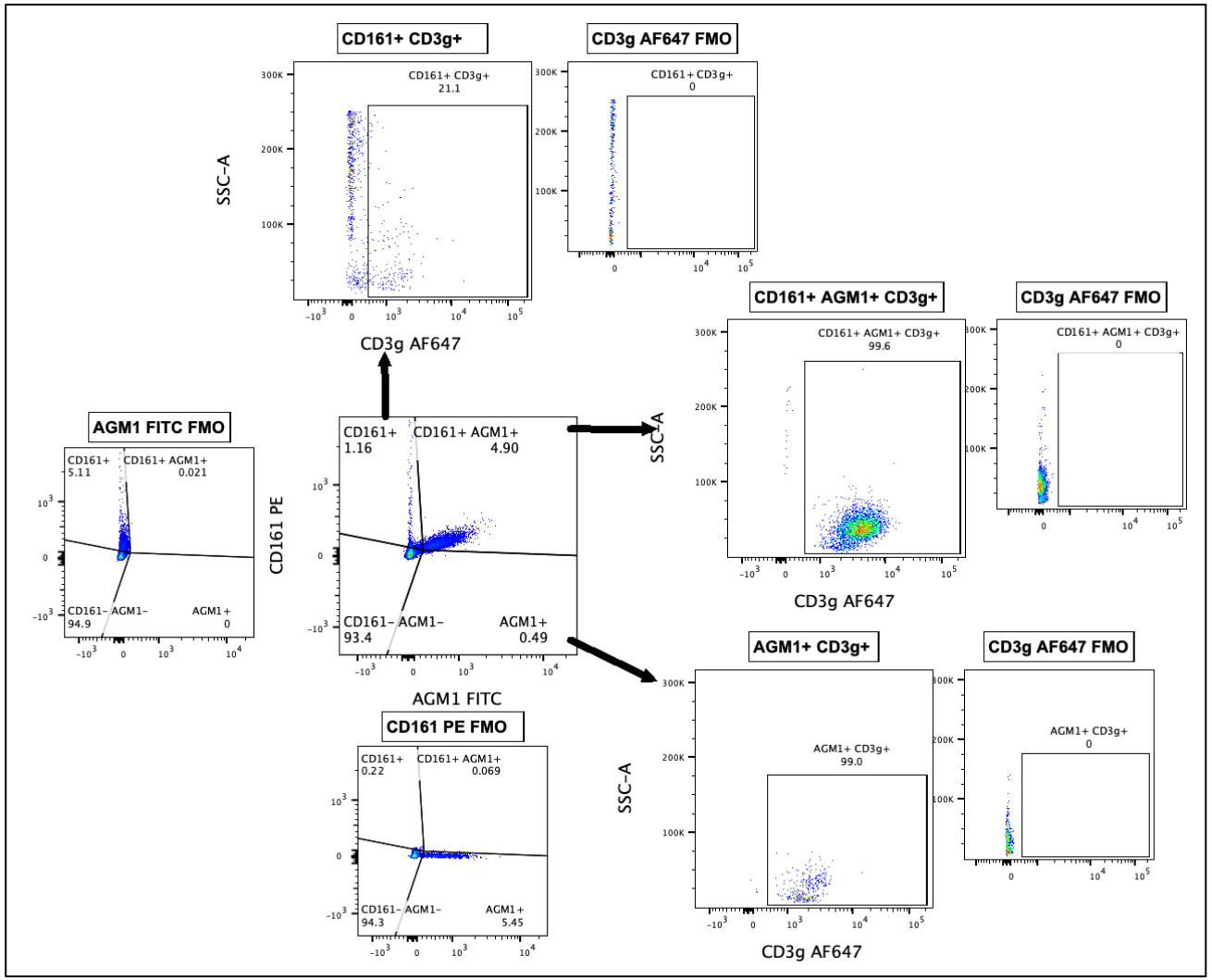

Figure I.40) Panel of anti-CD161 (PK136, PE), anti-AGM1 (polyclonal, FITC), and CD3γ (X-E2, AF647) staining of splenocytes analyzed on a FACSAria-III on one bat. 1.16% of splenocytes were $CD161^+$, 21.1% of those were also $CD3\gamma^+$. 4.9% of splenocytes were $CD161^+AGM1^+$, 99.96% of those cells were also $CD3\gamma^+$. 0.49% of splenocytes were $AGM1^+$, 99.0% of those were also $CD3\gamma^+$. Gates were drawn using FMOs. FCS files were analyzed in FlowJo V 10.8.1 Mac OS X.

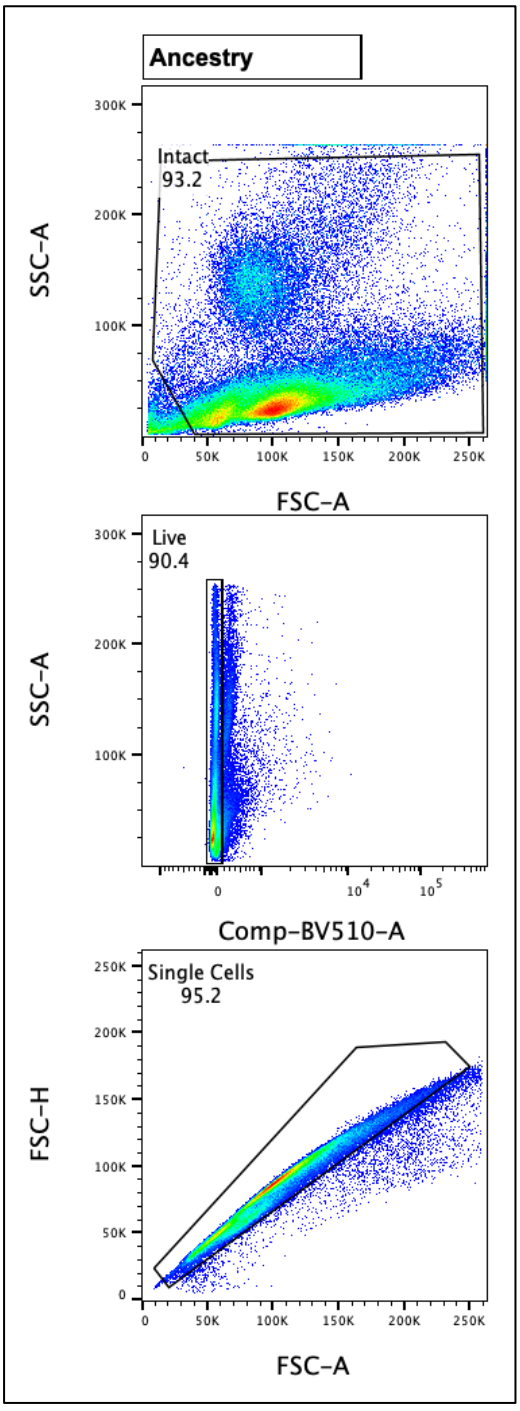

Figure I.41) Ancestry gating of **figure I.40**. Gating Strategy: Intact > Live > Single Cells. FCS files were analyzed in FlowJo V 10.8.1 Mac OS X. Gates were drawn based on FMOs.

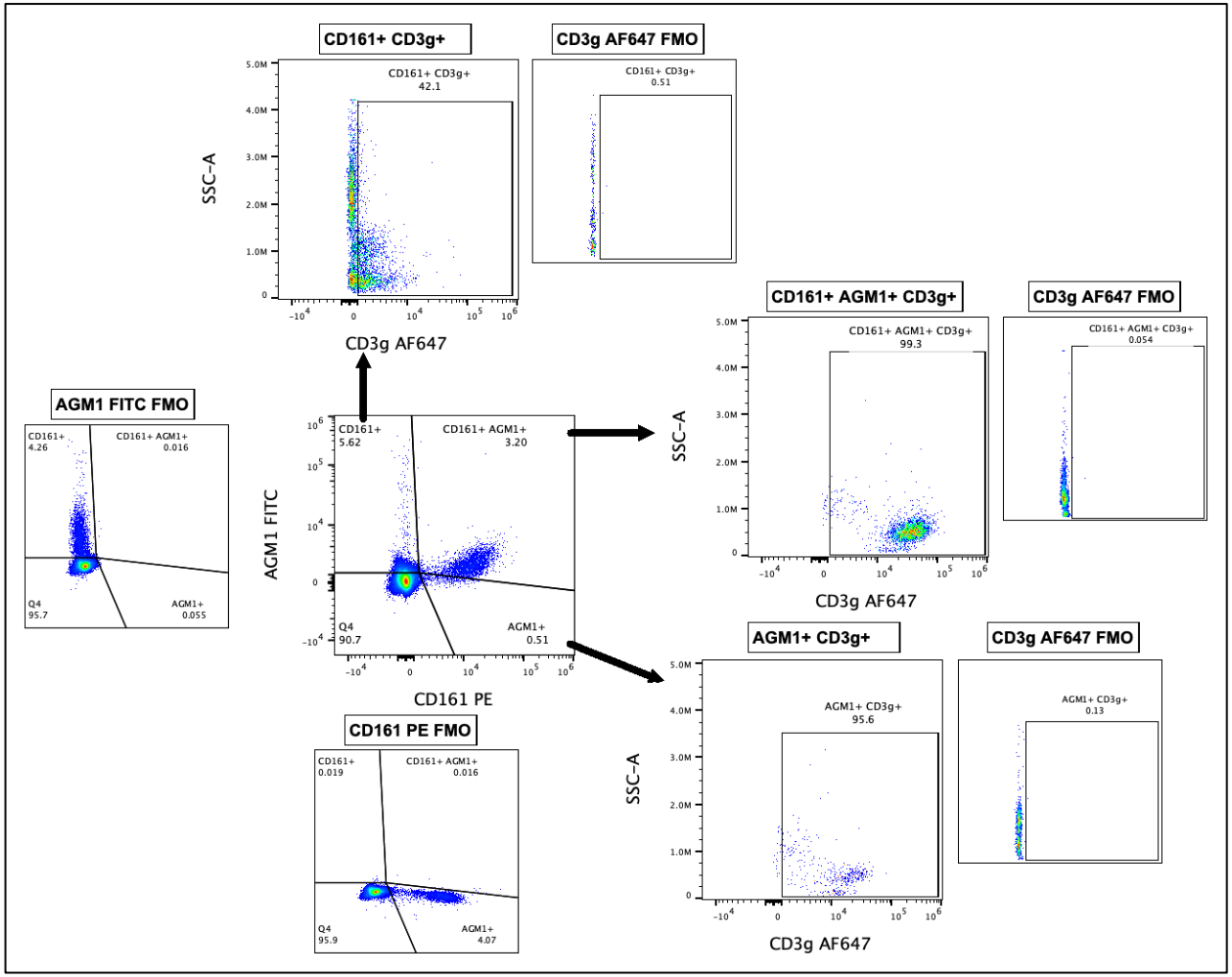

Figure I.42) Panel of anti-CD161 (PK136, PE), anti-AGM1 (polyclonal, FITC), and CD3γ (X-E2, AF647) stained splenocytes analyzed on a Cytek Aurora 4L 16V-14B-10YG-8R on one bat (the same sample analyzed by the FACSAria-III). 7.34% of splenocytes were $CD161^{+}$, 41.3% of those were also $CD3\gamma^{+}$. 3.20% of splenocytes were $CD161^{+}AGM1^{+}$, 99.3% of those cells were also $CD3\gamma^{+}$. 0.51% of splenocytes were $AGM1^{+}$, 95.7% of those were also $CD3\gamma^{+}$. Gates were drawn using FMOs. FCS files were analyzed in FlowJo V 10.8.1 Mac OS X.

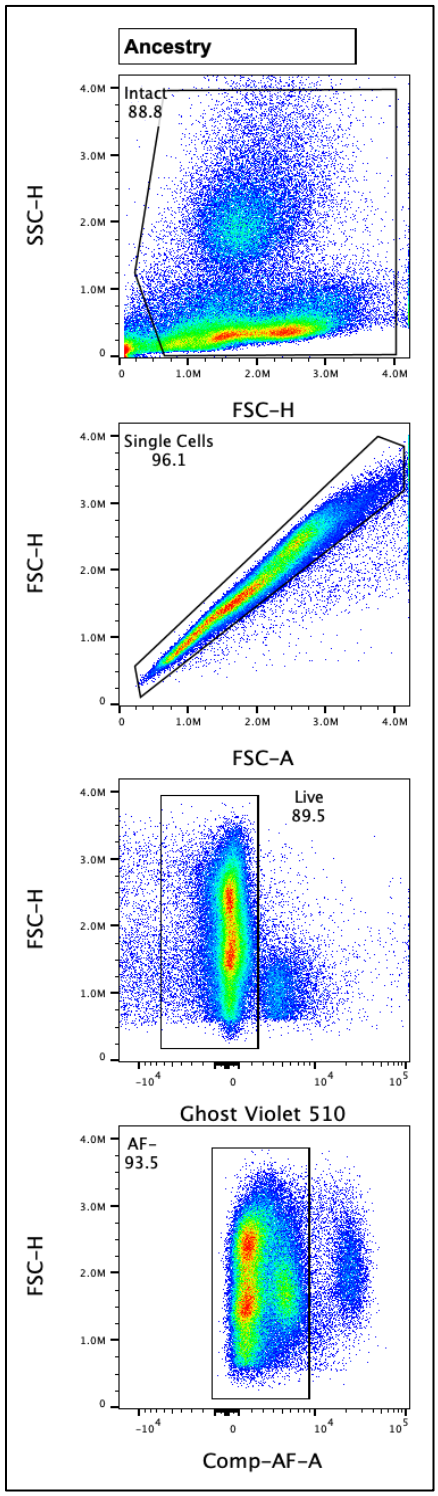

Figure I.43) Ancestry gating of **figure I.42**. Gating Strategy: Intact > Single Cells > Live > Autofluorescence negative. FCS files were analyzed in FlowJo V 10.8.1 Mac OS X. Gates were drawn based on FMOs.

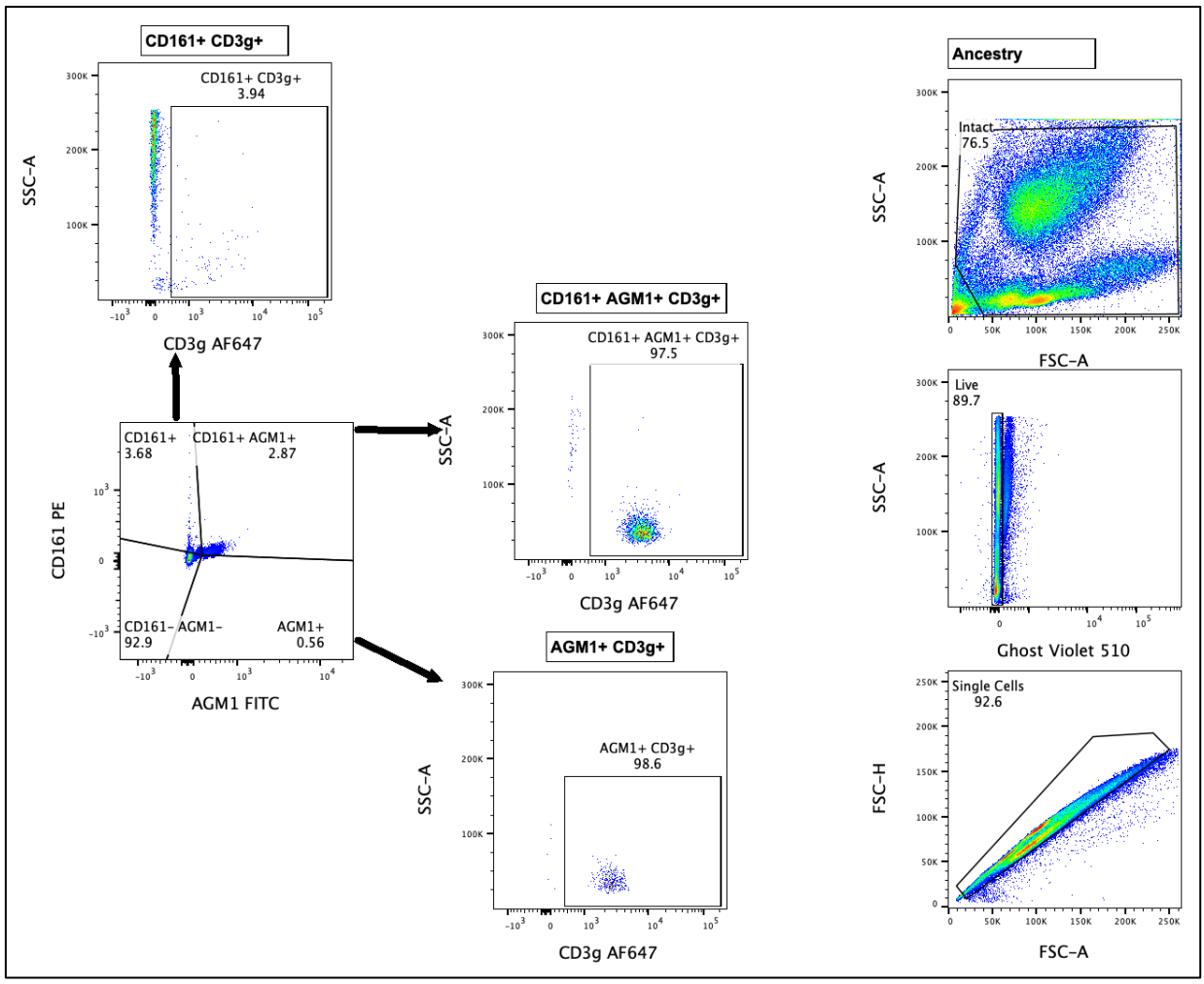

Figure I.44) PBMC panel of anti-CD161 (PK136, PE), anti-AGM1 (polyclonal, FITC), and CD3γ (X-E2, AF647) analyzed by FACSAria-III on one bat. 3.68% of splenocytes were $CD161^+$, 3.94% of those were also $CD3\gamma^+$. 2.87% of splenocytes were $CD161^+AGM1^+$, 97.5% of those cells were also $CD3\gamma^+$. 0.56% of splenocytes were $AGM1^+$, 98.6% of those were also $CD3\gamma^+$. Gates were drawn using FMOs. Ancestry gating (right): Intact > Live > Single Cells. FCS files were analyzed in FlowJo V 10.8.1 Mac OS X. Gates were drawn based on FMOs.

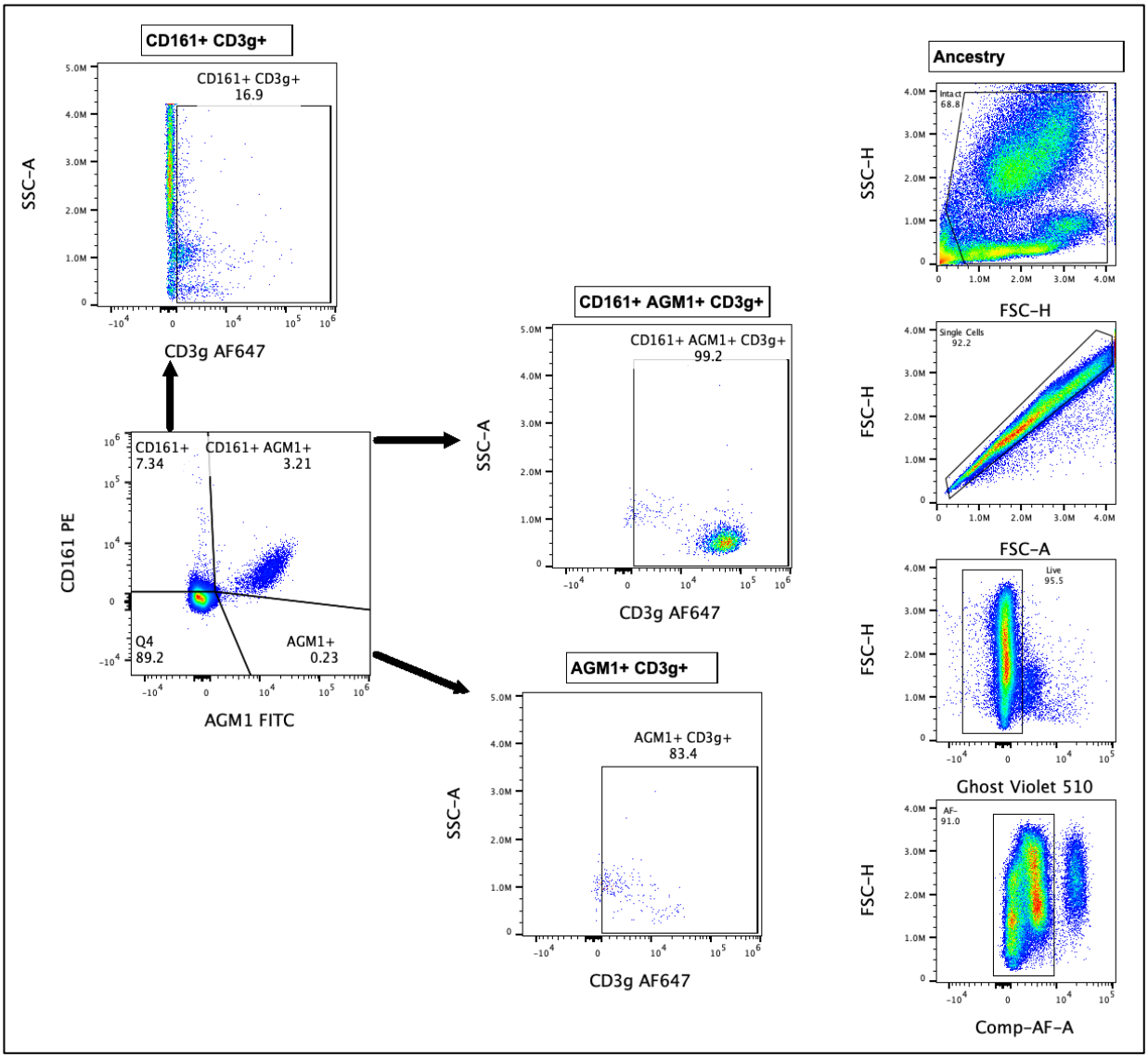

Figure I.45) PBMC panel of anti-CD161 (PK136, PE), anti-AGM1 (polyclonal, FITC), and CD3γ (X-E2, AF647) analyzed by Cytek Aurora 4L 16V-14B-10YG-8R on one bat. 7.34% of splenocytes were $CD161^{+}$, 16.9% of those were also $CD3\gamma^{+}$. 3.21% of splenocytes were $CD161^{+}AGM1^{+}$, 99.2% of those cells were also $CD3\gamma^{+}$. 0.23% of splenocytes were $AGM1^{+}$, 83.4% of those were also $CD3\gamma^{+}$. Gates were drawn using FMOs. Ancestry gating (right): Intact > Single Cells > Live > Autofluorescence negative. FCS files were analyzed in FlowJo V 10.8.1 Mac OS X. Gates were drawn based on FMOs.

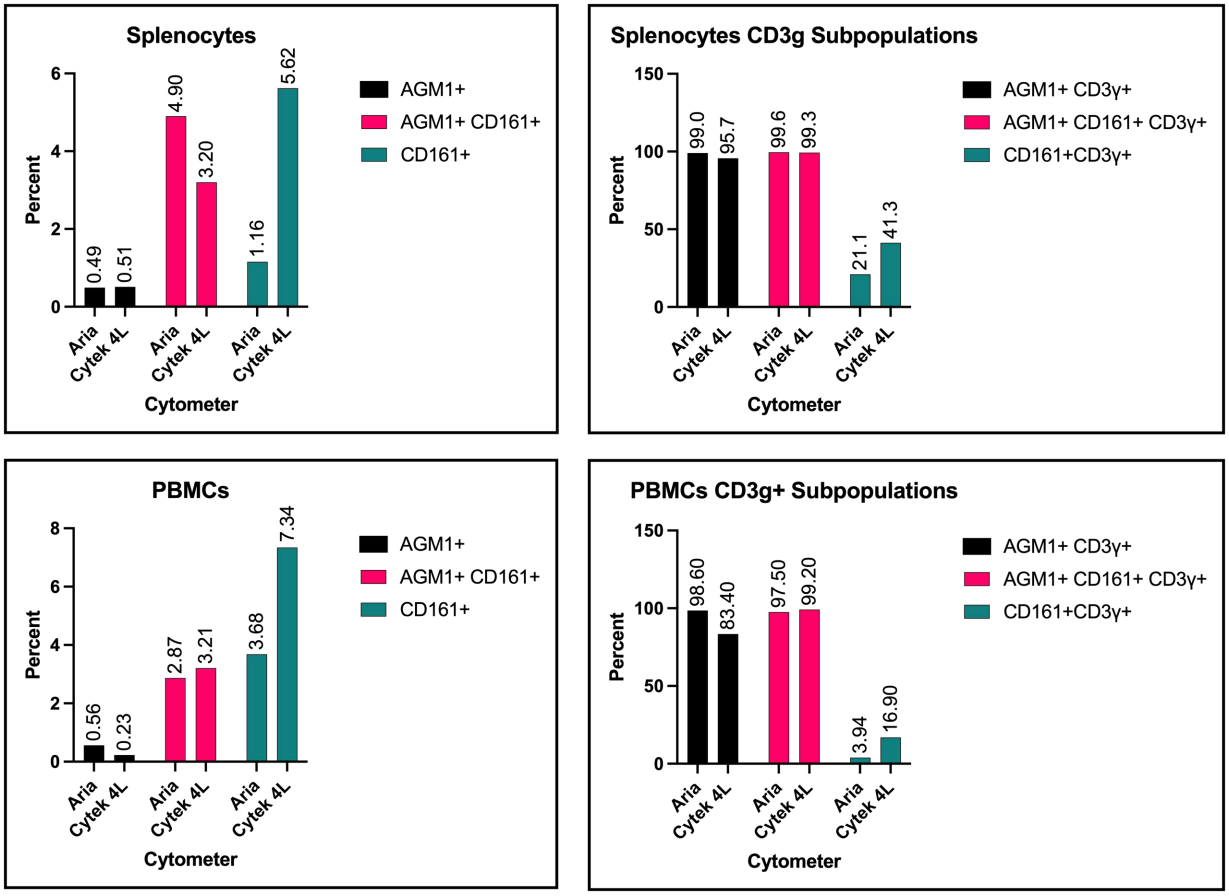

Figure I.46) Identical sample comparison of AGM1$^+$, CD161$^+$, AGM$^+$ CD161$^+$, and their CD3γ$^+$ subpopulations (percentage) on a spectral Cytek 4L cytometer with removal of highly autofluorescent populations vs. a traditional bandpass filter FACSAria-III cell sorter.

Cross-Reactive Clone	PK136 (Extracellular)		
Domain	Extracellular (Red)	Cytoplasmic (Cyan)	Combined
Identical Sites	58 (32.2%)	4 (10.5%)	62 (28.4%)
BLOSUM62	61.9%	35.1%	56.9%

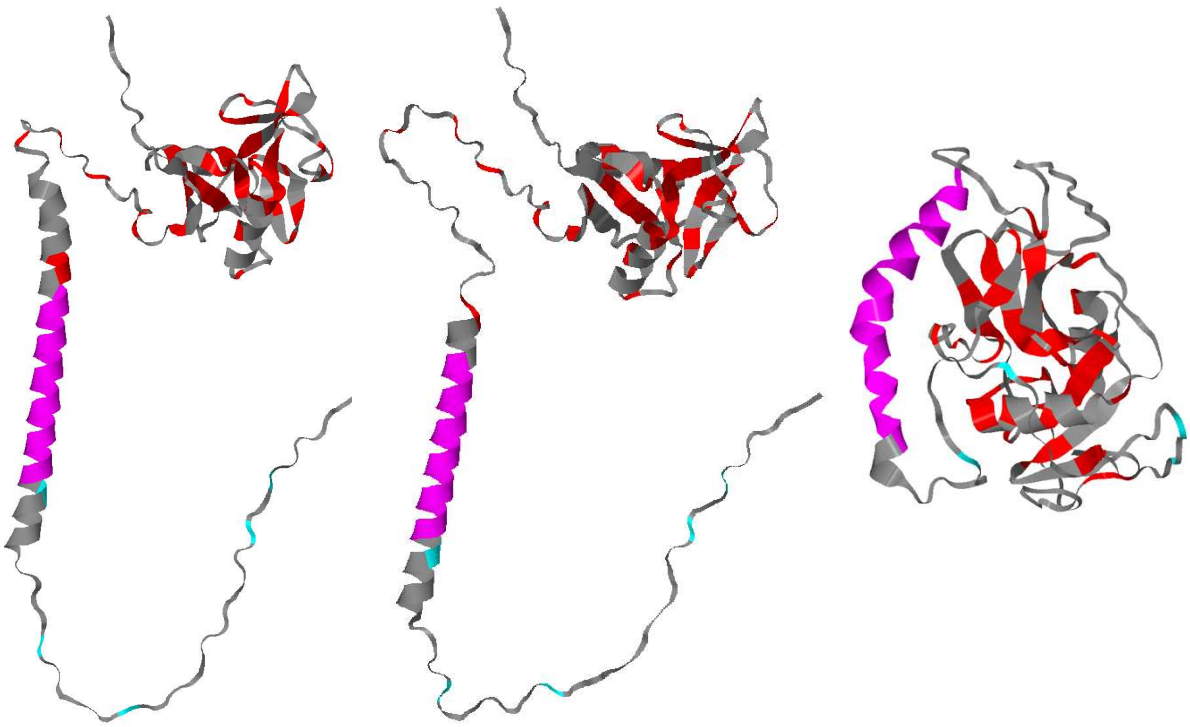

Figure I.46) Mouse CD161(KLRB1B right and KLRB1C center) and Jamaican fruit bat KLRF1 (left) three-dimensional models and protein homology. Mouse CD161 three-dimensional models were pulled from UniProt (KLRB1B UniProt P27812, KLRB1C UniProt P27814). Jamaican fruit bat KLRF1 three-dimensional model was generated using PHYR[2] (NCBI accession XP_037023746). Three-dimensional models represent proteins with signal peptides removed and transmembrane domains (magenta). Mouse CD161(KLRB1B and KLRB1C) and Jamaican fruit bat KLRF1 had 58 identical extracellular sites (red) or 32.2% of the extracellular domain, there are 4 identical cytoplasmic sites (cyan) or 35.1%. Accounting for peptides that are not identical but had similar properties and identical sites the extracellular domain has a BLOSUM62 value of 61.9% homology, the cytoplasmic domain has a BLOSUM62 value of 35.1% homology. The combined extracellular and cytoplasmic domains had 62 identical sites or 56.9%, and a BLOSUM62 value of 56.9% homology.

MHC-II

MHC-II or major histocompatibility class II is a polymorphic protein that binds to the T cell receptor for antigen presentation and is expressed on antigen presenting cells such as dendritic cells, macrophages, and B cells [21,163]. The CD4 co-receptor recognizes MHC-II and CD8 co-receptor recognizes MHC-I or major histocompatibility class I [21,163,204]. MHC-I and MHC-II both have regions known as peptide binding clefts where peptides are bound and presented to T cells (**Figure I.47**)[21]. Therefore, CD4 and CD8 work in conjunction with MHC-I and MHC-II to define the functionality of T helper or cytotoxic T cells in antigen recognition [21,163,204]. In humans, major

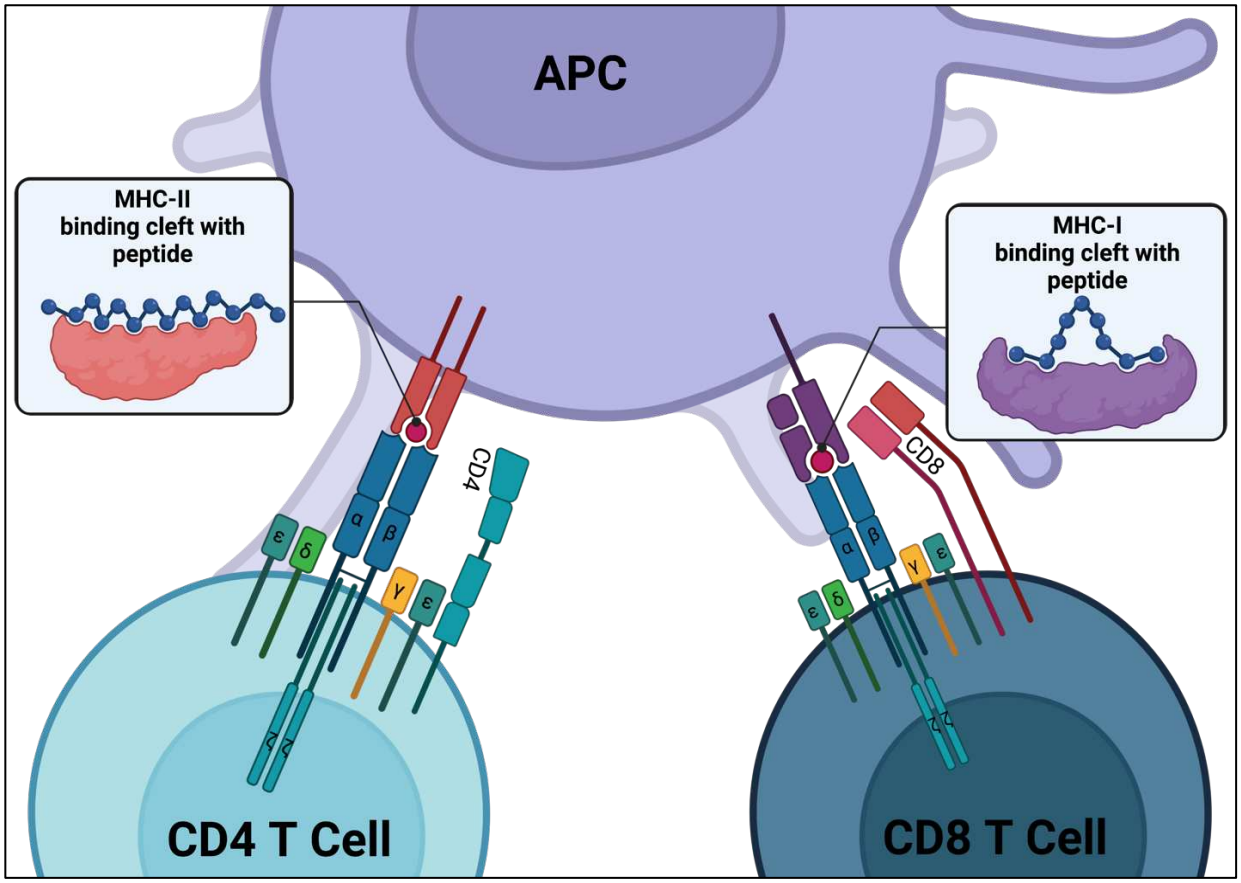

Figure I.47) Antigen presentation by MHC-II to CD4 T helper and MHC-I to CD8 T cell. Zoom magnification shows MHC binding clefts with bound peptide. Created with BioRender.com.

histocompatibility genes are called human leukocyte antigen or HLA genes and are located on chromosome 6. There are three pairs of MHC-II genes in humans *HLA-DR*, *HLA-DP*, and *HLA-DQ* [21]. In mice major histocompatibility genes are called H-2 genes and are located on chromosome 17. There are two pairs of MHC-II genes in mice *H2-A* (*I-A*) and *H2-E* (*I-E*) [21].

Mouse and Jamaican Fruit Bat MHC-II Protein Homology

One mouse reactive anti-MHC-II antibody clone (M5/114.15.2) cross reacted with Jamaican fruit bat splenocytes (**Figure I.48**) and disassociated laminal propria of the gastrointestinal tract (**Figure I.49**). This antibody reacts with I-A and I-E sub-regions of mouse MHC-II. Initial assessment of protein homology was carried out using NCBI protein blast by aligning mouse MHC-II (I-A UniProt P18468 and I-E UniProt P18469) to Jamaican fruit bat. NCBI protein alignment identified high homology with three Jamaican fruit bat sequences (NCBI accessions XP_037000184, XP_037009866, and XP_037018817) (**Figure I.50**). To further assess the protein homology, peptide sequences were downloaded into Geneious Prime (Mouse I-A UniProt P18468, mouse I-E UniProt P18469, Jamaican fruit bat NCBI accessions XP_037000184, XP_037009866, and XP_037018817). Alignment of mouse and Jamaican fruit bat MHC-II peptide sequences demonstrated that the mouse I-A and I-E subregions had 62 identical sites or 66.7% of the I-A and I-E regions. BLOSUM62 homology of the I-A and I-E sub-regions was 89.1% homologous. While this antibody does cross-react with Jamaican fruit bat MHC-II, further

investigation is required to identify what polymorphic variations of Jamaican fruit bat MHC-II clone M5/114.15.2 can bind.

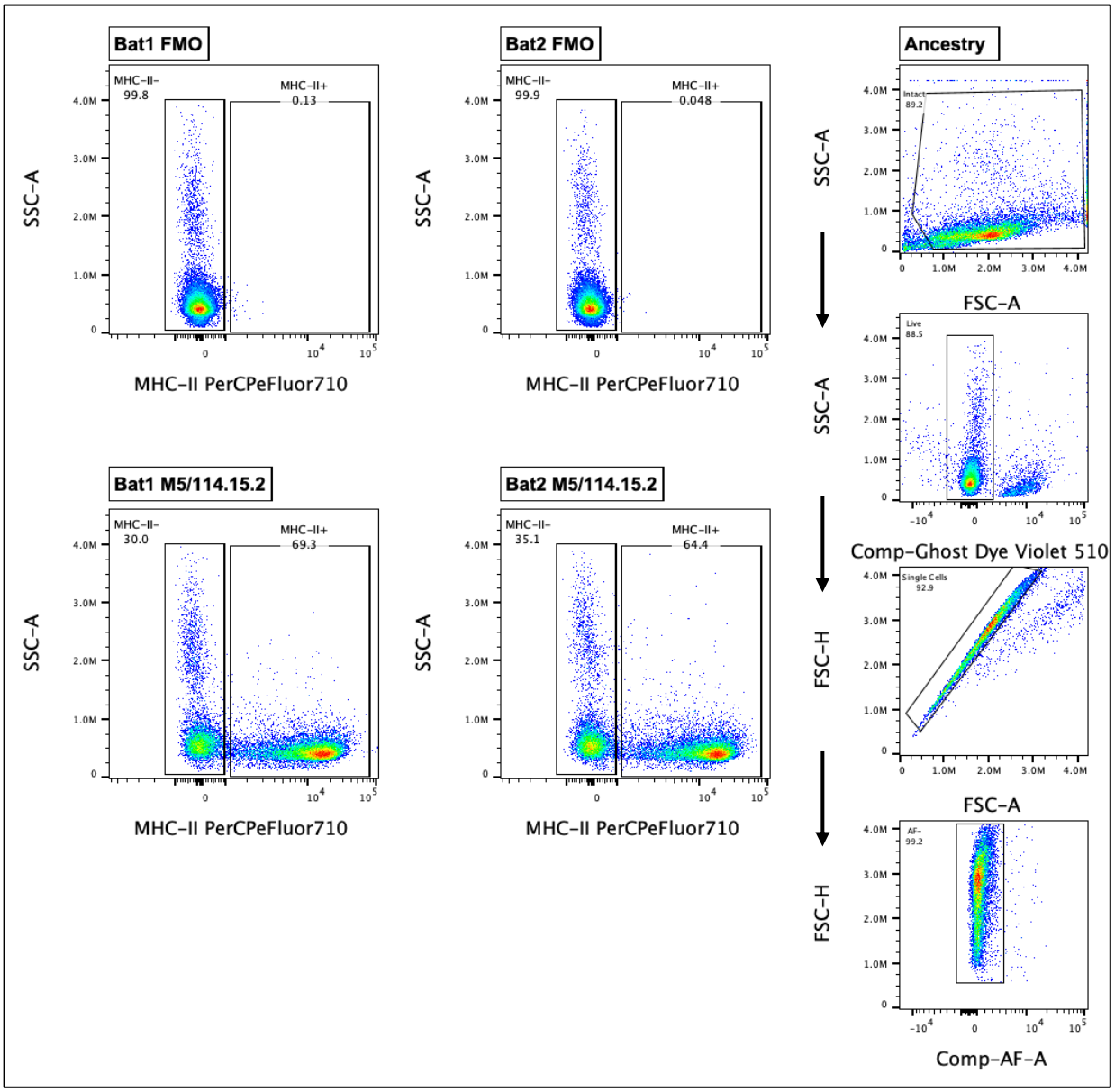

Figure I.48) Anti-MHC-II antibody clone (M5/114.15.2) cross-reacted with Jamaican fruit bat splenocyte single cell suspension from two bats. Gating strategy: ancestry gates (right) Intact > Live > Single Cells > Autoflorescence (AF)$^{-}$. MHC-II $^{+}$ gate determined by FMO control (top). MHC-II^{+} splenocytes averaged 66.85 %. Panel: MHC-II (PerCPeFluor710), primary amine viability (Ghost Violet 510). Analyzed in FlowJo V 10.8.1 Mac OS X. Gates were drawn based on FMOs.

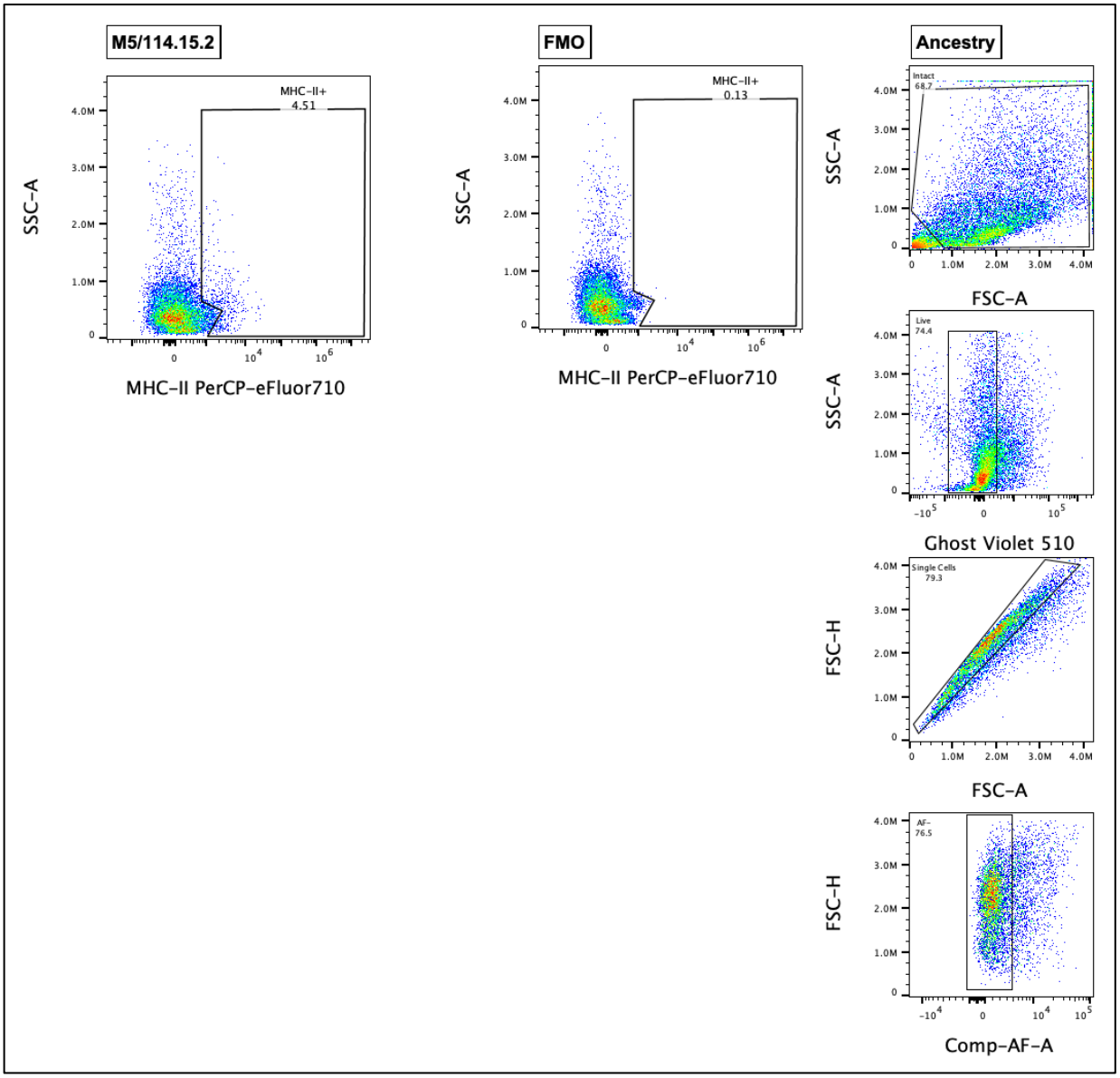

Figure I.49) Anti-MHC-II antibody clone (M5/114.15.2) cross-reacted with Jamaican fruit bat single cell suspension of disassociated lamina propria of the gastrointestinal tract from two bats. Gating strategy: ancestry gates (right) Intact > Live > Single Cells > Autoflorescence $(AF)^{-}$. MHC-II $^{+}$ gate determined by FMO control (top). MHC-II^{+} splenocytes averaged 4.51 %. Panel: MHC-II (PerCPeFluor710), primary amine viability (Ghost Violet 510). Analyzed in FlowJo V 10.8.1 Mac OS X.

Cross-Reactive Clone	**M5/114.15.2** (Extracellular)
Domain	I-A and I-E (Red)
Identical Sites	62 (66.7%)
BLOSUM62	89.1%

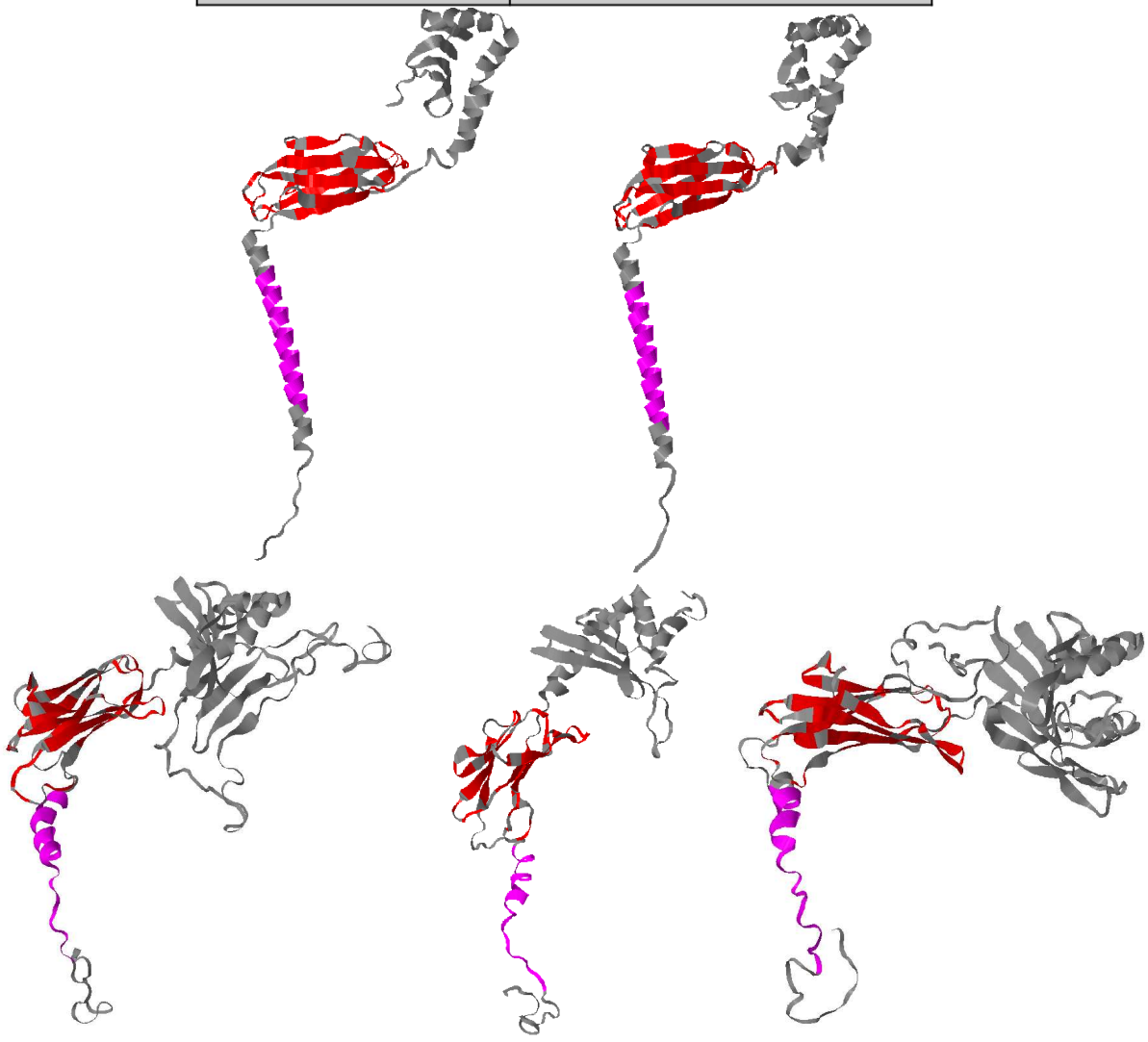

Figure I.50) Mouse MHC-II (I-A top right and I-E top left) and Jamaican fruit bat MHC-II three-dimensional models and protein homology (bottom). Mouse MHC-II three-dimensional models were pulled from UniProt (I-A UniProt P18468, I-E UniProt P18469). Jamaican fruit bat MHC-II three-dimensional models were generated using PHYR^2 (NCBI accessions XP_037000184 bottom left, XP_037009866 bottom center, and XP_037018817 bottom right). Transmembrane domains (magenta) and signal peptides (removed) were not included in the BLOSUM62 analysis. Mouse MHC-II (I-A and I-E) and Jamaican fruit bat MHC-II had 62 identical sites (red) or 66.7% of the I-A and I-E regions. Accounting for peptides that are not identical but had similar properties and identical sites the I-A and I-E regions had a BLOSUM62 value of 89.1% homology.

Appendix II

PRODUCTION OF HYBRIDOMAS TARGETING JAMACIAN FRUIT BAT LEUKOCYTE ANTIGENS CD4 AND CD8α

Purpose

Another method to overcome the limitation of bat specific reagents is to produce the reagents in-house. Production of hybridomas consume time but once the hybridomas are produced, cell culturing, collection of supernatants, and chromatography are the only techniques needed to produce antibodies. Production of hybridomas requires the design of a vaccine. Low molecular weight peptides ranging from 15 to 25 peptides perform like haptens resulting in poor to moderate antibody titers, as such low molecular weight peptides need to be conjugated to a carrier protein [229].

Methods

Jamaican fruit bat CD4 and CD8α protein sequences were submitted to the Phyre2 server to generate predicted 3D models of each protein. PDB files were imported into Geneious Prime, and the solvent-accessible peptide sequence were assessed. Peptide sequences chosen for CD4 (ENRKVSVVKTRQDRR) and CD8a (PVFLMYIGTRTKIAEGLESQISGQKFQNDG) were selected for antigen preparation (**Figure II.1**). Peptides had a cystine added at the C terminal ends for cysteine conjugation to keyhole limpet hemocyanin (KLH) carrier protein (**Figure II.2**).

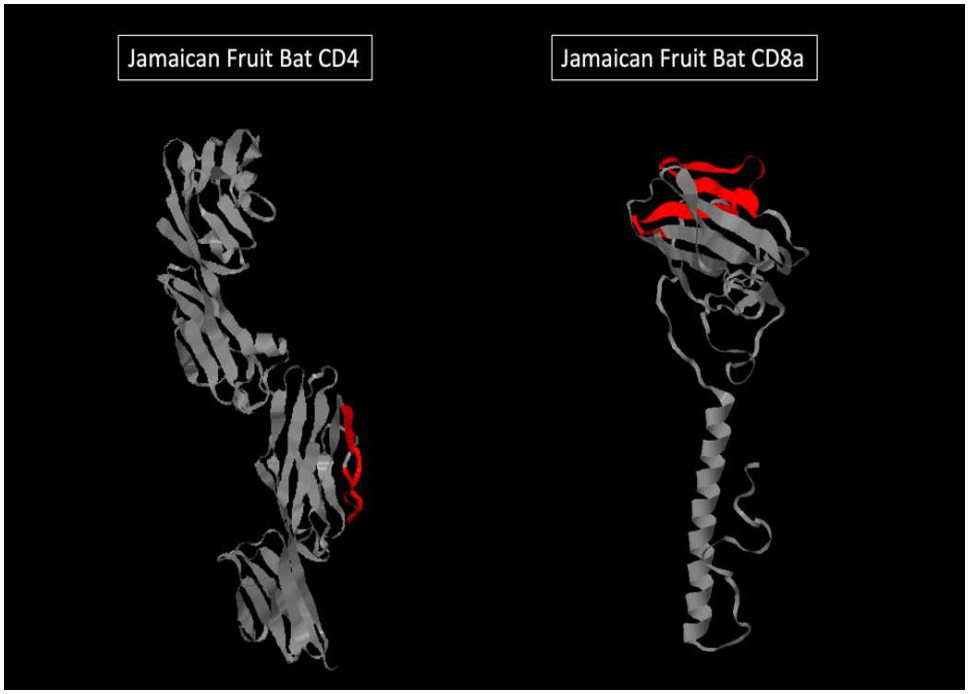

Figure II.1) Jamaican fruit bat three-dimensional models of CD4 and CD8α highlighting soluble-accessible antigenic peptides used for BALB/c mouse immunization. Three-dimensional models were generated with PHYR[2] using Jamaican fruit bat polypeptide sequences CD4 (NCBI accession XP_037016441) and CD8α (NCBI accession XP_036981493). CD4 antigenic polypeptide sequence ENRKVSVVKTRQDRR (red). CD8α antigenic polypeptide sequence PVFLMYIGTRTKIAEGLESQISGQKFQNDG (red).

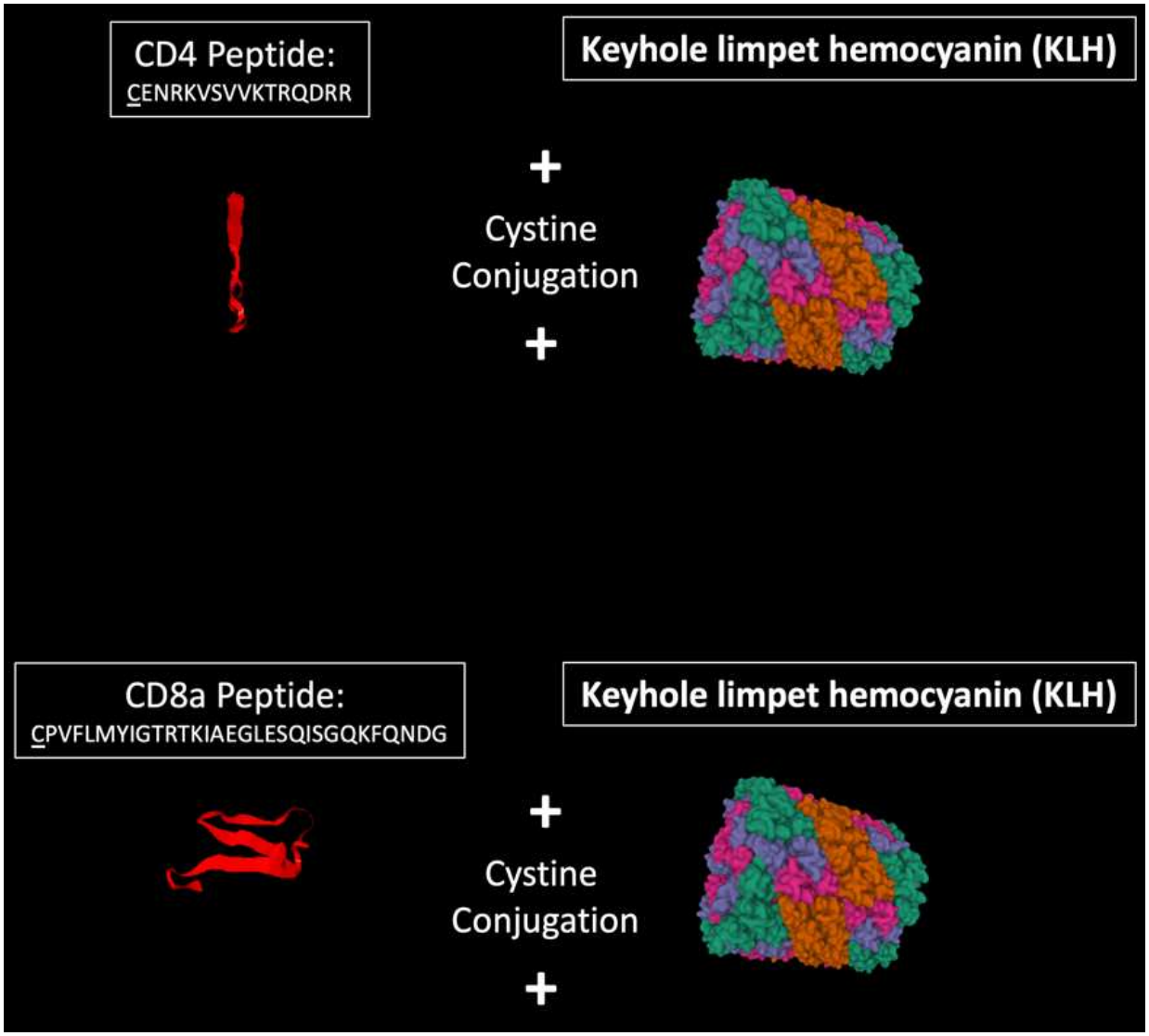

Figure II.2) Construction of vaccine immunogens for BALB/c mouse immunizations for hybridoma production. Three-dimensional models were generated with PHYR[2] using Jamaican fruit bat polypeptide sequences CD4 (NCBI accession XP_037016441) and CD8α (NCBI accession XP_036981493). Transmembrane domains (magenta) and signal peptides (removed) were not included in the BLOSUM62 analysis. Keyhole limpet hemocyanin PBD file was downloaded from RCSB protein data bank [2]. CD4 antigenic polypeptide sequence CENRKVSVVKTRQDRR (red). CD8α antigenic polypeptide sequence CPVFLMYIGTRTKIAEGLESQISGQKFQNDG (red). Underlined C's denote cystines that were added to polypeptide sequences for cystine conjugation to key hole limpet hemocyanin.

Anti-Jamaican fruit bat CD4 and CD8α hybridomas were produced by immunizing BALB/c mice intraperitoneally with 25 μg of the CD4 or CD8α peptides conjugated to KLH emulsified in incomplete Freund's adjuvant (IFA) (**Figure II.3**). Two BALB/c mice were boosted 4 weeks and 8 weeks after initial immunization with peptide-KLH in IFA. Screening of polyclonal serum was

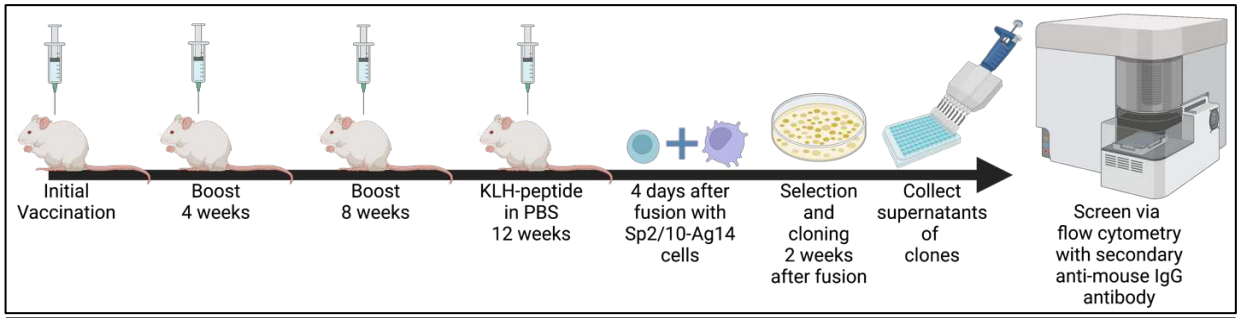

Figure II.3) Vaccination strategy of BALB/c mice for CD4cKLH and CD8αcKLH immunizations. Initial vaccination, 4-week boost, and 8-week boosts were administered in incomplete Freund's adjuvant. At week 12 final boost was administered in PBS. 4 days after final boost, spleens were harvested from BALB/c mice and fused with Sp2/10-Ag14 cells and were plated in semi-solid HAT selection media and cultured for 2 weeks. At 2 weeks clones were transferred to 96 well plates and were cultured for 2 days. Supernatants were then collected for reactivity screening via flow cytometry. Created with BioRender.com.

performed after the 4 weeks boost to assess reactivity with Jamaican fruit bat splenocytes (**Figures II.4 and II.5**) (CD4 data not shown). Twelve weeks post-initial immunization, mice were boosted with peptide-KLH in PBS and euthanized 4 days later. Spleens were harvested and processed into a single cell suspension and fused with Sp2/10-Ag14 cells. Fused cells were then cultured overnight for recovery, then plated on 100 mm Petri dishes with methylcellulose containing HAT medium for concurrent cloning and selection. Two weeks after fusion, 192 clones were transferred into two 96 well plates and cultured to expand clones (**Figure II.3**). To screen CD4 hybridomas Jamaican fruit bat splenocytes were incubated with hybridoma clone supernatants. Splenocytes were subsequently washed and then stained with a secondary anti-mouse IgG (FITC) antibody and analyzed on a 4 Laser Cytek Aurora flow cytometer (CD8α data not shown).

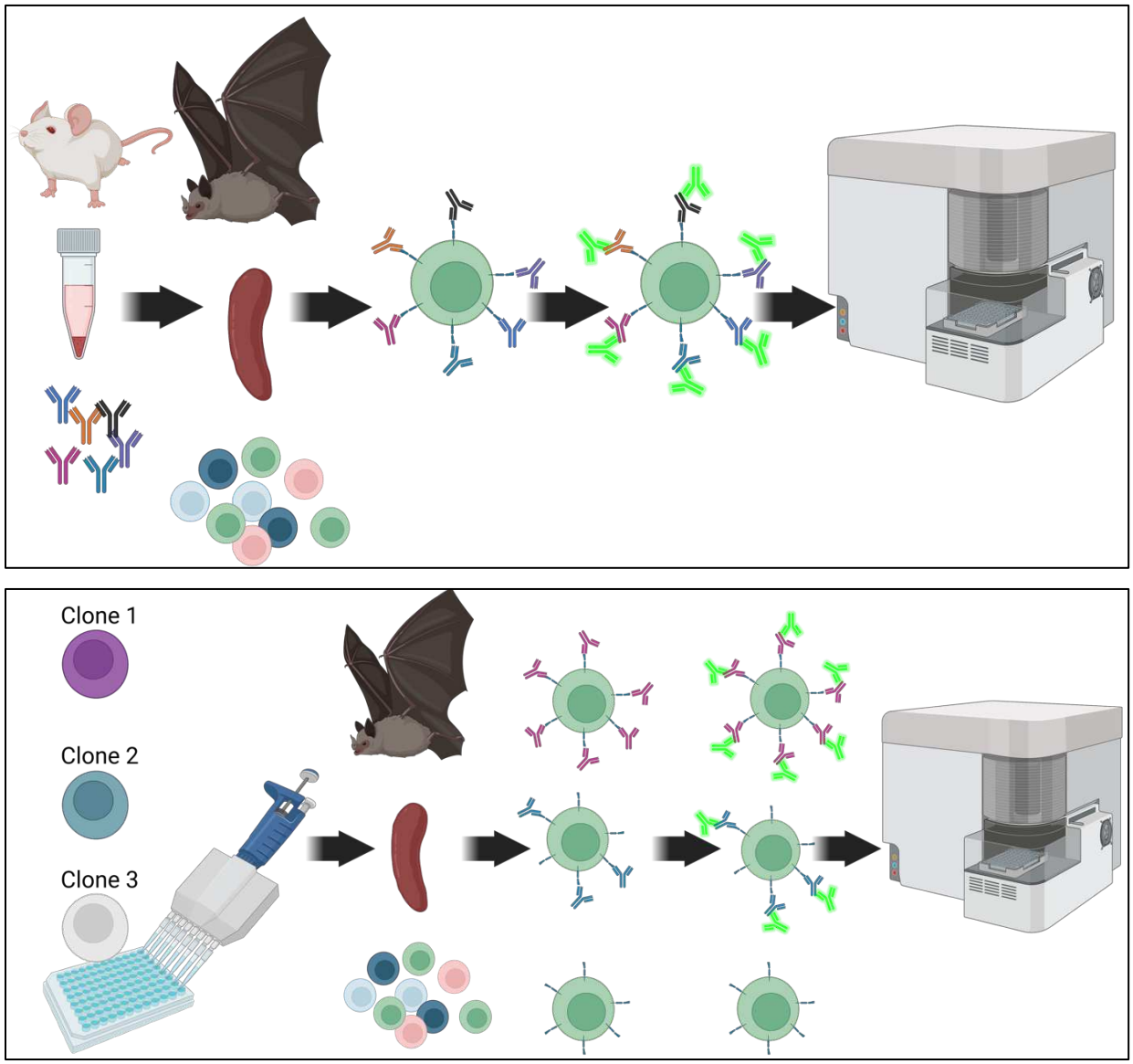

Figure II.4) Staining strategy for screening of polyclonal mouse serum for anti-CD8α reactivity (top) and staining strategy of monoclonal antibody supernatants for anti-CD4 reactivity (bottom). Serum was first collected from immunized mice (top) or collection of supernatants (bottom). Splenocytes were harvested from a Jamaican fruit bat and processed into a single cell suspension. Splenocytes were then incubated with mouse serum (top) or monoclonal supernatant (bottom), followed by an incubation with anti-mouse IgG FITC conjugated antibody. Splenocytes were than analyzed on a Cytek Aurora 4L 16V-14B-10YG-8R.

Results

Anti-CD4 Hybridoma Clones

Of the 192 screened hybridoma clones 23 clones were reactive with Jamaican fruit bat splenocytes. Interestingly, there was a range of reactivity with Jamaican fruit bat lymphocytes and monocytes (**Figure II.5**). Clone 1 demonstrated that 15.7% of splenocytes were $CD4^+$. Of the $CD4^+$ cells 69.4% were lymphocytes and 29.1% were $CD4^+$ monocytes as indicated by forward and side scatter. Clone 2 demonstrated that 8.95% of splenocytes were $CD4^+$. Of the $CD4^+$ cells 96.5% were lymphocytes and 3.19% were monocytes as indicated by forward and side scatter.

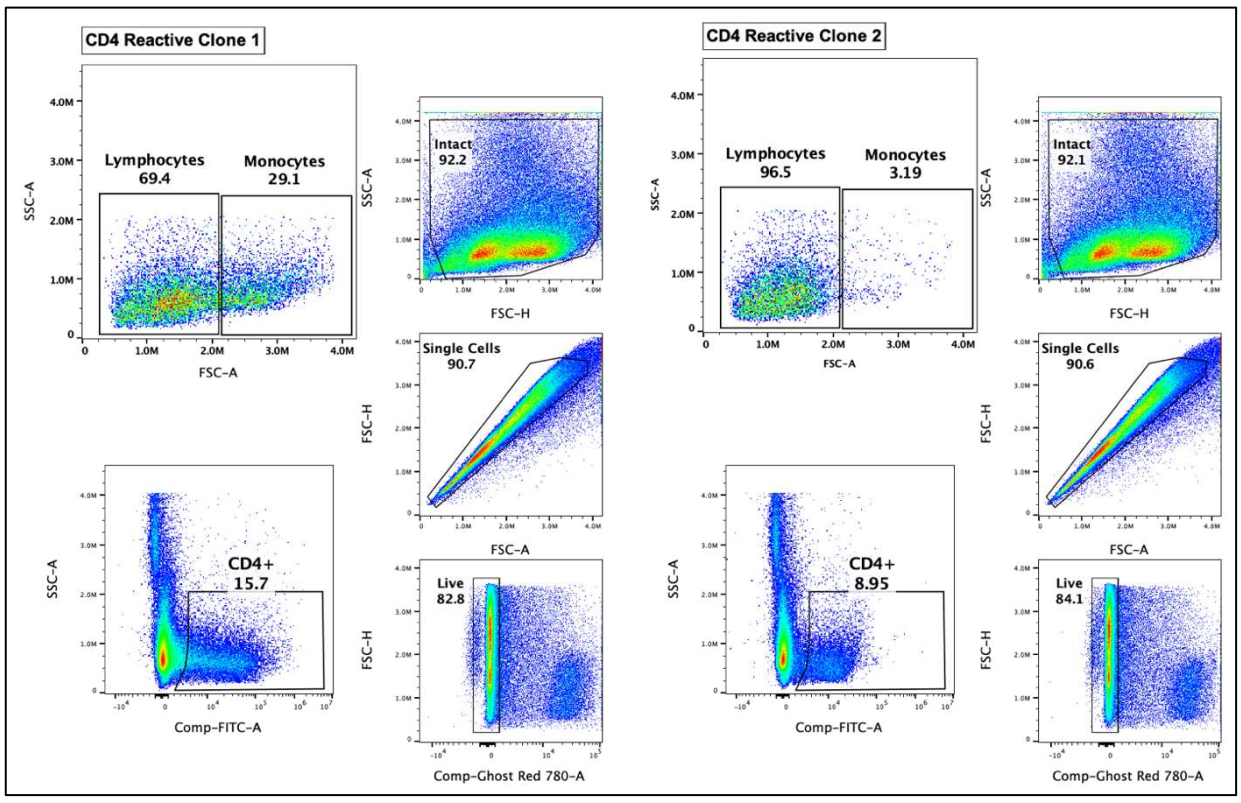

Figure II.5) Screening of hybridoma clones for anti-CD4 reactivity.

Anti-CD8α Polyclonal Serum

The polyclonal serum from the 4 week boost of the two mice reacted with Jamaican fruit splenocytes (**Figure II.6**). Serum from mouse 1 indicated 37.3% of the Jamaican fruit bat

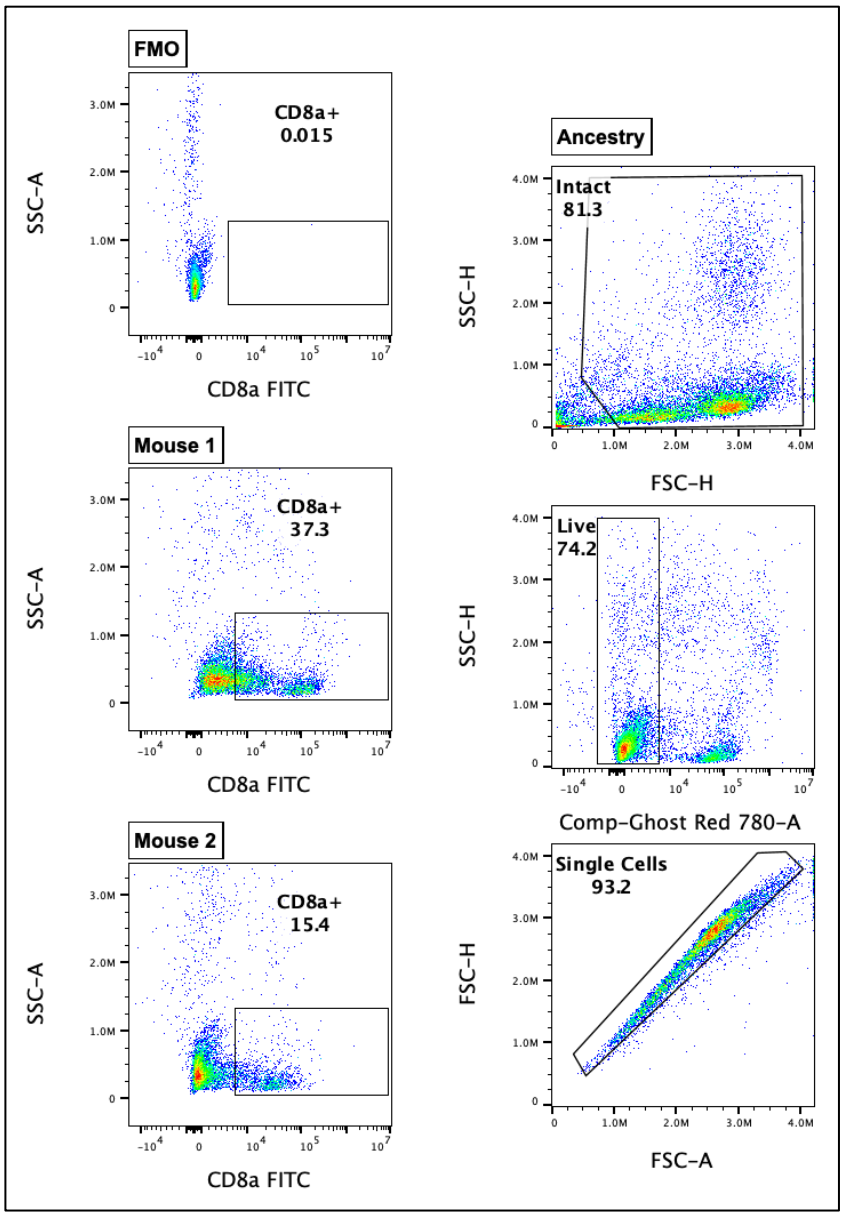

Figure II.6) Flow cytometry data demonstrating polyclonal mouse serum for reactivity with Jamaican fruit bat CD8α reactivity. Both immunized mice demonstrated reactivity with Jamaican fruit bat splenocytes. FCS files were analyzed using FlowJo V 10.8.1 Mac OS X. Gates were drawn based on FMOs.

splenocytes were CD8α$^+$. Serum from mouse 2 indicated 15.4% of the Jamaican fruit bat splenocytes were CD8a$^+$.

Discussion and Future Directions

The identification of 23 anti-CD4 hybridoma clones has provided multiple clones to further validate and characterize Jamaican fruit bat CD4$^+$ cells. More characterization is needed to identify ideal clones to be used for Jamaican fruit bat immunological assays and ensure a clone does not have off target binding. As previously stated, the variability of binding to monocytes is something that needs to be validated and investigated to properly identify if CD4$^+$ monocytes are 29.1% or closer to 3.19% of the CD4$^+$ population of splenocytes.

Currently the mice for CD8α-KLH immunization have had their second boost at 8 weeks, and the final boost, fusion, cloning and selection, and clonal screening need to be carried out. Similarly, to the anti-CD4 hybridomas, CD8α hybridomas will need to be validated and to identify if the CD8α$^+$ cells are truly CD8a$^+$.

APPENDIX III
MIFLOWCYT: THE MINIMUM INFORMATION ABOUT A FLOW CYTOMETRY EXPERIMENT COMPLIANCE APPENDIX

Overview

1. Purpose

The purpose of this study was to determine if our in-house made anti-CD3γ hybridoma (Clone X-E2, Alexa Fluor 647), and cross-reactive antibodies CD3ε (Clone Hit3a, FITC Tonbo biosciences), CD19 (Clone 1D3, PE-eFluor610, Thermo Fisher) are binding to the intended epitopes in Jamaican fruit bats *(Artibeus jamaicensis)* by cell sorting and RT-qPCR. Cell sorting was carried out on splenocytes from two male and two female naïve Jamaican fruit bats.

2. Keywords

Jamaican Fruit bat, Splenocytes, T cells, B Cells, CD3g, CD3e, CD19

3. Experimental Variables

I. Four naïve Jamaican Fruit *(Artibeus jamaicensis, Aj)* bats were used

- *Aj*1 male
- *Aj*2 male
- *Aj*3 female
- *Aj*4 female

II. Not sorted whole spleen single cell suspension RNA extraction samples

- Post-acquisition of unstained and FMO samples were pooled with each respective sample e.g., Aj1 unstained and FMOs pooled, Aj2 unstained and FMOs pooled etc. These were used as RT-qPCR controls.

III. Aj1-Aj4 sorted samples for RNA extraction

- $CD3\varepsilon^{+}$
- $CD3\gamma^{+}$

- $CD3\varepsilon^+$ $CD3\gamma^+$
- $CD19^+$

4. *Organization*

I. Name: Colorado State University, College of Veterinary Medicine

II. Address: 1350 Center Ave, Fort Collins, Co 80521

5. *Primary Contact*

I. Name: Tony Schountz

II. Email: tony.schountz@colostate.edu

6. *Dates*

I. Euthanasia and flow cytometry performed on April 11, 2022.

7. *Conclusion*

CD3γ, CD3ε, and CD19 monoclonal antibodies bind to intended epitopes, allowing for enrichment of $CD19^+$, $CD3\gamma^+$, $CD3\varepsilon^+$, and $CD3\gamma^+CD3\varepsilon^+$splenocyte populations.

8. *Quality Control Measures*

I. Whole spleen single cell suspension were used for RT-qPCR baseline controls to observe enrichment for CD3ε, CD3γ, and CD19 as described in section 3.II.

II. FMOs were used to draw sorting gates.

Flow Cytometry Specimen Details

9. Sample and Specimen Material Description

I. *Biological Sample Source Organism Description*:

- Taxonomy: Jamaican fruit bat *(Artibeus jamaicensis)*
- Colony: Colorado State University's captive breeding colony of Jamaican fruit bats
- Sex: 2 males and 2 females
    - Naïve Jamaican fruit bats were obtained directly from housed breeding colony.
- Jamaican fruit bats were anesthetized using isoflurane. Once anesthetized, cardiac puncture was performed, followed by thoracotomy. IACUC Protocol # 1034.

10. Sample Characteristics

Expected/analyzed cell types: T cells and B cells.

I. Treatment of Splenocytes

- Spleens were processed into a single cell suspension through a 70um cell strainer with 5 ml 1xPBS+ 5mM EDTA. Cells were then centrifuged (340xg for 10 minutes) and supernatant was decanted. The cell pellet was then resuspended in 10 ml ammonium chloride lysing buffer and incubated for 15 minutes on ice. Cells were then washed with 10 ml 1xPBS+ 5mM EDTA and spun at 340xg for 10 minutes and supernatant was decanted. Cells were then resuspended in 2 ml

1xPBS+ 5mM EDTA and counted using a hemocytometer and 0.4% trypan blue.

Staining of Samples

a. All fluorescence minus one (FMOs) staining was carried out in a 96 well v-bottom plate. 0.5 million splenocytes were used for each FMO control, and 1 million splenocytes were used for unstained controls.
    i. Following viability dye incubation – cells were quenched with 50ul FACS buffer (1xPBS, 5mM EDTA, 1% BSA, 0.5% sodium azide) and centrifuged (340xg for 5 minutes). Supernatant was aspirated. Cells were then washed 150ul FACS buffer, centrifuged (340xg for 5 minutes), and supernatant was aspirated.
    ii. Cells were then resuspended at 2 million cells per 100ul in Universal Fc Block (innovex Biosciences, NB309) and incubated for 30 minutes on ice.
    iii. Following incubation – Cells were quenched by bringing the volume up to 150ul with FACS buffer and centrifuged (340xg for 5 minutes). Supernatant was aspirated. Cells were then washed with 150ul FACS buffer, centrifuged (340xg for 5 minutes), and supernatant was aspirated.
    iv. Each sample was then resuspended in 100ul of respective antibody cocktail made in FACS buffer. Unstained cells were resuspended in 100ul FACS buffer. Cells were then incubated at 4°C in the dark for 30 minutes.
    v. Following incubation – Cells were quenched by bringing the volume up to 150ul with FACS buffer and centrifuged (340xg for 5 minutes).

Supernatant was aspirated. Cells were then washed with 150ul FACS buffer, centrifuged (340xg for 5 minutes), and supernatant was aspirated.

vi. Cells were transferred to 5 ml FACS tubes and resuspended in 500ul FACS buffer for flow cytometric analysis and cell sorting. Each sample was filtered through 70um mesh before being acquired on the FACS Aria III.

b. Remainder of cells were used for the full panel and stained in a 15 ml conical tube. Cells were resuspended at 2 million cells per ml in Ghost Dye Violet 450 viability dye (Tonbo bioscience, 13-0863) (1xPBS+ 5mM EDTA 1: 5,000 dilution) for 30 minutes on ice.

i. Following viability dye incubation – FACS buffer was added to bring the volume up to 15 ml and centrifuged (340xg for 10 minutes). Supernatant was decanted. Cells were then washed with 15 ml FACS buffer, centrifuged (340xg for 10 minutes), and supernatant was decanted.

ii. Cells were then resuspended at 2 million cells per 100ul in Universal Fc Block (innovex Biosciences, NB309) and incubated for 30 minutes on ice.

iii. Following incubation – FACS buffer was added to bring the volume up to 15 ml and centrifuged (340xg for 10 minutes). Supernatant was decanted. Cells were then washed with 150ul FACS buffer, centrifuged (340xg for 10 minutes), and supernatant was decanted.

iv. Each sample was then resuspended at 2 million cells per 100ul of antibody cocktail made in FACS buffer.

v. Cells were resuspended in FACS buffer at a concentration of 2 million cells/ml of FACS buffer in 5 ml FACS tubes for flow cytometric analysis and cell sorting. Each sample was filtered through 70um mesh before being acquired on the FACS Aria III.

c. Post-Sort Sample Handling.

i. The remainder of cells for unstained and FMOs for each Jamaican fruit bat were pooled together to use as the whole spleen single cell suspension for Trizol RNA extraction.

ii. The sorted samples with the whole spleen single cell suspensions were then centrifuged at 340xg for 10 minutes, and supernatant was decanted.

iii. 1 ml of trizol was added to each sample and vortexed.

iv. Samples were then incubated for 10 minutes at room temperature.

v. Samples were then placed in -20°C for storage to complete the RNA extractions the following day.

Table III.1) Table of flow cytometry reagents used for cell sorting.

Characteristic	Marker	Clone	Host	Fluorophore	Detector	Stock Concentration	Flow Dilution	Supplier	Catalog Number
T cells	CD3g	X-E2	Mouse	AlexaFluor 647	APC (660/20)	1mg/ml	1:100	Schountz Lab	N/A
T cells	CD3e	Hit3a	Mouse	FITC	FITC (530/30)	0.1mg/ml	1:20	Tonbo	50-0039
B cells	CD19	1D3	Mouse	PE-eFluor610	PE-Texas Red (616/23)	0.2mg/ml	1:800	Invitrogen	61-0193-82
Cell Viability	Primary Amines	N/A	N/A	Ghost Dye violet 450	BV421 (450/40)	N/A	1:5,000	Tonbo	13-0863
Fc Block	Fc Receptors	N/A	N/A	N/A	N/A	1X	100ul per 2 million cells	Innovex	NB309

Anti-CD3g X-E2 Antibody Production

I. X-E2 hybridomas were cultured in hybridoma culture medium (DMEM with L-glutamine 2mM), 5% FBS, 1x MEM non-essential amino acids (VWR, 11140-050), 1x penicillin/streptomycin, 21mM HEPES, 1mM sodium pyruvate, and 50ug/ml gentamicin. Incubation was carried out under 8%CO_2 atmosphere.
II. Supernatant from the hybridoma cell culture media was collected when media turned light orange.
III. Anti-CD3g X-E2 antibody was then purified using Pierce™ Protein A/G Plus UltraLink™ Resin (Themo Fisher, 53135) following manufacturer's protocol.
IV. Buffer exchange was then performed on the purified antibody using Slide-A-Lyzer™ Dialysis Cassettes, 7K MWCO, 3 mL in 1xPBS following manufacturer's protocol.
V. Antibody was then concentrated to 1mg/ml using Antibody Concentration and Clean-Up Kit (Abcam, 102778).
VI. Antibody was then conjugated with Alexa Fluor™ 647 NHS Ester kit (Thermo Fisher, A20186) following manufacturer's protocol

Single Color Controls

Single Color controls were stained using Ultra eComp, and ArcAmine beads, and were stained according to manufacturer's protocols. CD3g Alexa Fluor 647 in-house made antibody single color control was stained using Jamaican fruit bat splenocytes.

Table III.2) Compensation beads used for single color controls.

UltraComp eBeads	Invitrogen	01-2222
Arc Amine Beads	Invitrogen	A10346

Fluorescence Minus One Controls (FMOs)

FMOS were stained according to the following table:

Table III.3) FMO controls table.

	FMO Controls			
Reagent	CD3g Alexa Fluor 647	CD3e FITC	CD19 PE-eFlor610	Viability Ghost Dye violet 450
CD3g Alexa Fluor 647	–	+	+	+
CD3e FITC	+	–	+	+
CD19 PE-eFlor610	+	+	–	+
Ghost Dye Violet 450	+	+	+	–
Fc block	+	+	+	+

Instrument Details

11. Instrument Manufacturer

I. BD Biosciences

https://www.bdbiosciences.com/en-us

12. Instrument Model

I. BD FACS Aria III

https://www.bdbiosciences.com/en-us/products/instruments/flow-cytometers/research-cell-sorters/bd-facsaria-iii?utm_source=google&utm_medium=cpc&utm_content=&utm_campaign=7010L000000g23DQAQ&gclid=Cj0KCQjw1ZeUBhDyARIsAOzAqQJNiuUDYuyguZ4X4PCLmj_Mc_cJRVhoORPUpEYLPLPb2i5-K7c8EckaAjw5EALw_wcB

II. Serial Number: P64828200052

13. Instrument Configuration and Settings

I. Fluidics and Flow Cell

- The instrument has not been altered from manufacturer.

Light sources and Optics Configuration

Table III.4) FACS Aria III laser and filter configuration.

FACS Aria III Configuration

Lasers		LP	BP	
Blue 488nm	A	655	695/40	PerCP-Cy5.5
	B	502	530/30	FITC
	C	–	488/10	SSC
Red 633nm	A	735	780/60	APC-Cy7
	B	685	720/40	A700
	C	–	660/20	APC
Yellow 561nm	A	735	780/60	PE- Cy7
	B	680	710/50	PE-Cy5.5
	C	645	660/20	PE-Cy5
	D	595	616/23	PE-TxRed
	E	–	585/20	PE
Violet 405nm	A	735	780/60	BV786
	B	680	710/50	BV711
	C	650	660/20	BV650
	D	595	610/20	BV605
	E	502	525/50	BV510
	F	–	450/40	BV421

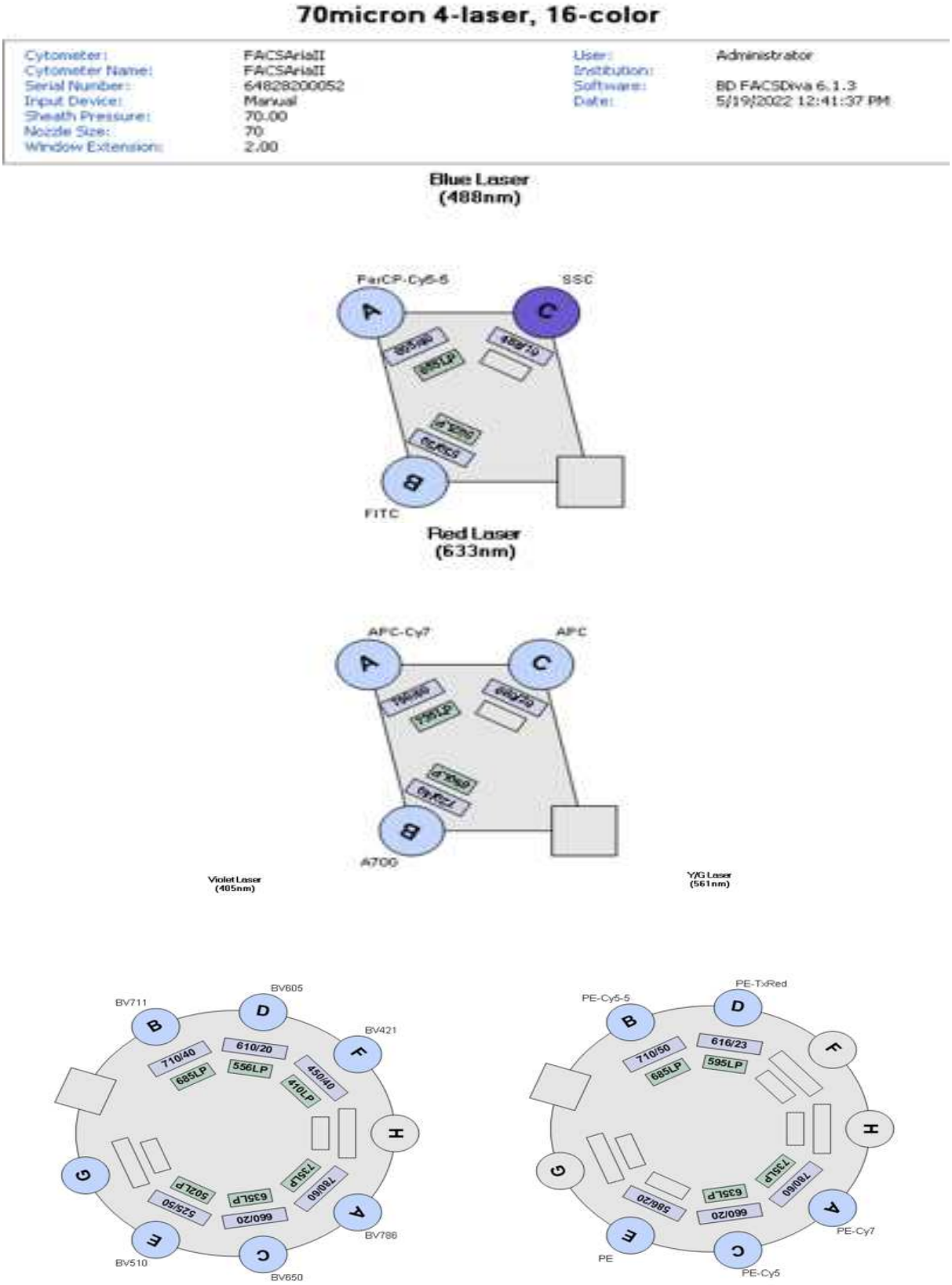

Figure III.1) Optical detectors and laser configuration.

Data Analysis Details

1. *List mode Data Files*

   I. FCS files have been uploaded to https://flowrepository.org/

   II. FCS files can also be obtained by contacting Dr. Tony Schountz.

2. *Compensation*

   I. FCS files were compensated using UltraComp eBeads (Invitrogen, 01-2222), ArC Amine beads (Life technologies, A10346) and Jamaican fruit bat splenocytes stained with anti-CD3g AF647 clone X-E2. FACSDiva's compensation matrix was used to calculate the compensation matrix.

II. Diva Compensation Matrix values in %:

Table III.5) FACS Diva compensation matrix.

	FITC-A	**PE-TxRed-A**	**BV421-A**	**APC-A**
FITC-A	100.0000	0.0014	0.5312	0.1008
PE-TxRed-A	0.0076	100.0000	0.0619	0.0458
BV421-A	0.0008	0.2095	100.0000	0.6785
APC-A	0.1102	0.3048	0.3107	100.0000

3. Data Transformation Details.

I. Purpose of Data Transformation

- Visualization and gating.

II. Data Transformation Description

- FACSDiva was used for visualization of data.

FACSDiva Version 6.1.3

- All fluorescent parameters are displayed in biexponential**.**

Gating Details

Gates were drawn using FMOs. $CD3\varepsilon^+$, $CD3\gamma^+$, $CD3\varepsilon^+$ $CD3\gamma^+$, and $CD19^+$ populations were sorted for each population until each sample ran out. Aj1 male data is used for Figures 2-7 and are representative of all samples.

Sort Reports

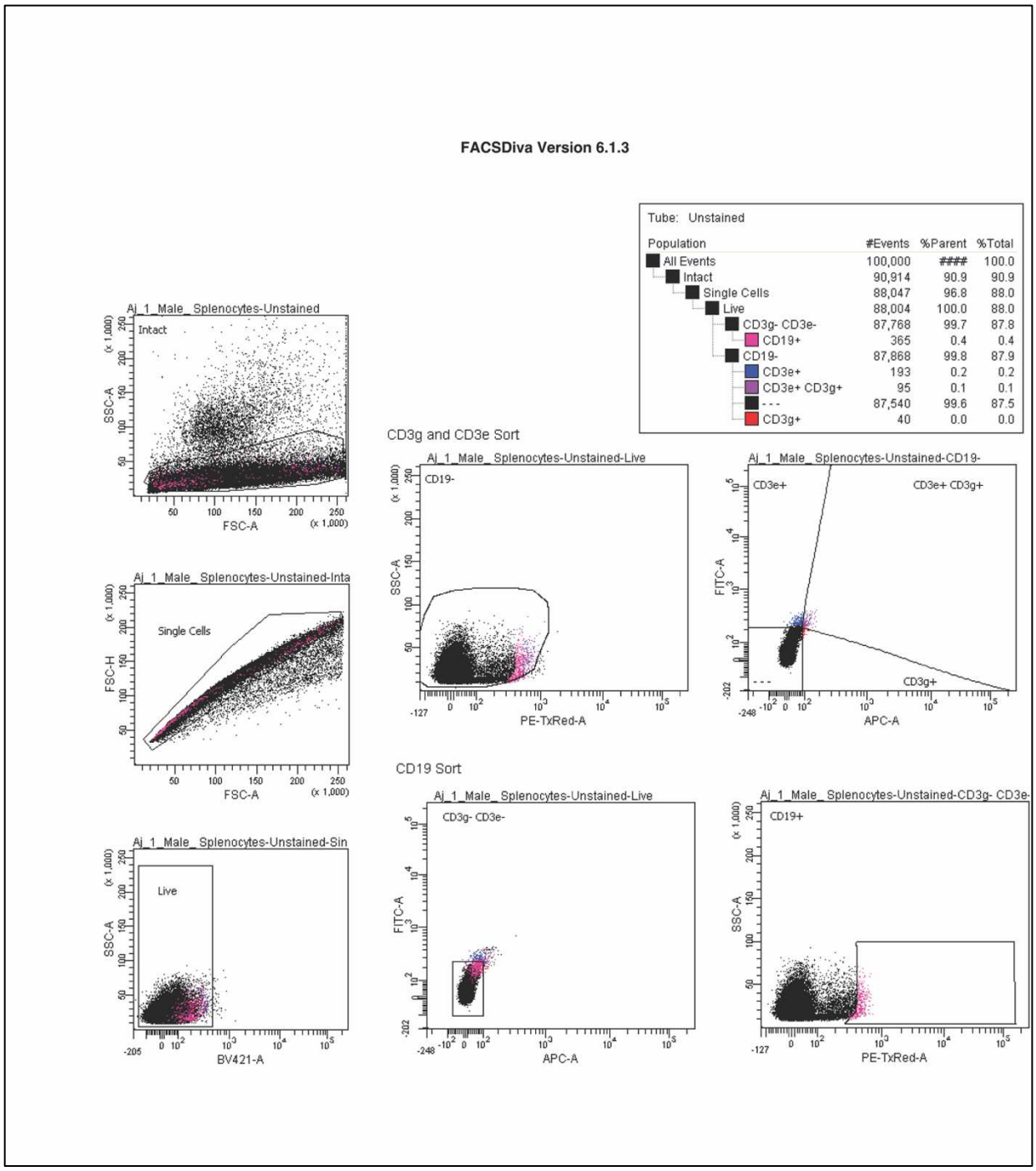

Figure III.2) Unstained *Aj*1 FACSDiva worksheet.

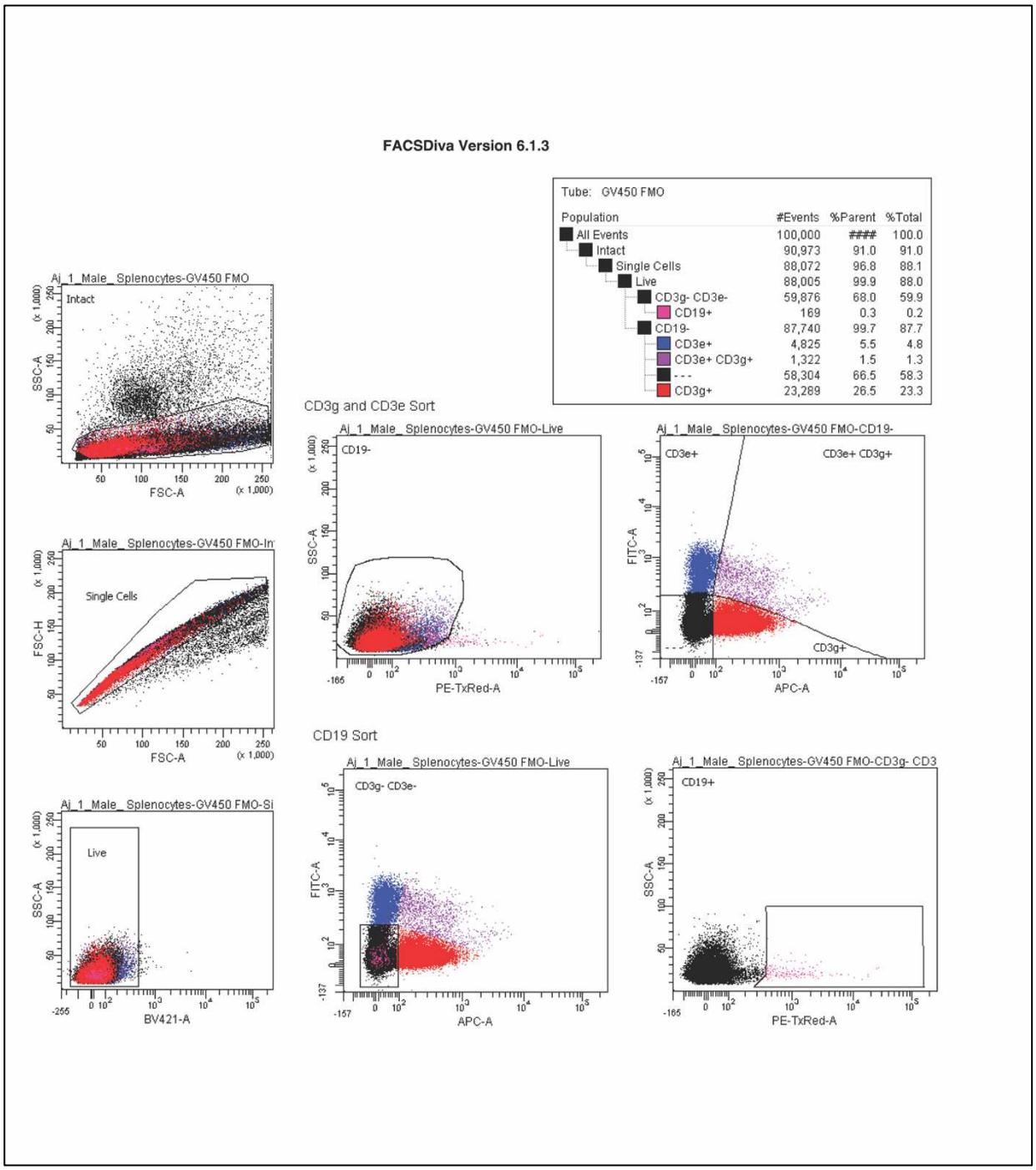

Figure III.3) GV450 *Aj*1 FACSDiva worksheet.

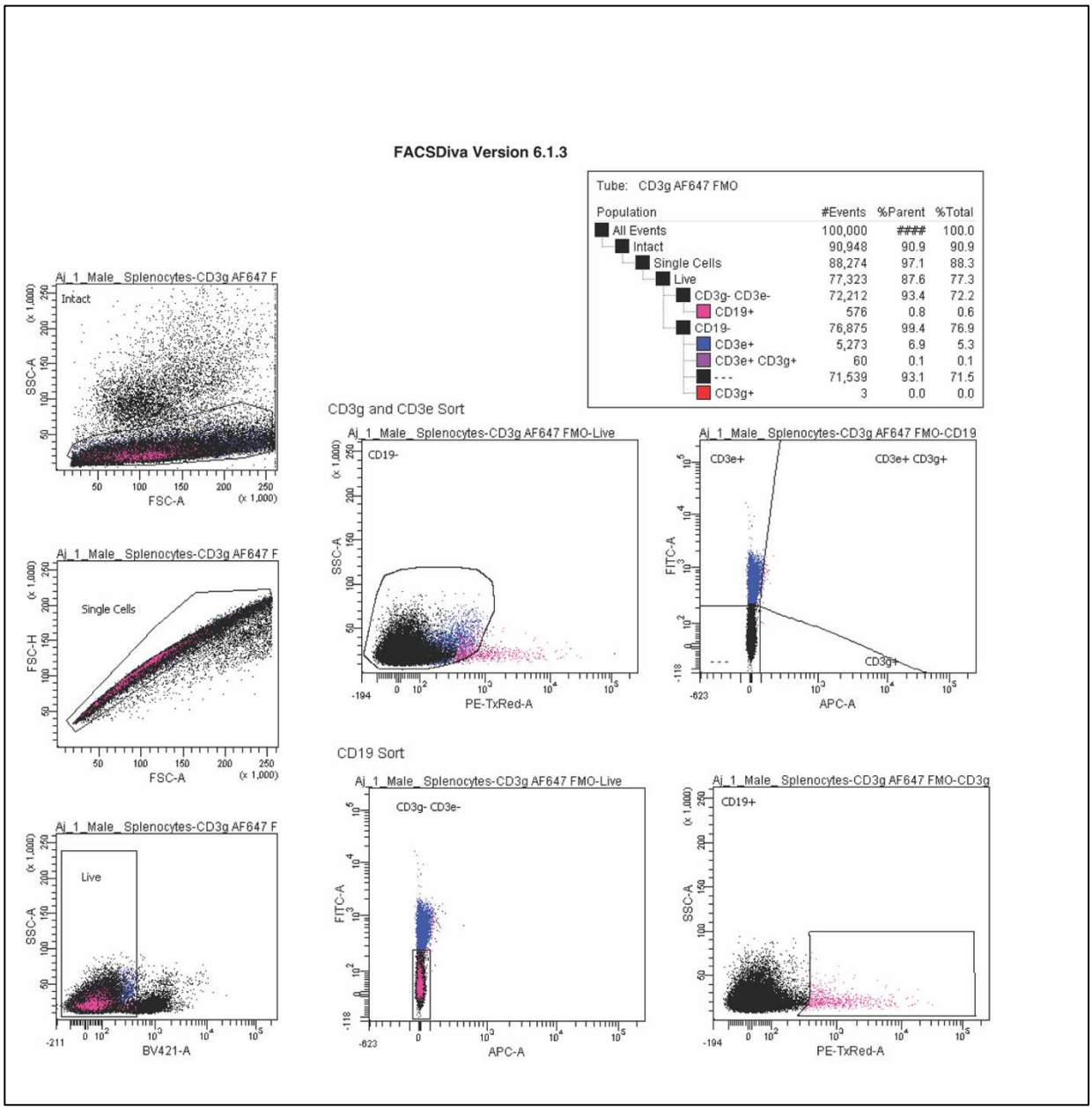

Figure III.4) CD3g AF647 FMO *Aj*1 FACSDiva worksheet.

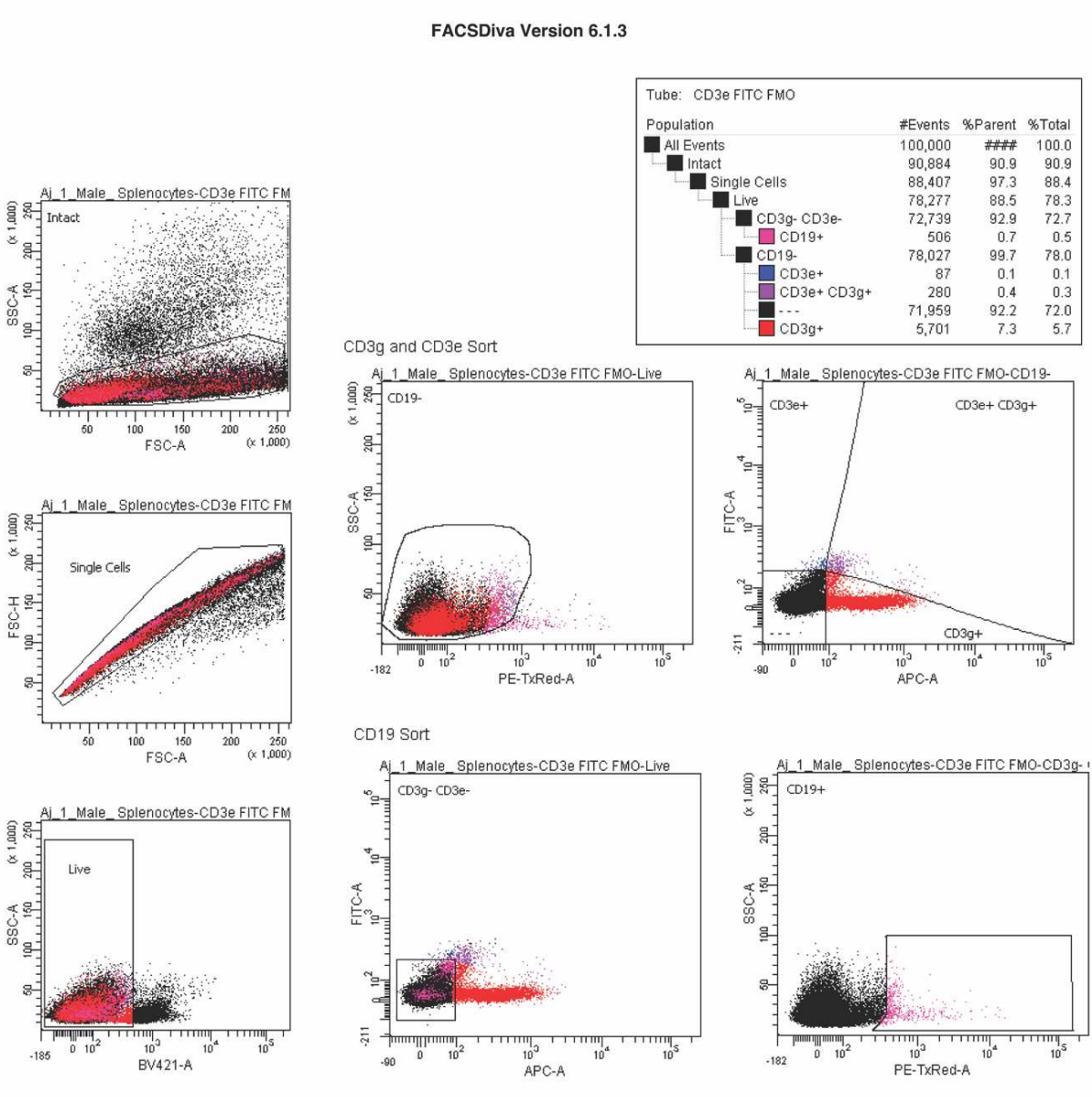

Figure III.5) CD3e FITC FMO *Aj*1 FACSDiva worksheet.

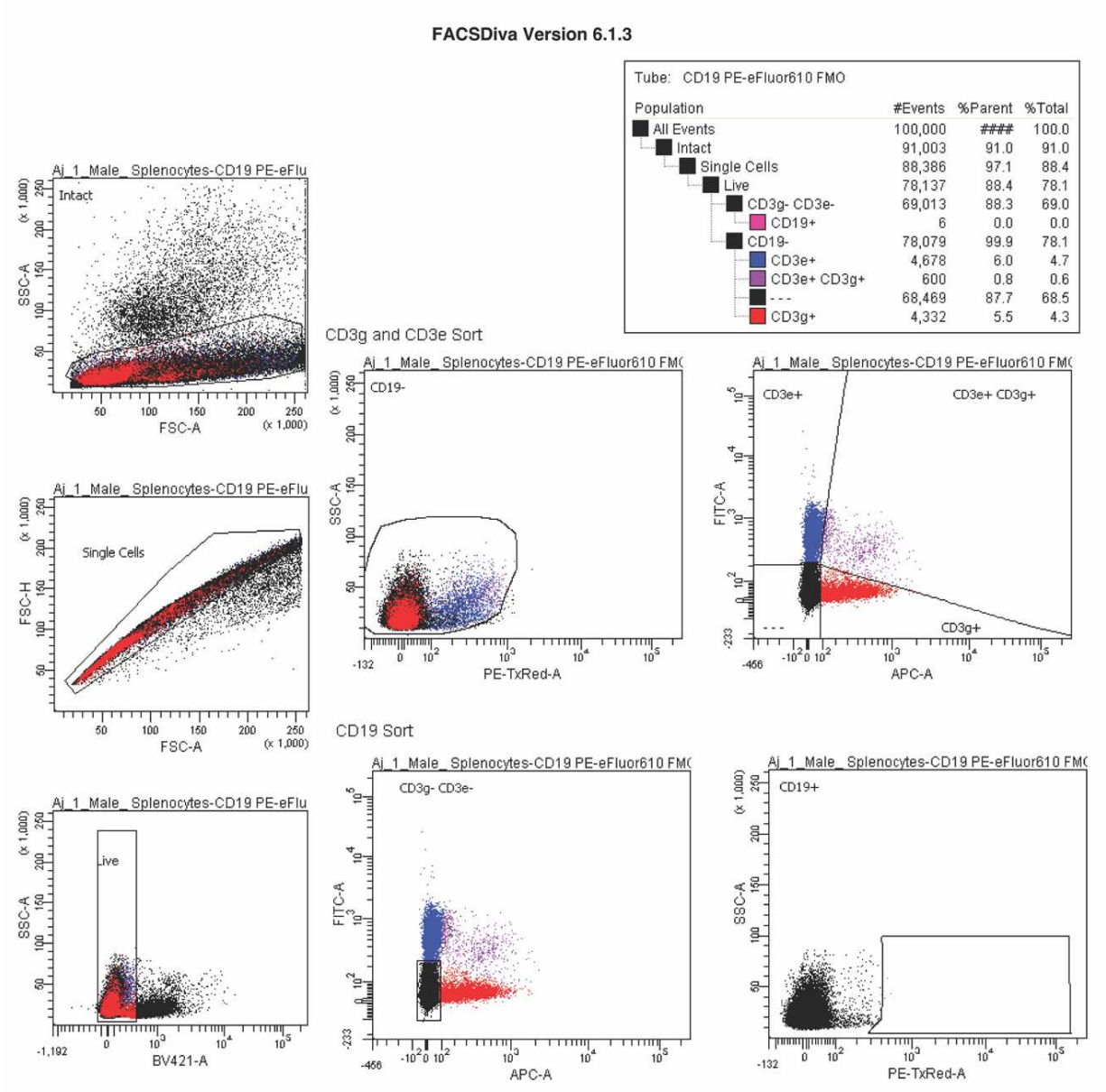

Figure III.6) CD19 PE-eFluor610 FMO *A*j1 FACSDiva worksheet.

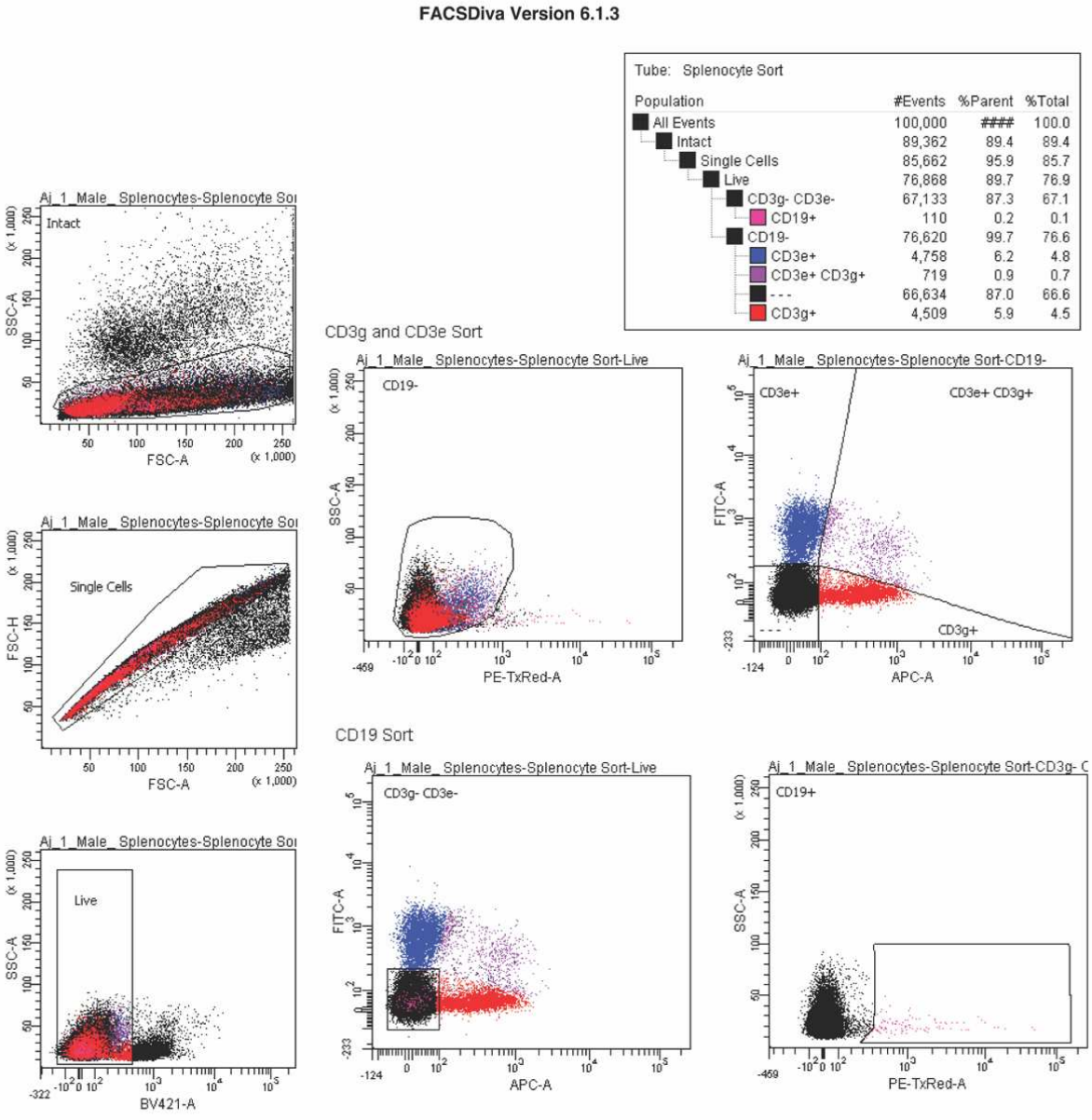

Figure III.7) Full panel sort sample *A*j1 FACSDiva worksheet.

Sort Reports

Experiment : Aj CD3g CD3e CD19 Sort Splenocytes_001 | Sort Report | Report Date : 2022.04.11 at 21:27:04
Specimen : Aj_1_Male_ Splenocytes | Device : 4 Tube
Tube : T and B Cell Sort | User ID : Administrator
Sort Layout : Sort Layout_002 | Cytometer : FACSAriaII (64828200052)
Application : FACSDiva Version 6.1.3

Sort Settings

Sort Setup	70 micron	Phase Mask	0
Frequency	86.2	Single Cell	Off
Amplitude	11.7	Sweet Spot	On
Phase	0.00	First Drop	211
Drop Delay	47.25	Target Gap	6
Attenuation	Off	Plates Voltage	5,000
Precision	Purity	Voltage Centering	-908
Yield Mask	32	Sheath Pressure	70.00
Purity Mask	32		

Side Stream Voltage (%)

Far Left	Left	Right	Far Right
100.00	35.00	35.00	100.00

Neighboring Drop Charge (%)

2nd	3rd	4th
18.00	9.00	4.00

Acquisition Counters

Threshold Count	11239760
Processed Events Count(evt)	12322436
Electronic Aborts Count(evt)	37932
Sort Elapsed Time(hh:mm:ss)	00:29:35

Sort Counters

	Far Left	Left	Right	Far Right
Sort Rate(evt/s)	21	220	249	7
Conflicts Count(evt)	3786	30150	24467	856
Conflicts Rate(evt/s)	2	16	13	0
Efficiency(%)	91	92	94	93

Sort Layout

Far Left	Left	Right	Far Right
CD3e+ CDg+ : 39035	CD3g+ : 390837	CD3e+ : 442189	CD19+ : 12538

Figure III.8) FACSDiva sort report Aj1 male.

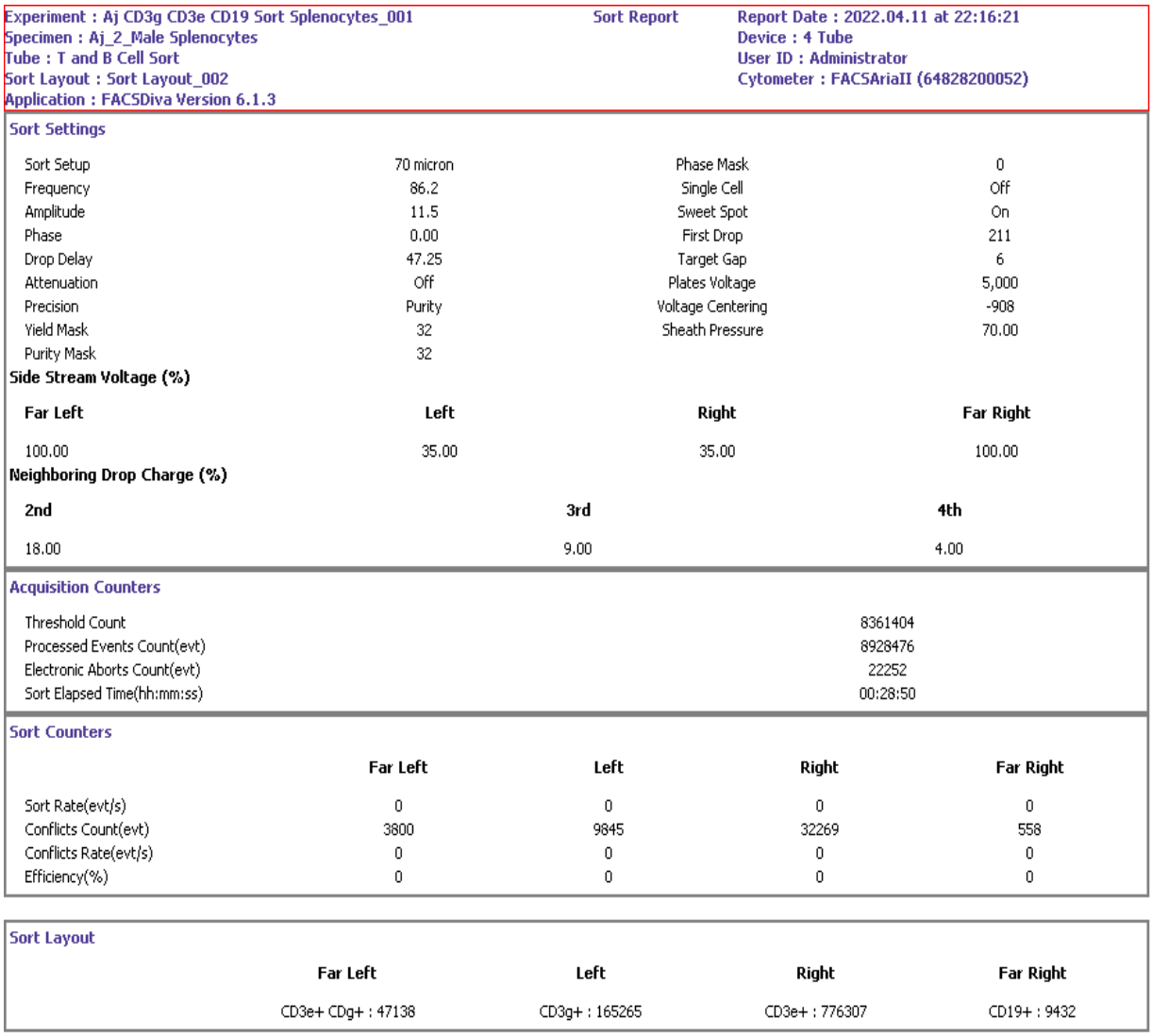

Experiment : Aj CD3g CD3e CD19 Sort Splenocytes_001
Specimen : Aj_2_Male Splenocytes
Tube : T and B Cell Sort
Sort Layout : Sort Layout_002
Application : FACSDiva Version 6.1.3

Sort Report

Report Date : 2022.04.11 at 22:16:21
Device : 4 Tube
User ID : Administrator
Cytometer : FACSAriaII (64828200052)

Sort Settings

Sort Setup	70 micron	Phase Mask	0
Frequency	86.2	Single Cell	Off
Amplitude	11.5	Sweet Spot	On
Phase	0.00	First Drop	211
Drop Delay	47.25	Target Gap	6
Attenuation	Off	Plates Voltage	5,000
Precision	Purity	Voltage Centering	-908
Yield Mask	32	Sheath Pressure	70.00
Purity Mask	32		

Side Stream Voltage (%)

Far Left	Left	Right	Far Right
100.00	35.00	35.00	100.00

Neighboring Drop Charge (%)

2nd	3rd	4th
18.00	9.00	4.00

Acquisition Counters

Threshold Count	8361404
Processed Events Count(evt)	8928476
Electronic Aborts Count(evt)	22252
Sort Elapsed Time(hh:mm:ss)	00:28:50

Sort Counters

	Far Left	Left	Right	Far Right
Sort Rate(evt/s)	0	0	0	0
Conflicts Count(evt)	3800	9845	32269	558
Conflicts Rate(evt/s)	0	0	0	0
Efficiency(%)	0	0	0	0

Sort Layout

Far Left	Left	Right	Far Right
CD3e+ CDg+ : 47138	CD3g+ : 165265	CD3e+ : 776307	CD19+ : 9432

Figure III.9) FACSDiva sort report Aj2 male.

Experiment : Aj CD3g CD3e CD19 Sort Splenocytes_001 | Sort Report | Report Date : 2022.04.11 at 22:57:18
Specimen : Aj_3_Female Splenocytes | Device : 4 Tube
Tube : T and B Cell Sort | User ID : Administrator
Sort Layout : Sort Layout_002 | Cytometer : FACSAriaII (64828200052)
Application : FACSDiva Version 6.1.3

Sort Settings

Sort Setup	70 micron	Phase Mask	0
Frequency	86.2	Single Cell	Off
Amplitude	11.5	Sweet Spot	On
Phase	0.00	First Drop	211
Drop Delay	47.25	Target Gap	6
Attenuation	Off	Plates Voltage	5,000
Precision	Purity	Voltage Centering	-908
Yield Mask	32	Sheath Pressure	70.00
Purity Mask	32		

Side Stream Voltage (%)

Far Left	Left	Right	Far Right
100.00	35.00	35.00	100.00

Neighboring Drop Charge (%)

2nd	3rd	4th
18.00	9.00	4.00

Acquisition Counters

Threshold Count	11016682
Processed Events Count(evt)	11133526
Electronic Aborts Count(evt)	42334
Sort Elapsed Time(hh:mm:ss)	00:25:12

Sort Counters

	Far Left	Left	Right	Far Right
Sort Rate(evt/s)	0	0	0	0
Conflicts Count(evt)	5305	13789	72610	919
Conflicts Rate(evt/s)	0	0	0	0
Efficiency(%)	0	0	100	0

Sort Layout

Far Left	Left	Right	Far Right
CD3e+ CDg+ : 45730	CD3g+ : 164233	CD3e+ : 1243632	CD19+ : 12056

Figure III.10) FACSDiva sort report Aj3 female.

Experiment : Aj CD3g CD3e CD19 Sort Splenocytes_001 | Sort Report | Report Date : 2022.04.11 at 23:50:09
Specimen : Aj_4_Female Splenocytes | Device : 4 Tube
Tube : T and B Cell Sort | User ID : Administrator
Sort Layout : Sort Layout_001 | Cytometer : FACSAriaII (64828200052)
Application : FACSDiva Version 6.1.3

Sort Settings

Sort Setup	70 micron	Phase Mask	0
Frequency	86.2	Single Cell	Off
Amplitude	12.1	Sweet Spot	On
Phase	0.00	First Drop	211
Drop Delay	47.25	Target Gap	6
Attenuation	Off	Plates Voltage	5,000
Precision	Purity	Voltage Centering	-908
Yield Mask	32	Sheath Pressure	70.00
Purity Mask	32		

Side Stream Voltage (%)

Far Left	Left	Right	Far Right
100.00	35.00	35.00	100.00

Neighboring Drop Charge (%)

2nd	3rd	4th
18.00	9.00	4.00

Acquisition Counters

Threshold Count	9636112
Processed Events Count(evt)	389304
Electronic Aborts Count(evt)	35001
Sort Elapsed Time(hh:mm:ss)	00:23:58

Sort Counters

	Far Left	Left	Right	Far Right
Sort Rate(evt/s)	0	0	0	0
Conflicts Count(evt)	1171	4518	8899	132
Conflicts Rate(evt/s)	0	0	0	0
Efficiency(%)	77	96	97	0

Sort Layout

Far Left	Left	Right	Far Right
CD3e+ CDg+ : 10427	CD3g+ : 66274	CD3e+ : 138479	CD19+ : 1888

Experiment : Aj CD3g CD3e CD19 Sort Splenocytes_001 | Sort Report | Report Date : 2022.04.12 at 00:05:30
Specimen : Aj_4_Female Splenocytes | Device : 4 Tube
Tube : T and B Cell Sort | User ID : Administrator
Sort Layout : Sort Layout_001 | Cytometer : FACSAriaII (64828200052)
Application : FACSDiva Version 6.1.3

Sort Settings

Sort Setup	70 micron	Phase Mask	0
Frequency	86.2	Single Cell	Off
Amplitude	12.1	Sweet Spot	On
Phase	0.00	First Drop	211
Drop Delay	47.25	Target Gap	6
Attenuation	Off	Plates Voltage	5,000
Precision	Purity	Voltage Centering	-908
Yield Mask	32	Sheath Pressure	70.00
Purity Mask	32		

Side Stream Voltage (%)

Far Left	Left	Right	Far Right
100.00	35.00	35.00	100.00

Neighboring Drop Charge (%)

2nd	3rd	4th
18.00	9.00	4.00

Acquisition Counters

Threshold Count	601918
Processed Events Count(evt)	599344
Electronic Aborts Count(evt)	583
Sort Elapsed Time(hh:mm:ss)	00:06:01

Sort Counters

	Far Left	Left	Right	Far Right
Sort Rate(evt/s)	0	0	0	0
Conflicts Count(evt)	216	223	677	6
Conflicts Rate(evt/s)	0	0	0	0
Efficiency(%)	0	100	100	0

Sort Layout

Far Left	Left	Right	Far Right
CD3e+ CDg+ : 3025	CD3g+ : 10985	CD3e+ : 44662	CD19+ : 655

Figure III.11) FACSDiva sort reports Aj4 female.

APPENDIX IV
RNA EXTRACTION OF ENRICHED CELL POPULATIONS BY FLUORESCENTLY ACTIVATED CELL SORTING USING TRIZOL

Purpose

This protocol is optimized for extraction of RNA from cells enriched by cell sorting. Cell sorting introduces FACS buffer and sheath fluid into the sample which interferes with trizol for an efficient RNA extraction. Additionally, when cells are sorted the static charges make the sorted droplets stick to the side of the FACS tube. During long sorts some of the droplets that contain cells will dry out on the sides of the FACS tubes – especially true of sorted populations less than 100,000 cells using a 70μm nozzle. As such, it is important to carry out the initial cell lysis using trizol in the FACS tube before transferring to the 2 ml microfuge tube.

Notes

- If you have the option, cool microcentrifuge to 4°C.
- Keep 70% ethanol and 100% isopropanol at -20°C.
- Trizol and all tips and tubes that have been in contact with trizol and chloroform must be labeled as "Trizol/Chloroform waste". DO NOT autoclave; place in plastic bag for hazardous waste.
- Trizol contains phenol, a strong acid and neurotoxin. Chloroform is also carcinogenic. Work with trizol and chloroform must be performed in a chemical fume hood. After step 18, it is safe to work outside the chemical fume hood.

Materials

- 2 ml microfuge tubes
- Trizol
- 100% molecular grade isopropanol
- 70% molecular grade ethanol
- Molecular grade water

- Molecular grade chloroform
- Molecular grade glycogen 20mg/ml
- Ribolock #EO0382

Protocol

1. After cells of interest have been sorted, spin at 340xg for 10 minutes.
2. Decant supernatant gently and as much as possible.
3. Add 1,000ul of Trizol into FACS tubes, cap, shake, and vortex.
4. Incubate at room temperature for 10 minutes.
5. Place in -20°C until ready to continue with RNA extraction.
6. Transfer to microfuge tubes after mixing well.
7. Add 200ul chloroform (µl Trizol x 0.2 for chloroform volume).
8. Vortex and incubate at room temperature for 5 minutes.
9. Spin at 12,000xg for 10 minutes.
    a. While waiting for spin – prepare tubes with 1ul glycogen.
10. Use a p200 to remove aqueous phase.
    a. Carefully pipette to not disturb the organic phase.
    b. Transfer to clean 2 ml microfuge tube.
11. To trizol tubes add an additional 500µl trizol and 100µl chloroform.
12. Vortex and incubate at room temperature for 5 minutes.
13. Spin at 12,000xg for 10 minutes.
    a. Carefully pipette to not disturb the organic phase.
    b. Transfer to the 2 ml microfuge tube that has the first collected aqueous phase.
14. Use p200 to obtain aqueous phase.

15. Add 300µl 100% isopropanol to aqueous phase.
16. Vortex, and spin for 20min at 12,000xg.
17. Remove most supernatant with P1000.
    a. Remove remining supernatant with P200 careful to leave the RNA/Glycogen pellet intact.
18. Wash with 500µl 70% ethanol.
    a. Can stop here and store at -20 in 70% ethanol.
19. Spin at 12,000xg for 10 minutes.
20. Set P1000 to 450µl, and P200 to 60µl to remove supernatant.
21. Wash with 500µl 70% ethanol.
    a. Can stop here and store at -20 in 70% ethanol.
22. Spin at 12,000xg for 10 minutes.
23. Set P1000 to 450µl, and P200 to 60µl to remove supernatant.
24. Let air dry for 5 minutes.
25. Add 20µl molecular grade H20.
26. NanoDrop using 2µl of RNA solution.
    a. If contaminants are found, add 100ul Trizol, 100ul chloroform, and vortex.
    b. Spin at 12,000xg for 10 minutes.
        i. Prepare clean precipitation 1.5 ml microfuge tubes with 1ul glycogen, and label.
    c. Set P200 to 65ul and remove aqueous phase and add to glycogen tubes.
    d. Add 50ul 100% Isopropanol and vortex.
    e. Spin at 12,000xg for 20 minutes.

f. Set P200 to 150ul to remove supernatant.

g. Wash with 500ul 70% ethanol.

h. Spin at 12,000xg for 10 minutes.

i. Set P1000 to 450ul, and P200 to 60ul to remove supernatant.

j. Wash with 500ul 70% ethanol.

k. Spin at 12,000xg for 10 minutes.

l. Set P1000 to 450ul, and P200 to 60ul to remove supernatant.

m. Let air dry for 5 minutes.

n. Add 20ul molecular grade H20.

o. NanoDrop.

27. Add 1ul Ribolock to each tube.

28. Store in -80°C freezer.

APPENDIX V

TISSUE HARVESTING OF INTRAEPITHELIAL AND LAMINA PROPRIA FRACTIONS OF THE GASTROINTESTINAL TRACT, BLOOD, BONE MARROW AND SPLEEN FOR FLOW CYTOMETRY AND CELL SORTING

Purpose

Tissue processing is the foundation of flow cytometry experimental success. The goal of tissue processing is to disassociate primary tissues into a single cell suspension with minimal cell aggregates and doublets to obtain data from single cells. Three primary goals need to be met, 1) Disassociate a tissue into an optimal single cell suspension 2) Obtain the optimal single cell suspension with highest possible cell viability 3) Maintain cells in a single cell suspension alive and prevent cell aggregates from forming after tissue disassociation.

Two methods, mechanical separation, enzymatic, or chemical disassociation achieve the first goal of obtaining a single cell suspension – sometimes more than one method is combined. An example of mechanical disassociation is the homogenization of a spleen through a 70μm mesh cell strainer or by macerating between two microscopy slides. Mechanical disassociation can also involve simply processing a tissue into smaller pieces using scissors or a scalpel. Chemical disassociation is often attained by using reducing agents such as dithioerythritol (DTE) or dithiothreitol (DDT) which break disulfide bonds in proteins. This method is often used in organs that contain epithelial tissue and endothelial tissue such as gastrointestinal tract tissue. Epithelial and endothelial cell tight junctions, such as claudins, which contain disulfide bonds which are reduced by DTT or DTE. Similar to chemical disassociation, enzymatic dissociation will break up matrixes that hold cells together, some such enzymes that can be of use are collagenases, trypsin, and proteinase K. Many tissues such as the gastrointestinal tract, lungs, and skin require a combination of mechanical, chemical, and enzymatic methods for a successful disassociation.

The second goal to obtain a high viability is often the most difficult. Different cell types can undergo more stresses, while others cannot. As such, each tissue will require a different disassociation method. However, there are a few guidelines that can help prevent unnecessary cell

death. 1) Keep processing times to an efficient minimum. 2) Keep all buffers and cells on ice or at 4°C unless a disassociation requires warmer temperatures (but quickly switch to cold buffers and storage on ice as soon as possible). 3) Wash disassociated cells as soon as possible in an appropriate cold buffer – chemical and enzymatic disassociation can often be toxic to cells. Dead cells are "sticky" and like to form aggregates with dead and live cells.

The third goal to maintain cells in a single cell suspension alive and prevent cell aggregates from forming after tissue disassociation can be attained by tailoring a FACS buffer specific to your sample type. Additives such as EDTA, DTE, DTT, DNase, and a protein like BSA or FBS in combination can produce a buffer that prevents aggregate formation and maintain cell viability throughout processing. Maintaining viability is of great importance if the goal is to culture cells after cell sorting. However, viability can be of secondary concern if preserving antigen accessibility is the primary concern. Another useful and important additive is sodium azide. Sodium azide is often only thought of as a preservative to prevent contamination of FACS buffer by bacterial and fungal growth. However, sodium azide performs other important functions for a flow cytometry experiment such as stabilization of tandem dyes, slows photo-bleaching, blocks antibody shedding, prevention of capping, modulization, and internalization of antigens. Sodium azide is toxic to cells because it is a metabolic inhibitor. Therefore, by inhibiting metabolism, the mechanisms of antigen internalization, modulization, and capping are slowed or prevented, especially if used in tandem with cold buffers and keeping samples on ice or at 4°C. However, it is best to forgo sodium azide if the goal of cell sorting is culturing sorted cells.

Notes

It is of high importance to perfuse the bat after it is euthanized with 60 ml of perfusion buffer (1x PBS, 5mM EDTA, 10units heparin/ml). Good perfusion is visualized by the color change of the intestines from a dark pink-red to a light pink color, lungs from a pink to white color, and the liver from a dark red to a brown color. This step is critical to remove erythrocytes from the intestines as using ammonium chloride red blood cell lysis buffer is not optimal for epithelial cell survival. Erythrocytes will make analysis of flow data more difficult, and as such, removal of erythrocytes helps to produce clean flow cytometry data.

It is also critical to immediately quench predigestion and digestion fractions with cold 1xPBS+5mM EDTA! If disassociated cells are left in predigestion or digestion buffer for extended periods, cell viability will be greatly reduced! Optimal cell viability achieved is 70-80% when following this protocol. Reduced viability is likely due to incubating for longer than 20 minutes or leaving disassociated cells in predigestion or digestion buffer without quenching and washing.

Harvest organs in this order:

a. Blood – go to Blood.

b. Spleen – go to Spleen.

c. Intraepithelial and lamina propria fractions of the intestines –go to Intestine.

d. Bone marrow – go to Bone Marrow.

1. Place spleen into 5 ml cold PBS, and store on ice.
2. Process organs in this order:

a. Blood.

b. Intestine.

c. Spleen.

d. Bone Marrow.

Materials

- Innovex Universal Fc Block.
- Viability dye.
    - Experiment dependent.
- Antibodies.
    - Experiment dependent.
- 1xPBS+5mM EDTA.
- RBC ammonium chloride lysis buffer.
- 70µm cell strainers.
- Lamina Propria Dissociation Kit Cat# 130-097-410.
- 96 well V-bottom plates.

Buffers and Solutions

- *Perfusion buffer*
    - 1xPBS.
    - 5mM EDTA.
    - 10units heparin.
- *1xPBS+ 5mM EDTA*
    - Store at 4°C or on ice.
- *FACS Buffer*
    - Store at 4°C or on ice.
    - 1xPBS.
    - 1%BSA (1-5%).
    - 0.5% Sodium Azide (0.1-1%).

- 5mM EDTA.

- *HBSS w*
  - Store at Room Temp
    - 50 ml 10xHBSS.
    - 5 ml 1M HEPES.
    - 0.07g $CaCl_2$ Hexahydrate [1.26mM].
    - 0.05g $MgCl_2$ Hexahydrate [0.5mM].
    - 0.05g $MgSO_4$ Hexahydrate [0.41mM].

- *HBSS w/o*
  - Store at Room Temp.
    - 50 ml 10xHBSS.
    - 5 ml 1M HEPES.

Buffers That Must Be Made the Day Of

- *Predigestion*

  (Recipe below makes 100 ml, but 80 ml is needed for 2 bats.)

  - Store at room temperature.
    - 94 ml HBSS w/o.
    - 5 ml FBS [5%].
    - 0.0154g DTT [1mM].
    - 1 ml 500mM EDTA [5mM].

- *Digestion*

  (Recipe below makes 5 ml for 2 digestions.)

  - Prewarm in 37°C water bath.
    - 4.4 ml HBSS w.
    - 250 µl FBS.
    - Enzymes are pre-aliquoted so use the entire vial.
      - 200 µl Enzyme D.
      - 100 µl enzyme R.
      - 25 µl Enzyme A.

Intestine

1. Place intestines on clean paper towel and keep moist with 1xPBS+5mM EDTA.
2. Cut the small and large intestine longitudinally so that the lumen is opened.
3. Cut intestine laterally into 0.5 cm pieces.
4. Place pieces into 50 ml conical tube (50 ml processing tube), wash 4 times with 10 ml. 1xPBS+5mM EDTA using a vortex on maximum.
5. Place 20 ml of Predigestion solution into the small and large intestine tubes.
6. Incubate at 37°C on continuous rotation on orbital rotator for 20 minutes.
7. Vortex on max for 10 seconds.
8. Strain Intestine pieces through 70µm cell strainer.
    a. Save the IEL supernatant in IEL 50 ml tube.
        i. Use a p1000 tip to help stir the intestine pieces to allow supernatant to pass through the cell strainer and add 1XPBS+5mM EDTA to 50 ml (**Figure V.1**).
        ii. Spin down IEL supernatant at 350xg for minutes and wash with 20 ml 1xPBS+5mM EDTA.
        iii. Resuspend in 5 ml 1xPBS+5mM EDTA and store on ice or in 4°C.
    b. Place Intestine pieces back into 50 ml processing tube.

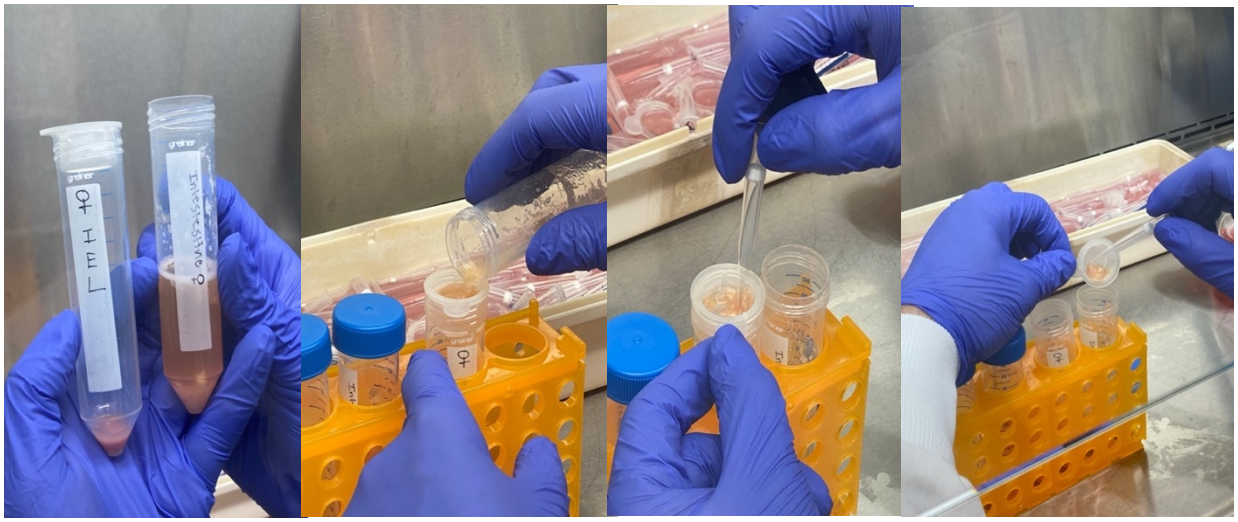

Figure V.1) Transfer technique of IEL supernatant.

9. Add 20 ml of fresh predigestion into 50 ml processing tube.
10. Incubate at 37°C on continuous rotation on orbital rotator for 20 minutes.
11. Vortex on max for 10 seconds.
12. Strain Intestine pieces through 70µm cell strainer.
    a. Save the IEL supernatant in IEL 50 ml tube.
        i. Use a p1000 tip to help stir the intestine pieces to allow supernatant to pass through the cell strainer and add 1XPBS+5mM EDTA to 50 ml (**Figure V.1**).
        ii. Spin down IEL supernatant at 350xg for 5 minutes and wash with 20 ml 1xPBS+5mM EDTA.
        iii. Resuspend in 20 ml 1xPBS+5mM EDTA and store on ice or in 4°C.
    b. Place intestine pieces back into 50 ml processing tube.
13. Add 20 ml of fresh HBSS w/o into processing tube.
14. Incubate at 37°C on continuous rotation on orbital rotator for 20 minutes.
15. Vortex on max for 10 seconds.

16. Strain Intestine pieces through 70µm cell strainer.
    a. Save the IEL supernatant in IEL 50 ml tube.
        i. Use a p1000 tip to help stir the intestine pieces to allow supernatant to pass through the cell strainer (**Figure V.1**).
        ii. Spin down IEL supernatant and wash with 20 ml 1xPBS+5mM EDTA.
        iii. Resuspend in 20 ml 1xPBS+5mM EDTA and store on ice or in 4°C.
17. Prepare digestion by adding 100 µL of Enzyme D, 50 µL of Enzyme R, and 12.5 µL of Enzyme A into a 15 ml tube containing the pre-heated 2.35 mL of digestion solution and mix gently.
    a. Transfer digestion buffer to the 50 ml tube containing intestinal pieces.
18. Incubate the sample for 30 minutes at 37 °C under continuous rotation using an orbital rotator.
19. Transfer the intestine tissue into the gentleMACS C Tube (C tube) and close C tightly.
20. Attach C tube it upside down onto the sleeve of the gentleMACS (**Figure V.2**).

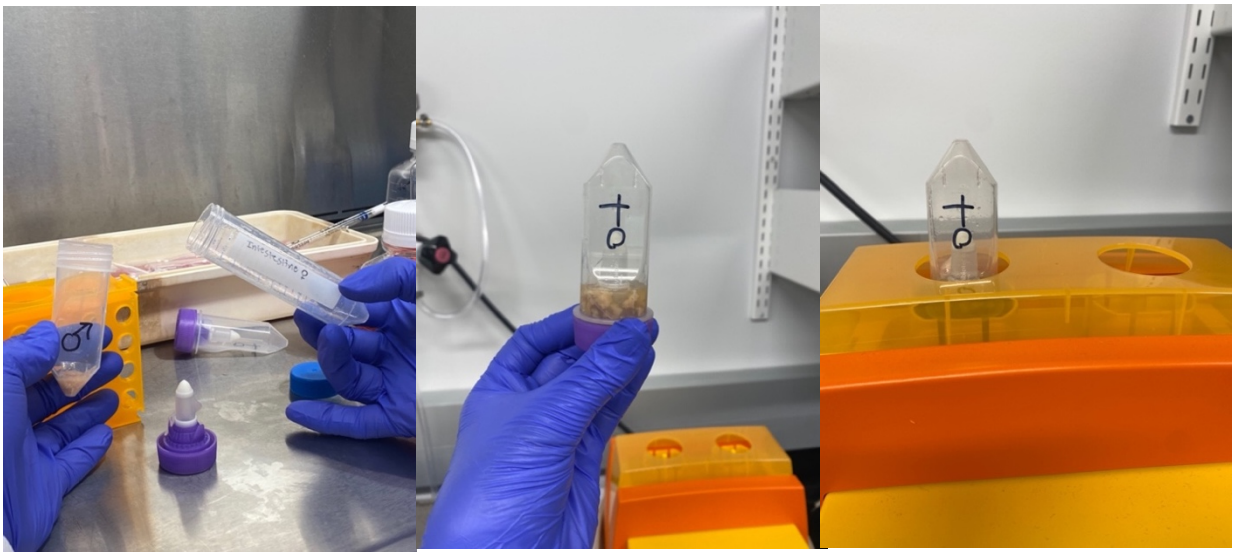

Figure V.2) Transfer of LP to C tube, and installation on instrument.

21. Run the gentleMACS Program m_intestine_01.

22. After termination of the program, detach C Tube from the gentleMACS and add 10 ml 1XPBS+5mM EDTA, close cap and invert several times.
23. Strain intestine pieces through 70µm cell strainer in a 50 ml tube.
    a. Save the LP supernatant.
        i. Use a p1000 tip to help stir the intestine pieces to allow supernatant to pass through the cell strainer and add 1XPBS+5mM EDTA to 50 ml tube (**Figure V.1**).
        ii. Spin down IEL supernatant at 350xg for 5 minutes and wash with 20 ml 1xPBS+5mM EDTA.
        iii. Resuspend in 20 ml 1xPBS+5mM EDTA and store on ice or in 4°C.
24. Procced to cell staining.

25. **Blood**

1. While bat is under anesthesia, perform terminal heart bleed using 3 ml syringe.
2. Immediately place blood into 45 ml 1x RBC buffer.
3. Mix, and place on orbital shaker for 10 minutes.
4. Place on ice.
5. Spin down 340×g 5 minutes and remove supernatant.
6. Wash with 1xPBS+5mM EDTA and transfer to 15 ml tube.
7. Spin down 340×g 5 minutes and remove supernatant.
8. In 15 ml tube, resuspend in 2 ml 1xPBS+5mM EDTA and store on ice or in 4°C.
9. Count cells.

Spleen

1. Process spleen through a 70µm cell strainer in a petri dish with 5 ml cold 1xPBS+5mM EDTA.
2. Remove single cell suspension and place into 15 ml tube.
3. Spin down and remove supernatant.
4. Resuspend in 10 ml cold 1x RBC lysis buffer.
5. Place on orbital rotator for 10 minutes.
6. Spin down 340×g 5 minutes and remove supernatant.
7. Wash with 1xPBS+5mM EDTA.
8. Spin down 340×g 5 minutes and remove supernatant.
9. In 15ml tube, resuspend in 2 ml 1xPBS+5mM EDTA and store on ice or in 4°C.
10. Count cells.

Bone Marrow

1. Prepare sterile 1 ml microfuge tubes by puncturing a hole in the bottom of the tube with a sterile 18g needle. Do this by placing the needle inside the tube and push out through the bottom.
2. Place 1 ml microfuge tubes inside 1.5 ml microfuge tubes. Set aside in a biosafety cabinet.
3. Remove humerus and femur bones from the bat.
4. Clean the bones of muscle and connective tissues.
5. Cut bones in half with scissors.
6. Place bones cut side down inside punctured 1 ml microfuge tubes.
7. Centrifuge at 200xg for 3-5 minutes.
8. Remove 1 ml microfuge tubes from 1.5 ml microfuge tubes.
9. Vigorously dislodge bone marrow pellet from the bottom of the microfuge tube with 800µl 1xPBS + 5mM EDTA using a P1000 pipette.
10. Force the bone marrow single cell suspension though 70µm mesh caps into a 5 ml FACS tube.

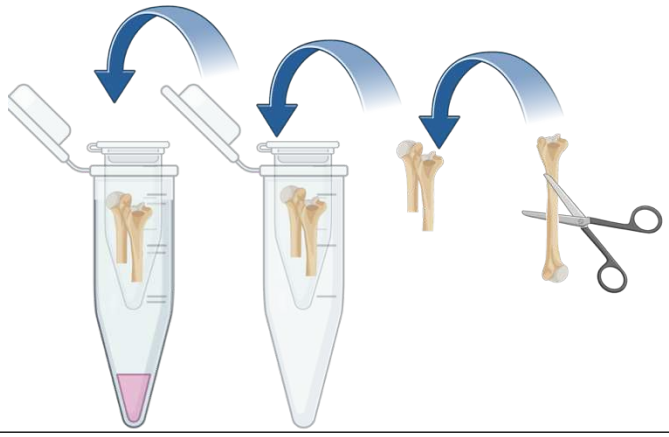

Figure V.3) Bone Marrow extraction method of using 1.5 ml and 1 ml microfuge tubes.

Cell Staining

Primary Amine Viability Staining

1. Count the number of cells for each organ sample using trypan blue.
2. Remove 1 million cells for unstained control.
3. Adjust cell volume for appropriate viability staining in 1xPBS + 5mM EDTA, then add primary amine viability dye.
    a. Ghost Violet 450 1:5,000
    b. Ghost Violet 510 1:5,000
    c. Ghost Blue 516 1:5,000
    d. Ghost Red 780 1:5,000
4. Incubate in the dark for 30min at 4°C or on ice.
5. Spin at 350xg for 5 minutes and decant.
6. Wash with FACS buffer.
    a. For 15 ml tubes add 12 ml FACS buffer.
    b. For 20 ml tubes add 40 ml FACS buffer.
7. Adjust cell concentration to 1.0x10^7 cells/ml.
8. Place 1million cells in each well of a 96 well V-bottom plate.
    a. Refer to your 96 well template.
9. Spin 340xg 5 minutes and decant.

Universal Fc Block

10. Resuspend in 100µl Universal Fc block.
11. Incubate in the dark for 30 min at 4°C or on ice.
12. Spin 340xg 3 minutes and decant.

13. Wash and spin two times with 150 µl FACS buffer

Antibody Staining (Experiment Dependent)

It is important to keep unstained cells and viability only samples on a separate plate, and samples are on opposite ends of the plate to ensure no cross-contamination of fluorescent reagents occurs. Unstained cells are a critical control for spectral flow cytometry. Also ensure fluorescence minus one controls (FMOs), and full antibody panel cocktails are made at the appropriate volumes and dilutions.

14. Extracellular antibody staining.
    a. Add antibody cocktails to appropriate samples.
15. Mix well with pipette.
16. Incubate in the dark at 4°C or on ice for 30 minutes.
17. Centrifuge for 5 minutes at 350xg for 5 minutes and decant.
18. Wash with 150µl FACS buffer, centrifuge for 5 minutes at 350xg, and decant
    a. If fixing cells, use freshly prepared 4% paraformaldehyde 1xPBS + 5mM EDTA solution.
    b. Incubate for 30 minutes in the dark.
    c. Centrifuge at 350xg for 5 minutes and decant.
    d. Wash with 150µl FACS buffer, centrifuge for 5 minutes at 350xg, and decant.
    e. Can store samples up to 3 days in the dark at 4°C.

APPENDIX VI
JAMAICAN FRUIT BAT GROWTH FACTOR GENE BLOCKS

Wnt3a

(Mouse IgK leader)
gcc acc atg gag aca gac aca ctc ctg cta tgg gta ctg ctg ctc tgg gtt cca ggt tcc act ggt

TCCCTGGCTGTTGGGCCCCAGTATTCGTCCCTGGGCACACAGCCCATCCTCTG
CGCCAGTATCCCAGGCCTAGTACCCAAACAGCTGCGCTTCTGCCGGAACTAC
GTGGAGATCATGCCCAGCGTGGCAGAGGGTGTCAGGATCAGCATCGAAGAGT
GTCAGCACCAGTTCCGTGGCCGCCGGTGGAACTGCACCACCATCAACAACAG
CCTGGCCATCTTTGGCCCTGTGCTGGACAAACTCTCTGCAGCCACCCGCGAGT
CTGCCTTCGTGCACGCCATTGCTGCAGCTGGTGTGGCCTTCGCTGTGACACGC
TCATGTGCTGAGGGCTCCGCTGCCATCTGTGGATGCAGCAGCCGTCACCTGG
GCTCACCTGGCCATGGCTGGAAGTGGGGCGGCTGCAGCGAGGACATCGAGTT
TGGAGGGATGGTATCCCGAGAGTTTGCAGATGCTCGGGAGAACAGGCCTGAT
GCCCGCTCTGCCATGAACCGCCACAACAATGAGGCAGGACGCCAACAGGCC
ATCGCCAGTCACATGCATCTCAAGTGTAAGTGCCACGGGCTGTCAGGGAGCT
GCGAGGTAAAGACCTGCTGGTGGTCGCAGCCCGACTTCCGCTCCATCGGCGA
CTTCCTCAAGGACAAGTATGACAGCGCCTCGGAGATGGTGGTGGAGAAACAC
CGAGAGTCGCGCGGCTGGGTGGAGACGCTGCGGCCTCGCTACACCTACTTCA
AGGTGCCCACGGAGCGTGACCTGGTCTACTACGAGGCGTCGCCCAACTTCTG
CGAGCCCAATCCTGAGACCGGCTCCTTCGGCACCCACGACCGCACCTGCAAC
GTGAGCTCACCAGGCATCGACGGCTGCGACCTGCTGTGCTGCGGCCGCGGGC
ACAATGCGCGCGCCGAGCAGCGCCTGGAGAAGTGCCTCTGCGTCTTCCACTG
GTGCTGTTACGTTAGCTGCCAGGAGTGCGCGCGCATCTACGACGTGCACACC
TGCAAG

(6X histidine tag STOP)

CATCATCACCACCATCACTGA

Noggin

(Mouse IgK leader)

gcc acc atg gag aca gac aca ctc ctg cta tgg gta ctg ctg ctc tgg gtt cca ggt tcc act ggt

ATGGATCGCTGTCCTAGTCTTGGTGTTACTCTTTATGCTCTTGTTGTTGTTCTT
GGTCTTCGTGCAGCACCTGCTGGTGGTCAACATTATCTCCACATCCGCCCGGC
CCCCAGCGACAACCTGCCCCTGGTGGACCTCATCGAGCACCCGGACCCTATC
TTTGACCCCAAGGAGAAGGATCTGAACGAGACGCTGCTACGCTCGCTGCTTG
GAGGCCACTACGACCCGGGCTTCATGGCTACCAGTCCACCAGAAGATCGACC
AGGTGGAGGTGGAGGAAGTGCTGGTAGTGCAGAAGATCTTGCTGAACTTGAT
CAACTTCTTCGACAGCGGCCGTCGGGGGCCATGCCGAGCGAGATCAAAGGGC
TGGAGTTCTCCGAGGGGTTGGCCCCGGGCAAGAAGCAACGCCTGAGCAAGA
AGCTGCGGAGGAAGTTACAGATGTGGCTGTGGTCTCAGACCTTCTGCCCGGT
GCTGTACGCTTGGAACGACCTGGGCAGCCGCTTTTGGCCGCGCTACGTGAAG
GTGGGCAGCTGCTTCAGCAAACGCTCGTGCTCTGTGCCGGAGGGCATGGTGT
GCAAGCCGTCCAAGTCTGTGCACCTCACCGTGCTGCGGTGGCGCTGTCAGCG
GCGCGGGGGCCAGCGCTGCGGCTGGATTCCCATCCAGTACCCCATCATTTCC
GAGTGCAAGTGCTCCTGC

(6X histidine tag STOP)

CATCATCACCACCATCACTGA

R-spondin-2

(Mouse IgK leader)

gcc acc atg gag aca gac aca ctc ctg cta tgg gta ctg ctg ctc tgg gtt cca ggt tcc act ggt

GAAGGATGTGAAGTTGGTCATTGGAGTGAATGGGGAACTTGTAGCAGAAATA
ATCGCACATGTGGATTTAAATGGGGTCTGGAAACCAGAACACGGCAAATTGT
GAAAAAGCCAGCGAAAGACACAATACCATGTCCGACCATCGCTGAGTCCAG
GAGGTGTAAGATGGCCATGAGGCATTGTCCAGGAGGTTGCAGAATAGAAAA
CTGTGATTCTTGCTTCAGCAAAGACTTTTGTACTAAGTGCAAAGCAGGTTTTT
ATTTGCATAGAGGCCGTTGCTTTGATGAATGTCCAGACGGTTTTGCACCATTA
GATGACACCATGGAATGTGTGAACATGCTTTTTCTTTCTTTTACAGCTAGTTA
TGTATCAAATCCCATTTGCAAGGGTTGCTTGTCTTGTTCTAAGGACAATGGGT
GCAGCCGATGTCAACAGAAGTTGTTCTTCTTTCTTCGAAGAGAAGGCATGCG
CCAGTATGGGGAGTGCCTCCATTCCTGCCCATCGGGTTACTATGGACACCGA
GCTCCAGATATGAACAGATGTGCACGTGAGCAGCTGACTTTTTCTGCCTCATT
TTATCATTTATGCCACTTA

(6X histidine tag STOP)

CATCATCACCACCATCACTGA

Epidermal Growth Factor
(Extracellular domain only. This is the only growth factor with a transmembrane domain)

(Mouse IgK leader)

gcc acc atg gag aca gac aca ctc ctg cta tgg gta ctg ctg ctc tgg gtt cca ggt tcc act ggt

CGAGGCGTTGGCCGACTGGCTATCGCTAGCTCTGGGCTGGTGTGGCCCAGTG
GAATAACGATTGATTTCTTAACTGACAAGTTGTATTGGTGCGATGCCATGCAG
TCTGTGATTGAAATGGCCAATCTGGATGGTTCAAAACGCCAAAGACTTGCCC
AGAACGATGTAGGTAGG

(6X histidine tag STOP)

CATCATCACCACCATCACTGA

Gastrin

(Mouse IgK leader)

gcc acc atg gag aca gac aca ctc ctg cta tgg gta ctg ctg ctc tgg gtt cca ggt tcc act ggt

CAGGGGCCGTGGGTGGAGGAAGAAGAAGCGTATGGATGGATGGACTTT

(6X histidine tag STOP)

CATCATCACCACCATCACTGA

APPENDIX VII

PRODUCTION OF CHEMICALLY COMPETENT ESCHERICHIA COLI FOR PLASMID TRANSFORMATION

Purpose

Chemically competent *E. coli* are used for many molecular biology experiments to allow for the *E. coli* to be transformed by a plasmid. Commercially available chemically competent cells are convenient but are not cost effective especially if all experimental controls are used.

Sterilization of Materials

- 1L Luria Broth.
- 1L 100mM CaCl2.
- 1L 100mM MgCl2.
- 100 ml 85mM CaCl2 15% glycerol w/v.
- Microcentrifuge tubes.
- 4x 50 ml conical tubes.

Day One

Make all solutions (make sure all solutions are chilled at 4C!).

Make overnight culture for the *E. coli* strain you want.

Day Two

Work on ice!

1. Inoculate four 500 ml flasks with 250 ml of LB with 2.5 ml of over-night culture. Grow in 37°C shaker.
2. Measure OD_{600} every hour, then every 20 minutes when OD_{600} gets to above 0.2.

3. When OD600 reaches 0.35-0.4, put cells on ice for 20-30 minutes shaking occasionally to cool evenly.
4. Place 50 ml of culture in four 50 ml tubes, spin at 3000xg for 15 minutes at 4°C, decant, and repeat until culture is used up.
5. Decant, resuspend in 5 ml cold 100mM MgCl2 then bring up to 50 ml, spin at 2000xg for 15 minutes at 4°C.
6. Decant, resuspend in 5 ml cold 100mM CaCl2 then bring up to 50 ml, leave on ice for 20 minutes, spin at 2000xg for 15 minutes at 4°C.
7. Decant and resuspend in 5 ml cold 85mM CaCl2 glycerol (collect into one tube) then bring up to 50 ml, spin at 1000xg for 15 minutes at 4°C.
8. Decant and resuspend in 2 ml cold 85mM CaCl2 glycerol.
9. Aliquot 50 µl into microcentrifuge tubes.
10. Snap freeze in liquid nitrogen or in isopropanol with dry ice.
11. Place in -80°C.

AF488 (Alexa Fluor 488)

Fluorophore type – synthetic cyclic ring compound.
Primary laser excitation – blue 488nm.
Max emission – 519nm.

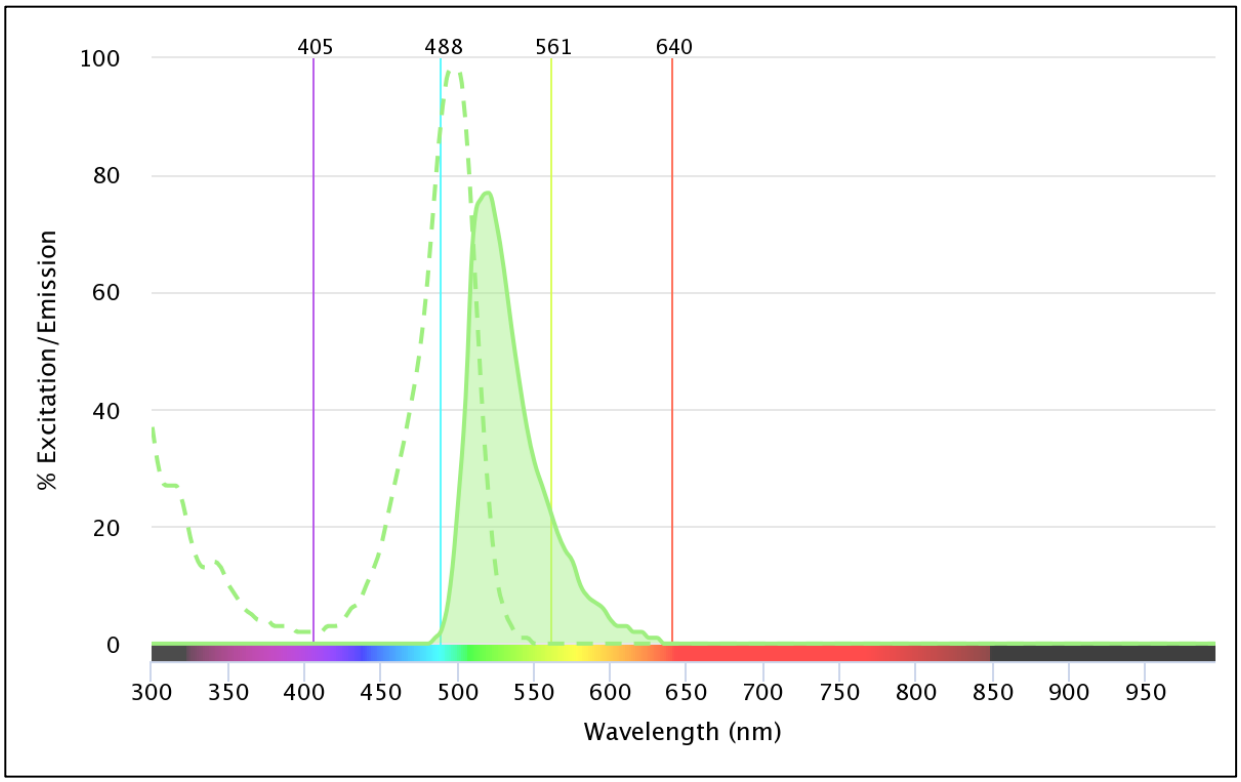

Figure G.1) AF488 (Alexa Fluor 488) excitation (dashed line) and emission (solid line with filled area) spectra normalized to 488nm blue laser line. Generated by FluoroFinder.

AF647 (Alexa Fluor 647)

Fluorophore type – synthetic cyclic ring compound.
Primary laser excitation – red 640nm.
Max emission – 670nm.

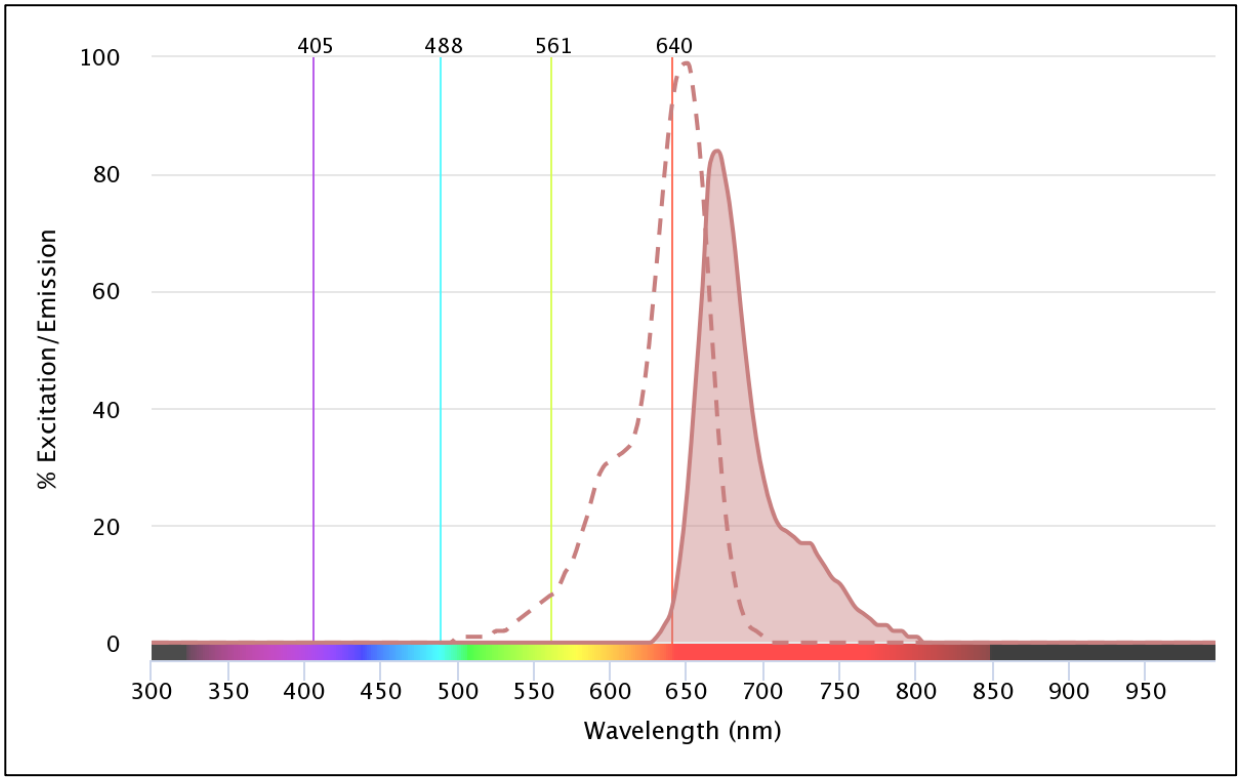

Figure G.2) AF647 (Alexa Fluor 647) excitation (dashed line) and emission (solid line with filled area) spectra normalized to 640nm red laser line. Generated by FluoroFinder.

APC (Allophycocyanin)

Fluorophore type – fluorescent trimer protein.
Primary laser excitation – red 640nm.
Max emission – 660nm.

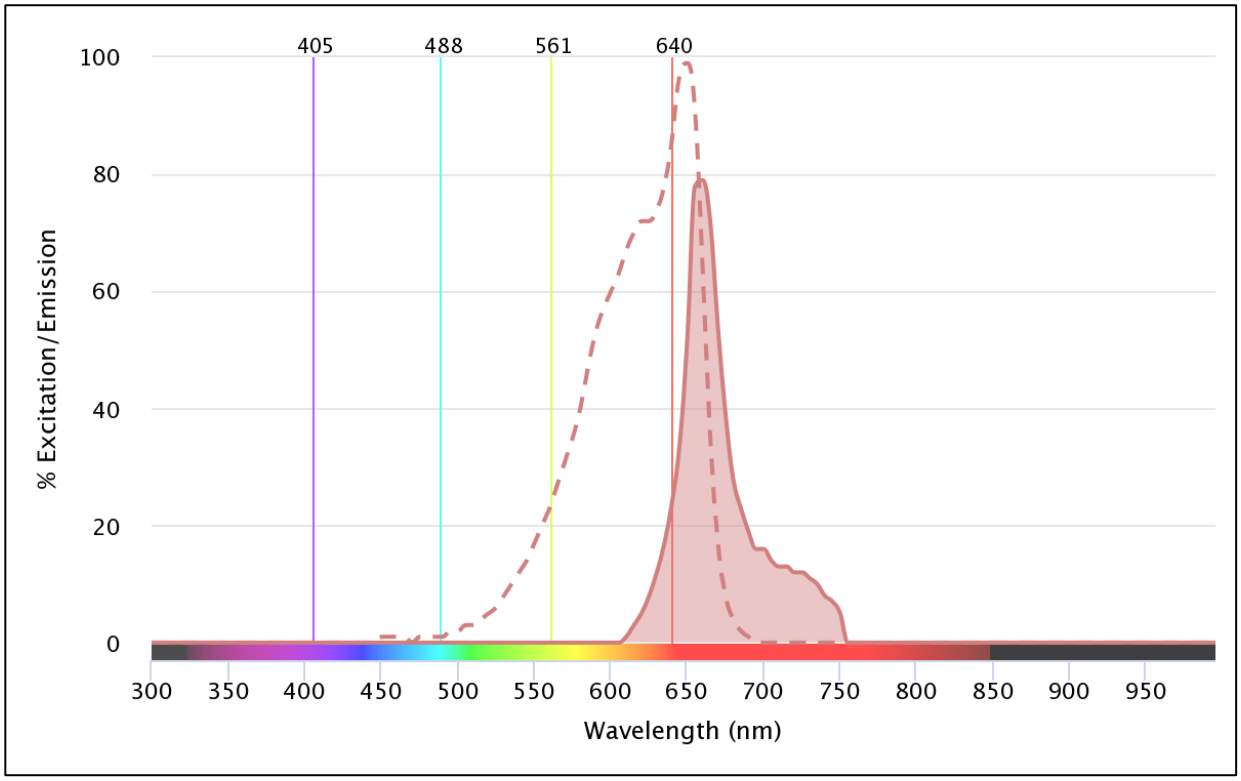

Figure G.3) APC (Allophycocyanin) excitation (dashed line) and emission (solid line with filled area) spectra normalized to 640nm red laser line. Generated by FluoroFinder.

APC-Fire750 (Allophycocyanin – Fire750)

Fluorophore type – fluorescent protein hexamer (APC) tandem synthetic ring compound (Fire750).
Primary laser excitation – red 640nm.
Max emission – 788nm.

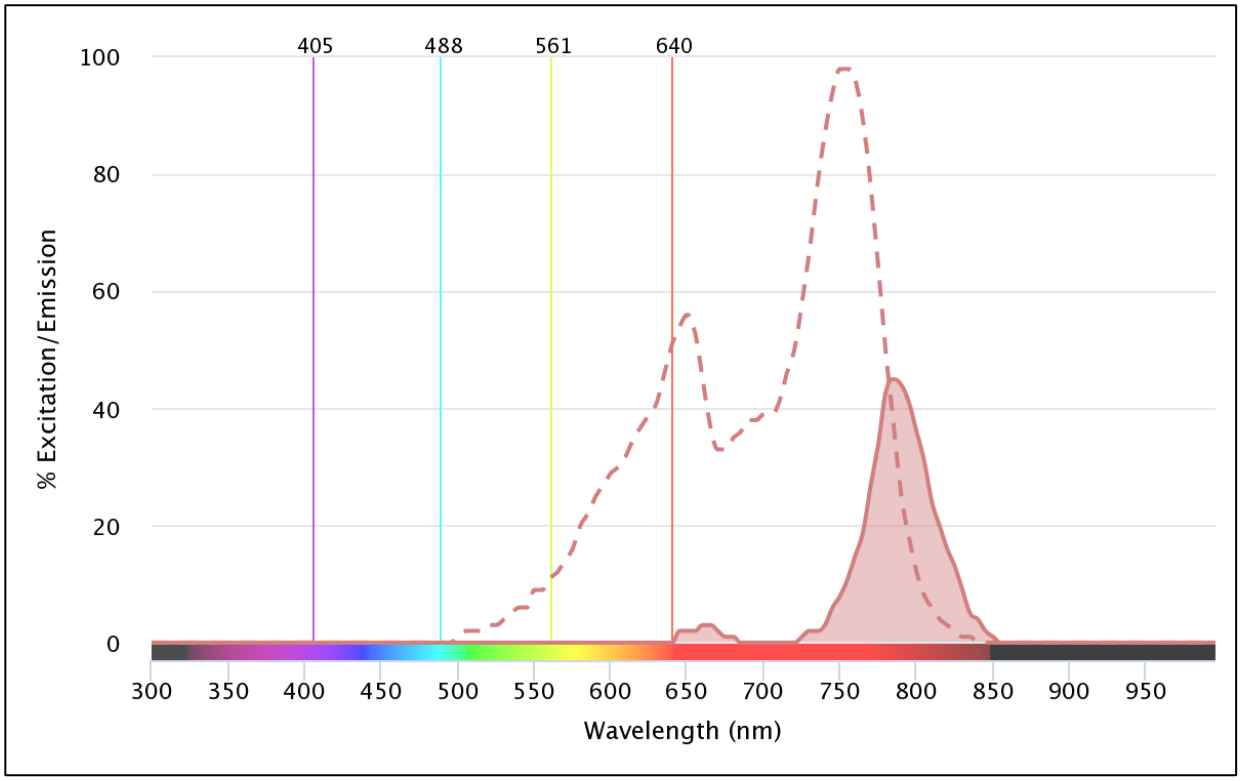

Figure G.4) APC-Fire750 (Allophycocyanin -Fire750) excitation (dashed line) and emission (solid line with filled area) spectra normalized to 640 nm red laser line. Generated by FluoroFinder.

BV421 (Brilliant Violet 421)

Fluorophore type – polymer dye.
Primary laser excitation – violet 405nm.
Max emission – 421nm.

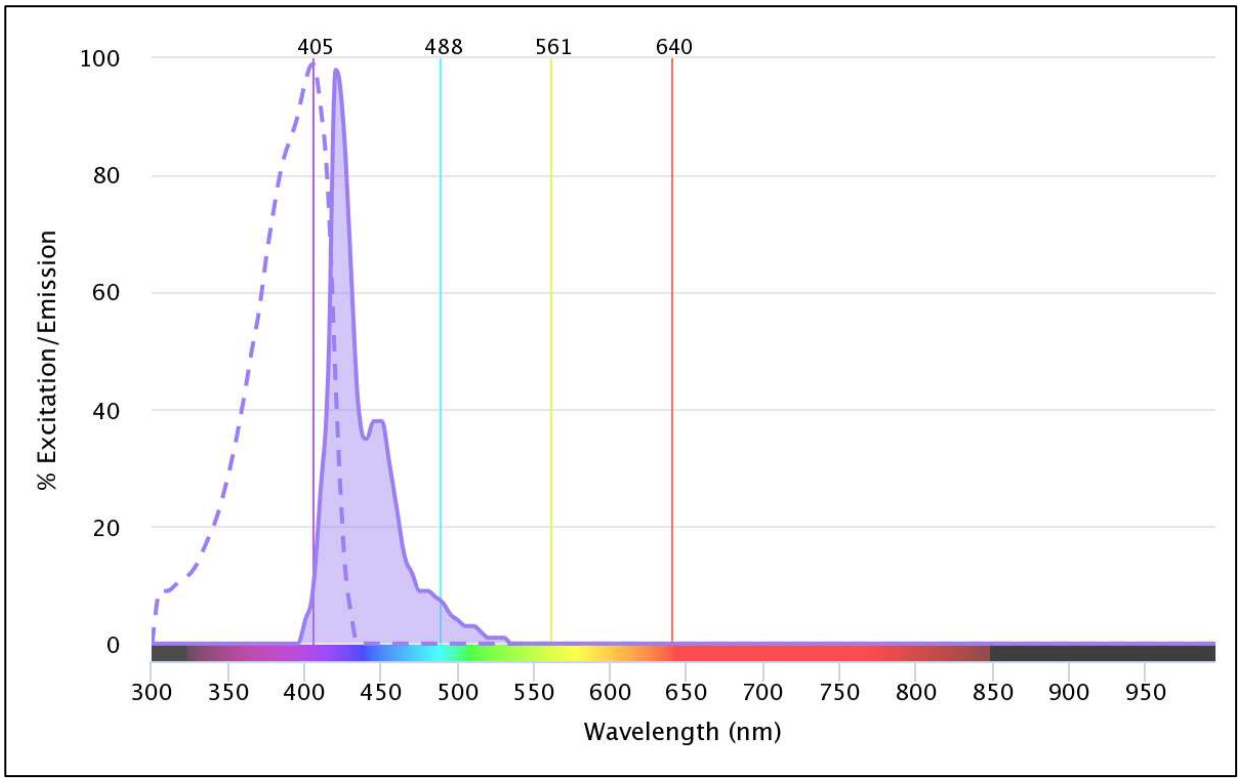

Figure G.5) BV421 (Brilliant Violet 450) excitation (dashed line) and emission (solid line with filled area) spectra normalized to 405nm violet laser line. Generated by FluoroFinder.

eFluor660

Fluorophore type – synthetic cyclic ring compound.
Primary laser excitation – red 640nm.
Max emission – 669nm.

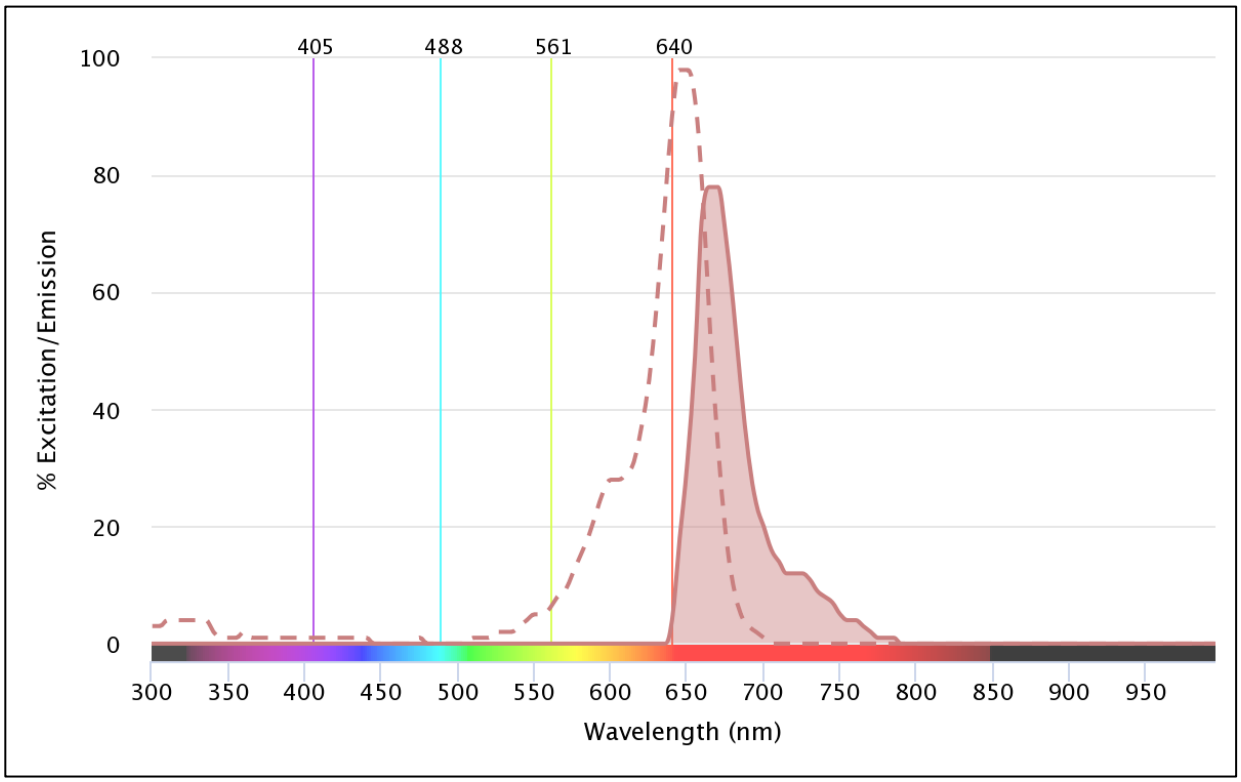

Figure G.6) eFluor660 excitation (dashed line) and emission (solid line with filled area) spectra normalized to 640nm red laser line. Generated by FluoroFinder.

FITC (Fluorescein isothiocyanate)

Fluorophore type – synthetic cyclic ring compound.
Primary laser excitation – blue 488nm.
Max emission – 525nm.

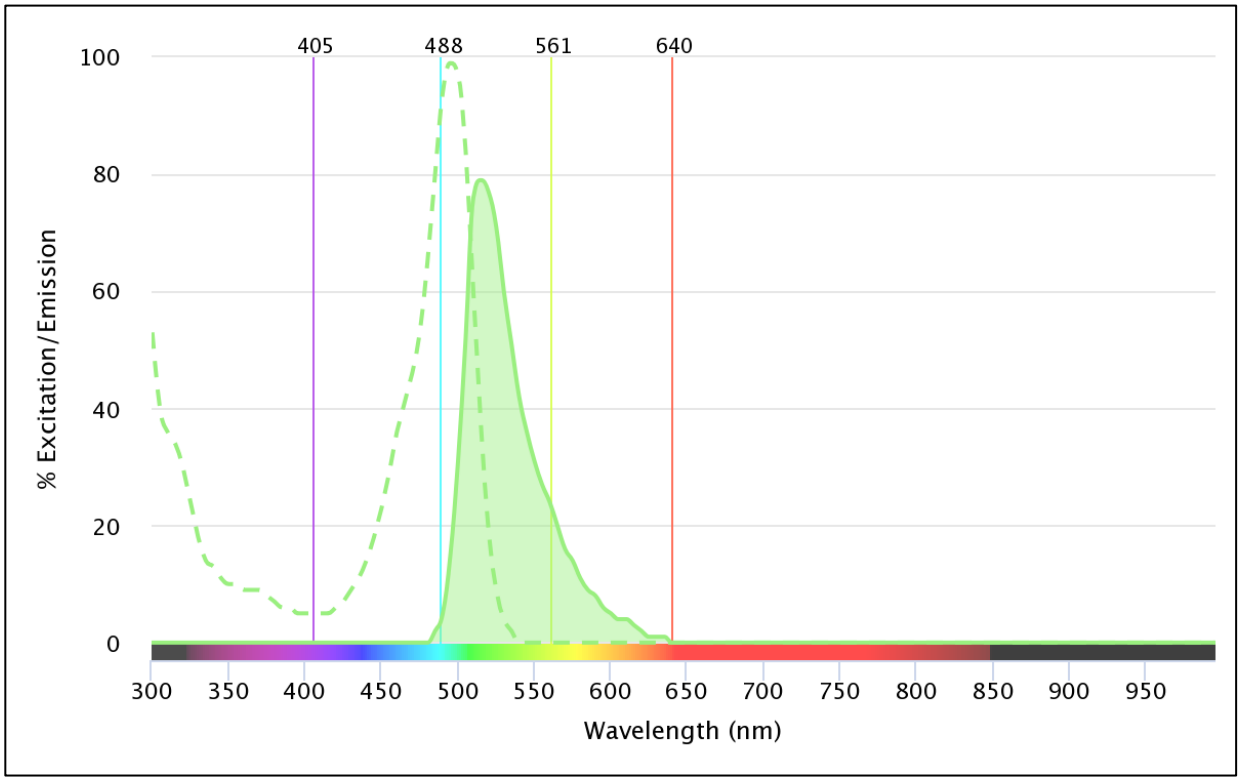

Figure G.7) FITC (Fluorescein isothiocyanate) excitation (dashed line) and emission (solid line with filled area) spectra normalized to 488nm blue laser line. Generated by FluoroFinder.

Ghost Violet 450

Fluorophore type – primary amine viability dye.
Primary laser excitation – violet 405nm.
Max emission – 447nm.

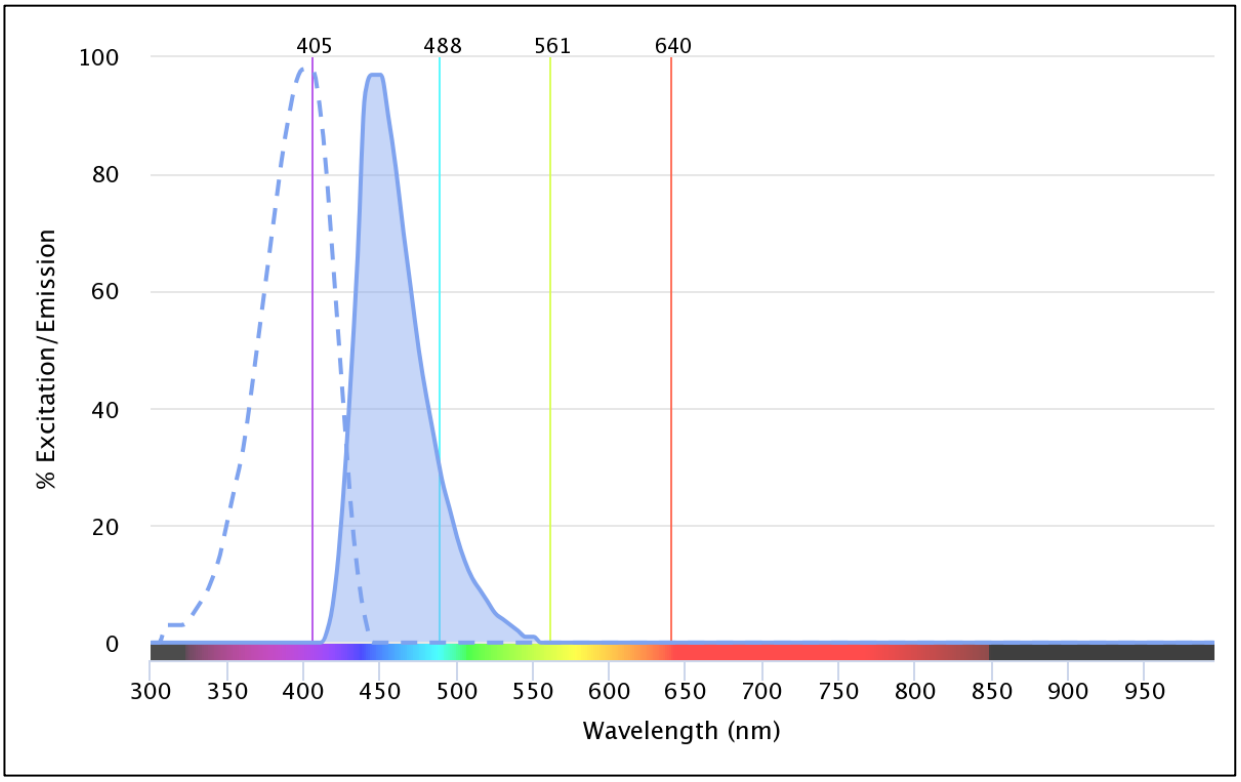

Figure G.8) Ghost Violet 450 primary amine viability dye excitation (dashed line) and emission (solid line with filled area) spectra normalized to 405 violet laser line. Generated by FluoroFinder.

Ghost Blue 516

Fluorophore type – primary amine viability dye.
Primary laser excitation – violet 405nm.
Max emission – 508nm.

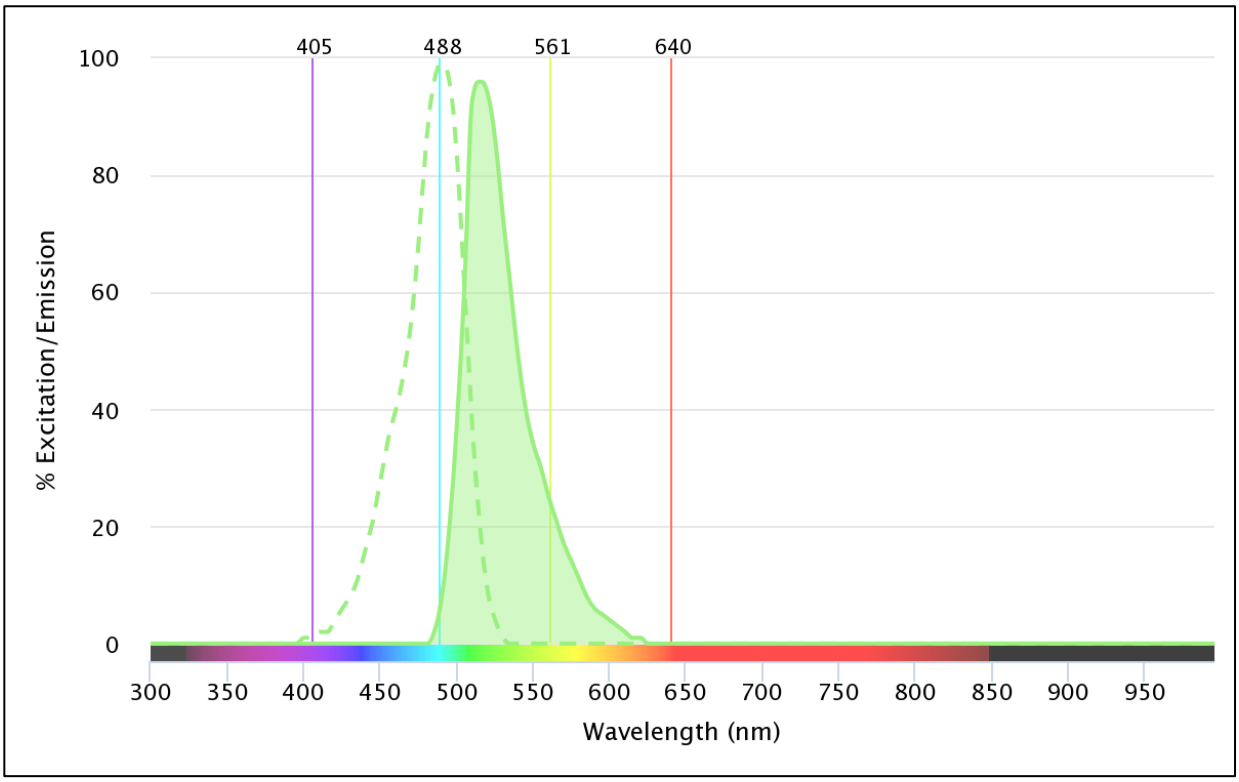

Figure G.9) Ghost Blue 516 primary amine viability dye excitation (dashed line) and emission (solid line with filled area) spectra normalized to 405 violet laser line. Generated by FluoroFinder.

Ghost Red 780

Fluorophore type – primary amine viability dye.
Primary laser excitation – red 640nm.
Max emission – 778nm.

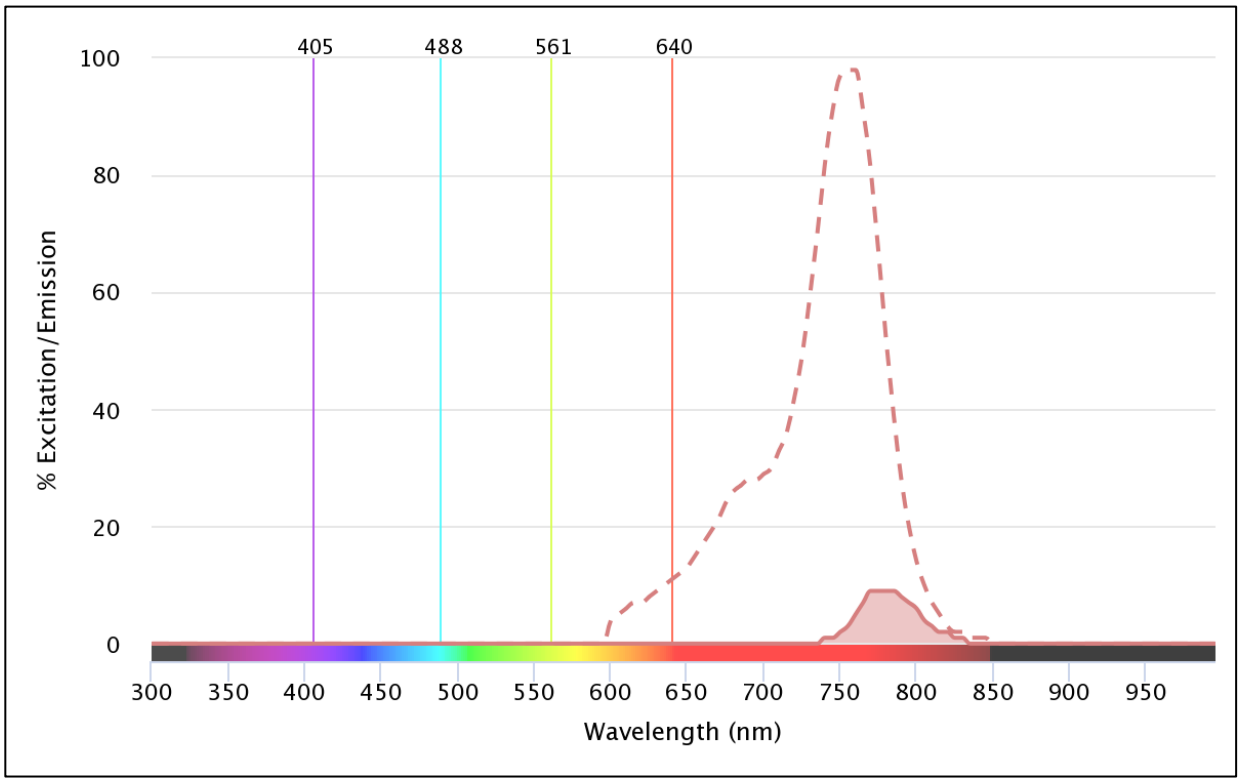

Figure G.10) Ghost Red 780 primary amine viability dye excitation (dashed line) and emission (solid line with filled area) spectra normalized to 640nm red laser line. Generated by FluoroFinder.

Ghost Violet 510

Fluorophore type – primary amine viability dye.
Primary laser excitation – violet 405nm.
Max emission – 508nm.

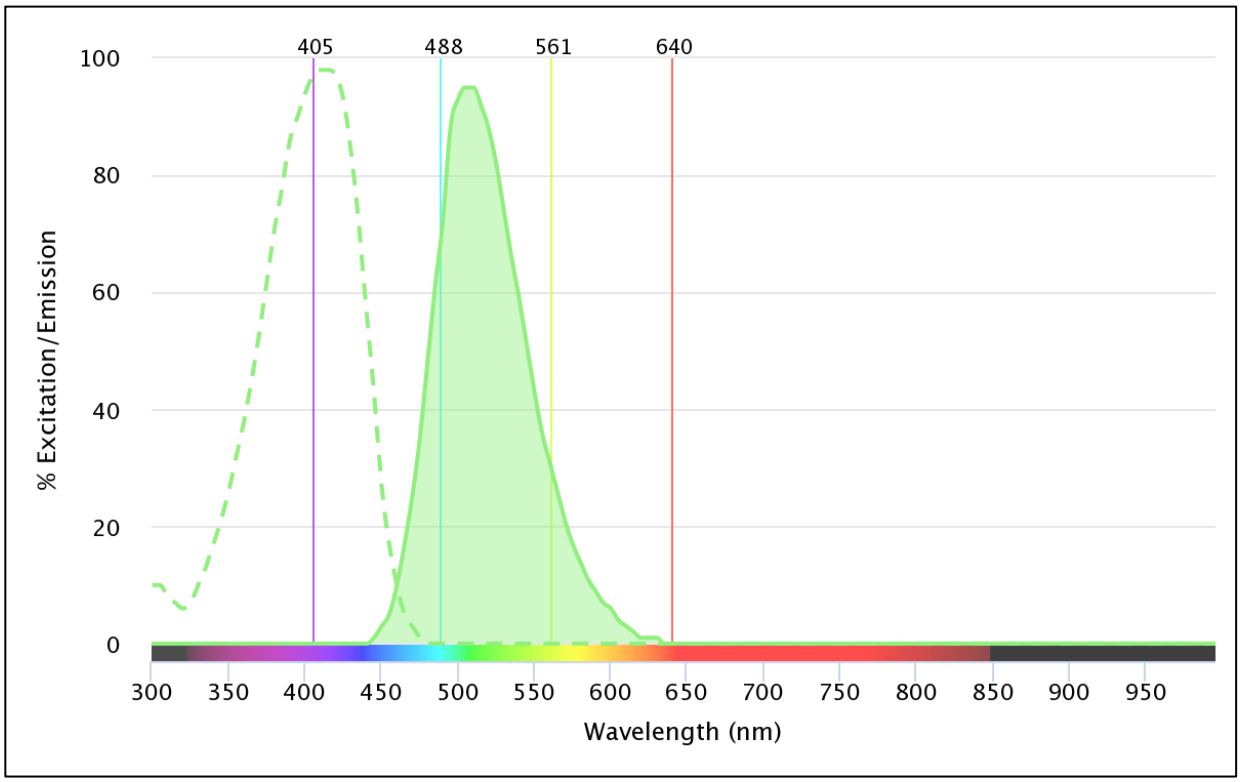

Figure G.11) Ghost Violet 510 primary amine viability dye excitation (dashed line) and emission (solid line with filled area) spectra normalized to 405 violet laser line. Generated by FluoroFinder.

PE (R-phycoerythrin)

Fluorophore type – fluorescent protein hexamer.
Primary laser excitation – yellow/green 561nm.
Max emission – 578nm.

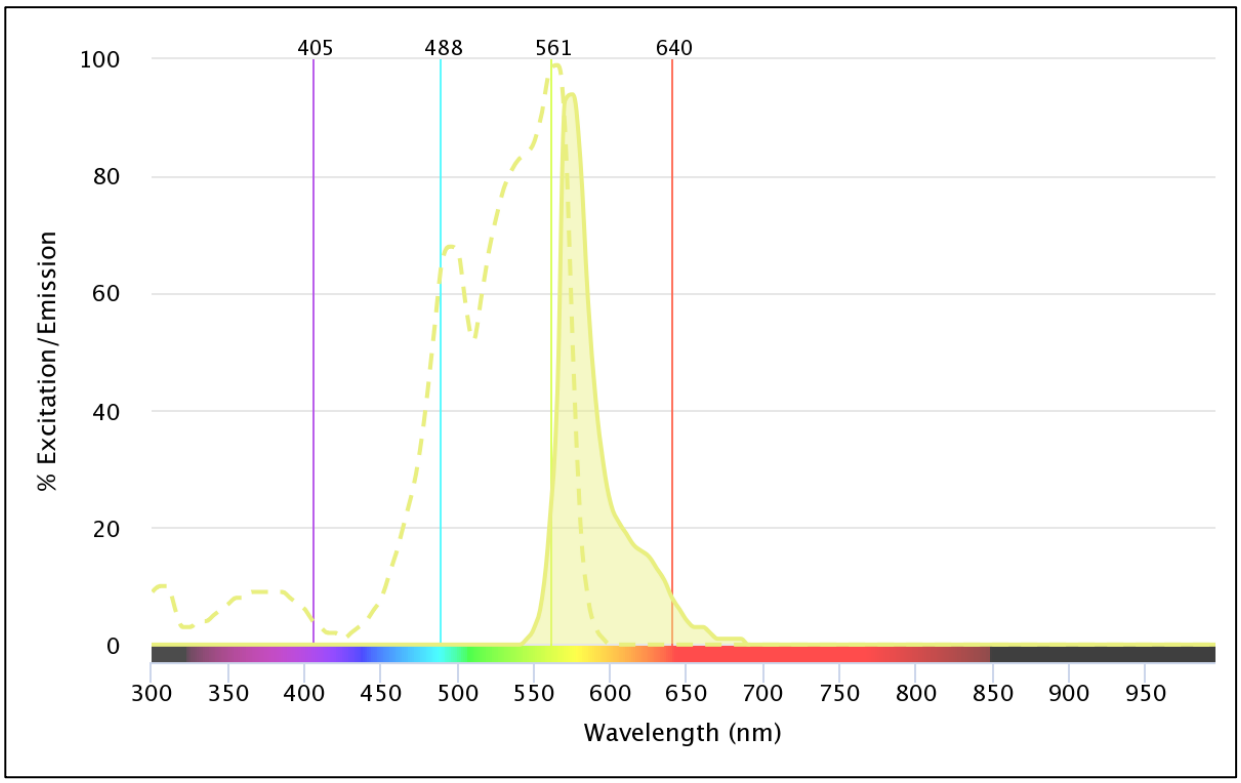

Figure G.12) PE (R- phycoerythrin**)** excitation (dashed line) and emission (solid line with filled area) spectra normalized to 561nm yellow/green laser line. Generated by FluoroFinder.

PE-Cy5 (R-phycoerythrin – Cyanine-5)

Fluorophore type – fluorescent protein hexamer (PE) tandem to synthetic cyclic ring compound (Cy5).
Primary laser excitation – yellow/green 561nm.
Max emission – 667nm.

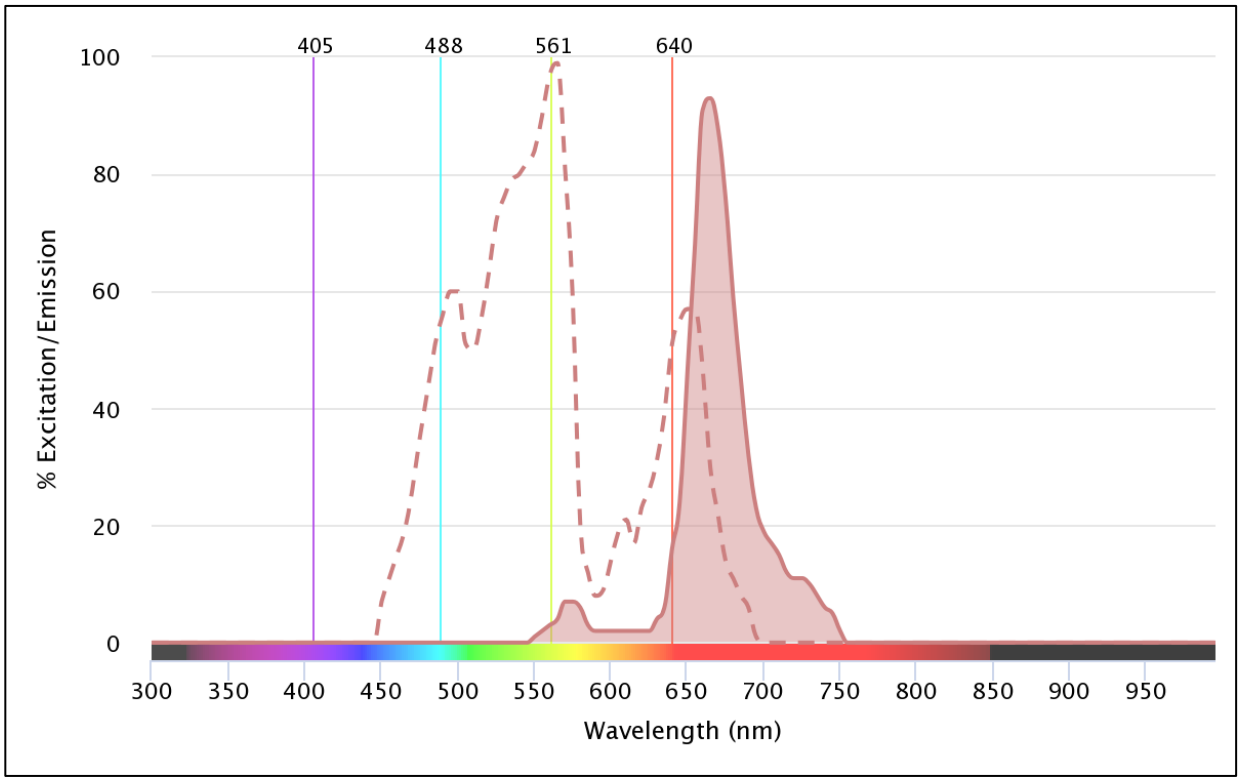

Figure G.13) PE-Cy5 (R- phycoerythrin –Cyanine-5) excitation (dashed line) and emission (solid line with filled area) spectra normalized to 561nm yellow/green laser line. Generated by FluoroFinder.

PE-Cy5.5 (R-phycoerythrin – Cyanine-5.5)

Fluorophore type – fluorescent protein hexamer (PE) tandem to synthetic cyclic ring compound (Cy5.5).
Primary laser excitation – yellow/green 561nm.
Max emission – 695nm.

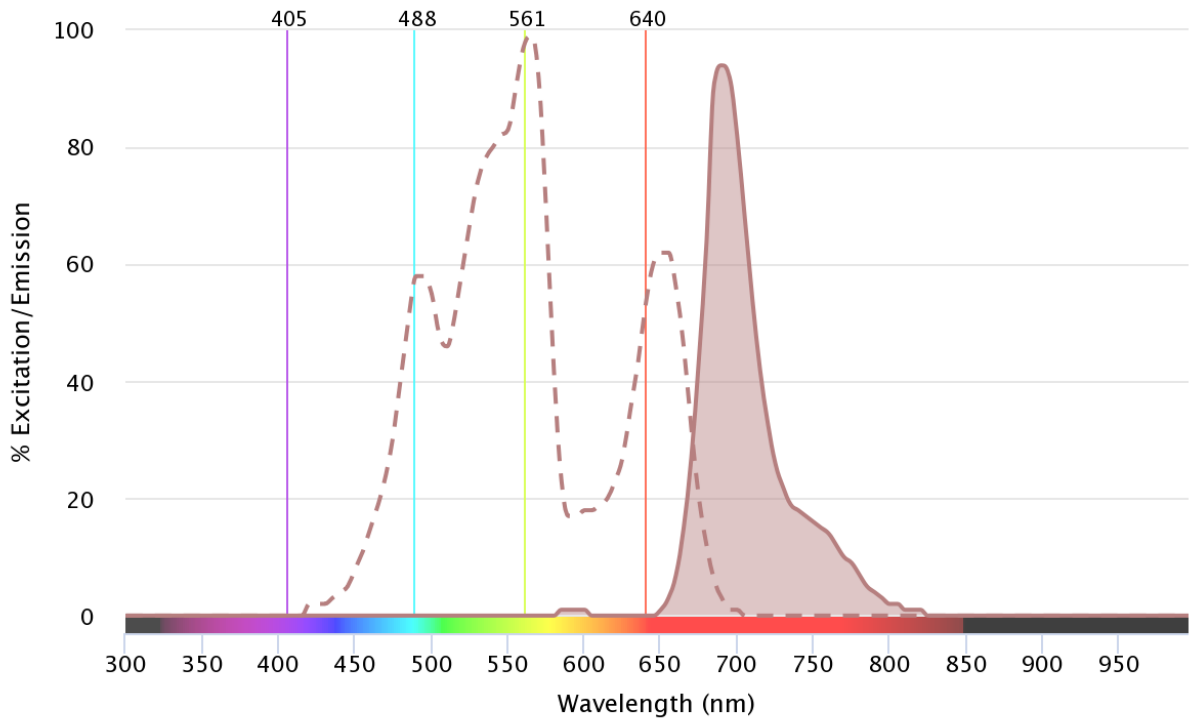

Figure G.14) PE-Cy5.5 (R- phycoerythrin –Cyanine-5.5) excitation (dashed line) and emission (solid line with filled area) spectra normalized to 561nm yellow/green laser line. Generated by FluoroFinder.

PE-Cy7 (R-phycoerythrin – Cyanine-7)

Fluorophore type – fluorescent protein hexamer (PE) tandem to synthetic cyclic ring compound (Cy7).
Primary laser excitation – yellow/green 561nm.
Max emission – 778nm.

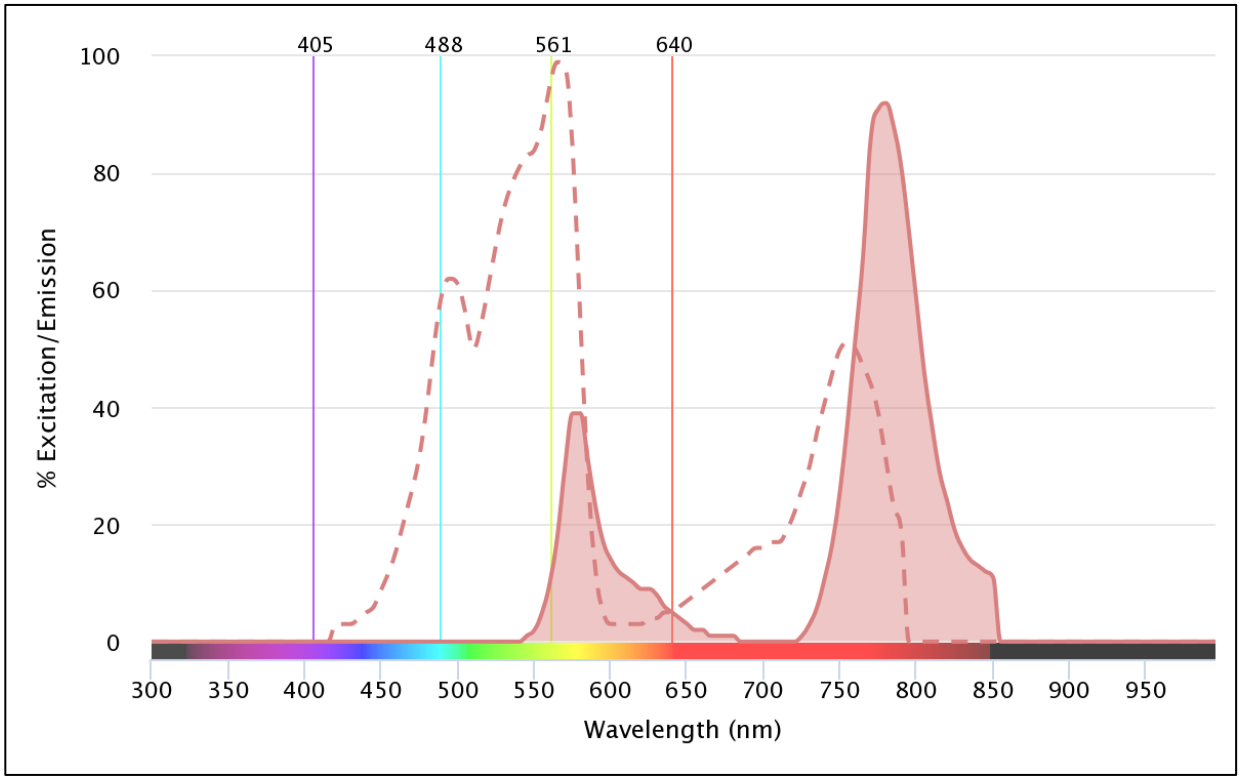

Figure G.15) PE-Cy7 (R- phycoerythrin –Cyanine-7) excitation (dashed line) and emission (solid line with filled area) spectra normalized to 561nm yellow/green laser line. Generated by FluoroFinder.

PE-eFluore 610 (R-phycoerythrin – eFluor 610)

Fluorophore type – fluorescent protein hexamer (PE) tandem to synthetic cyclic ring compound (eFluor 610).
Primary laser excitation – yellow/green 561nm.
Max emission – 607nm.

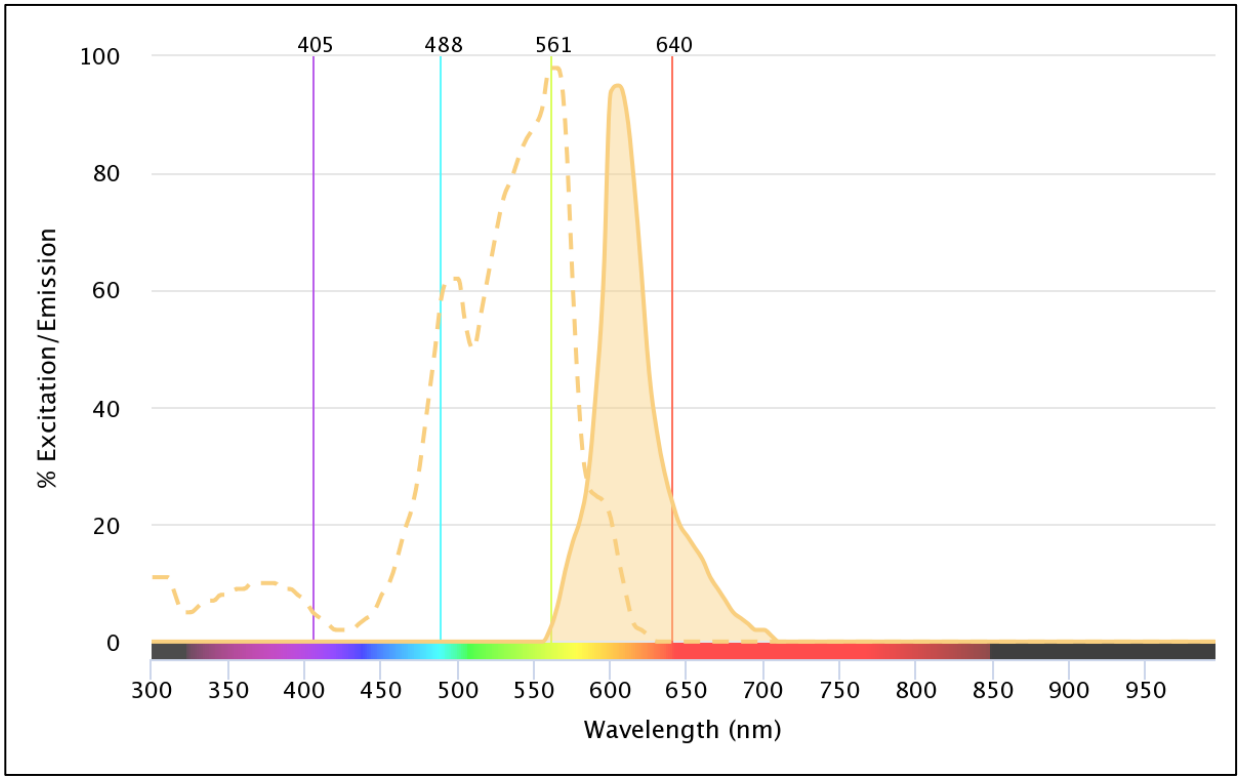

Figure G.16) PE-eFluor610 (R- phycoerythrin – eFluor 610) excitation (dashed line) and emission (solid line with filled area) spectra normalized to 561nm yellow/green laser line. Generated by FluoroFinder.

PerCP-eFluor 610 (Peridinin-Chlorophyll-Protein – eFluor 610)

Fluorophore type – fluorescent protein hexamer (PerCP) tandem to synthetic cyclic ring compound (eFluor 610).
Primary laser excitation – blue 488nm.
Max emission – 667nm.

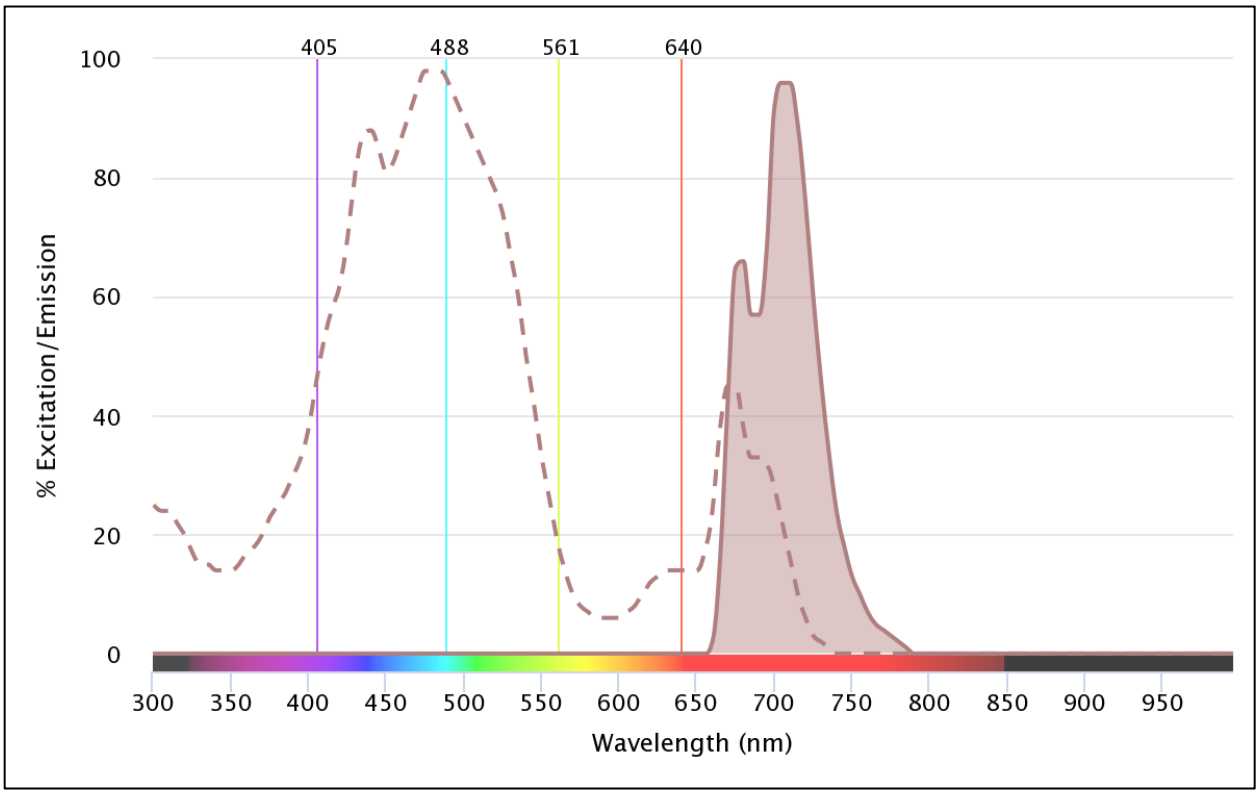

Figure G.17) PerCP-eFluor710 (Peridinin-Chlorophyll-Protein – eFluor 610) excitation (dashed line) and emission (solid line with filled area) spectra normalized to 488nm blue laser line. Generated by FluoroFinder.

LIST OF ABBREVIATIONS

AF ..... Autofluorescence
AGM1 ..... Asialo GM1
AICL ..... Activation-Induced C-Type Lectin
Aj ..... *Artibeus jamaicensis*
ANOVA ..... Analysis of Variance
BCR ..... B Cell Receptor
BLOSUM62 ..... Blocks Substitution Matrix
BSA ..... Bovine Serum Albumin
C3dg ..... complement opsonin C3dg
CD ..... Cluster of Differentiation
COVID-19 ..... Coronavirus Disease 2019
DAPI ..... 4',6-Diamidino-2-Phenylindole
DNA ..... Deoxyribonucleic Acid
DTT ..... Dithiothreitol
EDTA ..... Ethylenediaminetetraacetic acid
ELISA ..... Enzyme-Linked Immunosorbent Assay
ELISPOT ..... Enzyme-Linked Immunosorbent Spot
FBS ..... Fetal Bovine Serum
FCS ..... Flow Cytometry Standard
FMO ..... Fluorescence Minus One
FSC ..... Forward Scatter
HAT ..... Hypoxanthine-Aminopterin-Thymidine
HLA ..... Human Leukocyte Antigen
IACUC ..... Institutional Animal Care and Use Committee
IEL ..... Intraepithelial Lymphocyte
IFA ..... Incomplete Freud's Adjuvant
IFN ..... Interferon

IgG ..... Immunoglobulin G
IVA ..... Influenza A Virus

KLH ..... Keyhole Limpet Hemocyanin
KLRB1B .....Killer cell lectin-like receptor subfamily B, member 1
KLRB1C .....Killer cell lectin-like receptor subfamily B, member 1C
KLRC.....Killer cell lectin like receptor C
KLRD.....Killer cell lectin like receptor D
KLRF1 ..... Killer cell lectin like receptor F1
LB ..... Luria Broth
LLT1 ..... Lectin-Like Transcript-1
LOD ..... Limit of Detection
LOQ ..... Limit of Quantification
LP.....Lamina Propria
MDCK .....Madin-Darby canine kidney
MERS-CoV..... Middle East Respiratory Syndrome Coronavirus
MHC ..... Major Histocompatibility Complex
NCBI.....National Center for Biotechnology Information
OD..... Optical Density
PBMC .....Peripheral Blood Mononuclear Cells
PBS ..... Phosphate Buffered Saline
PCR..... Polymerase Chain Reaction
PHYR^2 .....Protein Homology/analogy Recognition Engine Version 2.0
RNA .....Ribonucleic Acid
RPS18 .....Ribosomal Protein S18
RT-qPCR .....Reverse Transcription-quantitative Polymerase Chain Reaction
SARS-CoV..... Severe Acute Respiratory Syndrome Coronavirus
SSC ..... Side Scatter
TCR..... T Cell Receptor
WNS..... White-Nose Syndrome
Wnt3A.....Wingless/Integrated Family Member 3A